University of Ljubljana

Faculty of Electrical Engineering

Anže Župančič

Treatment planning in biomedical applications of electroporation

DOCTORAL DISSERTATION

Mentor: prof. Damijan Miklavčič, Ph. D.

(University of Ljubljana, Slovenia)

Ljubljana, 2010

Declaration

The author hereby declares that the content of the thesis is a result of his own research work supervised by prof. Damijan Miklavčič. The results, which were collected in collaboration with other colleagues, are published in the presented papers. The published results of other authors are presented in the literature.

Anže Županič

Povzetek

Uvod

Če biološko celico izpostavimo dovolj visokemu zunanjemu električnemu polju, pride v celični membrani do strukturnih sprememb, ki omogočajo transport snovi skozi membrano. Elektroporacijo, kot se pojav imenuje po trenutno najbolj priznani teoriji o mehanizmih strukturnih sprememb, je mogoče nadzorovati s parametri električnih pulzov [Sugar in Neumann, 1984]. Električni pulzi nižjih napetosti celico elektroporirajo le začasno, tako da se po preteku nekaj minut celična membrana zaceli, celične funkcije pa se povrnejo v fiziološko stanje [Neumann et al., 1982]. Ta pojav se imenuje reverzibilna elektroporacija in ga večinoma uporabljamo za vnos snovi v celice. Električni pulzi višjih napetosti pa povzročijo ireverzibilno elektroporacijo, ki vodi v celično smrt [Rubinsky, 2007]. Ker je elektroporacijo mogoče doseči v vseh celicah, je postala ena izmed najpogosteje uporabljanih metod za doseganje transport snovi skozi celično membrano.

Elektroporacijo že nekaj časa uporabljajo tudi v medicinske namene. Trenutne aplikacije elektroporacije v medicini so elektrokemoterapija raka, ablacija tkiva z ireverzibilno elektroporacijo in genska elektrotransfekcija za gensko terapijo in gensko cepljenje. Elektrokemoterapijo, kjer se elektroporacijo uporablja za povečanje vnosa kemoterapevtskih učinkovin v tumorske celice, že nekaj let uporabljajo za zdravljenje kožnih in podkožnih tumorjev [Marty et al., 2006], prvi klinični testi ablacije z ireverzibilno elektroporacijo in genske elektrotransfekcije za gensko terapijo pa že kažejo pozitivne rezultate [Davalos et al., 2005; Heller et al., 2006]. Ena izmed zadnjih preprek še širši uveljavitvi teh aplikacij v kliničnem okolju je rutinsko doseganje primernih porazdelitev električnega polja v ciljnih tkivih.

V zadnjem desetletju so raziskovalci za napovedovanje porazdelitve električnega polja v tkivih in s tem tudi napovedovanje učinkov elektroporacije začeli uporabljati numerično modeliranje. Trenutno se za napovedovanje učinkov elektroporacije na nivoju tkiv uporabljajo statični [Miklavčič et al., 2000] in sekvenčni modeli [Šel et al., 2005], pri čemer prvi ne upoštevajo sprememb lastnosti snovi zaradi elektroporacije, drugi pa jih. Tako statični kot sekvenčni modeli uspejo dobro opisati elektroporacijo v izotropnih in homogenih tkivih, v heterogenih tkivih, kot je na primer koža, pa se rezultati sekvenčnih modelov mnogo bolje skladajo z eksperimentalnimi rezultati.

Glavni namen doktorske disertacije je bil razvoj postopka, s katerim bi lahko zagotovili primerno porazdelitev električnega polja v medicinskih uporabah elektroporacije. V ta namen smo na osnovi analize medicinskih slik, numeričnega modeliranja elektroporacije in optimizacije položajev elektrod ter napetosti med elektrodam izpeljali postopek za načrtovanje primerne porazdelitve električnega polja v tkivu. Ta omogoča individualno načrtovanje zdravljenja na osnovi določanja optimalnih položajev posameznih elektrod glede na ciljna tkiva in določanja optimalnih napetosti med posameznimi elektrodami. Za primere, kjer načrtovanje zdravljenja ni mogoče ali ni potrebno, pa smo določili osnovna vodila, ki povečujejo verjetnost doseganja primerne porazdelitve električnega polja in s tem uspešnosti zdravljenja.

Metode

Geometrije tkiv, ki smo jih uporabili v numeričnem modeliranju in načrtovanju zdravljenja z elektrokemoterapijo oziroma ablacijo z ireverzibilno elektroporacijo, smo sestavili iz medicinskih slik, na katerih so strokovnjaki z Onkološkega inštituta Ljubljana tkiva označili. Za sestavljanje geometrij smo uporabili dve metodi: metodo ravninskih krivulj [Liang et al., 2006] (Slika 1) in metodo volumetričnih slikovnih elementov [Astrom et al., 2009]. Metodo ravninskih krivulj smo uporabili za numerično modeliranje brez optimizacije in za preproste primere, kjer smo uporabili tudi optimizacijo, medtem ko smo za načrtovanje zdravljenja globoko ležečega tumorja z elektrokemoterapijo uporabili obe metodi. Geometrije elektrod smo zgradili z orodji, ki so na voljo v programu za numerično modeliranje s končnimi elementi Comsol Multiphysics (Comsol AB, Stockholm, Švedska).

Metoda končnih elementov [Silvester in Ferrari, 1992] je metoda za iskanje približnih rešitev parcialnih diferencialnih enačb. Bistvo metode leži v razdelitvi domene računanja na končne elemente, v katerih je približna rešitev enačb privzeta v obliki odsekoma zveznih funkcij. Približno rešitev enačb se tako izračuna zgolj na izbranih točkah v posameznih elementih, v prostoru med temi točkami pa je približna rešitev določena z obliko uporabljenih odsekoma zveznih funkcij – običajno so te funkcije linearne ali kvadratične. V modelih elektroporacije uporabljeni v naših raziskavah smo iskali rešitev Laplaceove diferencialne enačbe v obliki prostorske porazdelitve električnega potenciala:

$$-\nabla \cdot (\sigma \cdot \nabla V) = 0 \,, \tag{A.1}$$

kjer je σ električna prevodnost tkiva in V električni potencial. Pri tem smo uporabili sledeče robne pogoje: 1) konstanten električni potencial ($V = konstanta$) na aktivnih elektrodah in 2)

električno izolacijo ($\boldsymbol{n} \cdot (\boldsymbol{J_1} - \boldsymbol{J_2}) = 0$) na vseh zunanjih robnih ploskvah modela. Iz porazdelitve električnega potenciala je mogoče določiti jakost električnega polja:

$$E = -\nabla V, \qquad (A.2)$$

kjer je E jakost električnega polja. Jakost električnega polja je ključna količina za določanje elektroporacije, saj raziskave kažejo, da je mogoče prag elektroporacije določiti kot vrednost jakosti električnega polja.
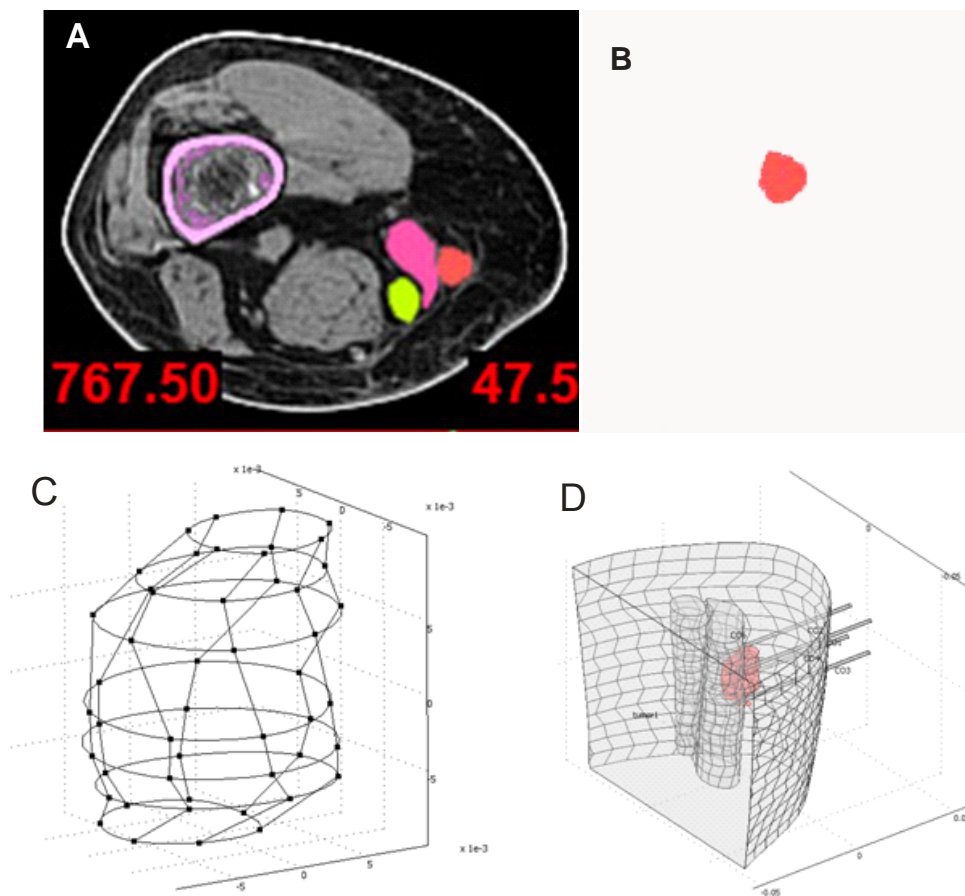
Slika 1. Gradnja 3D geometrije tumorja z metodo ravninskih krivulj. A) Segmentirane medicinske slike (na sliki je tumor rdeče barve) smo najprej spremenili v B) binarne matrike. C) Točke na robovih tumorja na vsaki sliki smo povezali med seboj, da smo zgradili zunanjo obliko geometrijskega objekta. D) Geometrijo tumorja smo izvozili v Comsol Multiphysics kot poln 3D-objekt skupaj z geometrijami preostalih relevantnih tkiv.

Elektroporacija povzroči spremembe v lastnostih elektroporiranega tkiva. Medtem ko je v statičnih modelih elektroporacije prevodnost tkiva med elektroporacijo konstantna, smo jo v sekvenčnih modelih opisali kot funkcijo odvisno od električnega polja $\sigma(E)$ [Šel et al., 2005; Pavšelj et al., 2005]:

$$\sigma(E) = \frac{\sigma_2 - \sigma_1}{E_{irr} - E_{rev}} \cdot E + \sigma_1 \; , \tag{A.3}$$

kjer je σ_1 oziroma σ_2 električna prevodnost ne-elektroporiranega oziroma elektroporiranega tkiva, E_{irr} oziroma E_{rev} pa prag ireverzibilne oziroma reverzibilne elektroporacije.

Visokonapetostni električni pulzi poleg elektroporacije v bioloških tkivih povzročajo tudi segrevanje. Segrevanje tkiv zaradi električnih pulzov smo opisali s Pennesovo biotoplotno enačbo [Pennes, 1948]:

$$\rho c \frac{\partial T}{\partial t} = \nabla \cdot (k \nabla T) - \rho_b c_b w_b (T - T_b) + Q_m + Q \; , \tag{A.4}$$

kjer je T temperatura, ρ gostota tkiva, c toplotna kapaciteta tkiva, ρ_b, c_b, w_b in T_b gostota, toplotna kapaciteta, pretok in temperatura krvi (v tem zaporedju), k toplotna prevodnost tkiva, Q_m toplota v tkivu nastala z metabolizmom in Q toplota v tkivu nastala zaradi zunanjih virov. Za hitrejšo oceno dviga temperature v tkivu pa smo uporabili:

$$\Delta T = (\sigma E^2 \, Nt) / \rho c \; , \tag{A.5}$$

kjer je N število električnih pulzov in t trajanje pulzov, σ, ρ in c pa so definirane že v enačbi A.4.

Za optimizacijo položajev elektrod in napetosti med njimi smo uporabili genetski algoritem [Holland, 1992], ki je kot vhod sprejemal porazdelitev električnega polja v modelu. Začetno populacijo rešitev smo določili naključno, pri tem pa smo upoštevali naslednje omejitve: nabor sprejemljivih razdalj med elektrodami, globin vstavljanja elektrod in napetosti med elektrodami. Rešitve so se iz generacije v generacijo razmnoževale (z verjetnostmi) glede na vrednosti njihovih objektnih funkcij:

$$F = \sum a_i \cdot E_{rev}^{i-cilj} - \sum b_j \cdot E_{irr}^{j-kritično} - \sum c_i \cdot E_{irr}^{i-cilj} - \sum d_j \cdot E_{rev}^{j-kritično}, \tag{A.6}$$

kjer so a_i, b_j, c_i in d_j uteži, ki predstavljajo pomen za pokritost ciljnega tkiva (^{cilj}) in ostalih tkiv (^{kritično}) z električnim poljem nad pragom reverzibilne ali ireverzibilne elektroporacije. Razmnoževanje je potekalo z operacijama križanja (A.7) in mutacije (A.8):

$$z_i = a_i \cdot x_i + (1 - a_i) \cdot y_i; \; a_i \epsilon [0,1] \; , \tag{A.7}$$

$$z_i = x_i + b_i \cdot x_i; \; b_i \epsilon [-p, p], \tag{A.8}$$

kjer so z_i rešitve v naslednji generaciji, x_i in y_i, rešitve v predhodni generaciji, a_i in b_i pa naključno izbrane uteži iz zgornjih intervalov.

Rezultati

Preučevanje elektroporacije v tkivu med dovajanjem električnih pulzov smo začeli z numeričnim modeliranjem porazdelitve električnega polja različnih polj igelnih elektrod, ki se uporabljajo za dovajanje električnih pulzov v klinični elektrokemoterapiji. Ugotovili smo, da je mogoče z elektrodami, razporejenimi v vrstah, dobiti boljše rezultate kot s heksagonalno postavljenimi elektrodami in da je za učinkovito izpostavitev tumorja električnemu polju elektrode najbolje postaviti okrog tumorja v vseh dimenzijah (Slika 2). Optimizacija položajev elektrod in napetosti z genetskim algoritmom je prej pridobljene rezultate potrdila, prav tako pa se je izkazala za zelo ponovljivo, saj se je postopek optimizacije v vseh primerih končal z rešitvijo, ki je predvidevala popolno pokritost tumorja z električnim poljem nad pragom reverzibilne elektroporacije.
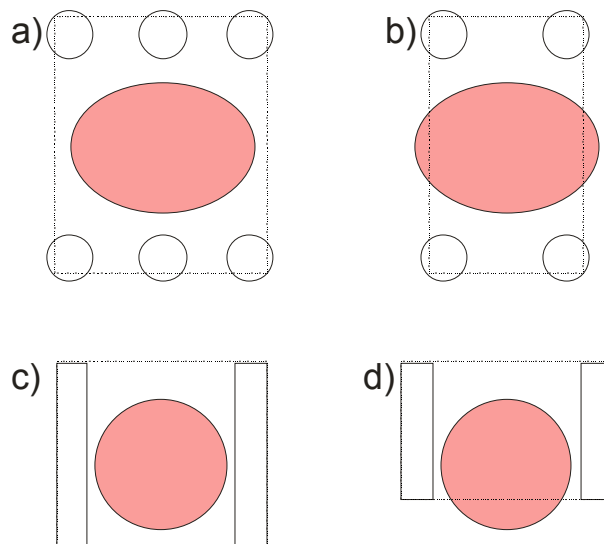

Slika 2. Ustrezen položaj igelnih elektrod glede na ciljno tkivo (a,c) in tipičen neustrezen položaj elektrod, ki zahtevajo za doseganje ustrezne porazdelitve električnega polja mnogo višje napetosti ali pa celo vodijo k nepopolni pokritosti ciljnega tkiva (b,d). (a,b) predstavljata presek tumorja in elektrod pravokotno na smer vstavljanja igelnih elektrod, medtem ko (c,d) predstavljata presek pravokotno na smer vstavljanja elektrod.

Nadaljevali smo z načrtovanjem ablacije podkožnega tumorja z ireverzibilno elektroporacijo. Optimizacija z genetskim algoritmom je pokazala, da je s postavljanjem posamičnih elektrod okrog tumorja mogoče doseči boljšo porazdelitev električnega polja, kot z uporabo vnaprej definiranega polja igelnih elektrod (tj. z dvema vrstama igelnih elektrod – Slika 2a). Pri postavljanju posameznih elektrod smo morali z optimizacijskim algoritmom

hkrati optimirati kar 19 parametrov, kar pa za algoritem ni predstavljajo večjih težav – v vseh simulacijah je optimizacija dala rezultat blizu optimalnega. Nadalje je bilo v bližino tumorja v model postavljeno kritično tkivo, kjer je bila ireverzibilna elektroporacija nezaželena. Z optimizacijo je bilo mogoče doseči popolno pokritost tumorja z električnim poljem nad pragom ireverzibilne elektroporacije, medtem ko je bilo pokritega zgolj 0,8 % kritičnega tkiva. Podobne rezultate smo dobili tudi pri optimizaciji elektrokemoterapije s posamičnim postavljanjem elektrod in dodano optimizacijo kotov vstavljanja elektrod v tkivo (36 parametrov).

Ker je glavna prednost ablacije z ireverzibilno elektroporacijo pred ostalimi ablacijskimi metodami njena »netermičnost« – smrt celic povzroča električno polje in ne visoka temperatura, smo poskusili v postopek načrtovanja zdravljenja vključiti tudi izračun porazdelitve temperature po tkivu med dovajanjem električnih pulzov. Ker je bilo računanje z biotoplotno enačbo (A.4) časovno zelo zamudno, smo poskusili z zelo konservativnim načinom ocenjevanja porazdelitve temperature (A.5), ki je čas optimizacije skrajšal za več kot 10-krat. Da optimalna rešitev, pridobljena na tak način, res ustreza »netermičnim« kriterijem, smo nato preverili še z izračunom porazdelitve temperature v tkivu z biotoplotno enačbo (A.4). Ugotovili smo, da parametri pulzov, ki jih trenutno uporabljajo pri ablaciji z ireverzibilno elektroporacijo, ne povzročajo pretiranega segrevanja (Slika 3), zato izračuna segrevanja ni potrebno vključiti v postopek načrtovanja zdravljenja, je pa potreben za preverjanje primernosti načrta zdravljenja po koncu optimizacije.

Učinkovita genska transfekcija v mišico ne zahteva tako natančne lokaliziranosti električnega polja kot elektrokemoterapija ali ablacija z ireverzibilno elektroporacijo. Vseeno pa je pomembno, da je čim večji del mišice izpostavljen električnemu polju nad reverzibilnim pragom elektroporacije in čim manjši polju nad ireverzibilnim pragom. Numerično modeliranje je pokazalo, da je nujno natančno opisati lastnosti tkiv, vključno z nelinearnimi in anizotropičnimi lastnostmi, in da se rezultati med statičnimi in sekvenčnimi modeli precej razlikujejo. S sekvenčnimi modeli smo izračunali povprečno 26 % večji volumen mišice, izpostavljene električnemu polju nad reverzibilnim pragom elektroporacije, medtem ko je bila razlika v izračunu električnega toka še precej večja (145 %).
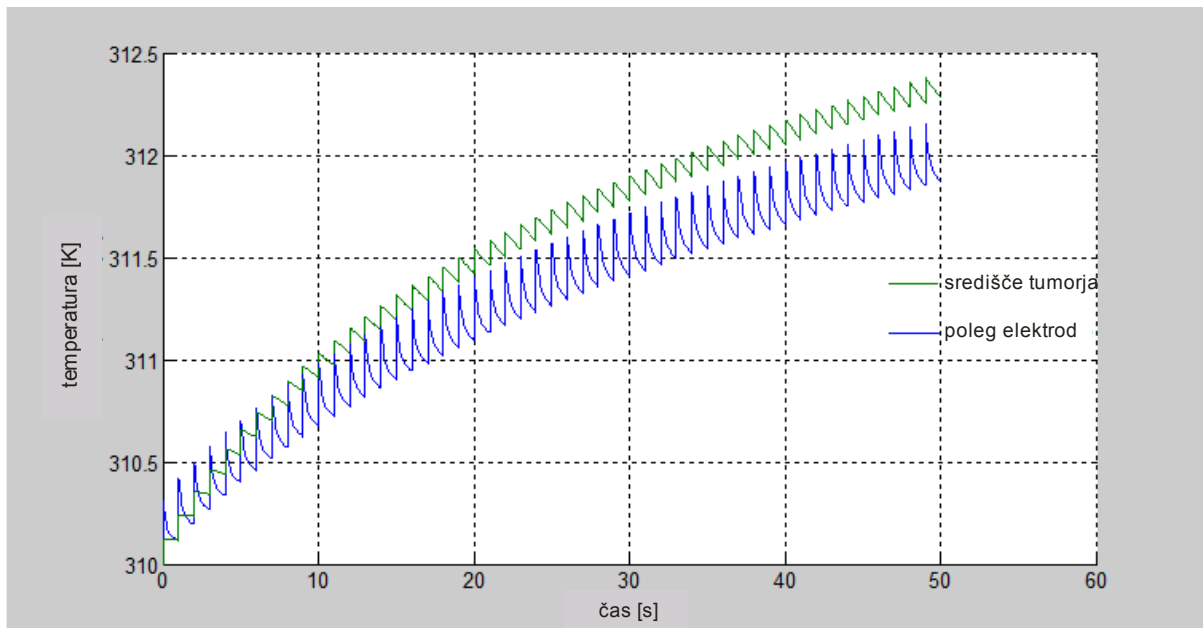
Slika 3. Temperatura v središču tumorja in v neposredni bližini elektrod po 50 100-mikrosekundnih pulzih napetosti 500 V izračunana z biotoplotno enačbo. Najvišja temperature v bližini elektrod je bila 39,1 °C (312,1 K), medtem ko je temperature v sredini tumorja dosegla 39,3 °C (312,3 K).

Parametrizacija in optimizacija položajev elektrod in napetosti sta pokazali, da je mogoče izpostaviti največji volumen mišičnega tkiva električnemu polju nad reverzibilnim pragom elektroporacije (in obenem majhen volumen polju nad ireverzibilnim pragom) z uporabo razmeroma velikih razdalj med elektrodami, z večjo globino vstavitve elektrod in z uporabo pravokotne orientacije električnega polja glede na orientacijo mišičnih vlaken.

Potem ko je bila uporabnost in robustnost postopka za načrtovanje porazdelitve električnega polja prikazana na hipotetičnih študijah aplikacij elektroporacije v medicini, smo postopek uporabili za načrtovanje prve elektrokemoterapije globoko ležečega tumorja na svetu. Z genetskim algoritmom smo določili dva načrta zdravljenja, enega s štirimi vstavljenimi elektrodami (ki je bil pred terapijo tudi izbran) in enega s petimi (Sliki 4 in 5). Čeprav je bila elektrokemoterapija uspešna zgolj delno – tumor se je zmanjšal, a nato je začel znova rasti –, smo pokazali, da je numerično načrtovanje zdravljenja v klinični elektrokemoterapiji mogoče. S preučitvijo izvedbe zdravljenja in postopka načrtovanja smo pokazali, da so bile za neuspeh verjetno odgovorne napake pri postavljanju elektrod okrog tumorja, nismo pa mogli povsem izključiti tudi napak v načrtu zdravljenja zaradi razlik med dejansko in upoštevano prevodnostjo tkiv uporabljenih v numeričnih modelih.
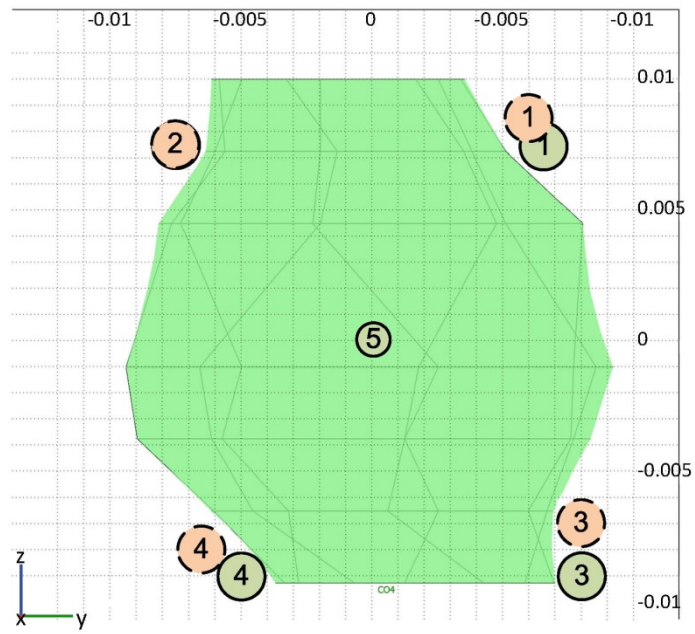
Slika 4. Položaji elektrod določeni z optimizacijo. Prikazana sta načrta zdravljenja s štirimi elektrodami (črtkani oranžni krogi) in petimi elektrodami (celi zeleni krogi). Optimalna položaja elektrode dve v obeh načrtih se prekrivata.
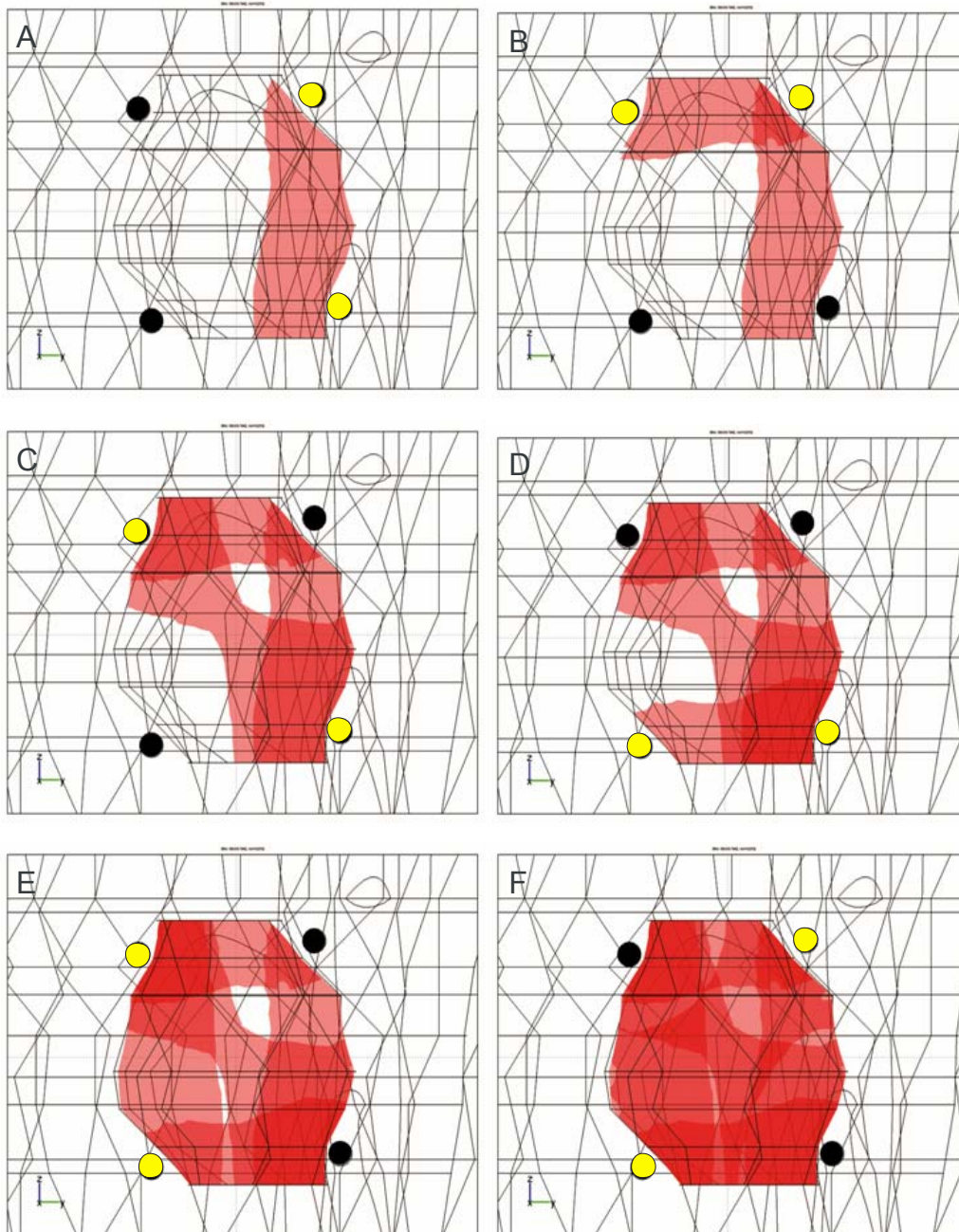
Slika 5. Pokritost tumorja z električnim poljem nad pragom reverzibilne elektroporacije za zaporedne serije električnih pulzov, pri čemer se menjajo aktivne elektrode (v rumeni barvi). Nekateri deli tumorja so pokriti z več serijami pulzov (temno rdeče), medtem ko so drugi pokriti samo enkrat (roza).

Analiza robustnosti načrta zdravljenja je pokazala, da na ustreznost načrta najbolj vplivajo prav vrednosti električnih prevodnosti posameznih tkiv in njihovih pragov elektroporacije ter natančnost pri postavljanju elektrod (Slika 6), zato bi bilo treba v prihodnje več pozornosti nameniti natančnim meritvam tkivnih lastnosti med elektroporacijo in načrtovanju sistema za natančnejše vstavljanje elektrod v tkiva.
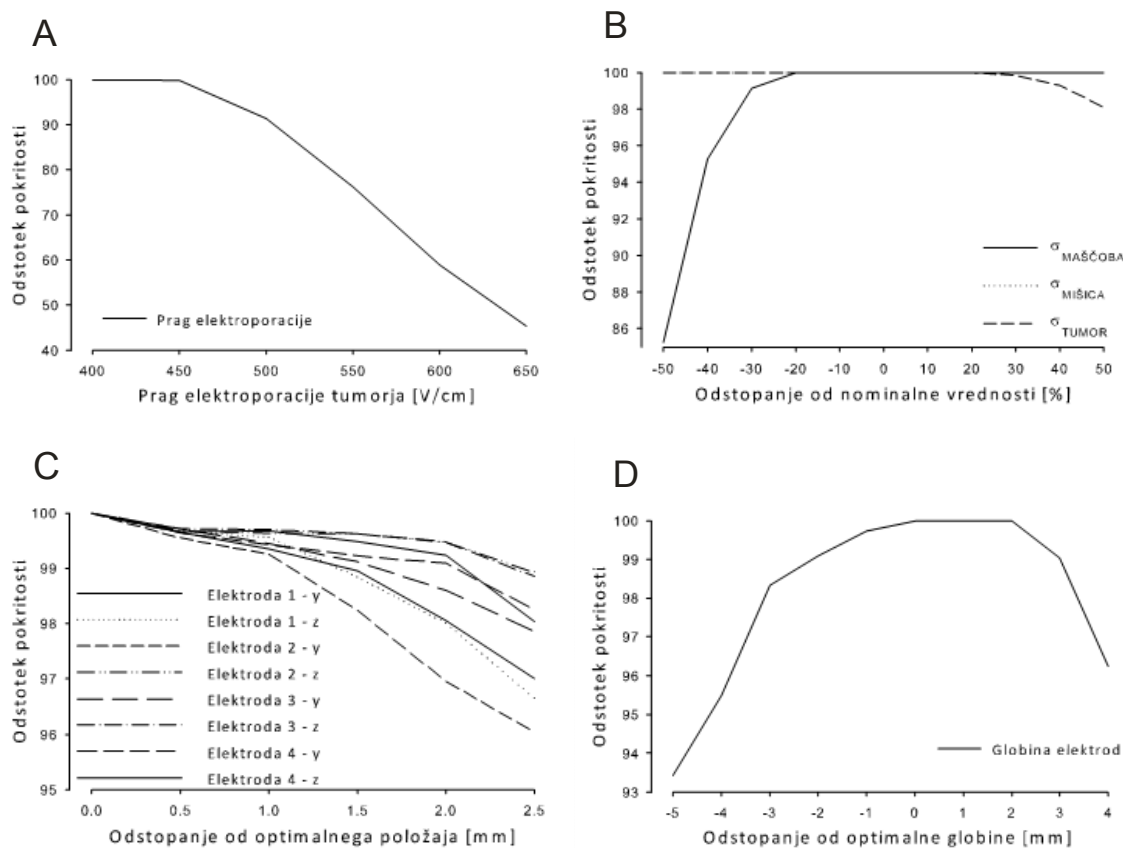
Slika 6. Analiza robustnosti načrtovanja elektrokemoterapije. A) Vpliv praga elektroporacije v korakih po 50 V/cm. B) Vpliv električne prevodnosti tkiva v korakih po 10 % vrednosti uporabljene pri načrtovanju zdravljenja – prevodnost mišičnega tkiva ni vplivala na rezultat, zato se njenega vpliva na sliki ne vidi (100 %). C) Vpliv napak v postavitvi elektrod v korakih po 0.5 mm od roba tumorja. D) Vpliv globine vstavljanja elektrod v korakih po 1 mm. Ordinatna os se od grafa do grafa razlikuje

V vseh primerih optimizacije položaja elektrod in napetosti med njimi smo med elektrokemoterapijo, ablacijo z ireverzibilno elektroporacijo in gensko elektrotransfekcijo ločevali zgolj z uporabo različnih objektnih funkcij, medtem ko smo uporabili enake numerične modele in optimizacijske algoritme. V zadnjem delu smo pokazali, da je tak pristop smotrn, saj smo na enakem modelu in geometriji dobili povsem različne rezultate, ko smo v objektni funkciji upoštevali pomembnosti porazdelitve električnega polja, ki pritičejo posamezni aplikaciji. Pri elektrokemoterapiji smo dosegli pokritost tumorja z električnim poljem nad reverzibilnim pragom elektroporacije, pri ablaciji nad ireverzibilnim pragom, medtem ko pri genski elektrotransfekciji nad reverzibilnim pragom in pod ireverzibilnim.

Zaključki

Rezultati našega dela kažejo, da sta numerično modeliranje in optimizacija položajev elektrod in napetosti med njimi zelo uporabna, celo ključna za doseganje primerne porazdelitve električnega polja v ciljnem tkivu. V elektrokemoterapiji in ablaciji tkiva z ireverzibilno elektroporacijo je treba doseči primerno porazdelitev električnega polja v (dobro) lokaliziranem tkivu, medtem ko je treba v bližnjih tkivih doseči čim nižje električno polje. Naši rezultati kažejo, da je v preprostejših primerih (kot je na primer zdravljenje podkožnih tumorjev) primerno porazdelitev polja mogoče doseči tudi brez optimizacije, s pravilno postavitvijo elektrod okrog ciljnega tkiva, medtem ko je v bolj kompleksnih primerih numerično načrtovanje porazdelitve električnega polja nujno. Pokazali smo tudi, da je mogoče v primeru genske elektrotransfekcije v mišico doseči izpostavitev večjega volumna tkiva električnemu polju nad reverzibilnim pragom, ne da bi bilo ob tem veliko tkiva izpostavljenega polju nad ireverzibilnim pragom.

Pokazali smo, da je v numeričnih modelih elektroporacije nujno upoštevati anizotropne tkivne lastnosti in da statični ter sekvenčni modeli elektroporacije vodijo k precej različnim izračunom porazdelitev električnega polja in toka v tkivu. Glede na naše rezultate je mogoče pri napovedovanju porazdelitve električnega polja v tkivu uporabiti tako statične (zgolj kot konservativno oceno) kot sekvenčne modele, medtem ko je za računanje tokov nujno uporabiti sekvenčne modele.

Z uporabo postopka za načrtovanje (elektroporacijskega dela) zdravljenja globoko ležečega tumorja, ki vključuje uvoz anatomskih podatkov iz medicinskih slik v programski paket za numerično računanje, natančno numerično modeliranje elektroporacije in optimizacijo parametrov elektroporacije, smo prikazali uporabnost numeričnega načrtovanja zdravljenja v medicinski uporabi elektroporacije in postavili osnovo za prihodnjo uporabo elektrokemoterapije za zdravljenje globoko ležečih tumorjev. Analiza robustnosti je pokazala, da je pomanjkanje podatkov o lastnostih bioloških snovi med elektroporacijo ena zadnjih pomanjkljivosti, preden se lahko robustno numerično načrtovanje zdravljenja začne redno uporabljati v klinični elektrokemoterapiji.

Abstract

Exposing biological cells to sufficiently strong external electric fields causes the electropermeabilization of cell membranes, followed by inflow/outflow of different molecules. The extent of electroporation, as the phenomenon is called according to the currently most widely accepted theory of electropermeabilization, can be controlled through parameters of applied electric pulses. Electroporation can thus be used to introduce various molecules into cells (using reversible electroporation) or to kill cells (irreversible electroporation). Electroporation can be achieved in all cell types, which is one of the reasons why it has become a widespread technique for inducing transport across the cellular membrane in biotechnology and also found its way into clinical practice.

Current medical applications of electroporation include electrochemotherapy of cancer, tissue ablation by irreversible electroporation of various tissues and gene electrotransfer for gene therapy and gene vaccination. Electrochemotherapy, a combination of electroporation and cytotoxic drugs, is already used routinely to treat cutaneous and subcutaneous tumor lesions. The first clinical trials of tissue ablation by irreversible electroporation and gene electrotransfer for gene therapy also show great promise. One of the few remaining challenges in these applications is routinely achieving an adequate electric field distribution in the targeted tissue.

In the last decade it has been shown that numerical modeling of electroporation can be used to predict the electric field distribution in biological tissue and thereby also the extent of tissue electroporation. There are currently two types of tissue-scale electroporation models: static models, which do not take the changes in tissue properties during electroporation into account, and sequential models, which do. Both types of models were used in previous studies to predict electroporation in homogeneous, isotropic tissues, however only the sequential models were able to explain electroporation of complex heterogeneous tissues such as skin and subcutaneous tumors. By comparing results of both models in electroporation of muscle tissue, we determined that on average the sequential models predict higher volumes of electroporated tissue than the static models (26 % higher) and higher total currents (145 % higher). This suggests that static models could be used to provide a conservative estimate of the volume of electroporated homogeneous tissues; however, sequential models would have to be used for the prediction of total electric current during electroporation.

To help achieve an adequate electric field distribution in tissue regardless of its complexity we designed a treatment planning procedure by means of medical image analysis, numerical modeling and optimization. Medical images were used to build 3D geometries of anatomical regions of interest, which were then imported into finite element software. Numerical modeling was used to evaluate the electric field distribution in the regions of interest. The modeling results provided an input for a genetic algorithm that was used to optimize the treatment parameters: electrode positions with respect to the target tissue and voltages between the electrodes.

By using numerical modeling and optimization of electroporation parameters for electrochemotherapy and ablation by irreversible electroporation of subcutaneous tumors we have shown that the coverage of the target tissue with a sufficiently strong electric field can be achieved with the least amount of healthy tissue damage by positioning the electrodes closely around the target tissue. The best electric field distributions for gene electrotransfer into muscle were achieved using large distances between electrodes, large depths of insertion and by positioning the electrodes in such a way that the electric field was perpendicular to the orientation of muscle fibers.

The optimization of electroporation parameters was performed by a genetic algorithm, designed specifically for this purpose. We tested the algorithm against different fitness functions, different numbers of parameters to optimize and different constraints. When tested on the same problem several times, the algorithm always returned an adequate solution in a reasonable amount of time, regardless of the complexity of the geometries used and the number of constraints or parameters that were optimized.

When we tried to use the genetic algorithm to optimize electroporation parameters for irreversible electroporation, accurate evaluation of the temperature distribution in the tissue for each set of electroporation parameters took too much time. Instead we proposed a simple evaluation of the temperature increase during the optimization, while a more accurate calculation was only performed after the optimal parameters were found.

In all optimization cases the same numerical models of electroporation (i.e. static or sequential) and the same optimization algorithm (genetic algorithm) were used; the main difference between the optimization was the choice of fitness functions. We showed that by choosing appropriate fitness functions, it is possible to obtain completely different solutions for electrochemotherapy, tissue ablation with irreversible electroporation and gene electrotransfection: for electrochemotherapy the target tissue was covered with an electric

field over the reversible electroporation threshold, for tissue ablation over the irreversible threshold and for gene electrotransfection between the reversible and irreversible threshold.

We used the designed treatment planning procedure for the world's first electrochemotherapy of a deep-seated tumor. Although complete response of the tumor was not achieved, the tumor did decrease in volume considerably before regrowing again. By reevaluating the treatment plan we showed that the reason for treatment failure was most likely in the inaccuracies in electrode positioning. Furthermore, the robustness analysis of the treatment plan showed that, apart from the electrode positioning, the lack of tissue-specific experimental data on tissue electrical conductivity and tissue electroporation thresholds remains one of the last hurdles for reliable numerical treatment planning in electroporation-based treatments.

Preface

The present PhD thesis is the result of numerical modeling and optimization algorithm development carried out during the PhD study period at the Laboratory of Biocybernetics, Faculty of Electrical Engineering, University of Ljubljana. Some of the results of the performed work have been published in international journals (or are submitted for publication) and will be referred to in the text by their corresponding roman numerals.

I: Corovic S, **Zupanic A,** Miklavcic D. Numerical modeling and optimization of electric field distribution in subcutaneous tumor treated with electrochemotherapy using needle electrodes. *IEEE Trans Plasma Sci* 36: 1665-1672, 2008.

II: Zupanic A, Corovic S, Miklavcic D. Optimization of electrode position and electric pulse amplitude in electrochemotherapy. *Radiol Oncol* 42: 93-101, 2008.

III: Zupanic A, Miklavcic D. Optimization and numerical modeling in irreversible electroporation treatment planning. In Rubinsky B (ed.), Irreversible electroporation, Springer Verlag, Berlin, 203-222, 2010.

IV: Miklavcic D, Snoj M, **Zupanic A,** Kos B, Cemazar M, Kropivnik M, Bracko M, Pecnik T, Gadzijev E, Sersa G. Towards treatment planning and treatment of deep-seated solid tumors by electrochemotherapy. *Biomed Eng Online* 9:10, 2010.

V: Kos B, **Zupanic A,** Kotnik T, Snoj M, Sersa G, Miklavcic D. Robustness of treatment planning for electrochemotherapy of deep-seated tumors. Submitted to *J Memb Biol.*

VI: Pavselj N, **Zupanic A,** Miklavcic D. Modeling electric field distribution in vivo. In Pakhomov AG, Miklavcic D, Markov MS (eds.) Advanced electroporation techniques in biology and medicine, CRC Press, New York, 2010. In print.

Table of contents

1. INTRODUCTION

Electricity has been used in medicine for centuries, even long before the effects of electric and magnetic fields on biological tissue were in anyway understood. As the knowledge of biological structures steadily increased, so has our understanding of the electric fields that our bodies generate and the effects external electric fields have on the body's internal structures [Rowbottom and Susskind, 1984]. In the last decades modern science and technology have made the use of electromagnetic devices in medicine ubiquitous. Measurements of internal electric fields are taken routinely in diagnostics and electric stimulation of excitable tissues is used to sustain life, rehabilitate injuries and improve the quality of life in general [Benedek et al., 2000].

Electric fields can affect not only excitable tissues, such as muscles and nerves, but also non-excitable tissues, either thermally, by generating heat inside the tissue or by inducing structural changes in cellular membranes. Numerous studies in the 1960s and 1970s have demonstrated that appropriate electric pulses can achieve electropermeabilization of biological cells that is followed by inflow/outflow of different molecules [Sale and Hamilton, 1967; Zimmermann et al., 1974]. This phenomenon was later termed electropermeabilization or electroporation, after a theory that explained the observed changes in membrane permeability in terms of formation of hydrophilic pores [Sugar and Neumann, 1984]. By controlling the electroporation parameters, it is possible to either transiently permeabilize cell membranes, which is called reversible electroporation [Neumann et al., 1982], or to kill cells, which is called irreversible electroporation [Rubinsky, 2007]. Reversible electroporation allows transient molecular transport through the pores; after a few minutes cellular membranes reseal and cell functions are restored [Rols and Teissie, 1990; Miklavcic and Puc, 2006c] (Figure 1).
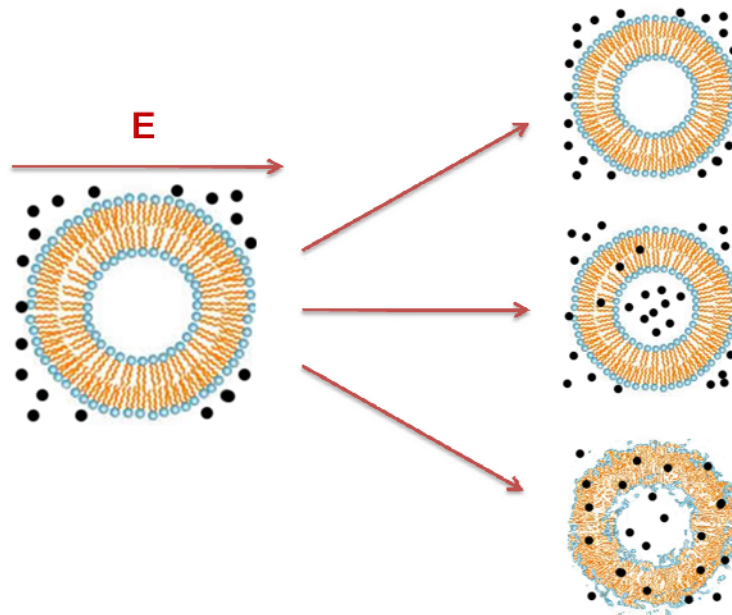
Figure 1. A cell exposed to an external electric field. If the amplitude of the electric field is low, there is no effect (top); increasing the amplitude of the electric field transiently permeabilizes the cell membranes; however the cell survives (reversible electroporation); further increasing the amplitude of the field kills the cells (irreversible electroporation).

Electroporation can be achieved in any cell type, which is one of the reasons why it has become a widespread technique for loading cells with substances that are otherwise difficult to load into cells [Tsong, 1991]. Reversible electroporation is widely used in biotechnology and medicine to introduce various molecules and agents into cells and tissues and for cell fusion [Zimmerman, 1982; Usaj et al., 2009]. The most advanced reversible electroporation-based medical treatments are cancer treatment by electrochemotherapy [Marty et al., 2006], gene electrotransfer (used for gene therapy and gene vaccination) [Heller et al., 2006] and transdermal drug delivery [Denet et al., 2004]. Irreversible electroporation has found its use in food sanitization [Heinz et al., 2002; Toepfl et al., 2006] and water treatment [Teissie et al., 2002] and is also being introduced into medicine for minimally invasive tissue ablation [Davalos et al., 2005].

After years of experiments on cells and small animals electroporation-based medical treatments are ready for use in the clinical environment; electrochemotherapy is already used routinely to treat cutaneous and subcutaneous tumor lesions [Marty et al., 2006], and first clinical trials for gene electrotransfer show great promise as well [Heller et al., 2006]. In all electroporation-based medical treatments routinely achieving an adequate electric field distribution in the targeted tissue and thereby controlling the electroporation remains one of

the few remaining challenges. The presented doctoral dissertation will focus on numerical modeling and optimization of the electric field distribution in targeted tissues by providing guidelines and tools for determining the appropriate electroporation parameters: the appropriate choice of electrodes and their positions in the body and the appropriate voltage.

1.1 Theory of electroporation

1.1.1 Induced transmembrane voltage

When a cell is exposed to an external electric field, a transmembrane voltage is induced on the cell membrane and superimposed on the resting membrane potential (from –20 to –70 mV, depending on cell type). When the total transmembrane voltage reaches a critical value (threshold ranging from 200 mV to 1 V, depending on cell type), electroporation of the membrane occurs and the flow of molecules in and out of the cell substantially increases [Neumann et al., 1982; Zimmermann, 1982; Neumann et al., 1989; Weaver et al., 1996; Miklavcic et al., 2000].

The induced transmembrane voltage ΔV for a spherical cell was first calculated by Schwan (Schwan, 1957):

$$\Delta V = 1.5 \, r \, E \, cos(\varphi) \tag{1.1}.$$

where r is the radius of the cell, E is the external electric field, and φ is the angle between the direction of the electric field and the selected point on the cell surface. The transmembrane voltage induced on a spherical cell is illustrated in Figure 2. A thorough analysis of Schwann's equations and their use as a model of electroporation can be found in [Kotnik et al., 1997]; the theory has been experimentally validated by the measurement of the transmembrane electric voltage with potentiometric molecular dyes [Pucihar et al., 2009]. For some geometrical shapes of cells, such as spheroids [Kotnik and Miklavcic, 2000] and cylinders, the transmembrane voltage can be derived analytically, while numerical and experimental methods have to be used for more complicated cell geometries [Pucihar et al., 2006].
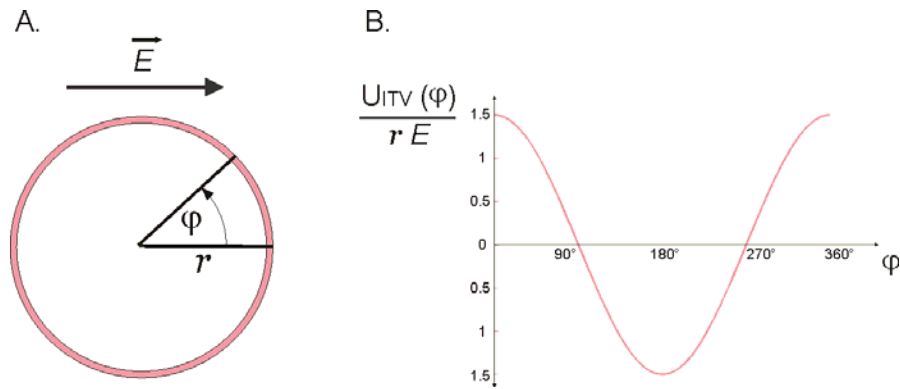
Figure 2. (A) A model of a spherical cell (r is cell radius and φ is the angle between the electric field E and the normal vector of the cell membrane) in an external electric field. (B) Dependence of the induced transmembrane potential (U_{ITV}) on the position on the cell membrane evaluated by Eq. 1.1.

1.1.2 Detection of electroporation

Although electroporation is currently the most widely accepted theory of electropermeabilization, the existence of pores has so far not been directly confirmed experimentally. Instead, electroporation was determined by measuring the cell membrane conductivity or the conductivity of a suspension of cells [Hibino et al., 1991; Kinosita and Tsong, 1979]. When the membrane is electroporated its conductivity increases in a few microseconds. After the initial surge in conductivity, the membrane starts to reseal and its conductivity begins to decrease, eventually returning to pre-electroporation values. A theoretical frame was developed that connects the changes of membrane conductivity during electroporation to changes of conductivity of cell suspensions [Pavlin and Miklavcic, 2003]. The increase in permeability of electroporated membranes is measured by the transport of different low-permeant molecules, such as fluorescent dyes (lucifer yellow, propidium iodide, calcein) or anti-cancer agents (bleomycin), or by measuring the release of intracellular molecules (Ca^{2+}, ATP) from the electroporated cells [Canatella et al., 2001; Macek-Lebar and Miklavcic, 2001].

1.1.3 Parameters for effective cell electroporation

The effectiveness of cell electroporation is determined by numerous factors, depending on both biological and physical parameters of the cells and the parameters of the electric pulses used. Cell shape, size, and orientation with respect to the applied electric field, as well

as cell density, all influence the transmembrane voltage induced by an external electric field. The effects of these cell parameters have been experimentally and numerically verified [Valic et al., 2003] (Figure 3a–d). It is therefore to be expected that different electric pulse parameters are needed for the electroporation of different cell lines [Cemazar et al., 1998]. However, the differences in cell size and shape cannot completely explain the measured differences; other factors, such as the resting membrane potential, the cytoskeleton structure of the cells, the membrane composition, and the extracellular environment, also play a role [Rols and Teissie, 1992; Sukhorukov et al., 2005, Kanthou et al., 2006].
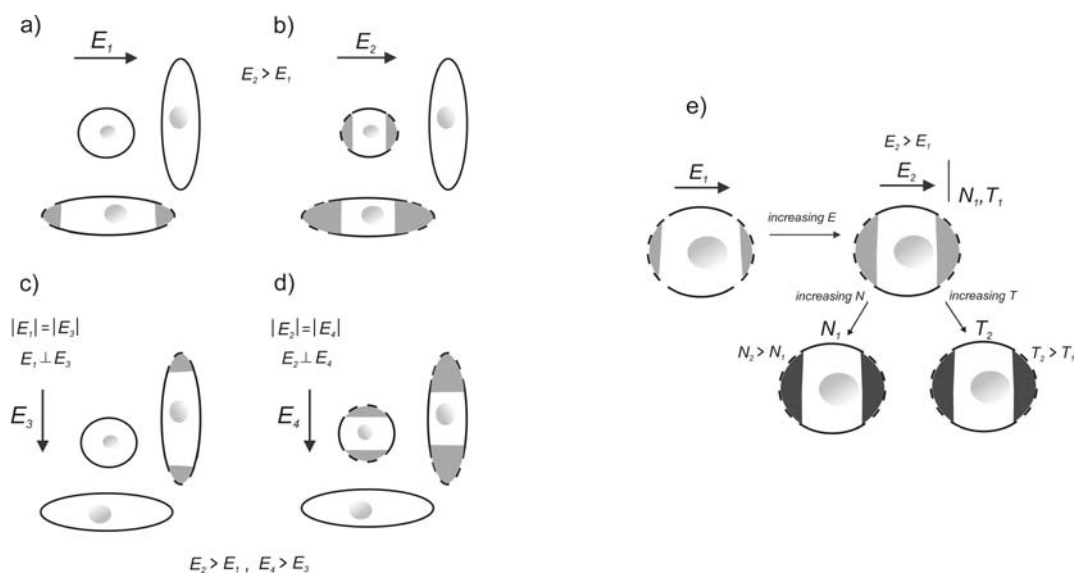
Figure 3. (a) Electric field parallel to elongated cell, (b) electric pulse amplitude is increased, (c) orientation of electric field is changed, (d) electric pulse amplitude is increased and (e) increasing the pulse amplitude increases the area of the membrane that is electroporated, while increasing the number of pulses or their duration does not affect the size of the electroporated area, but does however increase the extent of electroporation in the electroporated area. [Figure originally published in Kanduser and Miklavcic, 2008]

According to the theory of electroporation, pore formation is a stochastic process [Sugar and Neumann, 1984]. Using principles of statistical physics, models have been designed that predict the number, size and density of pores formed and maintained in the membrane of a single cell exposed to a single electrical pulse [Sung and Park, 1997; Saulis, 1997; DeBruin and Krassowska, 1999; Krassowska and Filev, 2007], as well as transport across the pores [Neumann et al., 1999]. Until recently [Kennedy et al., 2009], these models have been unable to predict experimentally suggested stable electropores and furthermore unable to match the inflow/outflow of molecules.

Parameters of the electric pulses used, such as the amplitude, duration, number of pulses and pulse repetition frequency, are also important for electroporation. While the amplitude of the pulses mostly affects the induced transmembrane voltage and thereby the area of permeabilized membrane, other electric pulse parameters affect electroporation in different ways (Figure 3e). Increasing the number of pulses and their duration increases the extent of membrane electroporation (presumably the number and size of pores formed) [Gabriel and Teissie, 1997; Krassowska and Filev, 2007]. An extensive analysis of the influence of the amplitude, number and duration of pulses on transport of small molecules into cells in vitro can be found in [Canatella et al., 2001; Macek-Lebar and Miklavcic, 2001; Macek-Lebar et al., 2002], while an analysis of cell survival can be found in [Gabriel and Teissie, 1995; Krassowska et al., 2003]. The effect of pulse repetition frequency on electroporation is more complex and is covered in [Pucihar et al., 2002; Miklavcic et al., 2005].

1.1.4 From cells to tissue

When a suspension of cells of low cell density is exposed to an external electric field, each cell feels the same electric field and the same (provided that cell are sufficiently similar) transmembrane voltage is induced across the cell membrane. In tissue and in dense cell suspensions the situation is much more complicated [Susil et al., 1998; Pavlin et al., 2002]. Cells are much closer together and their proximity affects the electric field that each cell is exposed to. Furthermore, in contrast to a cell suspension, tissues are usually not homogeneous; instead they are inherently heterogeneous, consisting of different cells (of different shapes, sizes, orientations) that are distributed in different densities [Miklavcic et al., 2006b]. The cells are also connected to each other through gap junctions and the extracellular matrix that can affect electroporation as well [Pucihar et al., 2007]. A further complication is that these tissue characteristics also affect tissue properties. Namely, the local electric field induced by an electric pulse depends on local electrical conductivity, which in turn depends on cell density, cell size, orientation, biological properties of cell, and other tissue properties, such as vascularization, hydration, ion content, and the extracellular matrix. Thus, tissue heterogeneity makes predicting the transmembrane voltage induced on tissue cells extremely difficult; it is consequently also extremely difficult to predict the thresholds at which electroporation would occur in a given tissue. Finally, electroporation increases the

conductivity of cells and tissues [Sel et al., 2005; Cukjati et al., 2007] and consequently changes the electric field distribution.

It is somewhat surprising that, regardless of the many difficulties mentioned so far numerical modeling has been rather successful in predicting electroporation outcomes in tissues. While the models that use the transport lattice method and incorporate electroporation on a single cell level, thereby calculating the number of pores in cells (assumed to be points) in the whole tissue, are more accurate, high computational costs make them inadequate for 3D modeling of electroporation [Gowrishankar and Weaver, 2006; Esser et al., 2007]. Instead, models based on the finite element method that model bulk tissue and consider electroporation to be a threshold phenomenon (tissues exposed to electric fields above a threshold are electroporated, while there is no electroporation if the tissues are exposed to electric fields below the threshold) are most often used. The electroporation thresholds for each tissue depend on the number and duration of the pulses used. In order for the models to predict the volume of electroporated tissue, thresholds need to be known beforehand.

Simple finite element models that did not take into account the changes of tissue properties (static models) were used to calculate the electric field distribution for electrochemotherapy of a realistic mouse tumor model [Semrov et al., 1998, Miklavcic et al., 1998] and in muscle tissue [Gehl et al., 1999]. Static models were also successfully used to predict the extent of electroporation in liver tissue and to determine liver-specific electroporation thresholds (E_{rev} - 360 V/cm, E_{irr} − 640 V/cm) [Miklavcic et al., 2000] by comparing the experimentally determined volume of molecular transport (reversible electroporation) and the volume of tissue damage (irreversible electroporation) and calculated surfaces of equal electric fields. Static models, however, were not able to predict tissue electroporation of a cutaneous tumor with plate electrodes, until the changes in tissue conductivity were taken into account [Sel et al., 2005; Pavselj et al., 2005] (Figure 4). These new "sequential models" (explained in detail in "Materials and methods") were also able to explain (and predict) why the electric current delivered during an electric pulse increases with the duration of the pulse if electroporation is achieved [Cukjati et al., 2007]. The changes in tissue conductivity during electroporation are also important for the detection and measurement of the extent of electroporation, either by measuring the electrical conductivity [Cukjati et al., 2007; Ivorra et al., 2009] or by electrical impedance tomography [Davalos et al., 2002; Davalos et al., 2004].
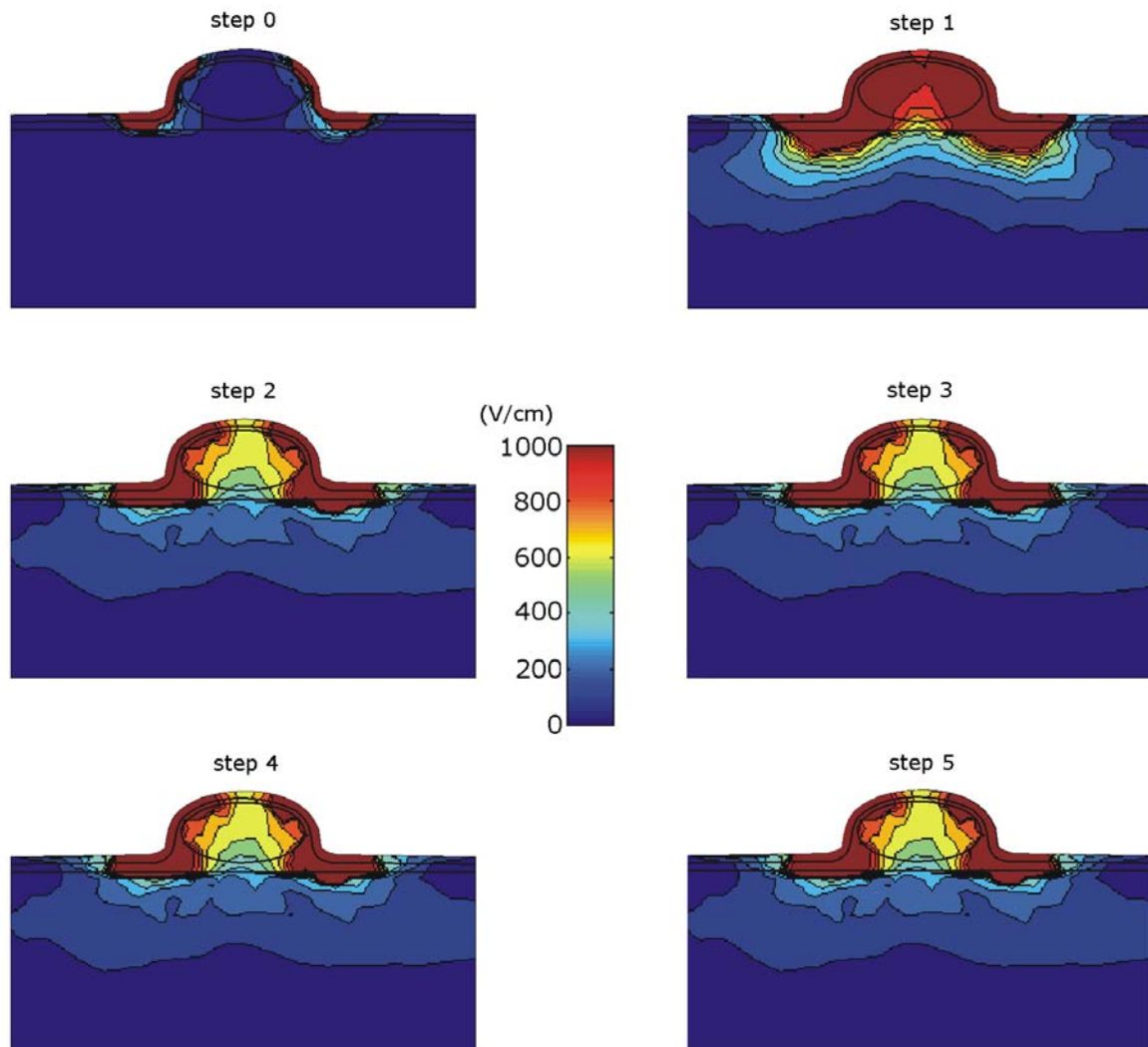
Figure 4. When a cutaneous tumor is exposed to an external electric field, most of the electric field is concentrated in the skin (step 0). However, when the skin is electroporated its conductivity increases and the electric field penetrates deeper into the tissue, where it electroporates other tissues (steps 1–5). [Figure was originally published in Pavselj et al., 2005]

The ability of sequential models to predict electroporation and the increased processing power of computers in the last years gave rise to the idea of numerically based treatment planning in electroporation-based treatments. As electroporation-based treatments depend on electric field distribution – a physical modality – a similar procedure as in radiotherapy treatment planning [Brahme, 1999] could be used. A feasibility study of numerical treatment planning for the electrochemotherapy of a brain tumor gave encouraging results [Sel et al., 2007]. The study used the sequential electroporation model and the sequential quadratic programming optimization method to determine the optimal distance between two electrodes and pulse amplitude – the obtained values achieved good coverage of

8

the tumor. A more complete treatment planning procedure, however, should also choose the appropriate electrodes (if more types are available), optimize the depth of electrode insertion and distance between electrodes (or groups of electrodes in an electrode array) with respect to the patient's anatomy, contact surface of the electrodes and the electric pulse parameters; indeed all the parameters that effect the electric field distribution in the tissue, and thereby electroporation [Miklavcic et al., 2006a]. Since in such a treatment planning procedure, numerical modeling would be used to evaluate the electric field distribution, its accuracy would be of the utmost importance. Accurate numerical modeling of electroporation requires accurate data on tissue properties; however, accurate tissue conductivity data are not readily available, most of all in the frequency region of interest to electroporation (DC and AC low frequencies). A recent systematic review of literature has shown that the values obtained by different groups can differ by more than 50 %, which was mostly attributed to differences in the measurement methods [Gabriel et al., 2009]. The situation is also critical regarding the data on electroporation-based increase in conductivity and electric field thresholds, where only a few studies exist [Miklavcic et al., 2000; Cukjati et al., 2007].

1.2 Electrochemotherapy

Electrochemotherapy is an antitumor treatment that uses locally applied high-voltage electric pulses in combination with chemotherapeutic drugs [Mir et al., 1991, Mir and Orlowski, 1999b; Sersa and Miklavcic, 2008a]. The electric pulses transiently permeabilize tumor cell membranes and thereby increase the uptake of chemotherapeutic drugs into the cells, causing cell death. Two chemotherapeutic drugs are currently used in the clinical environment: bleomycin and cisplatin. The effect of both was shown to be potentiated by electroporation both *in vitro* and *in vivo* by several folds [Orlowski et al., 1988; Poddevin et al., 1991; Mir et al., 1991; Sersa et al., 1995; Heller et al., 1995].

For electrochemotherapy to be efficient two conditions have to be met. The chemotherapeutic drug has to be present around tumor cells at the time when electric pulses are delivered, and secondly, all the cancer cells have to be reversibly electroporated. The former can be achieved with adequate intravenous or intratumoral injection of the chemotherapeutic drugs and the latter by choosing appropriate electrodes, positioning them appropriately and delivering electric pulses of appropriate parameters (such that the electric field is $E > E_{rev}$ in the entire tumor volume).

Since the first in vivo experiments in small animals [Okino and Mohri, 1987], electrochemotherapy has been used to treat various types of tumor lesions in animal models. Studies on orthotopic tumors of the brain [Salford et al., 1993], liver [Jaroszeski et al., 1997] and pancreas have shown promising results [Jaroszeski et al., 1999a]. The first human clinical trials were performed in 1991 [Mir et al., 1991]. This study was followed by several other clinical trials in patients that demonstrated high efficiency in antitumor treatment of tumors with different histologies [Rudolf et al., 1995, Heller et al., 1998; Heller et al., 1999, Rols et al., 2000, Rodrigez-Cuevas et al., 2001, Gothelf et al., 2003, Sersa et al., 2003, Rebersek et al., 2004, Snoj et al., 2005]. In 2006, standard electrochemotherapeutic operating procedures were defined for the treatment of cutaneous and subcutaneous tumor nodules of different histologies as a conclusion of a joint study of four European centers united in the ESOPE project [Mir et al., 2006; Marty et al., 2006]. For the electroporation part, square wave electric pulses with an amplitude over distance ratio of 1000–1300 V/cm, duration of 100 μs, and frequency of 1 Hz or 5 kHz have been defined as the standard. Objective response rate in the ESOPE study was 85 % regardless of tumor histology or drug used. Plate electrodes have been found to be suitable for treatment of protruding cutaneous tumors, while needle electrodes should be used in treatment of subcutaneous tumors. Clinical electrochemotherapy is currently used as a palliative treatment of cutaneous and subcutaneous tumor nodules of different malignances [Campana et al., 2008, Curatolo et al., 2008, Fantini et al., 2008, Quaglino et al., 2008, Snoj et al., 2009].

In order to improve the protocols of electrochemotherapy and extend its clinical scope to other, deep-seated types of tumors, equipment has to be improved and a treatment planning protocol has to be defined. The ESOPE protocols that have produced good results for cutaneous and subcutaneous lesions are not suitable for the treatment of larger lesions located deeper in the body. Since only special electrodes (needle or endoscopic electrodes [Soden et al., 2006]) can be used to treat deep-seated lesions, non-homogeneous electric field distributions are to be expected, which is why providing a voltage to distance ratio is no longer suitable for achieving an appropriate electric field distribution in the tumor. Therefore anatomy-based numerical treatment planning and accurate electrode positioning are crucial.

1.3 Tissue ablation by irreversible electroporation

In contrast to electrochemotherapy, irreversible electroporation does not require chemical agents to kill cells (Rubinsky et al., 2007). However, in order to achieve the death of all targeted cells, the electric field in the target tissue has to be above the irreversible threshold in the entire target volume ($E > E_{irr}$) and more pulses have to be applied (10 or more) compared to electrochemotherapy.

Irreversible electroporation did not receive much attention until it was discovered it can be used to kill cells without considerable thermal effects (Davalos et al. 2005; Al-Sakere et al., 2007; Edd et al., 2006; Miller et al., 2005). This discovery made irreversible electroporation a prime candidate for tissue ablation. Further studies have shown that tissue ablation by irreversible electroporation also has other advantages over other ablation methods: 1) irreversible electroporation is a non-thermal physical ablation modality, and therefore unaffected by blood flow (Miller et al., 2005); 2) delineation between treated (ablated) and untreated tissue after IRE is very sharp (Lee et al., 2007); 3) irreversible electroporation affects only cell membranes and leaves extracellular structures intact – preservation of microvasculature is possible (Lee et al., 2007; Maor et al., 2007; Onik et al., 2007); 4) irreversible electroporation elicits no immune response and can thus be used for the treatment of patients with immune system deficiency (Al-Sakere et al., 2007); 5) the procedure is relatively fast compared to other ablation techniques (Lee et al., 2007); 6) irreversible electroporation allows rapid regeneration of ablated tissue with healthy tissue (Rubinsky et al., 2007); 7) irreversible electroporation can be accurately numerically modeled – numerical models of reversible electroporation that have been developed for electrochemotherapy can be easily modified and implemented in irreversible electroporation modeling (Corovic et al., 2007; Edd and Davalos, 2007; Pavselj and Miklavcic, 2008a).

Irreversible electroporation was tested as an ablation modality in various medical applications, such as in ablation of cancer (Onik et al., 2007; Rubinsky et al., 2008), epicardial ablation (Lavee et al., 2007), prevention of restenosis after angioplasty (Maor et al., 2008), intracranial ablation (Loganathal et al., 2009) and kidney ablation (Leveillee et al., 2009). After encouraging primary results of these studies, researchers expressed the need for accurate planning that would: 1) guarantee that thermal effects would indeed be negligible; 2) take advantage of the sharp physical delineation between treated and untreated tissue to enable surgically precise ablation and 3) make procedures more reproducible. As in

electrochemotherapy, anatomy-based numerical treatment planning should be used to advance the use of irreversible electroporation in the clinical environment.

1.4 Gene electrotransfer

Research has shown that the uptake of plasmid DNA (and other macromolecules) differs from the uptake of smaller molecules such as chemotherapeutic drugs, as they are much larger than the predicted size of electropores. It seems that successful gene electrotransfer requires the electric pulses to not only reversibly electroporate the target cells but also to help move the negatively charged DNA molecules to the negatively charged cell membrane [Bureau et al., 2000; Satkauskas et al., 2002]. Structural changes in the cell membrane enable the DNA molecule to form a complex with the membrane that can later lead to uptake into the cell [Golzio et al., 2002; Teissie et al., 2005], and the electrostatic force moves the DNA molecule to the cell membrane by electrophoresis [Wolf et al., 1994; Viovy et al., 2000, Satkauskas et al., 2005]. This double role of electric pulses makes the choice of appropriate electric parameters much more difficult. Relatively high levels of transfection can be achieved using longer low-voltage pulses [Bettan et al., 2000], as well as using a combination of short high-voltage pulses and long low-voltage pulses [Bureau et al., 2000; Satkauskas et al., 2002].

For successful gene electrotransfer, plasmid DNA has to be present around the target cells before the electric pulses are applied [Mir et al., 1999]. This is sometimes difficult to achieve, because their large molecular size prevents them from being efficiently distributed throughout the targeted tissue [Zaharoff et al., 2002]. Instead, good DNA distribution has to be guaranteed by accurate local injection. It is also not necessary for the DNA to be transferred into all target cells (although a higher number of transfected cells is correlated to higher expression of the desired proteins), but only that enough DNA is transfected into enough cells (depending on the need of expression). The electric pulse parameters have to be chosen so that reversible electroporation is achieved (just above E_{rev}) in the target tissue, while limiting the amount of irreversible electroporation as much as possible, since damaged cells do not express the inserted DNA [Durieux et al., 2004].

Two medical applications of gene electrotransfer are currently under consideration: gene therapy [Heller et al., 2006], wherein the effects of defective genes responsible for disease development are corrected, and gene vaccination [Otten et al., 2004] that induces an immune response to an antigen protein expressed *in vivo*, which can be used against infectious

agents. Since electroporation-based gene therapy and vaccination are cost-effective and easily implementable they could be particularly useful for treatment of chronic diseases.

First studies showing an efficient *in vitro* gene transfection by electroporation pulses were published in 1982 [Neumann et al., 1982]. Since then a large body of evidence has shown that gene electrotransfer is efficient both *in vitro* and *in vivo*, and in a wide variety of tissues [Suzuki et al., 1998; Mir et al., 1998; Aihara and Myazaki, 1998; Rols et al., 1998; Gehl and Mir, 1999; Jaroszeski et al., 1999; Payen et al., 2001; Zhang et al., 2002; Gehl, 2003; Mir et al., 2005; Zampaglione et al., 2005; Prud'homme et al., 2006; Andre et al., 2008]. Gene electrotransfer has also been carried out in humans, and the first clinical trials for electroporation based gene therapy have already provided some promising results [Prud'homme et al., 2006; Heller et al., 2006; Daud et al., 2008].

In order to assure optimal conditions for electroporation-based gene therapy and vaccination (i.e. reversible and safe electroporation just above the reversible threshold value E_{rev}) the electrical parameters of electroporation need to be carefully selected [Miklavcic et al., 2000]. Anatomy-based numerical modeling can help us design better protocols and thereby control the extent of tissue where gene electrotransfer is achieved.

1.5 Aims

The goal of the present doctoral dissertation was to use numerical modeling and optimization techniques to provide guidelines and tools to determine the appropriate parameters for optimal electroporation for three electroporation-based treatments: electrochemotherapy, tissue ablation with irreversible electroporation, and gene electrotransfer for gene therapy and gene vaccination. Since electrochemotherapy is the most advanced of these therapies the majority of the work has focused on electric field distribution planning for electrochemotherapy. The treatment planning system has to provide for the acquisition of data from medical images and their conversion into 3D geometries, calculation of electric field distribution in these geometries and finally optimization of the electrical parameters of electroporation to best suit each of the electroporation-based treatments. In electrochemotherapy, the treatment planning procedure should provide the responsible physician with electrode positions and pulse amplitude that will result in reversible electroporation of the entire tumor volume while minimizing damage to the nearby critical tissue. In tissue ablation by irreversible electroporation, irreversible electroporation of the target tissue is desired, while the amount of heat generated by the pulses has to be controlled,

whereas in gene electrotransfer, as in electrochemotherapy, reversible electroporation is desired with the least amount of cell damage that would decrease the number of cells expressing the transfected genes and producing the desired proteins. Appropriate treatment planning can significantly increase treatment effectiveness for all three electroporation-based treatments.

2.   MATERIALS AND METHODS

The methods explained in the following sections can be divided into three categories, each crucial for the planning of electric field distribution for electroporation-based treatments: building a tissue geometry from medical images, numerical modeling of electroporation and optimization of electrode positions and voltages between the electrodes. The methods are explained in greater detail in the published scientific articles and articles submitted for publication that have been added in the Appendix. The results obtained in the study of prevention of thermal damage in irreversible electroporation (see 3.3 Prevention of thermal damage – IRE) and electric field distribution for gene electrotransfer into muscle (see 3.5 Electric field distribution in skeletal muscle – EGT) have not yet been published, therefore the methods are explained here in detail (see 2.2.3 Joule heating and 2.4 Gene electrotransfer into muscle tissue).

2.1 Building a 3D geometry from medical images
(articles II–VI)

Geometries used in the numerical modeling and treatment planning of electrochemotherapy and tissue ablation by irreversible electroporation were constructed from medical images (CT or MRI scans of patient anatomies) that were provided by the Institute of Oncology, Ljubljana. The obtained images have been segmented by oncology experts, i.e. all tissues of interest were clearly demarcated by different color coding. Two different methods were used to convert the segmented images to 3D geometries that could be imported into Comsol Multiphysics (Comsol AB, Sweden) – the planar contour method [Liang et al., 2006] and voxel import [Astrom et al., 2009]. The planar contour method was used in all cases where only numerical modeling was carried out, without the optimization of electrode positions, and in some simpler cases where optimization was performed. Voxel import was used when the numerical model was used in conjunction with the optimization for treatment planning for electrochemotherapy of a deep-seated tumor (see 3.6 Treatment planning for electrochemotherapy of a deep-seated tumor – ECT). Modeling of electrode geometries was carried out with a CAD tool available in Comsol Multiphysics.

2.1.1 Planar contour method

The conversion of segmented medical images to a 3D geometry was accomplished with an algorithm written in Matlab (Mathworks, USA) [Valic, 2006] (Figure 5). The algorithm works by first converting the medical images from the DICOM format into jpeg, and then into a binary matrix that contains only one tissue. The boundary of the tissue in each image is approximated by a spline using a certain number of points. A 3D geometry is built by first connecting each point on each image with the corresponding point on the neighboring images – the number of vertical lines created between two images is the same as the number of points used for the spline. Multiplying this number of vertical lines by the number of images used gives the total number of edges that define the object geometry. Finally, the segmented tissue representations are connected to each other using the vertical lines as guidelines.

The advantage of the planar contour method is that the imported geometries are geometrical objects in Comsol Multiphysics, which allows for greater accuracy in meshing and post-processing (integration over subdomain and boundaries). The disadvantage, however, is that in cases where objects are positioned close together (e.g. electrodes close to the tumor) Comsol Multiphysics is often unable to mesh the model. This can lead to difficulties when electrode position optimization is performed, since only electrode positions inside the target tissue or some distance away can be used and some potentially good solutions are discarded. Therefore, when treatment planning for electrochemotherapy was carried out, the voxel import method was used to construct the geometry used for optimization and the planar contour method was used to construct the (more accurate) geometry used in the treatment plan verification.
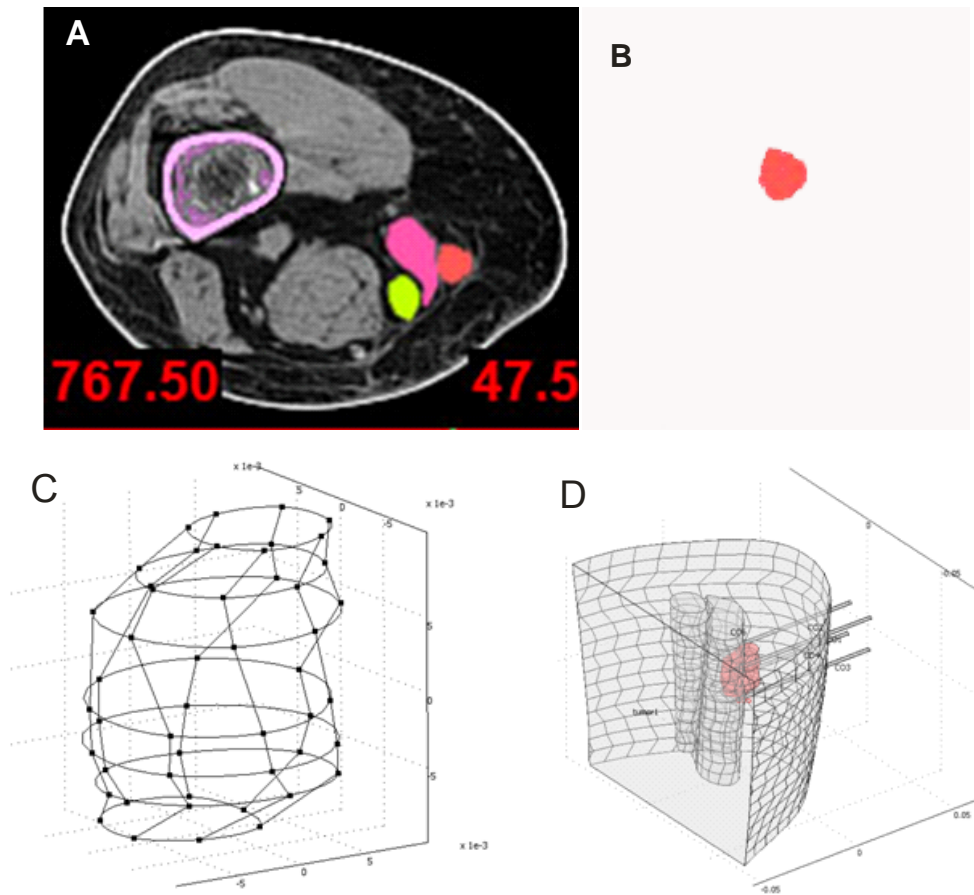
Figure 5. The process of building a 3D tumor geometry (see 3.6 Treatment planning for electrochemotherapy of a deep-seated tumor – ECT) with the planar contour method. A) Segmented medical images (the tumor is red) are taken and converted into B) binary matrices. C) Points on the boundaries of the tumor on each image are connected to the boundary points on each neighboring image to build the outer shape of the geometrical object. D) The tumor is imported into Comsol Multiphysics as a solid 3D object along with all other tissues of interest.

2.1.2 Voxel import

(article IV)

In the voxel import method, the DICOM images are first converted into matrices in Matlab, with each tissue having its own representative number (e.g. all muscle pixels are coded with 10, all tumor pixels with 20, etc.), and then imported directly into Comsol Multiphysics. This way all the tissues are present in a single geometrical object; however, the object can have distinct tissue properties that are defined by the numerical coding of the matrices. The electrodes are constructed separately in Comsol Multiphysics, each being its own geometrical object. The advantage of using the voxel import method is that the electrodes

17

can be positioned anywhere inside the model and there are no meshing issues, which makes optimization of electrode positions much simpler than with the planar contour method.

2.1.3 Electrode geometry
(articles I–VI)

Only needle-shaped electrodes were used in our models. The electrodes were geometrically modeled as cylinders of sizes similar to those used in various studies of electrochemotherapy, gene electrotransfer and irreversible electroporation in the last years [Gilbert et al., 1997; Puc et al., 2004; Mir et al., 2006]. In studies of electrochemotherapy and tissue ablation with irreversible electroporation (articles I–III and VI, see Results 3.1–3.4) electrodes with a diameter of 0.7 mm were used, while electrodes with a diameter of 1.8 mm were used in the treatment planning for the electrochemotherapy of a deep-seated tumor (articles IV and V, see Results 3.6). The different electrode arrays used are depicted in Figure 11 (see Results 3.1): 1) one electrode pair, 2) rows of needle electrodes (three and four electrode pairs) and 3) a hexagonal array of needle electrodes.

2.2 Numerical modeling
(articles I–VI)

Prediction of the electric field distribution inside biological tissues (with anisotropic and heterogeneous properties) of irregular shapes is only possible through numerical modeling. In the studies leading to this doctoral dissertation, the finite element method was used for numerical modeling because 1) current tissue electroporation models used the method and 2) several commercial numerical packages that utilize the method were available.

2.2.1 Finite element method

The finite element method (FEM) [Strang and Fix, 1973; Miller and Henriquez, 1990; Silvester and Ferrari, 1992] is a widespread numerical technique for finding approximate solutions to partial differential equations in complex geometries. The method essentially consists of assuming a piecewise continuous function for the solution of the given equations (and boundary conditions) and obtaining the parameters of the function in a manner that reduces the error in the solution. This is achieved by dividing the calculation domain (volume)

into discrete smaller elements (e.g. tetrahedral elements) that together form the mesh of the calculation domain. The approximate solution is only calculated on element nodes, while being defined on the elements by the chosen element shape functions (normally the functions are linear or quadratic although other forms are also possible). Reducing the size of the elements reduces the solution error; however, it increases the calculation time. If the approximate solution accuracy is only important in a certain part of the domain, it is possible to create a finer mesh in that part, while keeping the elements larger in other parts (Figure 6).
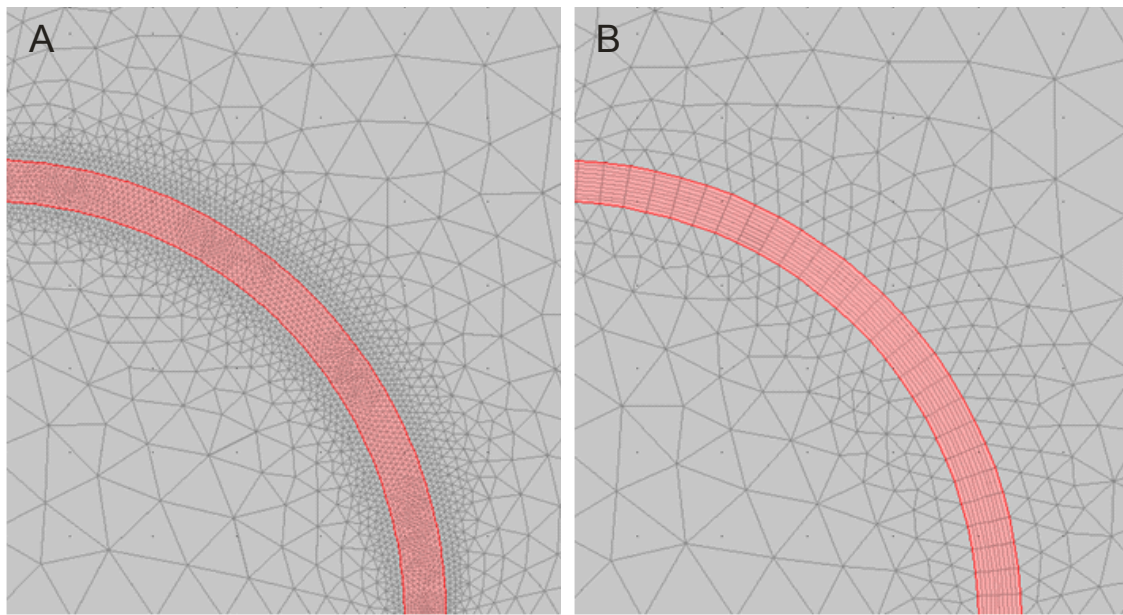
Figure 6. It is possible to define a very fine mesh in the region of interest and thus to increase the solution accuracy. A very fine mesh in the area of interest of (A) triangular elements (a total of 560 elements are used for the mesh) and of (B) rectangular elements (a total of 255 elements are used for the mesh).

All numerical models were built in commercially available software for the calculation of partial differential equations with the finite element method – Comsol Multiphysics (Comsol AB, Sweden). Comsol Multiphysics also features built-in multiphysics couplings, e.g. there are predefined couplings of equations for the calculation of Joule heating in materials as a consequence of energy generated by electromagnetic fields (the user can also define their own couplings). The Joule heating couple equations were used to calculate the temperature of biological tissue when electroporation pulses are applied in irreversible electroporation. The process of building and calculating a mathematical model in Comsol Multiphysics is illustrated in Figure 7.
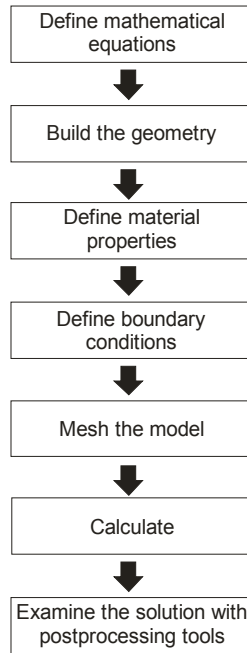
Figure 7. The process of building and calculating a mathematical model in Comsol Multiphysics. The order in which the first four stages are performed is not relevant.

2.2.2 Electric field distribution

(articles I–VI)

In all used models the electric field distribution was determined by solving the Laplace equation for static electric currents:

$$-\nabla \cdot (\sigma \cdot \nabla V) = 0 \,, \tag{2.1}$$

where σ is tissue conductivity and V is electric potential. The boundary conditions used in our calculations were as follows: 1) constant potential ($V = const.$) on the surface of the active parts of the electrodes, 2) continuity ($\boldsymbol{n} \cdot (\boldsymbol{J_1} - \boldsymbol{J_2}) = 0$) on all other interior boundaries and 3) insulation ($\boldsymbol{n} \cdot \boldsymbol{J} = 0$) on the inactive parts of the electrodes and outer boundaries of the model. Tissue properties used in the models are listed in Table 1. We sometimes used different values of tissue conductivity and electroporation thresholds for the same tissue, which was mostly due to using the most recent data available at the time (see Appendix for details) [Smith et al., 1986; Gabriel et al., 1996; Gabriel et al., 2009; Haemmerich et al., 2009]. Hereafter, all models that only utilized constant values for tissue conductivity during electroporation will be called "static models".

Table 1. Electrical tissue properties used in the numerical models [Smith et al., 1986; Gabriel et al., 1996; Miklavcic et al., 2000; Cukjati et al., 2007; Gabriel et al., 2009; Corovic et al., 2010]

Tissue	σ_1 [S/m]	σ_2 [S/m]	E_{rev} [V/cm]	E_{irr} [V/cm]
Tumor	0.4 [I–III]			900 [I–II,IV,VI,]
	0.2 [IV,VI]	0.7 [IV,VI]	400 [I–II,IV,VI]	800 [III]
Healthy tissue	0.2 [I–III]		400 [I–II]	900 [I–II]
	0.15 [VI]	0.5 [VI]	250 [VI]	600 [VI]
Muscle	0.135* [IV]	0.47* [IV]	80* [IV]	450
	0.75** [IV]	2.62** [IV]	200** [IV]	900 [IV]
Fat	0.018 [IV]	0.065 [IV]	100 [IV]	900 [IV]

* in the direction parallel to muscle fibers
** in the direction perpendicular to muscle fibers
σ_1 conductivity of non-electroporated tissue
σ_2 conductivity of electroporated tissue
I–VI articles in which the particular tissue property value was used

In all models in which the change of tissue properties was taken into account (sequential models), electric conductivity was modeled as an electric field-dependent function $\sigma(E)$ [Sel et al., 2005; Pavselj et al., 2005]:

$$\sigma(E) = \frac{\sigma_2 - \sigma_1}{E_{irr} - E_{rev}} \cdot E + \sigma_1 \,, \tag{2.2}$$

where σ_1 and σ_2 are electrical conductivities of non-electroporated and electroporated tissues respectively, and E_{irr} and E_{rev} are the thresholds of irreversible and reversible electroporation respectively. Eq. 2.2 is valid for the duration of the electric pulse. Namely, in Eq. 2.2 electric conductivity can only increase as a result of the tissue being exposed to the electric field above the electroporation threshold, and can never decrease. After the pulse, the cells begin to reseal and the electric conductivity decreases, however this is not modeled by Eq. 2.2. Since the use of a function that can only increase is not possible in Comsol in the continuous form, a four-step approximation of the function was used instead (Figure 8). To determine the steady state electric field distribution a subroutine was used that modeled the dynamics of electroporation as a discrete process with a sequence of static model calculations (steps). In the first step, the static electric field distribution was calculated, and in the second step, the tissue conductivity was determined based on electric field distribution from the previous step:

$$\sigma(k) = f(E(k-1)) \,, \tag{2.3}$$

where k stands for the step number. In the third step the new electric field distribution resulting from the changed conductivities was calculated, in the fourth step tissue conductivity changed according to the new electric field distribution, and so on. In the presented studies

(see article IV, Results 3.5 and 3.6) seven steps were used before the calculations were stopped, as this has been determined to be sufficient in previous studies [Pavselj et al., 2005].
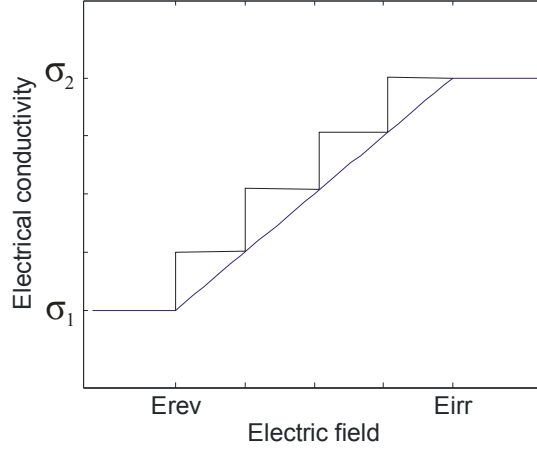
Figure 8. Tissue electrical conductivity during electroporation is described by an electric field dependent function.

2.2.3 Joule heating

As one of the main advantages of tissue ablation by irreversible electroporation compared to other ablation techniques is its non-thermal nature, it is important that the electric pulses do not cause thermal damage. The most commonly used equation for heat modeling in tissues is the Pennes bioheat equation [Pennes, 1948]:

$$\rho c \frac{\partial T}{\partial t} = \nabla \cdot (k \nabla T) - \rho_b c_b w_b (T - T_b) + Q_m + Q \, , \qquad (2.4)$$

where T is temperature, ρ is tissue density, c is tissue heat capacity, ρ_b, c_b, w_b and T_b are blood density, heat capacity, perfusion rate and temperature, respectively, k is tissue heat conductivity, Q_m is the spatial heat rate generated in tissue by the metabolism and Q is the spatial heat rate generated in tissue by external sources. Since exact calculation of the temperature increase for each set of treatment parameters investigated in the treatment planning process could take too long, a simpler change in temperature evaluation is also used:

$$\Delta T = (\sigma E^2 \, Nt)/\rho c \, , \qquad (2.5)$$

where σ is tissue electrical conductivity, E is electric field, N is number of pulses and t is duration of pulses. Compared to the bioheat equation, Eq. 2.5 does not take into account heat dissipation between the pulses, heat dissipation by blood perfusion or heat generated by metabolic processes; thus the calculated temperature increase is much higher. Only if the

maximum conservative temperature evaluation by Eq. 2.5 at the distance of 1 mm from the electrodes was above 50 °C [Davalos and Rubinsky, 2008], was a modified version of the bioheat equation evaluated:

$$\rho c \frac{\partial T}{\partial t} = \nabla \cdot (k \nabla T) + Q \; . \tag{2.6}$$

In comparison to Eq. 2.4 metabolic heat generation and perfusion were omitted, since their contribution in the short span of a single pulse is negligible [Davalos and Rubinsky, 2008]. Furthermore, it has been shown that electroporative pulses induce a vascular lock in the affected tissue [Edd et al., 2006; Sersa et al., 2008]. Thermal damage was evaluated by cumulative equivalent minutes over 43 °C T_{43} [Pearce, 2009]:

$$T_{43} = \begin{cases} t \cdot 2^{T-43} \, , T \geq 43°C \\ \frac{t}{4^{43-T}} \, , T < 43°C \end{cases} . \tag{2.7}$$

In all calculations the initial value for the temperature was set to the physiological temperature (37 °C) and the adiabatic boundary condition $\frac{\partial T}{\partial n} = 0$ (n is the normal vector of the surface boundary) was used on all outer surface boundaries of the model. The calculated temperatures were therefore higher than in reality. The values of tissue density (ρ = 1050 kg/m^3), heat capacity (c = 3600 J/(kg·K)) and thermal conductivity (k = 0.512 W/(m·K)) were taken from the literature [Lackovic et al., 2009].

2.2.4 Robustness analysis
(article V)

The robustness of the treatment plan generated for the electrochemotherapy of a deep-seated tumor (see Results 3.6.1–3.6.3) was evaluated using the same numerical model as the treatment planning and parametrizing the model inputs: electrical conductivity values and electroporation thresholds. The volume of the tumor covered by the electric field higher than the reversible electroporation threshold was calculated while changing a single model parameter at a time. The effects of errors in electrode positioning and voltage used were analyzed as well.

Every parameter was varied in five steps from the optimal position, and the level of tumor volume coverage was determined for each parameter value. Electrode positions perpendicular to the axis of insertion were varied in 0.5 mm steps away from the tumor in two perpendicular directions; depth of electrode insertion was varied in 1 mm steps in both directions (deeper and shallower penetration than optimal); voltages were varied in steps of

100 V below the optimal values; electrical conductivities were varied in steps of 10 % of the values used in the model in both directions (higher and lower values than those used in the model); and electroporation thresholds were varied in steps of 50 V/cm above the values used in the model.

2.3 Optimization
(articles I–IV, VI)

For electroporation-based treatment to be efficient, an adequate electric field distribution in the tissues has to be achieved. This can be done by correct electrode positioning and the use of adequate electric pulses. A combination of numerical modeling and optimization can provide both. In the studies leading to this doctoral dissertation, a genetic algorithm was used to determine the appropriate parameters for electrochemotherapy, tissue ablation by irreversible electroporation, and gene electrotransfer.

2.3.1 Genetic algorithm
(articles I–IV, VI)

The genetic algorithm [Holland, 1992] (Figure 9) was written in Matlab 2007a (Mathworks, USA) and was run together with the finite element models using the link between Matlab and Comsol Multiphysics. The initial population of solutions was generated randomly (vectors of real numbers $X = (x_1, x_2, \ldots, x_n)$), taking into account the following model constraints: range of distances between electrodes, range of depth of electrode insertion into tissue, and range of voltages between the electrodes. These constraints were chosen in order to respect the calculation domain size and COMSOL meshing capabilities. Solutions were selected for reproduction proportionally to their fitness according to the defined fitness function. The selected solutions reproduced by cross-over or mutation. When cross-over takes place, each new solution $Z = (z_1, z_2, \ldots, z_n)$ is a random linear combination of parent solutions x and y:

$$z_i = a_i \cdot x_i + (1 - a_i) \cdot y_i; \quad a_i \epsilon [0,1] , \tag{2.8}$$

where z_i are parameters of the new solution, x_i and y_i are parameters of the parents' solutions and a_i is a scalar value randomly chosen from the presented interval. When mutation takes place each new solution is a random variation of one parent solution x:

$$z_i = x_i + b_i \cdot x_i; \quad b_i \epsilon [-p, p] \,, \tag{2.9}$$

where b_i is a scalar value randomly chosen from the presented interval and p is the "distance" of mutation considered acceptable for the optimization procedure.

Cross-over and mutation as reproduction methods were chosen according to pre-set probabilities (normally around 80 % of the reproductions are cross-overs while the rest are mutations), with the exception that the top ranking (elite) solutions could not be subjected to mutation. The genetic algorithm was terminated after 300 generations (we established that the fitness function of the best solution in the population normally reaches a plateau before the 300th iteration) or when termination conditions were fulfilled.
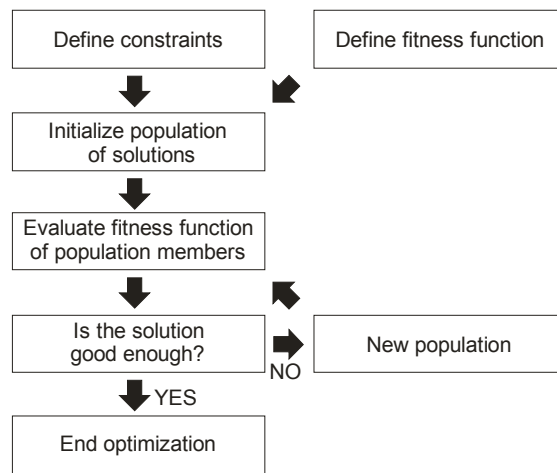
Figure 9. The process of optimization with a genetic algorithm.

Optimization with genetic algorithms has both its advantages and disadvantages compared to other optimization methods. On the one hand, the genetic algorithm does not require the fitness function to be differentiable, both linear and non-linear constraints can be implemented easily, it allows for the optimization of continuous, discrete and categorical parameters (e.g. type of electrodes) at the same time, and does not depend on the quality of the initial guess. Because the final result of the optimization is the whole final population, it is possible to design the algorithm in such a way that it produces topologically different solutions, thereby providing an additional option for the attending physician to choose from. On the other hand, the stochastic nature of the genetic algorithm does not allow it to return the true minimum/maximum, but only an approximation. It also takes more time to generate a solution with a genetic algorithm that with other optimization methods. Nevertheless, in cases where numerous parameters are optimized (as is the case in electroporation-based treatments, where electrode positions and pulse parameters together can reach up to 30 parameters), the

genetic algorithm is generally more likely to reach a solution. This has already been established in radiotherapy treatment planning, where genetic algorithms are a widespread optimization method [Ezzel, 1996; Wu and Zhu, 2001; Bevilacqua et al., 2007].

2.3.2 Fitness functions
(articles I–IV, VI)

The fitness functions for the genetic algorithm were defined arbitrarily for each electroporation-based treatment that the optimization was carried out for:

$$F = \sum a_i . E_{rev}^{i-target} - \sum b_j \cdot E_{irr}^{j-critical} - \sum c_i \cdot E_{irr}^{i-target} - \sum d_j \cdot E_{rev}^{j-critical} \;, \quad (2.10)$$

where F is fitness, E_{rev} and E_{irr} volume fractions of tissue exposed to electric field over the reversible and irreversible threshold, respectively, ($^{i-target}$) and ($^{j-critical}$) represent target and critical tissues – the summation is over all tissues designated as target or critical tissues, and a_i, b_j, c_i and d_j are weights set according to the importance of coverage of each tissue with the corresponding electric field. For instance, the weights for electrochemotherapy in Eq. 2.10 were set according to the following reasoning: the most important thing is to cover all target tissues by an electric field above the reversible thresholds; keeping critical tissues (e.g. large vessels or the spinal cord) from being damaged by an electric field above the irreversible threshold is less important; keeping the target tissues (tumors that we want to kill by electrochemotherapy) from being damaged by the electric field is even less important, and keeping the critical tissue from being reversibly electroporated is the least important. Therefore the weights in Eq. 2.10 were set as $a_i > b_j > c_i > d_j$. Similar arguments lead to fitness functions for the optimization of tissue ablation by irreversible electroporation (Eq. 2.11) and gene electrotransfer (Eq. 2.12).

$$F = \sum a_i . E_{irr}^{i-target} - \sum b_j \cdot E_{irr}^{j-critical} - \sum c_j \cdot E_{rev}^{j-critical} \quad (2.11)$$

$$F = \sum a_i . E_{rev}^{i-target} - \sum b_i \cdot E_{irr}^{i-target} - \sum c_j \cdot E_{irr}^{j-critical} - \sum d_j \cdot E_{rev}^{j-critical} \quad (2.12)$$

When treatment planning was carried out for electrochemotherapy of a tumor in the thigh, the weights in the fitness function were set after consulting with the attending physician.

2.3.3 Comsol Multiphysics and geometry optimization
(articles I–IV, VI)

Although Comsol Multiphysics provides some basic optimization techniques, they are only intended for the optimization of scalar and vector parameters and not for the optimization of geometry or topology. Namely, when optimizing (or parametrizing) scalar and vector parameters, the matrices used for calculation retain the same form and size, as neither the number or shape of finite elements used nor the indices of the boundaries where boundary conditions used are defined change. When optimizing the geometry of a model, the boundary indices change with each calculation. Since Comsol Multiphysics has no available solution (and neither did any other available numerical modeling packages) for geometry optimization, a simple algorithm was defined that takes care of changing boundary indexes (Appendix A) during the optimization procedure.

2.4 Gene electrotransfer into muscle tissue

Efficient gene electrotransfer into biological cells requires that DNA is present around the cells and that the electric pulses 1) electroporate the cells and 2) electrophoretically drive the DNA molecules towards the cell membranes. Since a correlation between the volume of electrotransfected muscle tissue, the amount of transfected DNA, and the desired clinical response has so far not been established, we focused on maximizing the volume of electrotransfected muscle tissue without causing tissue damage. In this preliminary study, only reversible and irreversible electroporation of muscle tissue was studied, while the influence of the electrophoretic effect of the electric pulses was not taken into account.

Muscle geometry and muscle tissue properties were taken from a recent study in which the authors determined the reversible and irreversible electroporation thresholds for muscle tissue for parallel and perpendicular orientations of the external electric field with respect to muscle fiber orientation [Corovic et al., 2010]. Muscle was modeled in realistic size in order to provide guidelines for clinical gene electrotransfection for gene therapy and gene vaccination. Electrical conductivity of muscle tissue was considered anisotropic with 0.135 S/m in the direction perpendicular to muscle fibers and 0.7 S/m in the direction parallel to the fibers. The conductivity increased by a factor of 3.5 for electroporated tissue [Cukjati et al., 2007]. The reversible and irreversible thresholds were taken, as determined by [Corovic et

al., 2010] to be: 1) E_{rev} = 80 V/cm and E_{irr} = 450 V/cm for an electric field parallel to muscle fibers and 2) E_{rev} = 200 V/cm and E_{irr} = 450 V/cm for an electric field perpendicular to muscle fibers. Two different needle electrode arrays were used in the modeling process, one needle electrode pair and three needle electrode pairs (Figure 11). The electrodes were 5 cm long and 0.7 mm in diameter.

To determine the best electrode positions and electric pulse parameters for gene electrotransfer into muscle tissue the following parameters were analyzed: 1) distance between rows of electrodes (4–28 mm, 4 mm step for three needle electrode pairs; 4–36 mm for one needle electrode pair), 2) distance between electrodes in a row (4–28 mm, step of 4 mm), 3) depth of electrode insertion into muscle tissue (10–40 mm; 10 mm step), 4) voltage between electrodes (400–2400 V, 200 V step for three needle electrode pairs; 1000–3000 V for one needle electrode pair) and 5) angle of the applied electric field with respect to the orientation of muscle fibers (0–90 °; 22.5 ° steps). The quality of a given set of parameters was evaluated by the volume of muscle tissue that was reversibly and irreversibly electroporated (see 3.5 Electric field distribution in skeletal muscle – EGT), determined by using the sequential model of electroporation (see 2.2.2 Electric field distribution). To evaluate the developed optimization algorithm (see 2.3 Optimization) an optimization with the genetic algorithm was carried out for the same parameters.

3. RESULTS

The work presented in the doctoral dissertation spans the entire process of designing a treatment planning procedure for the electroporation part of electroporation-based treatments. Since the requirements of such a procedure are ease of use, efficiency, and robustness, many details with respect to geometry building, numerical models, optimization methods, efficiency and robustness have to be considered. The results are presented in such a way that every following section adds a new layer to the final treatment planning procedure, thereby showing the workflow of designing a treatment planning procedure from start to finish. As each new layer is based on a hypothetical or real case of electroporation-based treatment in practice, each section heading is annotated by the appropriate acronym: ECT for electrochemotherapy, IRE for tissue ablation by irreversible electroporation, and EGT for gene electrotransfer for gene therapy and gene vaccination.

In section 3.1 we compared electric field distributions in a subcutaneous tumor (different tumor geometries were used) for different needle electrode arrays, and tested the genetic algorithm as an optimization tool for the positions of needle electrodes and voltages between the electrodes in electrochemotherapy. A fitness function was chosen (see 3.1.2) to reflect the desired electric field distribution for electrochemotherapy: 1) the whole tumor exposed to electric fields above the reversible electroporation threshold and 2) as little as possible healthy tissue exposed to electric fields over the irreversible threshold.

In section 3.2 we used the same subcutaneous tumor geometry and the genetic algorithm to optimize the position of different needle electrode arrays (only distances between electrodes and voltage for tissue ablation with irreversible electroporation). We used a different fitness function for the optimization to reflect the desired electric field distribution in tissue ablation by irreversible electroporation (see 3.2). We also added a critical tissue to the model, which should, if possible, not be irreversibly electroporated at all, and the positions of all electrodes were optimized, instead of using the positions of a prearranged array as in section 3.1.

Since the advantage of tissue ablation by irreversible electroporation to other ablation modalities is its non-thermal nature, optimization of electrode position and voltages was repeated in section 3.3, only this time the temperature distribution was also calculated to ensure that no thermal damage would be caused by the electric pulses.

In section 3.4, optimization was again performed for electrochemotherapy and the position of each electrode was optimized along with the angle of its insertion. In total, 36

parameters were optimized; a number similar to the number of parameters that would be used in clinical treatment planning.

In section 3.5, the electric field distributions obtained by different electrode positions and voltages between electrodes were compared for gene electrotransfer into skeletal muscle, a tissue with anisotropic tissue properties. Again we used a different fitness function for the optimization to reflect the desired electric field distribution in gene electrotransfer (see 3.5). The electric field distributions obtained by static and sequential (see 2.2.2) electroporation models, with conductivity and electroporation thresholds modeled as isotropic and anisotropic tissue properties, were compared to each other to determine which models and which properties should be used in treatment planning.

In section 3.6, we used the developed algorithms for 3D geometry generation from medical images, numerical models of electroporation and the genetic algorithm to plan an electrochemotherapy treatment of a deep-seated tumor. As the size of the treated tumor was too great to achieve good electric field coverage with a single set of electric pulses, a sequence of pulses was used instead, with each set of pulses applied between different electrodes (see Figure 38). A partial response of the treated tumor was achieved; we consequently reevaluated the treatment plan according to the electrode positions used during treatment to try to better understand the treatment outcome. We also performed a robustness analysis of the treatment plan to evaluate which parameters have the greatest effect on its quality and must be considered priorities in future research. Finally, in section 3.7 we compared the results of optimization, while varying the chosen fitness functions. We showed that by controlling the weights of the fitness function it is possible to achieve a treatment plan for each electroporation-based application: electrochemotherapy, tissue ablation with irreversible electroporation and gene electrotransfer.

3.1 Electric field distribution in a subcutaneous tumor – ECT

(articles I, II)

Needle electrodes have been in use for some time in experimental and clinical electrochemotherapy of cutaneous and subcutaneous tumors [Gilbert et al., 1997; Puc et al., 2004; Mir et al., 2006]. We used numerical modeling and optimization to compare different needle electrode arrays for their effectiveness in exposing subcutaneous tumors of different

shapes to electric fields over the reversible threshold E_{rev}, while not damaging too much healthy tissue. All electric field representations in this section are based on the legend presented in Figure 10. The different arrangements of electrodes, different tumor geometries and the model of the tumor inside healthy tissue are shown in Figures 11–14.
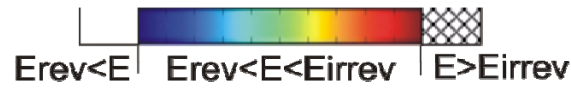
Figure 10. False color legend used in Figures 15–18, indicating the local electric field distribution within the tissue models. White represents non-electroporated tissue ($E < E_{rev}$), colors represent reversibly electroporated tissue (400 V/cm = $E_{rev} < E < E_{irr}$ = 900 V/cm) and pattern represents irreversibly electroporated tissue ($E > E_{irr}$).
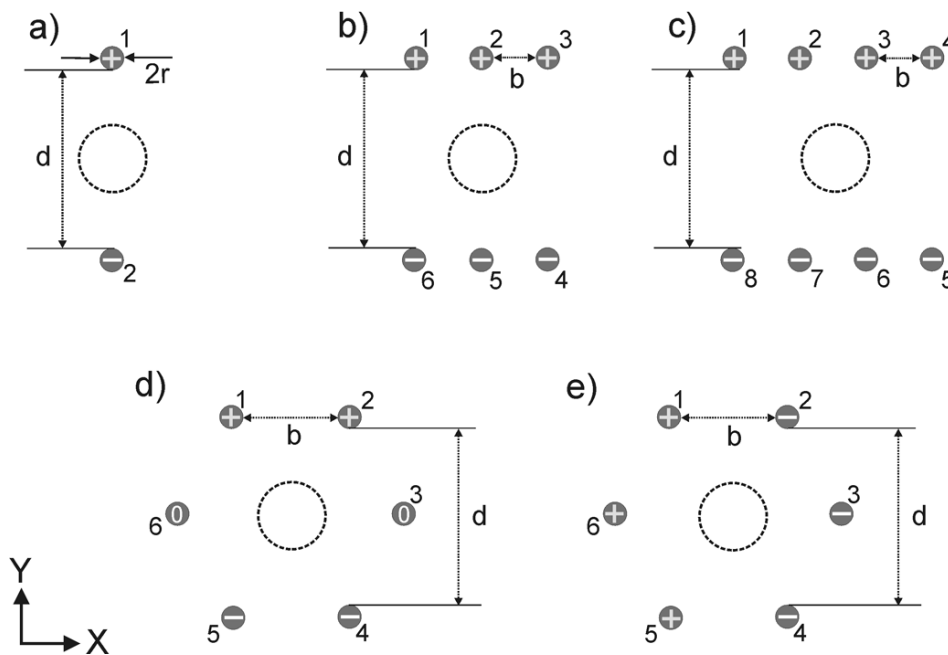
Figure 11. Needle electrode polarities and arrangement with respect to the tumor (dashed line): a) one needle electrode pair; b) three needle electrode pairs; c) four needle electrode pairs; d) 2×2 hexagonal needle electrode array (2 electrodes on positive potential, 2 on negative and 2 grounded); and e) 3×3 hexagonal needle electrode array (3 electrodes on positive potential and 3 on negative potential). d and b are the distance between opposite sets of electrodes and distance between electrodes of the same row (parallel needle electrode arrays) or distance between neighboring electrodes (hexagonal needle electrode array) respectively.
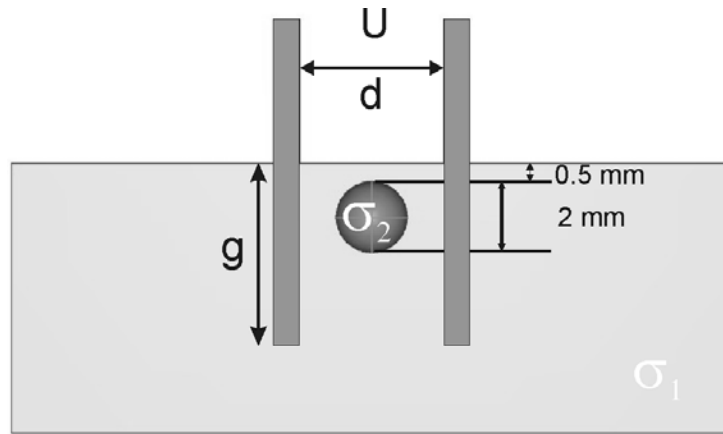
Figure 12. Cross-section of a subcutaneous tumor in healthy tissue between two needle electrodes, where U is the applied voltage between the electrodes; g is the depth of needle insertion; and d is the distance between the electrodes as indicated in Figure 11. The tumor is located 0.5 mm below the surface of the model.
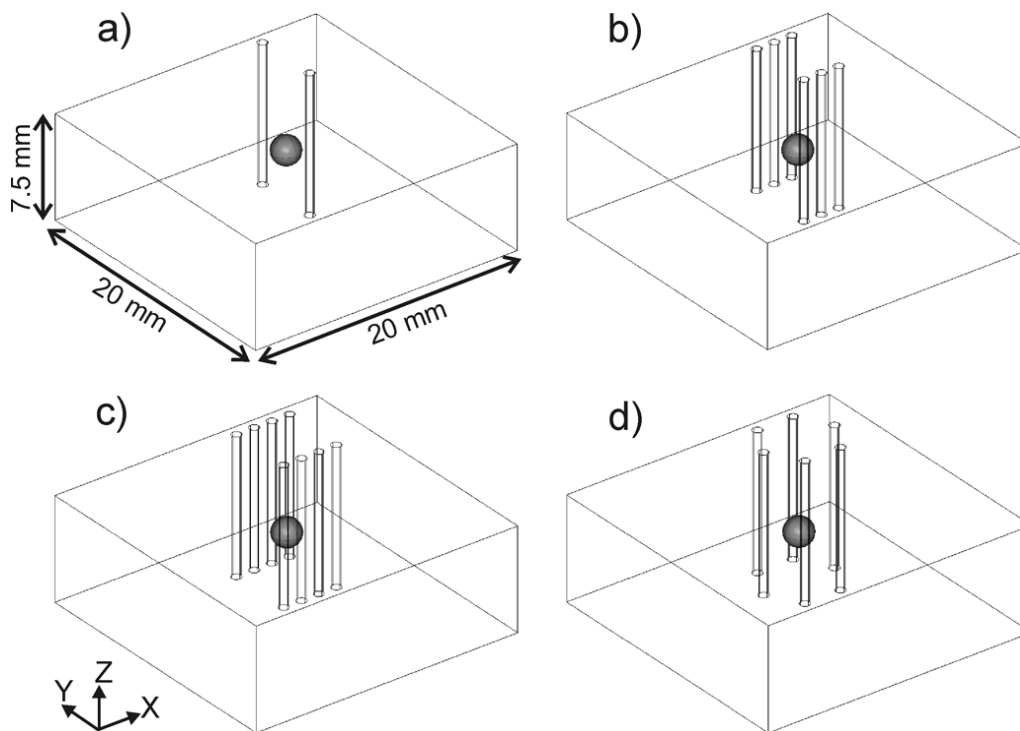
Figure 13. 3D geometry of a subcutaneous tumor with four needle electrode geometries analyzed: a) one needle electrode pair; b) three needle electrode pairs; c) four needle electrode pairs and d) a hexagonal needle electrode array.
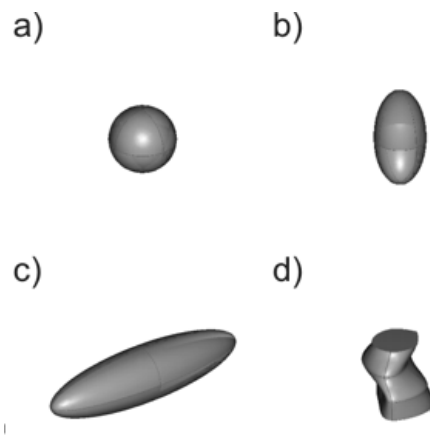
Figure 14. 3D subcutaneous tumor geometries. a) sphere; b) and c) ellipsoids; d) realistic tumor geometry obtained from medical images [Sel et al., 2007].

3.1.1 Comparison of different needle electrode arrays by numerical modeling (article I)

The electrode arrays were positioned around a spherical subcutaneous tumor (Figure 13), and critical voltages (U_C) at which the whole tumor volume was reversibly electroporated ($E > E_{rev}$) were determined by incrementally increasing the voltage applied to the electrodes from 100 V (in steps of 10 V). The critical voltages differed substantially between the electrode arrays, with four needle electrode pairs requiring the lowest and one needle electrode pair the highest voltage (Table 2). When a voltage of 290 V (the determined U_C for three needle electrode pairs) was applied to the other needle electrode arrays, not all arrangements resulted in complete coverage of the tumor (Table 3, Figures 15 and 16). One needle electrode pair failed to provide adequate coverage at any depth of insertion, and either of the hexagonal arrays failed to provide adequate coverage at the insertion depth of 3 mm. Healthy tissue was most heavily damaged by the 3x3 array and by one needle electrode pair which also caused the electric field to be the least homogeneous. Best results were achieved by three and four needle electrode pairs, with four needle pairs producing around 25 % more electric current. The preference for three needle electrode pairs was consistent with a previous 2D study [Corovic et al., 2007].

Table 2. Calculated values of critical voltage U_c, total electric current I, reversibly electropermeabilized tumor volume V_{Trev}, and reversibly and irreversibly electropermeabilized healthy tissue V_{Hrev} and V_{Hirrev} are given for all analyzed electrode geometries and polarities and for depths of electrode insertions $g = 3$ mm and $g = 5$ mm. All volume values are normalized by tumor volume V_T. Distances between opposite sets of electrodes d and distances between electrodes of the same row b (needle electrode arrays) or between neighboring electrodes b (hexagonal needle electrode array) were kept constant at $b = 0.65$ mm (parallel needle electrode arrays), $b = 4/\sqrt{3}$ mm (hexagonal needle electrode array) and $d = 4$ mm in all simulations.

Electrode configuration and polaririty	g [mm]	U_C [V]	I [A]	$\dfrac{V_{Trev}}{V_T}$	$\dfrac{V_{Hrev}}{V_T}$	$\dfrac{V_{Hirrev}}{V_T}$
one-needle pair	5	400	0.248	1	29.96	6.14
	3	440	0.175	1	21.00	5.14
three-needle pairs	5	260	0.270	1	31.86	1.71
	3	290	0.198	1	24.86	2.35
four-needle pairs	5	240	0.294	1	43.78	2.43
	3	280	0.234	1	29.21	2.14
2x2 hexagonal array	5	290	0.301	1	38.36	3.64
	3	350	0.234	1	30.64	4.92
3x3 hexagonal array	5	280	0.463	1	42.43	9.71
	3	310	0.330	1	31.4	8.07

Table 3. Calculated values of total electric current I, reversibly electroporated tumor volume V_{Trev}, reversibly and irreversibly electroporated healthy tissue V_{Hrev} and V_{Hirrev} for all analyzed electrode geometries, and polarities for depths of electrode insertions $g = 3$ mm and $g = 5$ mm. All volume values are normalized by tumor volume V_T. Distances between opposite sets of electrodes d and distances between electrodes of the same row b (needle electrode arrays) or between neighboring electrodes b (hexagonal needle electrode array) were kept constant at $b = 0.65$ mm (parallel needle electrode arrays), $b = 4/\sqrt{3}$ mm (hexagonal needle electrode array) and $d = 4$ mm in all simulations. Voltage was set to $U = 290$ V in all simulations.

Electrode configuration and polaririty	g [mm]	U [V]	I [A]	$\dfrac{V_{Trev}}{V_T}$	$\dfrac{V_{Hrev}}{V_T}$	$\dfrac{V_{Hirrev}}{V_T}$
one-needle pair	5	290	0.180	0.08	17.21	2.71
	3	290	0.115	0.03	10.42	2.00
three-needle pairs	5	290	0.301	1.00	37.21	2.79
	3	290	0.198	1.00	24.86	2.36
four-needle pairs	5	290	0.354	1.00	45.86	2.86
	3	290	0.236	1.00	30.64	2.42
2x2 hexagonal array	5	290	0.291	1.00	36.86	3.29
	3	290	0.190	0.41	22.93	2.71
3x3 hexagonal array	5	290	0.471	1.00	44.07	10.57
	3	290	0.308	0.99	29.07	7.00

Figure 15. Local electric field distribution for the models with a) and b) one needle electrode pair, c) and d) three needle electrode pairs, e) and f) four needle electrode pairs, shown for two depths of electrodes' insertion $g = 5$ mm (a, c, e) and $g = 3$ mm (b, d, f). Electric field distribution is shown in three central perpendicular planes XY, YZ and XZ all passing through the center of the tumor (see Figure 10 for details). Geometrical details are given in the caption to Table 3. Voltage applied between the electrodes was 290 V.
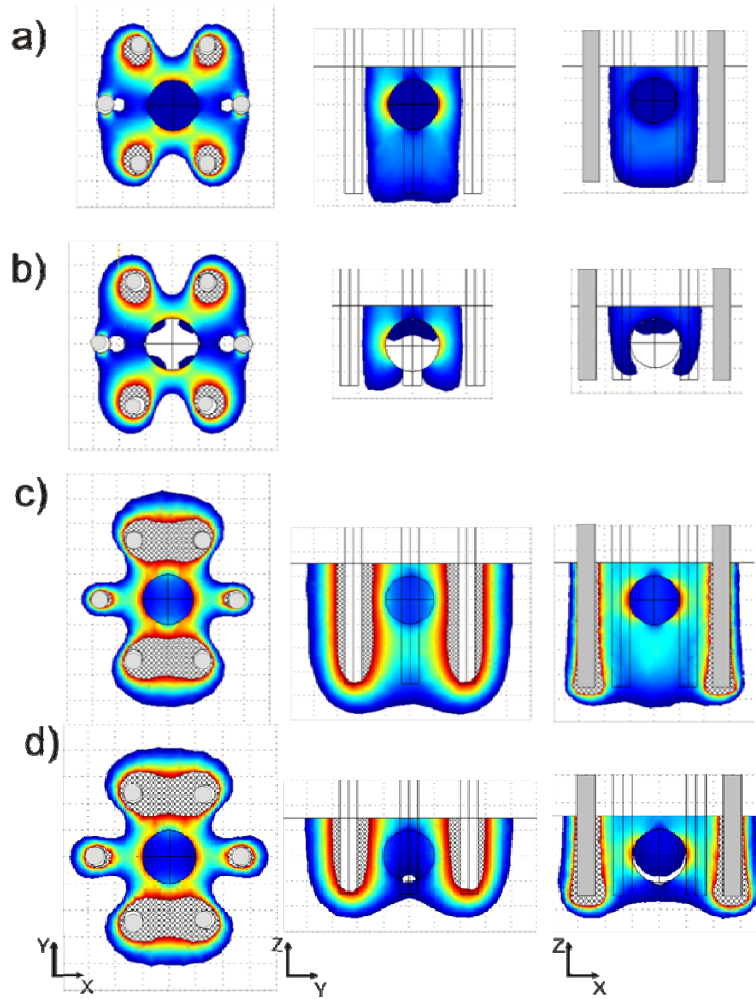
Figure 16. Local electric field distribution for the models of a) and b) 2x2 hexagonal needle electrode array, c) and d) 3x3 hexagonal needle electrode array, shown for two depths of electrodes' insertion $g = 5$ mm (a, c) and $g = 3$ mm (b, d). Electric field distribution is shown in three central perpendicular planes XY, YZ and XZ all passing through the center of the tumor (see Figure 10 for details). Geometrical details are given in the caption to Table 3. Voltage applied between the electrodes was 290 V.

3.1.2 Optimization of needle electrode arrays

(article I,II)

The optimization of distances between electrodes (*b* and *d*), depths of electrode insertion and voltages between the electrodes (four parameters in total) was carried out with the genetic algorithm for all needle electrode arrays, except the one needle electrode pair. The optimization was carried out for each of the tumor geometries presented in Figure 14 (including realistic tumor geometry) to see if a particular array is more suitable for a particular tumor shape than others. The fitness function used was:

$$F = 100 \cdot V_{Trev} - 10 \cdot V_{Hirr} - V_{Hrev} - V_{Tirr},$$

where V_{Trev} is the volume of reversibly electroporated tumor, V_{Tirr} is the volume of irreversibly electroporated tumor, V_{Hrev} is the volume of reversibly electroporated healthy tissue and V_{Hirr} is the volume of irreversibly electroporated healthy tissue. The weights in front of the volumes were chosen according to their general significance to successful treatment. Efficient electrochemotherapy requires the entire tumor volume to be at least reversibly electroporated; its weight is therefore highest, i.e. +100. It is also desired that healthy tissue is not damaged by the electric pulses, and the weight of V_{Hirr} is set accordingly to −10. While irreversible electroporation of the tumor is not desired, it has so far not been shown that it has a negative effect on the treatment outcome (weight −1). Reversible electroporation of healthy tissue has also not been shown to have any significant clinical effects (weight −1).

Table 4. Optimized electrode positions around the spherical tumor and voltages applied for all analyzed electrode geometries and polarities. Calculated values of total electric current I, reversibly electropermeabilized tumor volume V_{Trev}, and reversibly and irreversibly electropermeabilized healthy tissue V_{Hrev} and V_{Hirr} are given for all optimum solutions. All volume values are normalized by tumor volume V_T.

Electrode configuration and polaririty	b [mm]	d [mm]	g [mm]	U_C [V]	I [A]	$\dfrac{V_{Trev}}{V_T}$	$\dfrac{V_{Hrev}}{V_T}$	$\dfrac{V_{Hirrev}}{V_T}$
three-needle pairs	0.70	4.04	3.15	272	0.20	1	23.64	1.86
four-needle pairs	0.67	4.10	3.20	265	0.25	1	28.29	1.65
2x2 hexagonal array	1.71	3.47	3.57	256	0.24	1	21.86	2.34
3x3 hexagonal array	1.71	3.47	2.90	246	0.32	1	21.64	5.14

Table 5. Optimized electrode positions and voltages applied for all analyzed electrode arrangements and tumor geometries. Calculated values of total electric current through tissue (I), fraction of reversibly permeabilized target tissue (V_{Trev}/V_T) and normalized volume of damaged healthy tissue (V_{Hirr}/V_{sph}) are given for all optimized solutions. Normalizing factor in the latter case is the volume of the spherical tumor.

Tumor	Electrode geometry	b [mm]	d [mm]	Insertion depth [mm]	U [V]	I [A]	V_{Trev}/V_T	V_{Hirrev}/V_{sph}
	3 pairs	0.70	3.4	1.1	210	0.45	1	1.00
	4 pairs	0.70	3.4	0.9	210	0.52	1	1.03
	3x3	1.30	3.7	0.3	200	0.55	1	3.58
	2x2x2	1.30	3.7	0.3	220	0.32	1	1.77
	3 pairs	0.70	3.4	0.9	220	0.65	1	1.59
	4 pairs	0.70	3.6	0.9	220	0.75	1	1.39
	3x3	1.30	3.7	0.3	210	0.89	1	6.31
	2x2x2	1.30	3.7	0.7	220	0.47	1	2.51
	3 pairs	2.60	3.4	0.9	320	0.88	1	7.40
	4 pairs	1.60	3.4	0.7	320	0.96	1	7.08
	3x3	4.30	12.2	0.5	550	1.19	1	15.84
	2x2x2	4.60	13.0	0.1	1160	1.25	1	31.22
	3 pairs	0.75	3.4	0.9	270	0.65	1	3.17
	4 pairs	0.70	3.4	0.7	270	0.70	1	3.39
	3x3	1.80	5.1	1.1	320	1.07	1	11.44
	2x2x2	1.60	4.5	0.9	320	0.55	1	5.45

Compared to critical voltages in Table 2, the voltages obtained by optimization were lower, and less healthy tissue was irreversibly and/or reversibly electroporated (Table 4 – values for the spherical tumor). In addition, coverage of the whole tumor was achieved with all needle electrode arrays and for all tumor geometries (Table 5). Again, three and four needle electrode pairs produced the best solutions for all tumor shapes, with the lowest voltages necessary and the least amount of healthy tissue damage (Figures 17 and 18). The hexagonal arrays required very high voltages to cover the ellipsoid tumor – which is partly due to the fact that the angle of rotation of the needle electrode array was not an optimization parameter. If that had been the case, lower voltages would have also been achieved using hexagonal arrays, although they would have probably still been higher than with other electrode arrays.
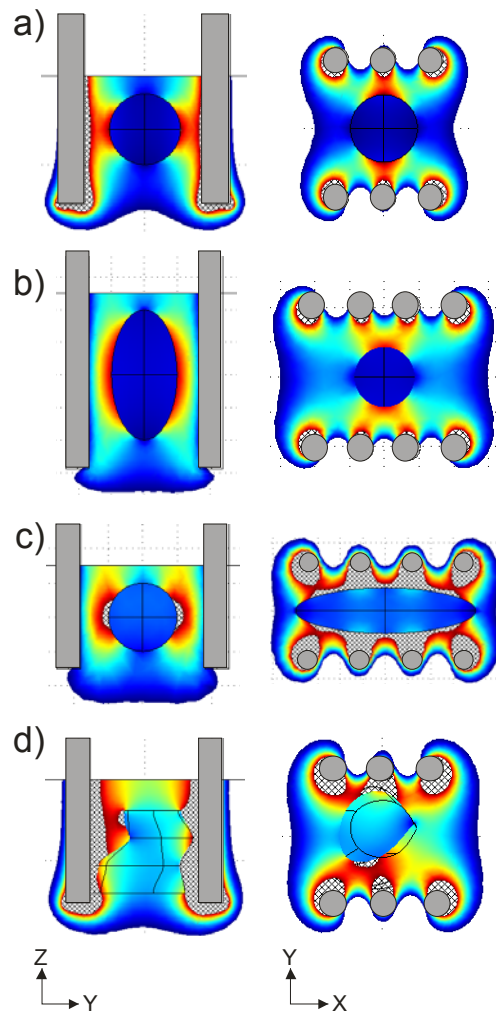
Figure 17. Local electric field distribution for the optimized models. In each case only the best electrode configuration is given: a) three needle pairs for the spherical tumor; b) and c) four needle pairs for both ellipsoid geometries; d) three needle pairs for the realistic tumor. The electric distribution is shown in two central perpendicular planes, YZ and XY, both passing through the center of the tumor (see Figure 10 for details). Corresponding optimized parameters are given in Table 5.
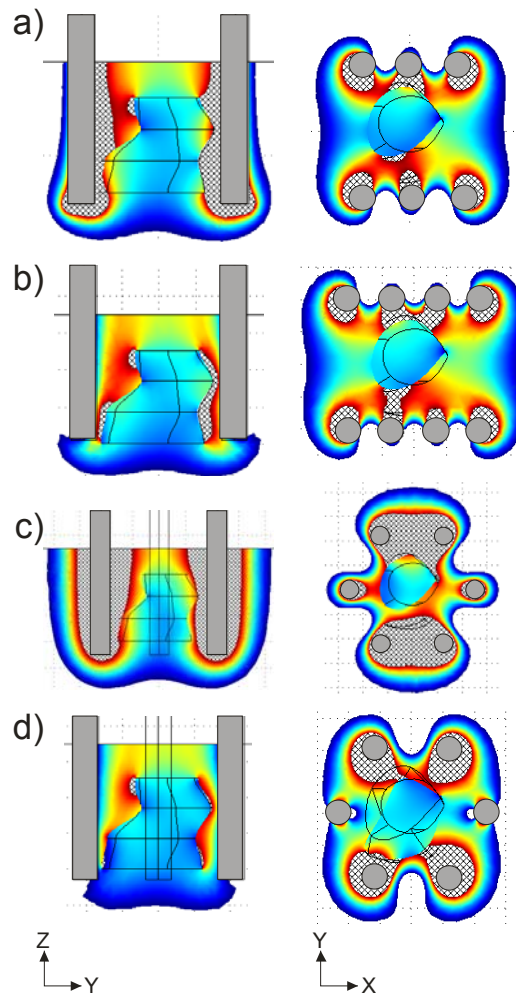
Figure 18. Local electric field distribution for the optimized model of the realistic tumor with a) three needle pairs; b) four needle pairs; c) 3x3 hexagonal needle electrode array; d) 2x2x2 hexagonal needle electrode array. The electric distribution is shown in two central perpendicular planes, YZ and XY, both passing through the center of the tumor (see Figure 10 for details). Corresponding optimized parameters are given in Table 5.

To analyze the reproducibility of the optimization results, optimization of each electrode array/tumor geometry combination was run 50 times. Although the time at which the algorithm reached the best solution was different in each run, and the solutions reached in individual runs did not match each other perfectly, a good solution was reached in a given number of iterations in all runs (Figure 19). The differences between individual optimized parameter were very small; typically the positions of the electrodes differed by around 0.1 mm and the voltages by around 10 V.
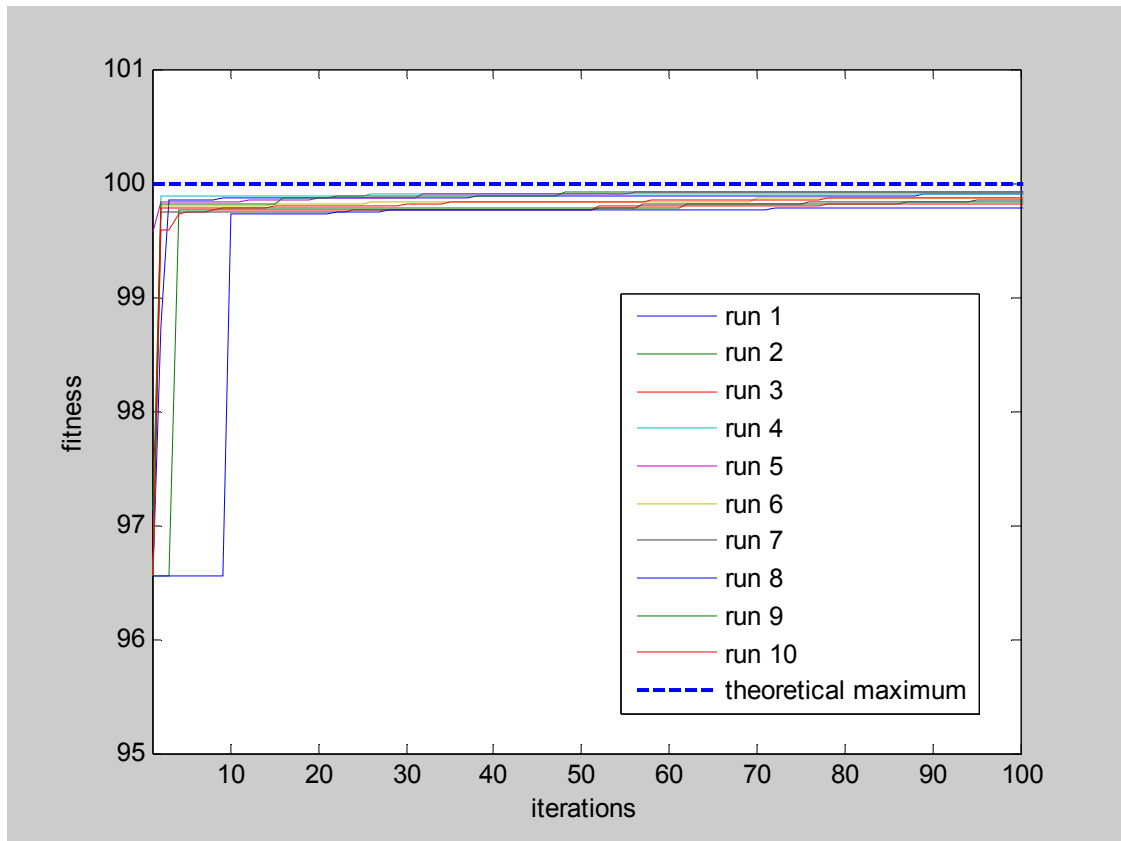
Figure 19. Fitness of the best solution in population for 10 randomly chosen optimization runs. All runs produced very good solutions early in the optimization process (in iteration 10), while there were only minor improvements later, until the last iteration. The initial population of solutions was chosen randomly, with one seeded solution (F = 96.54), which was obtained with respect to the ESOPE standard protocol [Mir et al., 2006]. This solution achieved complete coverage of the tumor with $E > E_{rev}$, however, it also caused substantial healthy tissue damage.

3.1.3 Guidelines for needle electrode ECT of subcutaneous tumors

It can be seen from all the optimized voltages and positions of the electrode arrays that the best results (complete coverage of the tumor and the least healthy tissue damage) are obtained by putting the electrodes around the tumor in such a way that the active parts of the electrodes (or their projections) cover a bigger volume than the tumor (Figure 20).
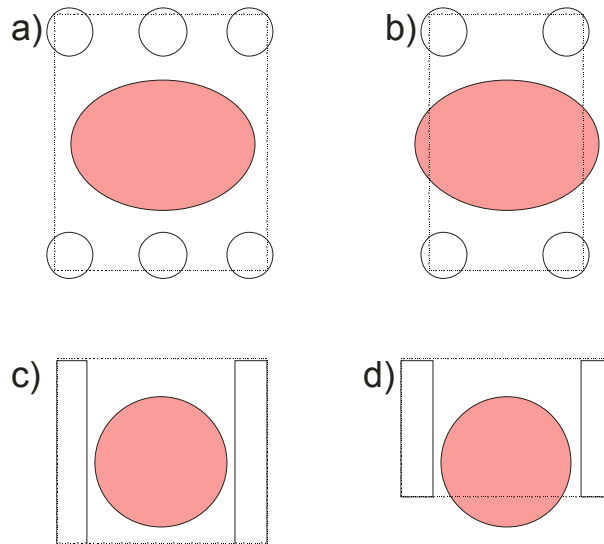
Figure 20. Best electrode positions for complete coverage of a subcutaneous tumor with an adequate electric field (a, c) and typical positions of electrodes that require much higher voltages to cover the tumor or lead to inadequate coverage (b, d). (a, b) are presented in a cross-section perpendicular to the direction of needle electrode insertion, while (c, d) are presented in a cross-section parallel to electrode insertion.

In general the studied parameters affect the electric field distribution in the tumor in the following ways: 1) if the distance between electrodes is increased, a higher voltage is needed to achieve the same electric field strength and the isofield lines in the middle curve upwards (Figure 15d), thereby increasing the probability of inadequate coverage of the lower part of the tumor; 2) if electrode insertion is too shallow, the lower part of the tumor is not covered; increasing insertion depth also increases the total electric current produced by the pulses; 3) the determination of adequate voltage depends strongly on electrode and tumor positions – if the values were optimized each time, much lower voltage would be needed for successful electroporation, and the danger of not covering a part of the tumor with the electric field above the reversible electroporation threshold would decrease.

3.2 Electric field distribution in a subcutaneous tumor – IRE

(article III)

For the optimization of irreversible electroporation parameters, the geometry used was the same as in the previous section (i.e. a realistic tumor), with an additional geometrical object – a critical tissue which was used to simulate an important organ of the body whose exposure to high electric fields is extremely undesirable (Figure 21). The goal of the optimization in this case was to achieve irreversible electroporation ($E > E_{irr}$) of the entire tumor volume, while sparing the critical tissue. Optimization used the following fitness function:

$$F = 10000 \cdot V_{Tirr} - 200 \cdot V_{Cirr} - V_{HTirr},$$

where indices $_T$, $_C$ and $_{HT}$ are the tumor, critical tissue and healthy tissue respectively. The weights in front of the volumes were chosen with similar reasoning as for the fitness function in electrochemotherapy. Efficient tumor tissue ablation by irreversible electroporation requires the entire tumor volume to be irreversibly electroporated; its weight is therefore highest. Irreversible electroporation of critical and healthy tissue in not desired; however, damage to critical tissue can have severe clinical consequences – it is therefore weighted more heavily that irreversible electroporation of non-critical healthy tissue. We presumed that reversible electroporation of healthy and critical tissue does not cause adverse clinical effects.
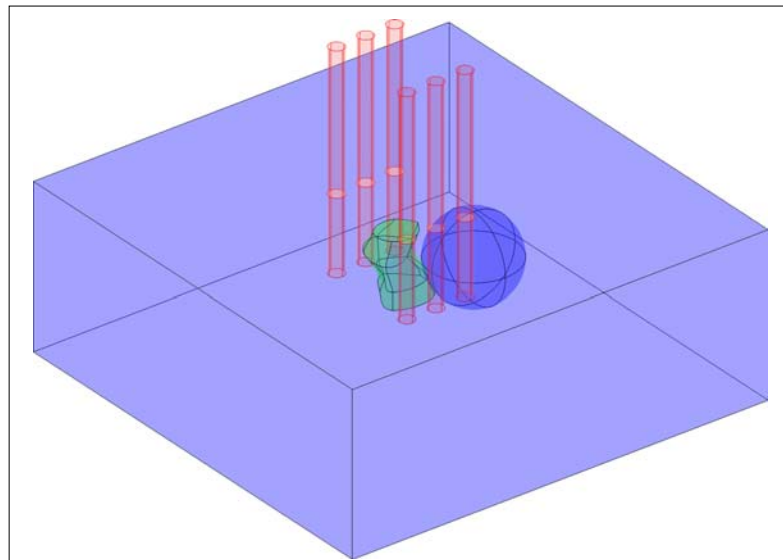
Figure 21. Model geometry for the optimization of irreversible electroporation: healthy tissue (light blue); tumor (green) [Sel et al., 2007]; critical tissue (dark blue).

3.2.1 Three needle electrode pairs

Optimization was performed for the needle electrode array that performed best in the optimization of electroporation parameters for electrochemotherapy – three needle electrode pairs. The optimized parameters were: distance between rows of electrodes, distance between electrodes in a row, depth of electrode insertion, center point of the electrode array, and the voltage between rows of electrodes; six parameters in total.

The final treatment plan is presented in Figures 22 and 23. The electric field distribution is rather homogeneous; the field is very high only close to the electrodes, and just above the irreversible threshold inside the tumor. Electric field is also quite high in the critical tissue closest to the tumor; the irreversible threshold is exceeded in 2.43 % of the critical tissue (Table 6).

Figure 22. Local electric field distribution for the treatment plan with three needle electrode pairs is shown in the XY plane through the center of the tumor. The optimal voltage on the electrodes was determined to be 500 V (voltage was defined as the difference between electric potentials of the rows of needle electrodes – see Figure 11b). White arrow marks part of the tumor where the electric field is barely above the irreversible electroporation threshold (800 V/cm). The electric field is shown in the range from 800 V/cm (irreversible threshold) to 3200 V/cm; values above 3200 V/cm are shown in dark red.

Figure 23. Tumor, critical tissue and irreversibly electroporated area are presented as contours in the XY plane (left) at three different depths (top row: 8 mm; middle row: 23 mm; bottom row: 38 mm) and in the XZ plane (right) at three different cross-sections (middle row: tumor center; top row and bottom row: 1.2 mm from tumor center).

3.2.2 Six individual needle electrodes

Optimization was also carried out for six individual electrodes positioned around the tumor. In this case the optimized parameters were: x and y coordinates of each of the electrodes, electric potential on each electrode and depth of electrode insertion (equal for all electrodes); 19 parameters in total, significantly more than in the three needle pair case.

The resulting treatment plan is presented in Figures 24 and 25. The electric field is not as homogeneous as in the case of three needle pairs: the field around the electrodes and within the tumor is much stronger. Nevertheless, only 0.8 % of the organ at risk is exposed to electric fields above the irreversible threshold (Table 6), which makes (according to the fitness function) this electrode configuration better than three needle pairs. The irregular positioning

of the electrodes and different potentials on each electrode result in an electric field distribution that is more successful in "avoiding" high electric fields in the critical tissue, however, this is achieved at the expense of a stronger electric field elsewhere.

Table 6. Treatment planning parameters V_{Tirr} V_{Cirr} and treatment planning (computational) time. V_{Tirr} and V_{Cirr} are normalized by their tissues' respective volumes. All values were calculated using the optimal parameters acquired by the optimization procedure.

	F	V_{Tirr} [%]	V_{Cirr} [%]	calculation time [h]
Three needle pairs	9995.0	100	2.4	1.5
Six electrodes	9998.1	100	0.8	4.2
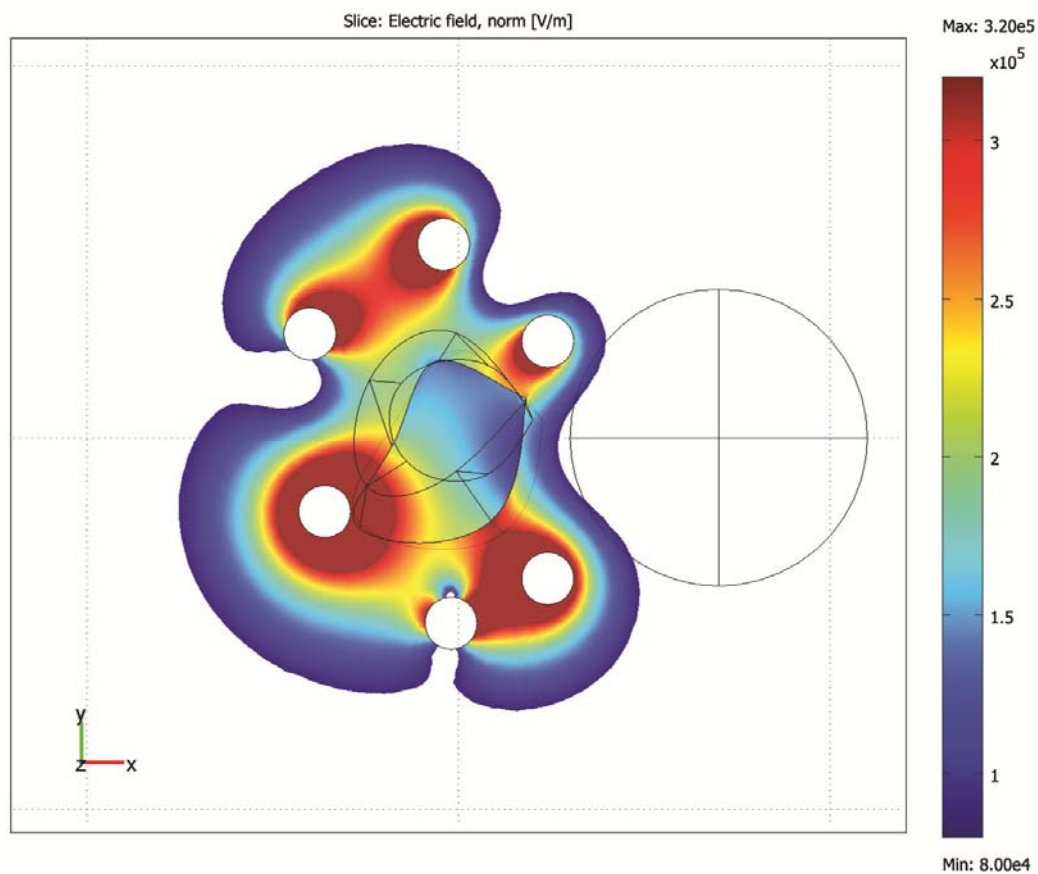
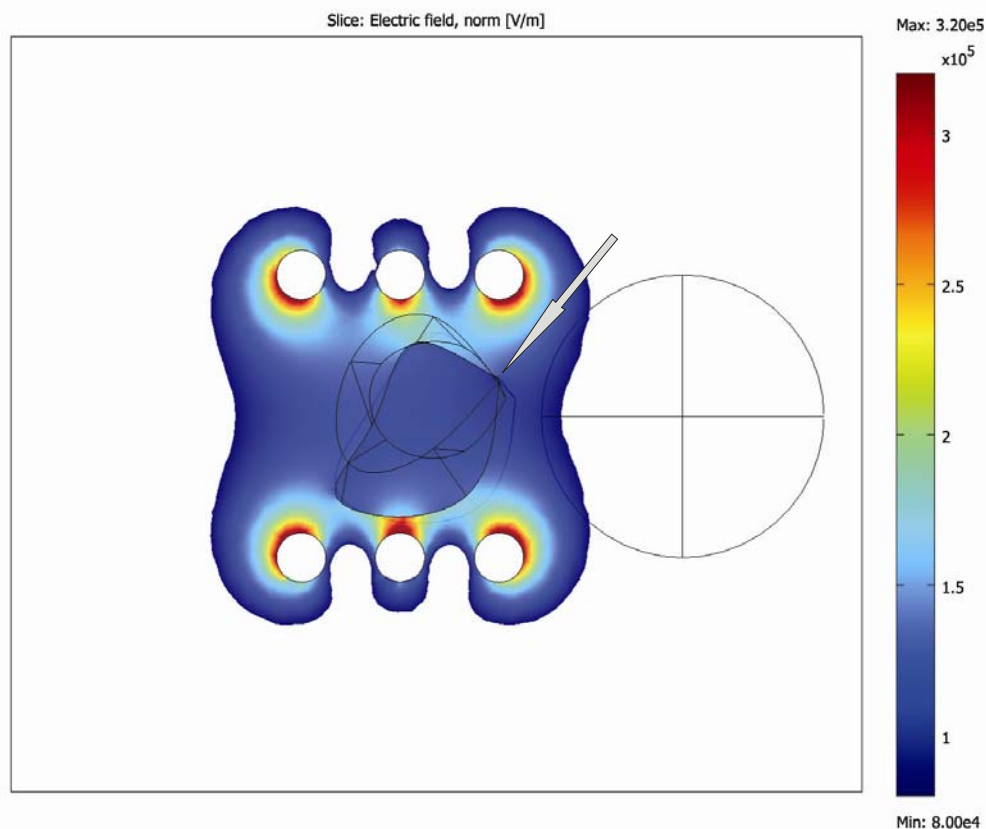Figure 24. Local electric field distribution for the treatment plan with six individual needle electrodes is shown in the XY plane through the center of the tumor. The optimal potentials for each electrode were determined to be 825 V, 825 V, 900 V, 500 V, 0 V and 300 V (starting at the top and moving clockwise). For better comparison, the same color legend as in Figure 22 is used (800 V/cm–3200 V/cm).
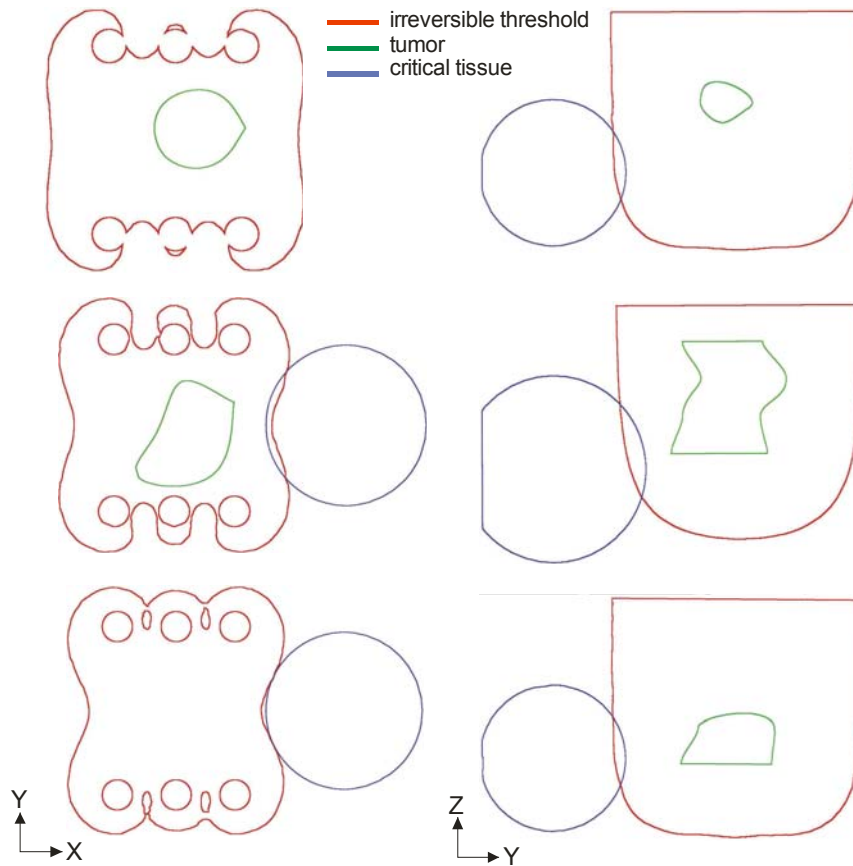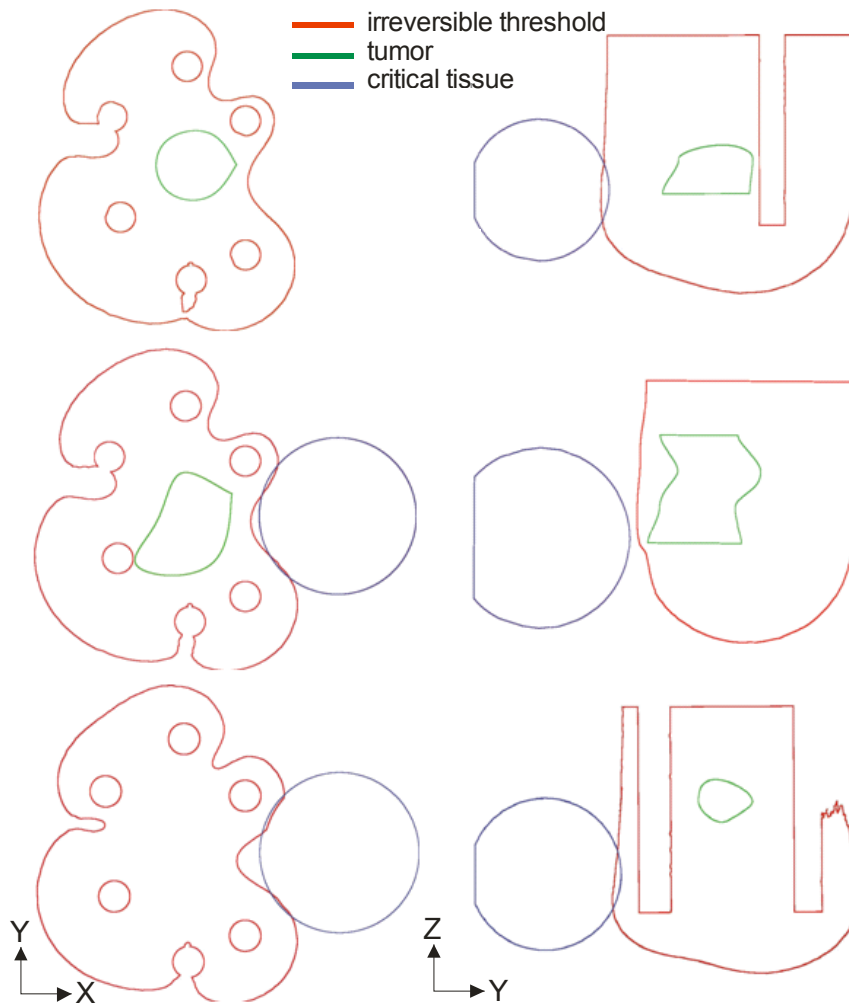
Figure 25. Tumor, critical tissue and irreversibly electroporated area are presented as contours in the XY plane (left) at three different depths (top row: 8 mm; middle row: 23 mm; bottom row: 38 mm) and in the XZ plane (right) at three different cross-sections (middle row: tumor center; top row and bottom row: 1.2 mm from tumor center).

3.3 Prevention of thermal damage – IRE

Since the main advantage of tissue ablation by irreversible electroporation is its non-thermal nature, it is very important to keep the temperature increase due to electroporation pulses under the thermal damage threshold. The model used for the optimization of electroporation parameters for irreversible electroporation was modified to include the calculation of temperature increase during pulse delivery using the modified bioheat equation (Eq. 2.6). The obtained temperature distribution in time and space was used to calculate thermal damage (Eq. 2.7), which was used in the fitness function of the genetic algorithm:

$$F = 10000 \cdot V_{Tirr} - 200 \cdot V_{Cirr} - V_{HTirr} - 100\, T_{43}.$$

The temperature was evaluated for 50 pulses of 100 µs and pulse repetition frequency of 1 Hz, a combination that produced good results in a recent study of prostate cancer ablation [Rubinsky et al., 2008].

3.3.1 Optimization and temperature calculation

After only a few iterations of the optimization it became clear that an exact calculation of temperature distribution was not feasible, as the calculation of the temperature distribution took minutes for each set of pulses, while the calculation of only the electric field distribution took seconds. This would mean that the entire optimization process would have taken a week or so, which was not acceptable.

Instead a conservative evaluation of the temperature distribution according to (2.5) was used for screening for possible thermal damage. Only if a temperature increase above 50 °C was determined by Eq. 2.5, was the evaluation of the bioheat equation performed. In this way it was possible to reduce the bioheat equation evaluation to less than 12 % of all calculations performed during the optimization, which meant that the optimization procedure took only 29 hours. Nevertheless, this still presented an almost 20-fold increase compared to optimization without calculating the temperature distribution. The treatment plan obtained by the optimization of the electric field and temperature did not however differ significantly from the one without temperature calculations (Figure 22).

The results indicate that much higher temperatures are achieved when Eq. 2.5 is used (Figure 26) instead of the modified bioheat equation (Eq. 2.6) (Figure 27) (center of the tumor: 47.1 °C vs. 39.3 °C). The modified bioheat equation takes into account heat dissipation, which results in lower temperature in the areas where most of the Joule heating is

generated (electrodes, tumor) and also in lower temperatures next to the electrodes compared to the tumor temperatures. This effect is the result of the electrodes behaving as a heat sink due to their high thermal conductivity.
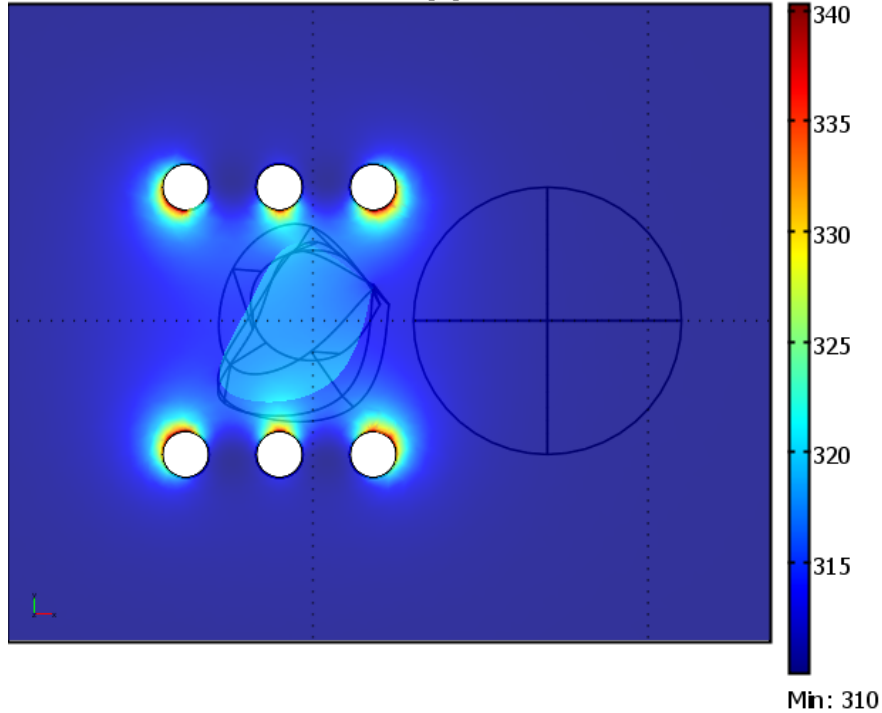
Figure 26. Temperature distribution after 50×100 μs pulses of 500 V, as evaluated by Eq. 2.5. The maximum temperature reached was 67.3 °C (340.3 K) in the vicinity of the electrodes, while the temperature in the center of the tumor reached 47.1 °C (323.5 K). The units of the color scale are K.

Figure 28 shows how the temperature changes during and after each pulse in the tumor and near the electrodes. Due to high electrode thermal conductivity, the temperature around the electrode decreases substantially between pulses, while it does not change as much within the tumor. A further decrease in computation time was achieved by not evaluating the bioheat equation at all. The optimization fitness function was thus changed to:

$$F = 10000 \cdot V_{Tirr} - 200 \cdot V_{Cirr} - V_{HTirr} - 100 \, (T - 43°C),$$

where T is the temperature in the center of the tumor as evaluated by Eq. 2.5. In this case optimization took 1.5 hours and the obtained treatment plan again did not differ significantly from the one obtained without calculating the temperature distribution (Figure 22).
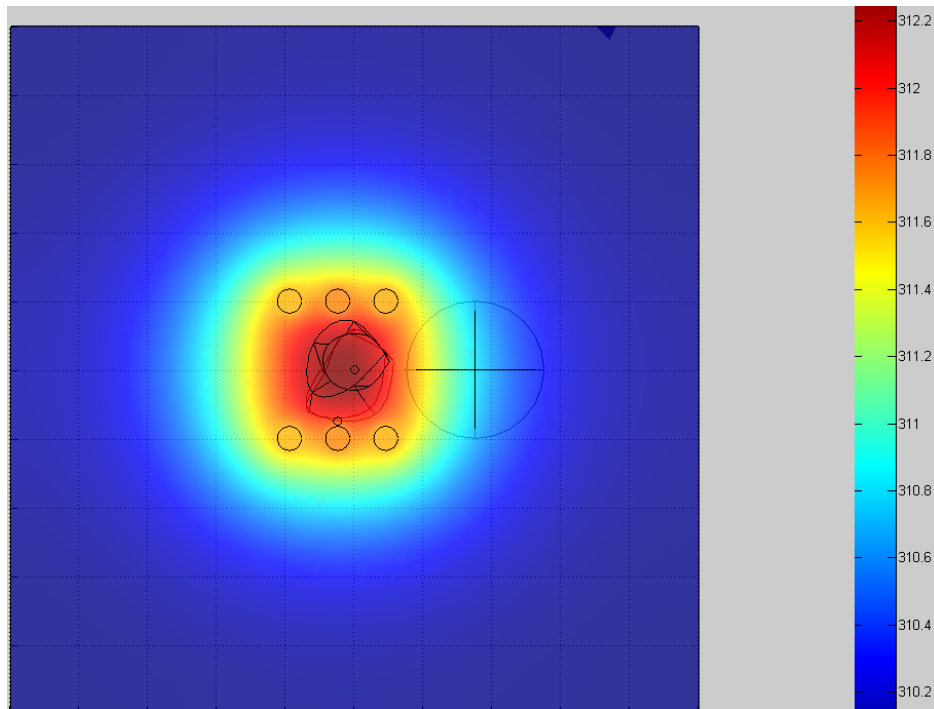
Figure 27. Temperature distribution after 50×100 µs pulses of 500 V, as evaluated by the bioheat equation (Eq. 2.6). In the vicinity of the electrodes the temperature reached 39.1 °C (312.1 K), while the temperature in the center of the tumor reached 39.3 °C (312.3 K). The units of the color scale are K.
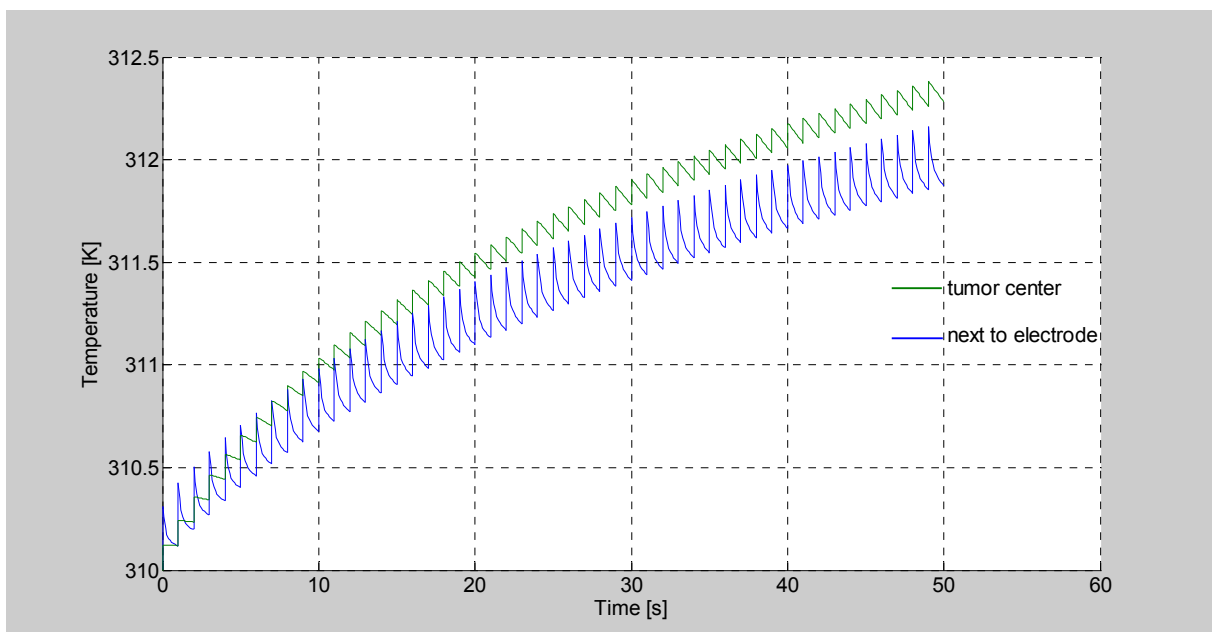
Figure 28. Temperature in the tumor center and next to one of the electrodes during 50 100 µs pulses of 500 V, as evaluated by the bioheat equation (Eq. 2.6). In the vicinity of the electrodes the temperature reached 39.1 °C (312.1 K), while the temperature in the center of the tumor reached 39.3 °C (312.3 K).

3.4 Electric field distribution in a subcutaneous tumor – ECT 2

(article VI)

The optimization was carried out for the same model as in section 3.2.2 (six individual electrodes), except that new parameters were added to the optimization. Insertion depth was optimized for each electrode, as were the angles of electrode insertion with respect to the center of the tumor – the azimuth angle φ and the elevation angle θ. The elevation angle was constrained to a maximum of 20 ° (otherwise the electrode geometries could coincide with each other, which could lead to an error in the calculation), while there were no constraints for the azimuth angle. 36 parameters were optimized. The fitness function was also changed from the one used in section 3.1 to:

$$F = 10 \cdot V_{Trev} - 2 \cdot V_{Cirr} \,,$$

where V_{Trev} is the volume of reversibly electroporated tumor and V_{Cirr} is the volume of irreversibly electroporated critical tissue. Irreversible electroporation of healthy tissue and tumor tissue have been left out, as has been reversible electroporation of healthy tissue, as both did not significantly affect the results in section 3.1.

3.4.1 Optimization of angle insertion

The increase in number of parameters had very little effect on the genetic algorithm; the optimization was completed in less than 5 h. The optimized electrode positions were very similar to the ones obtained for irreversible electroporation (see Figure 24); however, the obtained potentials on individual electrodes were different (Figure 29), as expected. Interestingly, although irreversible electroporation of the tumor was not part of the fitness function, the treatment plan resulted in almost 50 % of the tumor being irreversibly electroporated, while critical tissue was spared almost entirely (only 0.3 % was irreversibly electroporated).
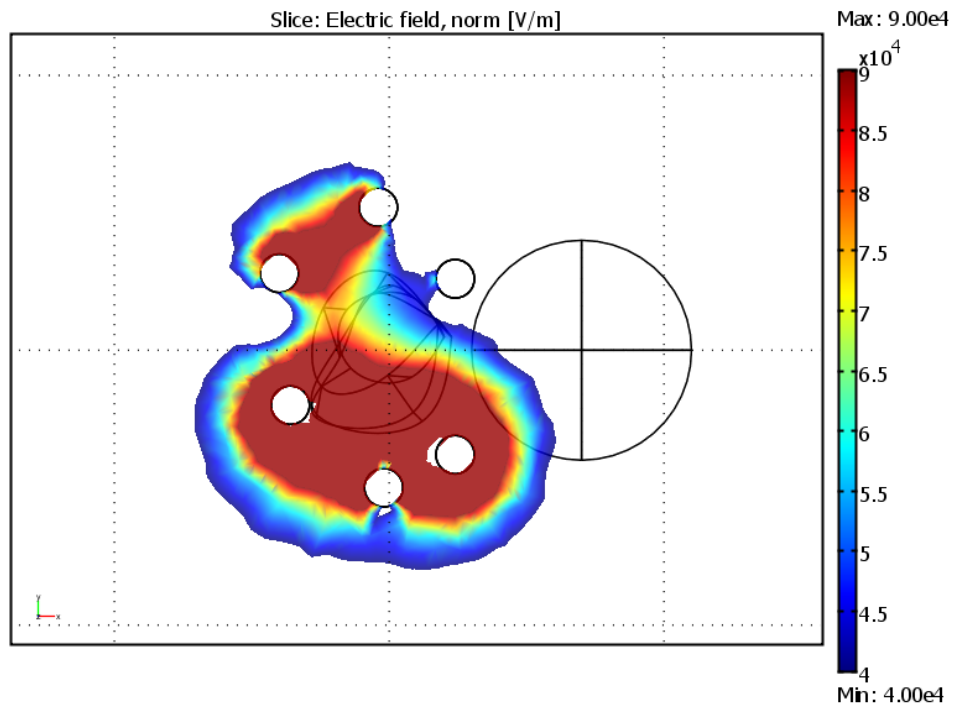
Figure 29. Electric field distribution in the XY plane through the center of the tumor. The optimal potentials for each electrode were determined to be 275 V, 255 V, 500 V, 300 V, 0 V and 100 V (starting at the top and moving clockwise). The electric field is shown in the range from 400 V/cm (reversible threshold) to 900 V/cm (irreversible threshold); values above 900 V/cm are shown in dark red.
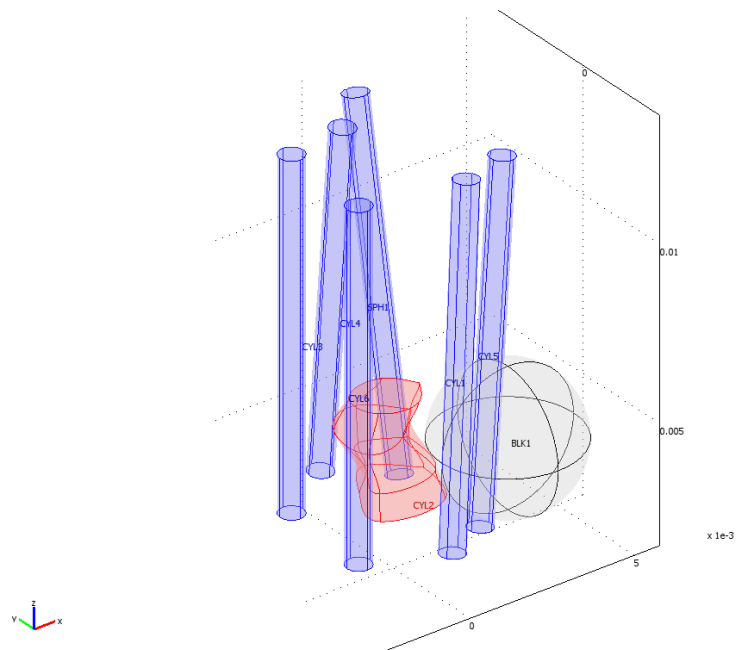
Figure 30. The optimized elevation and azimuthal insertion angles for individual electrodes were 5 ° and 270 °, 10 ° and 90 °, 5 ° and 15 °, 5 ° and 30 °, 0 ° and 145 °, 0 ° and 15°.

The elevation angles obtained by the optimization were small or zero (Figure 30), which suggests that parallel insertion of electrodes would give adequate results. In fact, by changing all the angles from their optimized values to zero, only the volume of irreversibly electroporated critical tissue increased from 0.30 % to 0.37 % for this specific geometry, while the whole tumor volume was reversibly electroporated in both cases. There was also almost no difference between the electrode insertion depths ; five were inserted to the same depth, while another was inserted 1 mm deeper than the others.

3.5 Electric field distribution in skeletal muscle – EGT

In this section we present a model electroporation of skeletal muscle, a tissue of choice for gene therapy and gene vaccination, since it allows for long-term expression of the transfected genes. One of the essential conditions for efficient gene electrotransfer is that the cells should only be electroporated reversibly, and not irreversibly. Parameterization and optimization of needle electrode positions and potentials were used to determine the optimal parameters for exposing as much muscle volume as possible to electric fields above the reversible threshold and at the same time as little as possible to fields above the irreversible threshold (in order to achieve efficient gene expression). Muscle tissue properties and geometry were taken from a previous study [Corovic et al., submitted for publication] (see the Methods section 2.4). Two different needle arrays were used: one needle electrode pair and three needle electrode pairs (Figure 11). Both parameterization and optimization used the following fitness function to evaluate the solution quality:

$$F = \left\{ \begin{matrix} 0 \, , \ if & V_{irr} > 1 cm^3 \,|\, I_{tot} > 30A \\ V_{rev} - V_{irr}, & otherwise \end{matrix} \right\} \, ,$$

where V_{rev} is the volume of reversibly electroporated muscle tissue and V_{irr} the volume of irreversibly electroporated muscle tissue. The fitness function evaluates the volume of muscle tissue exposed to an electric field between the reversible and irreversible electroporation threshold, where gene electrotransfer can occur. By adding the constraints for volume of irreversibly electroporated tissue and total current, extensive damage to muscle tissue is avoided and compliance with electric pulse generator limitations guaranteed.

3.5.1 Isotropic vs. anisotropic tissue properties

We first compared the electric field distribution between models using isotropic and anisotropic muscle tissue properties. Using anisotropic conductivities resulted in a much more heterogeneous electric field distribution (Figure 31), with less tissue reversibly electroporated than when using isotropic properties. Due to the obvious differences between using isotropic and anisotropic properties, it is clear that anisotropic properties have to be taken into account when modeling electric field distribution together with different electroporation thresholds in the parallel and perpendicular direction with respect to muscle fibers.
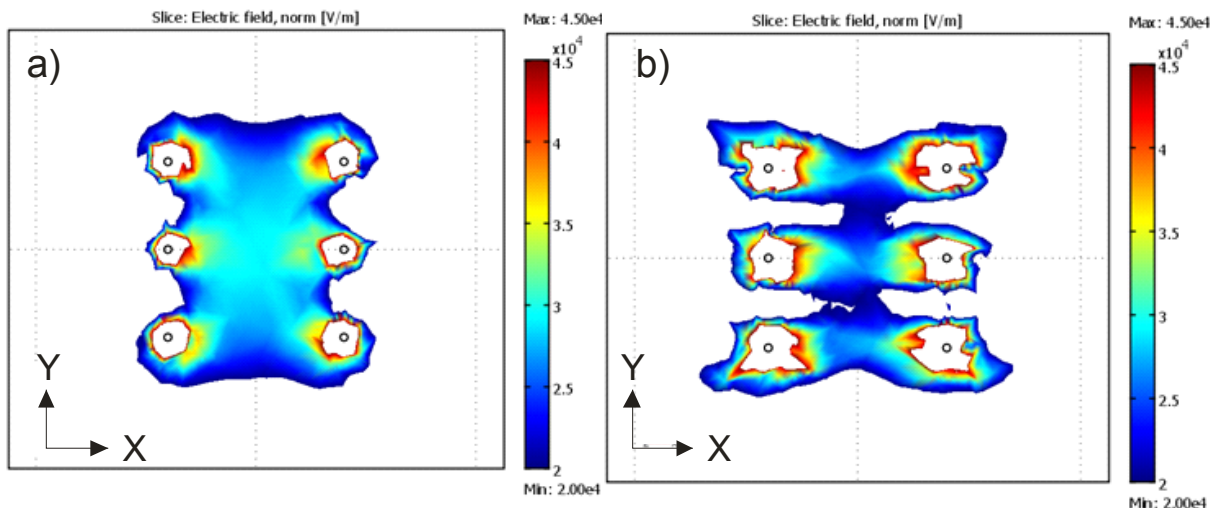
Figure 31. Electric field distribution in the muscle for a) isotropic conductivity (0.135 S/m) and b) anisotropic conductivity (0.135 S/m perpendicular to muscle fibers – y, z direction – and 0.75 S/m parallel to muscle fibers – x direction). Identical conditions were used in both models: U/d = 600 V/1.6 cm, depth of electrode insertion 3 cm. The electric field is presented in a plane perpendicular to electrode insertion in the depth of 2 cm.

3.5.2 Static vs. sequential models of electroporation

Sequential models of electroporation were first designed to mimic the process of electroporation of the skin and underlying tissues, which static models could not achieve. However, calculation of sequential models takes at least five times longer than that of static models. Furthermore, sequential models built in Comsol require well-defined geometric objects to work properly. It is not possible to use them if the model geometry is built using the

voxel import method. By comparing the results of static and sequential models (for three needle electrode pairs) in muscle electroporation, it was possible to quantify the difference between the predicted volumes of muscle tissue exposed to electric fields above the electroporation thresholds. The final electric field distribution in the sequential model (Figure 32a) and the one obtained from the static model (Figure 31) were not very different. The sequential model predicted values that were on average 1.26 ± 0.25 times higher than in the static model for three needle electrode pairs.
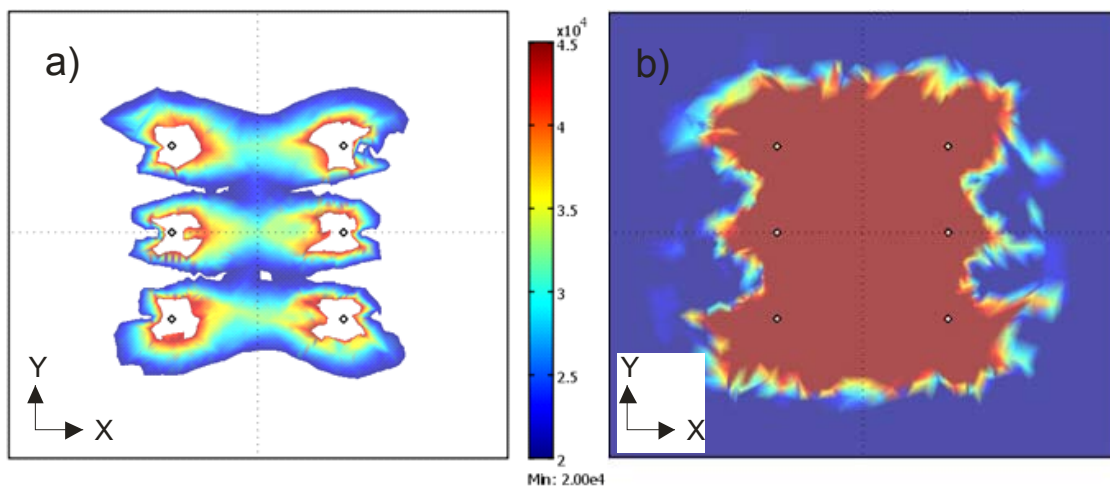
Figure 32. a) Electric field distribution in the muscle after the final step of the sequential model. The scale is in V/m. Identical conditions as in Figure 31 were used. b) Muscle area where electrical conductivity has changed during electroporation (in red).

The differences were much greater with respect to the evaluation of the total electric current flowing through the model. Here the sequential model compared to the static model predicted values for three needle electrode pairs that were 2.45 ± 0.55 times higher on average. The volume of electroporated tissue can also be evaluated by looking at the volume in which conductivity has changed during electroporation (Figure 32b). In fact, according to electroporation theory, this should be a more accurate predictor of electroporation than the electric field after the final step in the sequential model. In the parameterization, volumes of electroporated tissue evaluated by changes in conductivity were 1.15 ± 0.14 times higher than values evaluated by the electric field.

3.5.3 Guidelines for EGT into muscle tissue

In the parameterization, the effects of distance between electrodes, depth of insertion, angle of the electric field with respect to muscle fiber orientation and voltage between the electrodes on the volume of muscle exposed to electric fields above the reversible electroporation threshold were studied, since this is crucial for efficient gene electrotransfer. The maximum values of the fitness function for each of the parameters are presented in Figures 33 and 34.
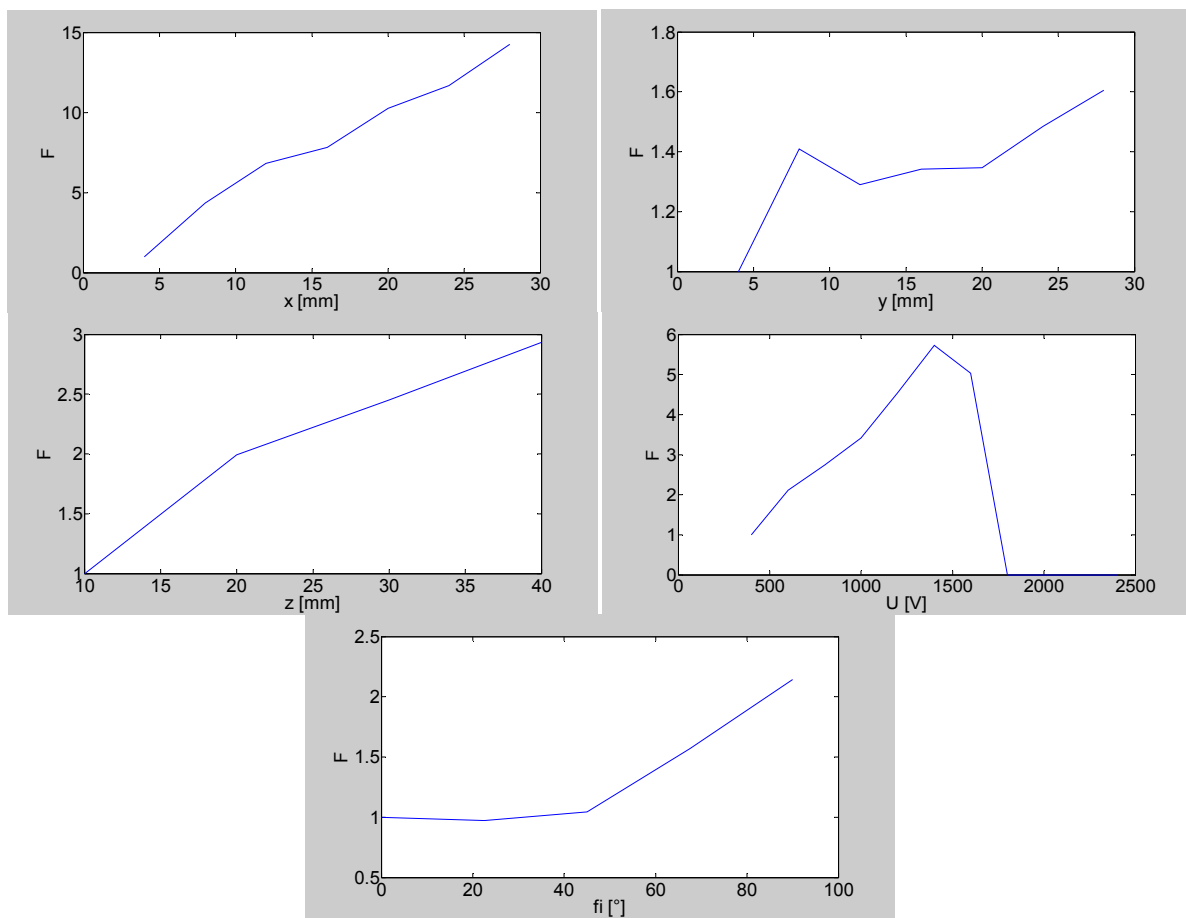
Figure 33. Maximum values of obtained fitness functions depending on the distance between electrodes (*x, y*), depth of electrode insertion (*z*), voltage between the electrode rows (*U*) and angle of electric field with respect to muscle fiber orientation (*fi*) for three needle electrode pairs. Fitness function values are normalized to the first maximum value obtained for that parameter (e.g. the maximum fitness function calculated for 400 V was used to normalize maximum fitness functions calculated for other voltages). The sequential model was used for all calculations.

As expected, increasing the distance between electrodes or their insertion depths increases the average fitness function. The results for the angle between electric field and muscle fiber orientation were somewhat ambiguous: for three needle electrode pairs, the

perpendicular orientation gave better results than other orientations, while for one needle electrode pair, the parallel orientation gave the best results (although the difference between perpendicular and parallel orientation was only 10 %). For three needle electrode pairs, the highest fitness functions were calculated for voltages of 1400 V, while in the case of voltages above 1800 V, the current and electroporated volume constraints were always violated, and the fitness function was therefore always evaluated as 0 (Figure 33). Similar results were obtained for one needle electrode pair; only the peaks were moved slightly towards higher voltages.
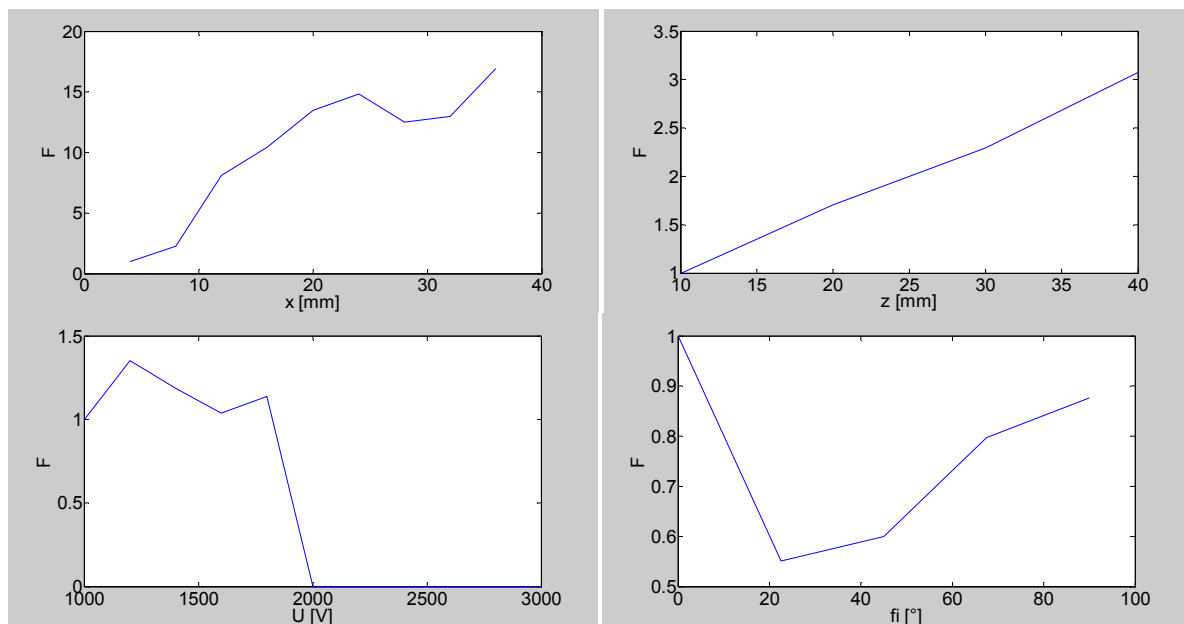
Figure 34. Maximum values of obtained fitness functions depending on the distance between electrodes (*x*), depth of electrode insertion (*z*), voltage between the electrode rows (*U*) and angle of electric field with respect to muscle fiber orientation (*fi*) for one needle electrode pair (see Figure 33 for other details).

The maximum values of the fitness function were obtained for the following parameters: $x = 28$ mm, $y = 28$ mm, $z = 40$ mm, $U = 1400$ V, $\varphi = 90\,°$ for three needle electrode pairs and $x = 36$ mm, $z = 40$ mm, $U = 1200$ V, $\varphi = 0\,°$ for one needle electrode pair (Figures 35 and 36). The optimal parameters resulted in 79.1 cm^3 of muscle tissue being reversibly electroporated when using three needle electrode pairs, and 28.9 cm^3 when using one needle electrode pair.
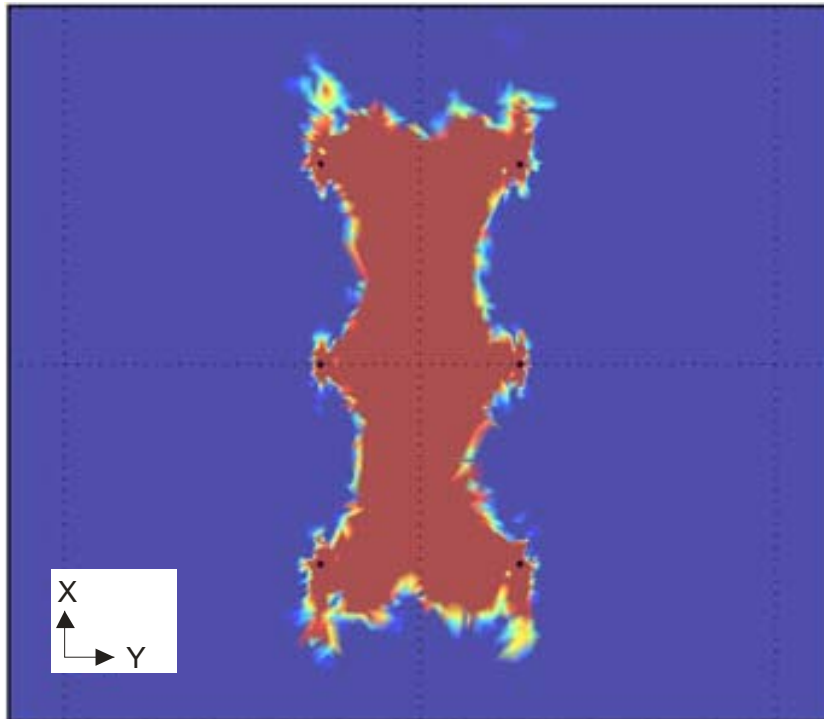
Figure 35. Electric field above the reversible threshold (in red) in the muscle for the optimal parameters determined by the parameterization – three needle electrode pairs. The field is shown at the depth of 2 cm perpendicular to electrode insertion.
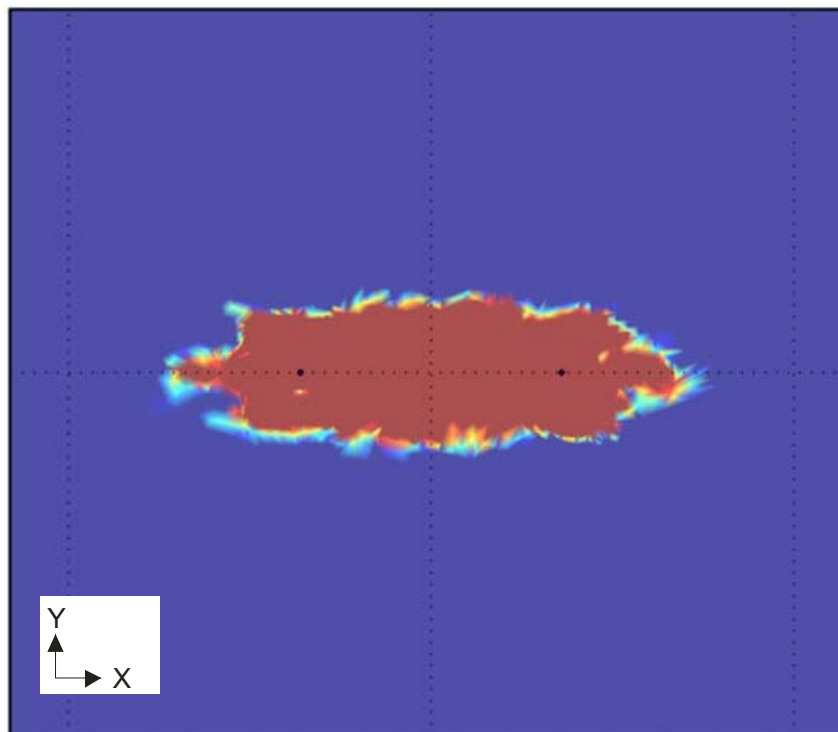
Figure 36. Electric field above the reversible threshold (in red) in the muscle for the optimal parameters determined by the parameterization – one needle electrode pair. The field is shown at the depth of 2 cm perpendicular to electrode insertion.

3.5.4 Optimization of EGT

Optimization was only carried out for the sequential model of electroporation with three needle electrode pairs, and the optimum solution determined by the algorithm matched the optimum found by the parameterization study (Figure 35). The optimization algorithm took 3 hours to determine the optimum, while the parameterization had to run for 2 days and 9 hours.

3.6 Treatment planning for electrochemotherapy of a deep-seated tumor – ECT

(articles IV,V)

Complete treatment planning was carried out for electrochemotherapy of a melanoma metastasis seated in the thigh of a patient – the first case of electrochemotherapy of a deep-seated tumor in the world. A 3D geometry was built based on computer tomography images (Figure 5) of the region of interest. The static model of electroporation was used to determine the optimum electrode positions and voltages between the electrodes, and the sequential model of electroporation was used to determine the total current. Optimization was performed with the genetic algorithm presented in previous sections, with the following fitness function:

$$F = 100V_{Trev} - 10V_{Hirr},$$

where V_{Trev} and V_{Hirr} are the tumor volume exposed to electric fields above the reversible threshold and healthy tissue volume exposed to electric fields above the irreversible threshold respectively. As the treated tumor was too big to allow for good electric field coverage with a single set of electric pulses, a sequence of pulses was used instead, with each set of pulses applied between different electrodes (see Figure 38). The following parameter constraints were used in the optimization: electrodes could only be positioned outside the tumor (except for the center electrode – Figure 37) and the maximum acceptable potential on the electrodes was 3000 V (technical limitation of the electric pulse generator Cliniporator Vitae™).

The resulting treatment plan was used in electrochemotherapy of the deep-seated tumor and tumor growth was followed. After obtaining data of the actual parameters used (that differed somewhat from the proposed treatment plan), the electric field distribution in the tumor was reevaluated. Finally, a robustness analysis of treatment planning was carried

out to determine the most important factors that influence the quality of the treatment in clinical electrochemotherapy.

3.6.1 Treatment plan

(article IV)

Treatment planning was carried out for two different electrode configurations; the geometry of the model can be seen in Figure 5. The first configuration was with five electrodes, with the central electrode inserted in the tumor and the other four electrodes distributed around the tumor, while the second configuration was with four electrodes outside the tumor (Figure 37). Results of the optimization were electrode positions and minimum voltages for each needle electrode pair (Table 7). In case of four electrodes, 18 parameters were optimized (x, y, z coordinate of each electrode, and voltage between each needle electrode pair), while in the case of five electrodes, 21 parameters were optimized for (for the center electrode, x, y were set at the tumor center).

Table 7. Distances between electrodes and voltages between electrodes for the treatment plan with 4 electrodes and the treatment plan with 5 electrodes.

4 electrodes	Distance [mm]	Voltage [V]	5 electrodes	Distance [mm]	Voltage [V]
1-2	14	2000	1-2	14	2000
1-3	16	2700	1-3	17	2500
1-4	21	3000	2-4	13	2500
2-3	22	2900	3-4	17	2000
2-4	16	2700	1-5	10	1700
3-4	15	2000	2-5	10	1700
			3-5	10	1700
			4-5	12	1700

The predicted electric currents were all below the limit of 50 A (Cliniporator Vitae[TM]). Electrode positions outside the tumor were similar in both configurations, i.e. very close to the tumor surface; however the fifth electrode inside the tumor significantly reduced the required voltage to achieve efficient membrane electroporation of cells in the whole tumor, thereby reducing damage to healthy tissue. Maximum voltages required were 3000 V and 2500 V in the four and five electrode configuration respectively. The volume of irreversibly permeabilized tissue according to treatment plan was 13.8 cm^3 (of that 11.5 cm^3 adipose tissue

and 2.33 cm^3 muscle tissue) in the four electrode configuration and 12.3 cm^3 (of that 10.4 cm^3 adipose tissue and 1.88 cm^3 muscle tissue) in the five electrode configuration. Insertion depth was a few millimeters deeper than the tumor, slightly penetrating the muscle tissue. Tumor coverage by successive electric pulses is shown in Figure 38. Although the treatment plan with 5 electrodes was assessed as the better of the two, insertion of the central electrode into the tumor proved difficult during the electrochemotherapy treatment, therefore the 4 electrode treatment plan was adopted.
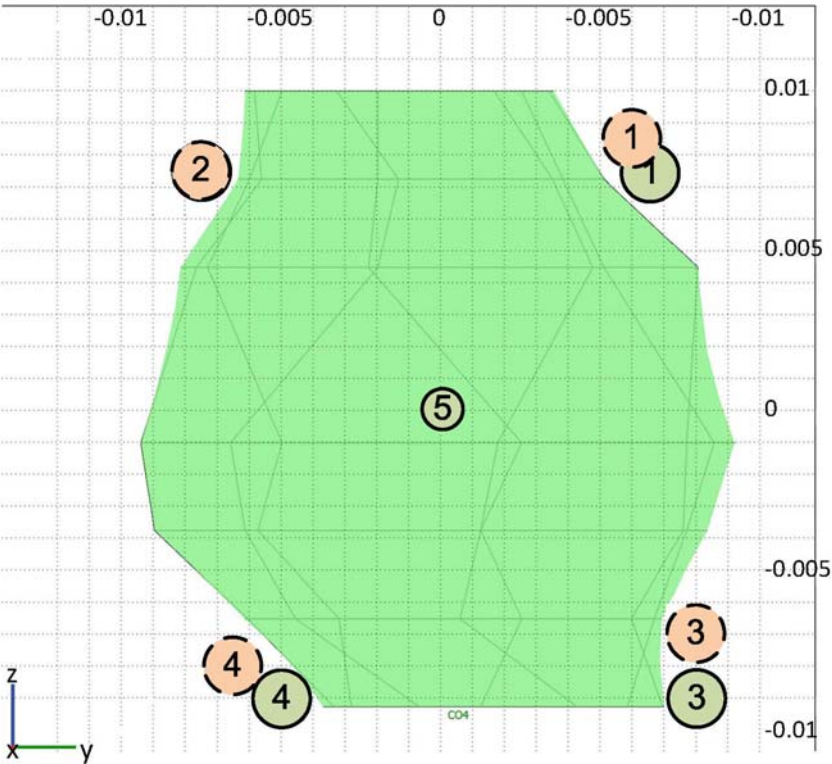
Figure 37. Electrode positions according to treatment plan. Electrode positions for four (dashed line circles) and five (solid line circles) electrodes are shown. The presented tumor cross-section is a parallel projection of the tumor on a plane parallel to the skin surface. The optimal position of electrode 2 was determined to be the same by both treatment plans.
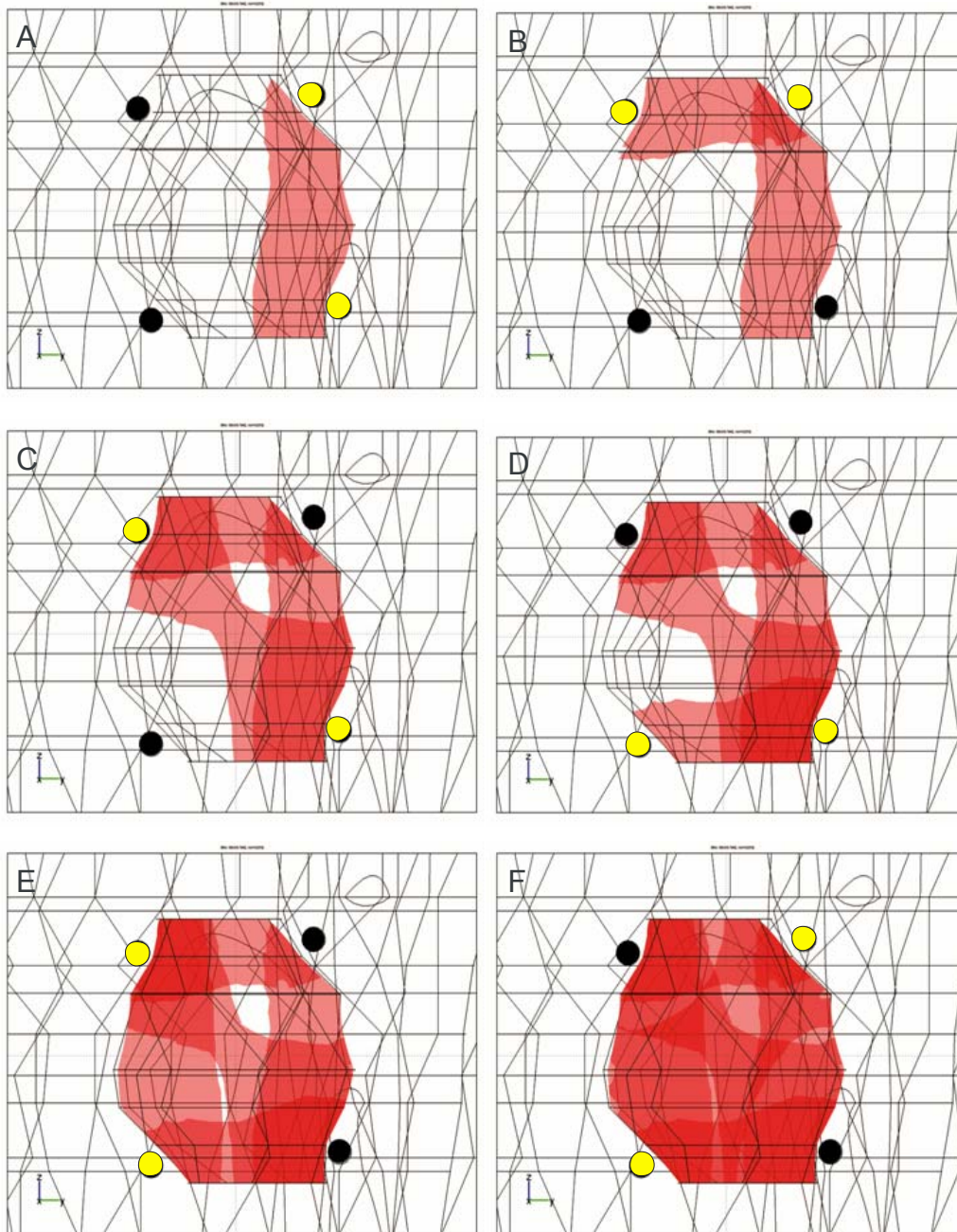
Figure 38. Coverage of the tumor by an electric field above the reversible threshold by successive pulses delivered between different active electrodes (yellow circles). Some parts of the tumor are covered by more than one electric pulse (dark red), while others are only covered by a single electric pulse (pink). The presented tumor cross-section is a parallel projection of the tumor on a plane parallel to the skin surface.

3.6.2 Treatment results

(article IV)

The patient reported no discomfort after the treatment and left the hospital after 2 days. The response to the treatment with electrochemotherapy was followed ultrasonographically by experts at the Institute of Oncology Ljubljana (Figure 39). The first post-operative ultrasound showed a substantial decrease in tumor volume (more than 50 %), while the second showed a regrowth of tumor tissue. In February 2009, i.e. 52 days after electrochemotherapy was performed, the metastasis was excised.
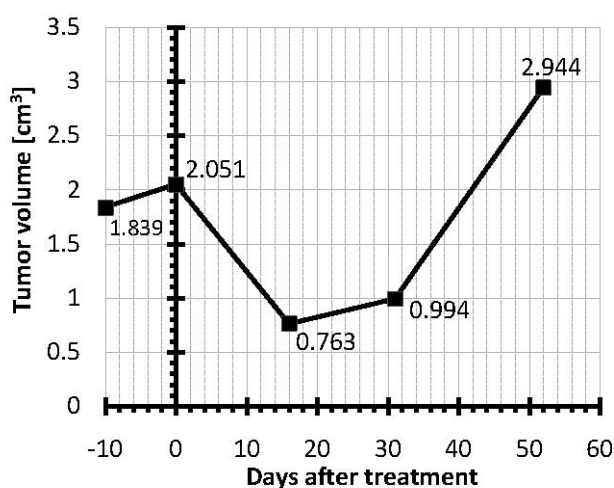
Figure 39. The figure shows tumor size 10 days before the treatment, at the time of the treatment itself and during the follow-up as determined by ultrasound measurements. Regrowth of the tumor was observed at day 31 and the tumor was excised at day 52.

Histologically, the metastasis showed partial necrosis, estimated to represent 40–50 % of the tumor. It was, however, not possible to discriminate between spontaneous and induced necrosis. However, there was indirect evidence of the electrochemotherapeutic effect; i.e. the presence of fat necrosis and obliterated blood vessels in the tissue around the tumor (Figure 40). These observations would not be expected in a fast-growing untreated metastasis.
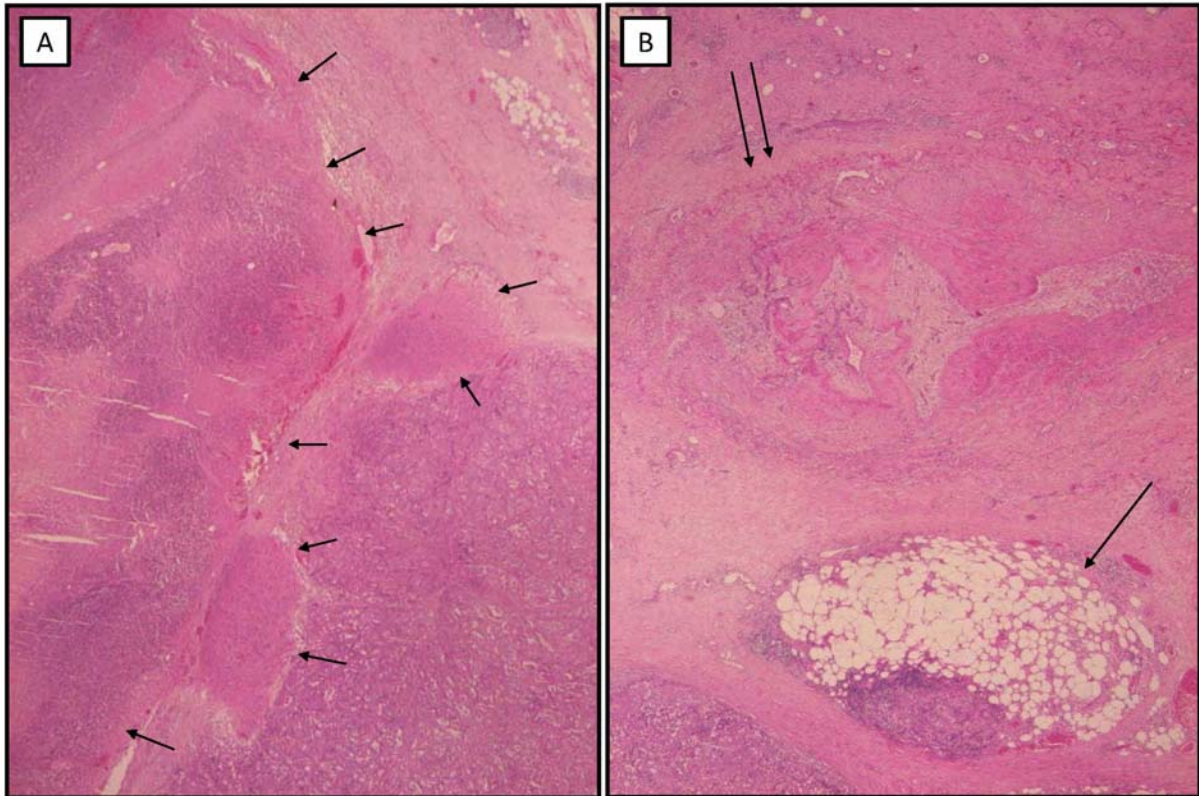
Figure 40. Histology of melanoma metastasis treated by electrochemotherapy. The tumor (A) shows partial necrosis (short arrows). In the surrounding tissue (B), fat necrosis (long arrow) and obliterated blood vessels (double arrow) are visible (H&E, original magnification 20x).

3.6.3 Reexamination of the treatment plan
(article IV)

After the treatment, the geometry of the numerical model was updated according to the measurements taken during the operating procedure and photographic documentation of the treatment. Specifically, the four electrode positions in the model were changed according to these measurements (Figure 41).

We compared the maximum value of electric current measured by Cliniporator Vitae during electric pulse delivery to the current predicted by the numerical model. Good agreement was obtained between measurements and calculations, as presented in Table 8. Finally, tumor coverage with an electric field above reversible threshold was recalculated using the electrode positions used in the actual electrochemotherapy treatment, and the volume of reversibly permeabilized tumor was determined to be approximately 94 % (Figure 42), enough for some tumor cells to survive and the tumor to begin regrowing.
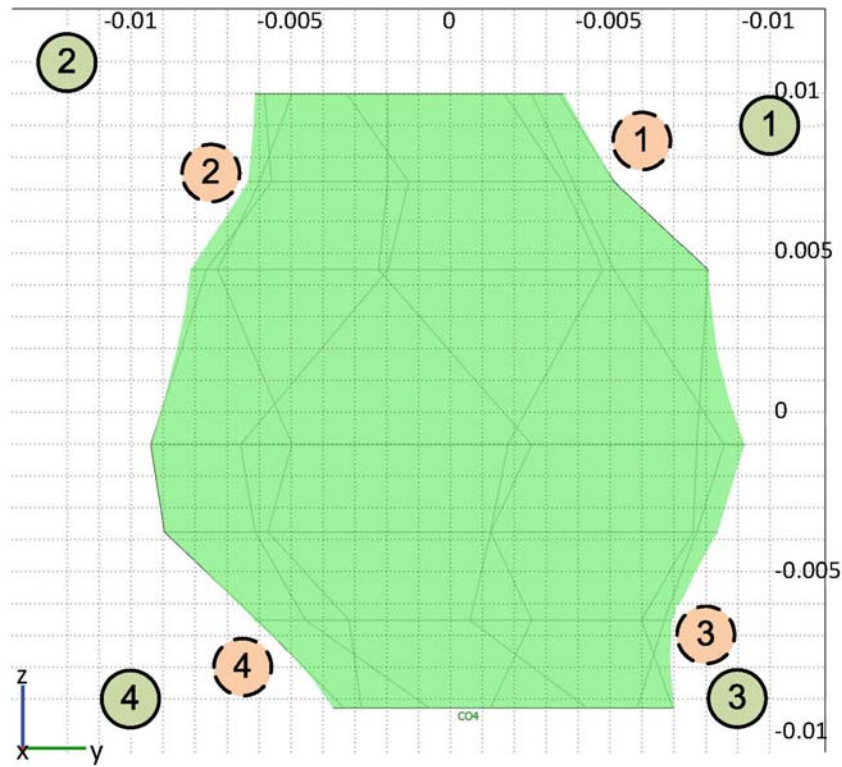
Figure 41. Electrode positions according to treatment plan (dashed orange circles) and actual electrode positions during treatment as determined by ultrasonography and photographic documentation (solid green circles). The tumor cross-section shown is a parallel projection of the tumor on a plane parallel to the skin surface.

Table 8. Agreement between electrical currents measured during delivery and steady-state current calculated in the numerical model.

Electrode pair	Measured current [A]	Calculated current [A]	Error [%]
1-2	16	16.2	1
1-3	18	17.3	–4
1-4	10	9.5	–5
2-3	19	17.2	–9
2-4	9	8.4	–7
3-4	9	8.0	–11
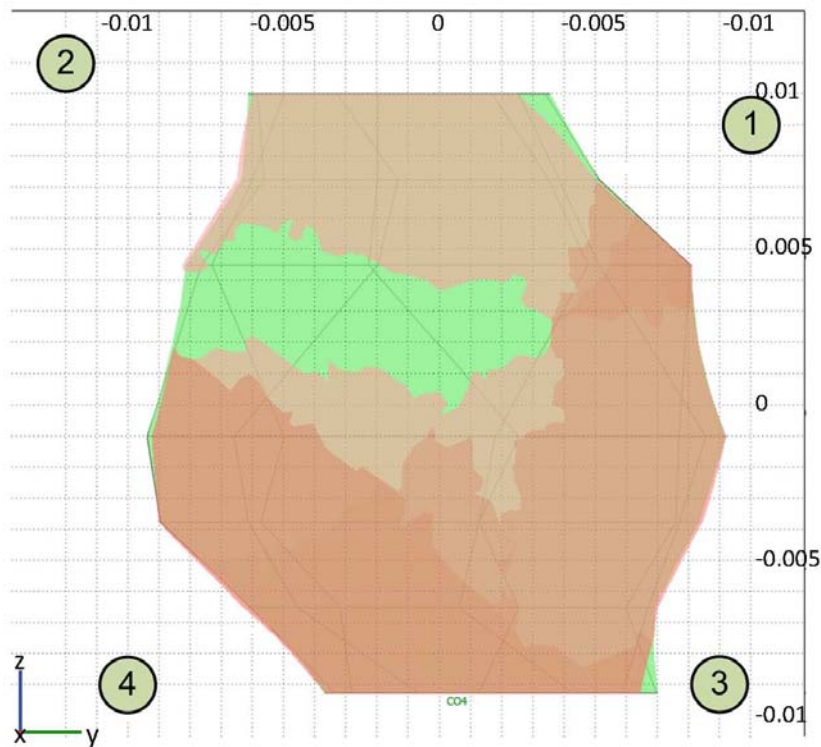
Figure 42. Numerical prediction of reversible electroporation of the tumor after the application of all electric pulses in a plane parallel to the skin surface, passing through the centre of the tumor. Green color represents tumor tissue that was not electroporated, while shades of brown represent tissue electroporated by one or more pulse sequences (from lighter to darker shade).

3.6.4 Robustness analysis

(article V)

Robustness analysis showed that decreasing the voltage on a single needle electrode pair by 300 V does not affect tumor coverage at all (Figure 43), while decreasing the voltage by 500 V causes a small volume (ranging from 0.05 to 0.2 %) to be below the threshold. This can be explained by the fact that most of the tumor volume is covered by more than a single a pair of electrodes (Figure 43). Therefore, an effectiveness decrease in a single needle electrode pair does not affect the end result as dramatically as might be expected.
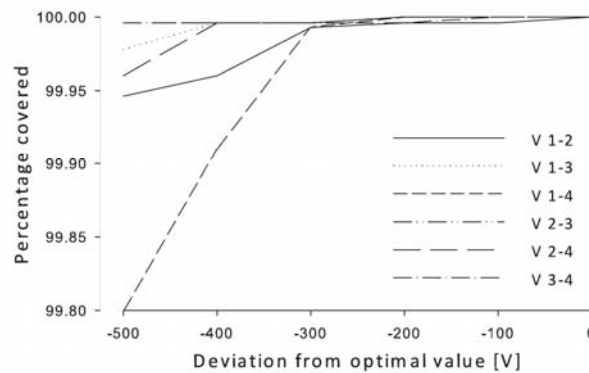
Figure 43. Robustness analysis – dependence of tumor coverage with an electric field above the reversible electroporation threshold on different parameters. Effect of reducing voltage on a single needle electrode pair in steps of 100 V. See Table 8 and Figure 42 for details on electrode pairs and voltages between them.

The biggest drop in tumor coverage was observed when the tumor reversible electroporation threshold was increased (Figure 44A) – increasing the threshold from 400 V/cm to 650 V/cm reduced tumor coverage to 45 %. The ratio of conductivities between the tumor and surrounding tissue (in this case adipose) was also determined to be an important factor (Figure 44B). When the conductivity of adipose tissue is lowered or, alternatively, the conductivity of the tumor is increased, the ratio of $\sigma_{TUMOR}/ \sigma_{FAT}$ increases and the treatment effectiveness is reduced significantly. If this ratio is changed from 10 as in the original treatment plan to 20, tumor coverage is reduced to 85 %. Electrode positions are also a critical parameter (Figure 44C,D), as electrode insertion is the part of the procedure most prone to errors. Mispositioning a single electrode by 2 mm can already reduce tumor coverage from 100 % to less than 97 %. However, if all electrodes miss their target, the results are affected greatly. When all electrodes are moved away from the tumor diagonally by 0.7 or 1.4 mm (effectively increasing the distance between the electrodes and the distance between the electrodes and the tumor), the tumor coverage decreases to 87 or 66 % respectively. The depth of insertion is important as well, although we assumed at this point that all electrodes were positioned at the same depth. Since the active surface of the electrodes is only 3 cm in length (size chosen to be comparable with tumor size) and the rest of the electrode length is insulated, inserting them either too deep or too shallow can decrease tumor coverage, e.g. by 6 % when electrodes are inserted 5 mm too deep (Figure 44D).
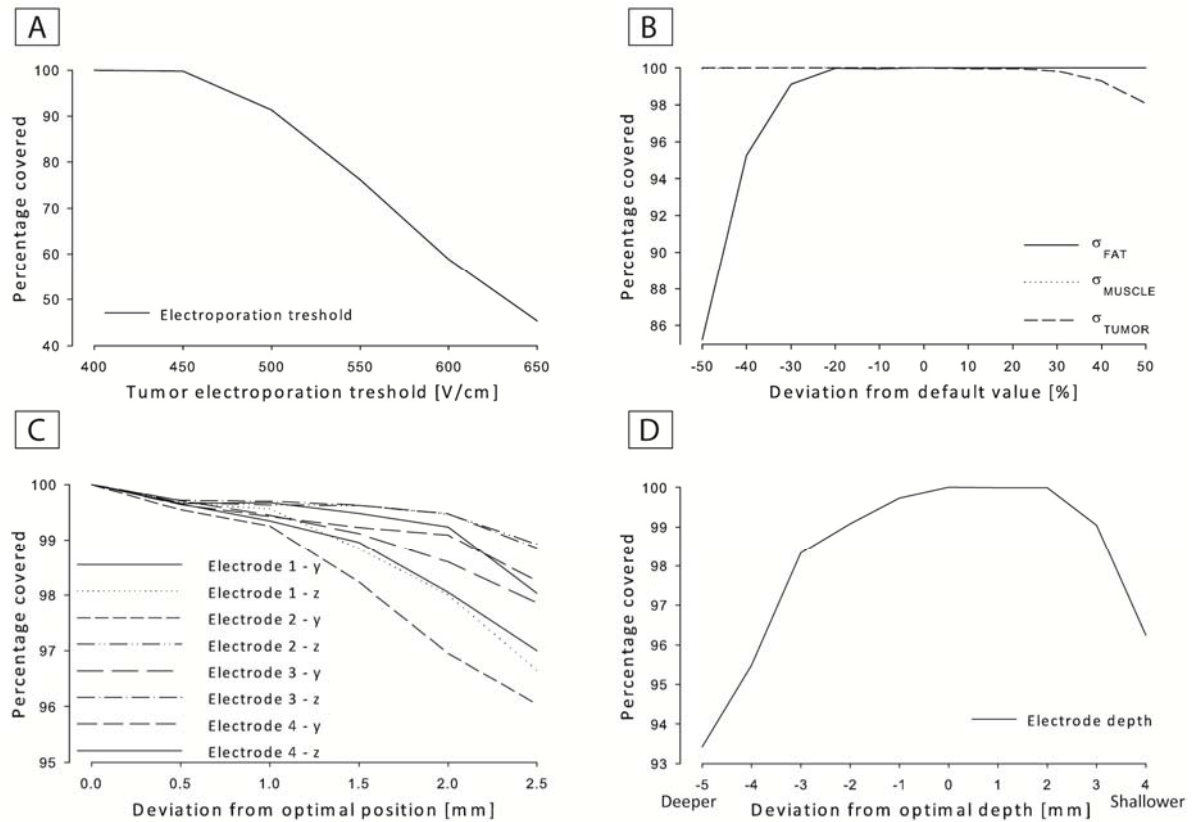
Figure 44. Robustness analysis – dependence of tumor coverage with an electric field above the reversible electroporation threshold on different parameters. A) Effect of deviations of tumor electroporation threshold in steps of 50 V/cm. B) Effect of deviations of tissue conductivities from values used in treatment planning in steps of 10 % of the values used. C) Effect of errors in electrode positions along a single axis in steps of 0.5 mm away from tumor surface. D) Dependence on depth of insertion of all electrodes. Note that the plots do not share the same vertical scale.

3.7 Electric field distribution in a subcutaneous tumor - ECT, IRE, EGT

In previous sections numerical models of electroporation were used to optimize the electrode positions and voltages between electrodes for electrochemotherapy, tissue ablation by irreversible electroporation or gene electrotransfer. In all optimization cases the same numerical models of electroporation (i.e. static or sequential) and the same optimization algorithm (genetic algorithm) were used; the main difference between the optimization was the choice of the fitness function. For electrochemotherapy (at least) reversible electroporation of the target tissue was sought, for tissue ablation irreversible electroporation of the target tissue and for gene electrotransfer reversible electroporation without irreversible

electroporation. In this section we analyzed, how the choice of fitness function affects the calculated optimum and whether it is possible to obtain reliably different results for electrochemotherapy, tissue ablation with irreversible electroporation and gene electrotransfer by choosing appropriate fitness function weights.

We used the same geometry as in sections 3.2 and 3.4 (see Figure 21): a realistic tumor in the vicinity of a critical tissue. The optimization parameters were the positions of six individual electrodes and the electric potential on each electrode. Nine different fitness functions were arbitrarily set (F_{1-3} for electrochemotherapy, F_{4-6} for tissue ablation with irreversible electroporation and F_{7-9} for gene electrotransfer):

$$F_1 = 100000V_{Trev} - 10V_{Tirr} - 50000V_{Cirr} - 10V_{Hirr}$$
$$F_2 = 100000V_{Trev} - 10V_{Tirr} - 200V_{Cirr} - 10V_{Hirr}$$
$$F_3 = 100000V_{Trev} - 10V_{Cirr} - 10V_{Hirr}$$

$$F_4 = 100000V_{Tirr} - 50000V_{Cirr} - 2V_{Hirr}$$
$$F_5 = 100000V_{Tirr} - 200V_{Cirr} - 2V_{Hirr}$$
$$F_6 = 100000V_{Tirr} - 10V_{Cirr} - 10V_{Hirr}$$

$$F_7 = 100000V_{Trev} - 50000V_{Tirr} - 50000V_{Cirr} - 10V_{Hirr}$$
$$F_8 = 100000V_{Trev} - 50000V_{Tirr} - 200V_{Cirr} - 10V_{Hirr}$$
$$F_9 = 100000V_{Trev} - 200V_{Tirr} - 10V_{Cirr} - 10V_{Hirr}$$

where V_{Trev} and V_{Tirr} are tumor volume exposed to electric fields over the reversible electroporation threshold and over the irreversible threshold, respectively, and V_{Cirr} and V_{Hirr} are volumes of critical tissue and healthy tissue exposed to electric fields over the irreversible electroporation threshold, respectively. All optimization runs were terminated after 200 iterations and took approximately 2 hours each.

3.7.1 Fitness function analysis

Using different fitness functions in the optimization algorithm resulted in different solutions (Table 9, Figure 44), with the in group variability being much lower than the between group variability – i.e. the difference between the solution obtained by different electrochemotherapy fitness functions (F_{1-3}) was much smaller than the difference between the electrochemotherapy and e.g. the tissue ablation solutions (F_{4-6}). The main differences between the groups were in the two most important fitness function factors: reversible electroporation was achieved in the tumor for electrochemotherapy and gene electrotransfer, while irreversible electroporation was achieved for tissue ablation. As the second most important parameters for gene electrotransfer was V_{Tirr}, very little irreversible electroporation was achieved in the tumor compared to electrochemotherapy (Figure 45a,c). In turn, the second most important parameters for electrochemotherapy V_{Cirr} caused that the electric field in the critical tissue to be below the irreversible threshold (Figure 45a). Since V_{Hirr} was not an important factor in any of the fitness functions, it was expected that tissue ablation solutions would cause the most healthy tissue damage, since tissue ablation requires the highest electric fields.

Table 9. Optimization results for different fitness functions are presented as volumes of reversibly and irreversibly electroporated tissues (see fitness function equations above) and the average electrode distance from the center of the tumor (R).

	Fitness function	F	V_{Trev} [%]	V_{Tirr} [%]	V_{Cirr} [%]	V_{Hirr} [mm^3]	R [mm]
ECT	F_1	99994.34	100	48.9	0	76.7	23.4
	F_2	99998.76	100	7.5	0	48.7	23.2
	F_3	99999.41	100	30.8	0	59.3	22.8
IRE	F_4	99449.79	100	100	1.1	103.6	22.8
	F_5	99998.23	100	100	0.4	135.9	22.1
	F_6	99998.72	100	100	2.1	106.6	22.0
EGT	F_7	99999.40	100	0	0	60.0	25.3
	F_8	99899.08	100	0.2	0.2	52.5	25.7
	F_9	99985.40	100	6.9	1.9	60.7	24.3

The optimum electrode positions between the solutions are all very similar, only the positions of electrodes for gene electrotransfer are somewhat further away from the tumor than for the other two applications (Table 9). This is most likely due to V_{Tirr} being a strong negative factor in the gene electrotransfer fitness functions; the electrodes had to be positioned away from the tumor in order not to cause too much irreversible electroporation inside the tumor, however they may cause irreversible electroporation inside healthy tissue.
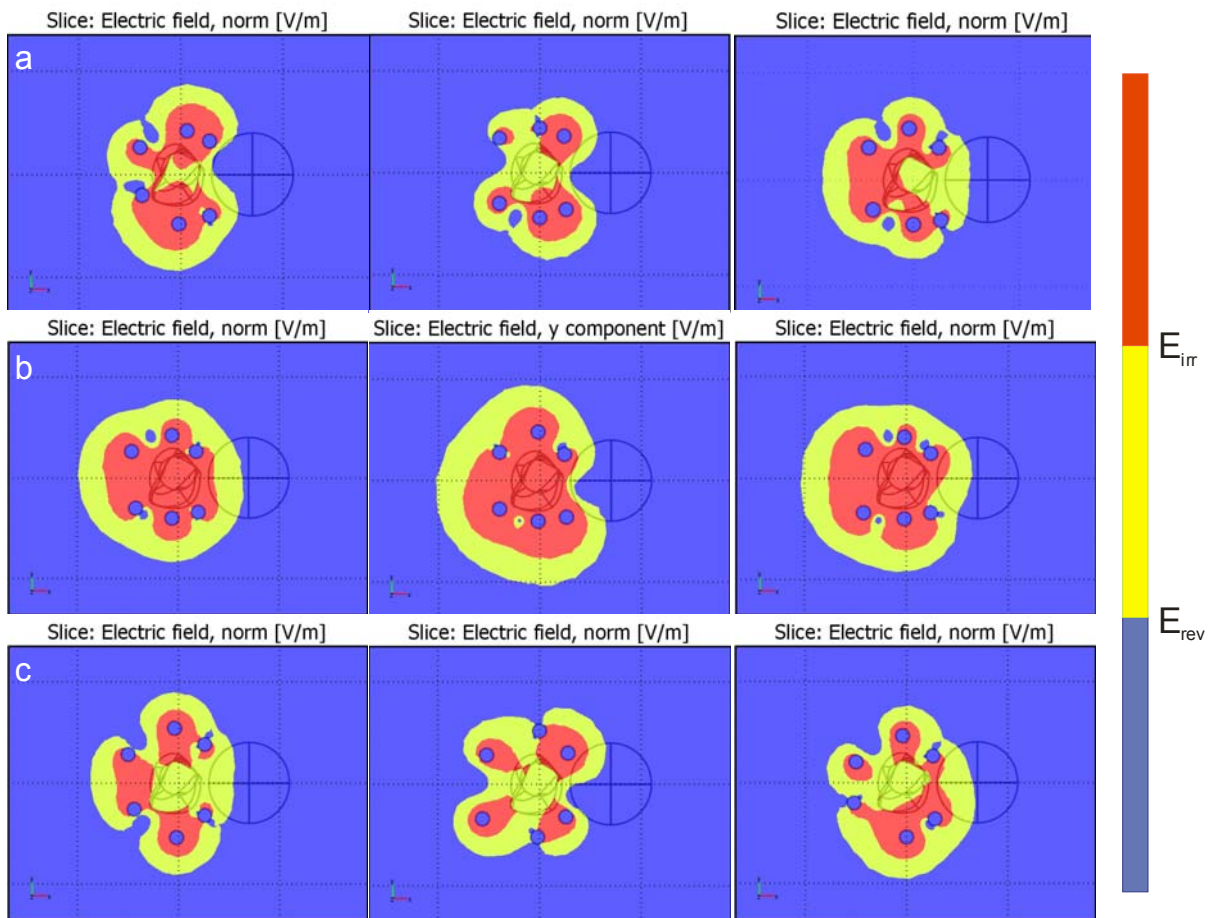
Figure 45. Local electric field distribution obtained treatment plan with six individual needle electrodes is shown in the XY plane through the center of the tumor for a) electrochemotherapy (F_{1-3}), b) tissue ablation with irreversible electroporation (F_{4-6}) and c) gene electrotransfer (F_{7-9}). The electric field is presented as three separated regions, blue: the electric field is under the reversible electroporation threshold; yellow: the electric field is between the reversible and irreversible threshold and red: the electric field is above the irreversible electroporation threshold.

In the electrochemotherapy fitness functions the importance of avoiding electric fields over the irreversible electroporation threshold in the critical tissue decreased from F_1 to F_3. This did not seem to affect the outcome, since critical tissue was successfully sparred in all three cases. There were big differences in the volume of irreversibly electroporated tumor tissue between the three cases, however V_{Tirr} was not an important factor in the fitness function, therefore this was most probably caused by the stochastic nature of the genetic algorithm.

In the tissue ablation by irreversible electroporation fitness functions the importance electric fields over the irreversible electroporation threshold also decreased from F_4 to F_6.

Again, this did not affect the outcome, however this was mostly caused by a relatively bad solution obtained for F_4 that was much worse than the solution for F_5 (Table 9). On the other hand, F_6 did cause the biggest volume of critical tissue damage, as was expected.

In the gene electrotransfer fitness functions the importance of avoiding electric fields over the irreversible electroporation threshold in the tumor and the critical tissue decreased from F_7 to F_9. The optimization results matched the fitness functions, with F_7 causing the least damage to tumor and critical tissue and F_9 the most damage.

The results show that the highest weight factor in the fitness functions effects the optimized solutions the most, followed by the second and third highest weights factors. If factors carry the same weights (as in F_{1-3}, F_6, F_7 and F_9) the conflict between the factors and the otherwise highest weight factor decide how they will affect the optimized solution. For instance, in F_6 the weights of both V_{Cirr} and V_{Hirr} are set to -10, but a lot less critical tissue is exposed to electric fields above the irreversible threshold, since it is easier to avoid damage to the critical tissue than to the healthy tissue, while keeping the target tissue exposed to electric field above the irreversible threshold. This suggests that it is possible to obtain adequate results in the optimization by setting the fitness function weights.

4.   DISCUSSION

The goal of the present doctoral dissertation was to use numerical modeling and optimization techniques to provide guidelines and tools to determine the appropriate parameters for optimal electroporation for three electroporation-based treatments: electrochemotherapy, tissue ablation with irreversible electroporation, and gene electrotransfer for gene therapy and gene vaccination. We developed a treatment planning procedure that provides for the acquisition of data from medical images and their conversion into 3D geometries, calculation of electric field distribution in these geometries and finally optimization of the electrode positions and voltages between the electrodes to best suit each of the electroporation-based treatments. For building the 3D geometry from medical images we analyzed and improved existing methodologies – the planar contour method and voxel import method [Valic, 2006; Astrom et al., 2009] (see 2.1 Building a 3D geometry from medical images for details). For the numerical modeling we used static and sequential finite element electroporation models [Miklavcic et al., 2000; Pavselj et al., 2005] (see 2.2 Numerical modeling for details) and for the optimization we chose the genetic algorithm that is often used in radiotherapy treatment planning [Wu and Zhu, 2001; Bevilacqua et al., 2007] (see 2.3 Optimization for details). Since the requirements of a treatment planning procedure are ease of use, efficiency, and robustness, many details of the procedure had to be considered. In this section these details are discussed in the same order as their analysis was presented in the Results section.

4.1 Electric field distribution in a subcutaneous tumor – ECT
(articles I, II)

We first tested the geometry building, numerical models and optimization algorithm on a 3D model of a subcutaneous tumor for electrochemotherapy with needle electrodes. Similar modeling has already been performed in 2D and our results could thereby be easily validated [Corovic et al, 2007]. In section 3.1 needle electrode arrays that have been used in experimental and clinical electrochemotherapy of subcutaneous tumors in recent years were compared. By examining the results of numerical modeling in 3D and optimization of electroporation parameters, we determined that rows of needle electrodes (three pairs and four pairs) produce better results than hexagonal electrode arrays. The results agree well with

previous 2D studies [Dev et al, 2003; Corovic et al, 2007], however we did not take into account that electric pulses can be delivered in series between different electrodes in an array, which was shown to effect both the extent of electroporation and the electric field distribution [Sersa et al, 1996; Gilbert et al, 1997]. If this would have been taken into account, the hexagonal electrodes would most probably be more positively evaluated. Regardless of the needle electrode arrays used, we determined that positioning the electrodes around the tumor in all dimensions provides the best electric field distribution (Figure 20).

Optimization with the genetic algorithm (three parameters were optimized: distance between electrodes in the array, depth of electrode insertion, and the voltage of applied electric pulses) always (each optimization was run 50 times) resulted in complete coverage of the tumor, regardless of the needle electrode array or tumor geometry used. Although the time at which the algorithm reached the best solution was different in each run, and the solutions reached in individual runs did not match each other perfectly, a good solution was reached in a given number of iterations in all runs (Figure 19). This suggests that the designed optimization algorithm was very robust.

4.2 Electric field distribution in a subcutaneous tumor – IRE

(article III)

In section 3.2 we tested the treatment planning procedure for tissue ablation with irreversible electroporation, the most recent electroporation-based treatment [Rubinsky, 2007]. The same geometry as in section 3.1 was used, while the number of optimization parameters was increased to six for three needle electrode pairs and to 19 for six individual electrodes. Also, a critical tissue, whose integrity was very important, was added to the model. Both calculated treatment plans provided electroporation treatment parameters that covered the tumor with electric fields above the irreversible electroporation threshold, while leaving the critical tissue relatively undamaged. According to our fitness function, the treatment plan that utilized six individual electrodes was better, as it caused less damage to the critical tissue. However, the weights of the fitness function in our case were set arbitrarily; in the clinical environment, the weights of the fitness function would have to be set according to an analysis of several cases of tissue ablation with irreversible electroporation, or several different sets of weights could be set in the treatment planning procedure and the results presented to the attending physician. He/she would then have to make an educated choice between the presented treatment plans.

Optimization was carried out five times for each case and an adequate solution was obtained each time, which suggests that the optimization algorithm reaches a good solution for any number of parameters used. Using more parameters resulted in a somewhat better solution but also required more than twice the computational time. When deciding on the number of parameters for the optimization, the desired accuracy of the ablation procedure would have to be weighed against the time needed to plan the treatment (other factors, e.g. options available due to electric pulse generator characteristics, such as number of available channels, maximum allowed output voltage and current, and circumstances of the particular treatment, will also have a role in process).

In tissue ablation with irreversible electroporation, a higher number of pulses are applied to the target tissue compared to electrochemotherapy. More pulses increase the probability of cell death at certain electric field strength, therefore it is possible to lower the electric field electroporation thresholds by increasing the number of applied pulses [Canatella et al., 2001]. Although the electroporation model used in this section did not take into account the effects of number or duration of pulses on the final outcome, the modularity of the designed treatment planning procedure should be comparably effective in optimization based on the probability models of electroporation [Golberg and Rubinsky, 2010].

4.3 Prevention of thermal damage – IRE

As the main advantage of tissue ablation with irreversible electroporation compared to other ablation modalities is its non-thermal nature, we added a multiphysics component to the used models to calculate the increase of temperature cause by the electric pulses. On a desktop PC the evaluation of temperature distribution during the optimization procedure using the bioheat equation took too long to be of practical use. We therefore considered less accurate estimates that were able to reduce the computation time. A decrease in used time was achieved by estimating the temperature increase by Eq. 2.5. As Eq. 2.5 was designed to overestimate the actual temperature and thereby the induced thermal damage, its use in avoiding unnecessary calculations is justified.

When we evaluated the temperature increase in the tissue for average parameters used in tissue ablation [Rubinsky et al., 2008] (50 100 μs pulses with the repetition frequency of 1 Hz and U/d of approximately 2000 V/cm), we determined that even when a large number of high-voltage pulses is used, thermal damage only occurs in the vicinity of the electrodes, if at

all, while the temperature in the majority of the target and healthy tissue will remain below the thermal damage threshold. It seems that more rigorous temperature distribution calculation and its inclusion in the treatment planning process will only become necessary if: 1) even more pulses are used, 2) the pulses induce higher electric fields in the tissue or 3) the pulse repetition frequency that currently maintains a relatively low temperature by providing enough time for heat dissipation is increased.

Numerical modeling was used before to evaluate the temperature increase and consequent thermal damage in biological tissue due to application of high-voltage electric pulses [Davalos and Rubinsky, 2008; Shafiee et al., 2009; Maor et al., 2010]. In these studies it was established that a range of electric pulse parameters exists that should not cause thermal damage, a result that was confirmed in our study. Nevertheless, none of our studies took into account the changes in tissue properties during electroporation. Since a recent study in nanosecond electroporation suggests that incorporating the increase in tissue conductivity into numerical models results in higher temperatures than without the increases [Esser et al., 2009], it is quite possible that our approach underestimated the temperature increase. Still, the obtained values were so far below the thermal threshold that this does not change our conclusions that the pulses currently used in tissue ablation with irreversible electroporation.

4.4 Electric field distribution in a subcutaneous tumor – ECT 2
(article VI)

In section 3.4, the genetic algorithm was again tested for electrochemotherapy of a subcutaneous tumor, however this time 36 parameters were optimized, a number that should suffice for clinical treatment planning of electrochemotherapy. Along with electrode positions, already optimized in section 3.2, the angles of electrode insertion were also added to the optimized parameters. The increase in the number of parameters did not cause any problems and the calculation was still relatively fast, which suggests that the optimization algorithm in its tested form could be used for treatment planning of electrochemotherapy in the clinical environment. Since the optimized angles of insertion in our model were all very close to 0° (insertion perpendicular to skin), it is unclear whether their optimization is actually relevant for clinical treatment planning.

4.5 Electric field distribution in skeletal muscle – EGT

Successful gene electrotransfer requires the electric pulses to reversibly electroporate the target cells and move the negatively charged DNA molecules to the negatively charged cell membrane. Relatively high levels of transfection can be achieved using longer low-voltage pulses [Bettan et al., 2000], as well as using a combination of short high-voltage pulses and long low-voltage pulses [Bureau et al., 2000; Satkauskas et al., 2002]. In the latter case the short high-voltage pulses reversibly electroporate the cells, while the long low-voltage pulses electrophoretically move the DNA to the cell membranes. In section 3.5 the high-voltage pulses of this double pulse procedure were optimized for gene electrotransfer in muscle tissue. Muscle geometry was taken from a previous study, in which in vivo gene electrotransfer into a mouse *tibialis cranialis* muscle was combined with numerical modeling to determine electroporation thresholds for muscle tissue in the directions perpendicular and parallel to muscle fibers [Corovic et al., 2010].

We first determined that anisotropic tissue properties have to be taken into account when designing accurate numerical models of electroporation, as the predicted electric fields between models with isotropic and anisotropic properties differed significantly. We furthermore compared static and sequential models of electroporation and determined that the volumes of electroporated tissue predicted by both models differed by 26 % on average (sequential models predicted higher volumes). If changes in conductivity were used to determine the electroporated volume instead of the electric field, the sequential models produced values that were 45 % higher on average. The difference was even greater with respect to calculation of total electric current, where sequential models produced 145 % higher results. It seems that static models regularly underestimate the volume of electroporated tissue and severely underestimate the total current running through the tissue, as has also been determined by experiment on simple isotropic tissue [Ivorra and Mir, 2009]. This suggests that static models could be used to provide a conservative estimate of the volume of electroporated homogeneous tissue, however, sequential models have to be used for the prediction of total electric current during electroporation.

The parametric analysis of electrode positions and voltage between the electrodes suggests that in order to achieve optimal electric field distribution for gene electrotransfer, it is best to use large distances between electrodes and large depths of insertion, and to position the electrodes (electric field) perpendicular to the orientation of muscle fibers in case where three needle electrode pairs were used and parallel to the muscle fibers when only one needle

electrode pair was used. Similar results for one needle electrode pair were obtained by [Aihara and Miyazaki, 1998] in experiments on mice. It seems that high volumes of reversible electroporation in muscle tissue can be achieved without causing extensive irreversible electroporation. Similar results were obtained in a recent study of in mice, where electric pulse parameters for gene electrotransfer were compared for efficiency [Tevz et al., 2008] Nevertheless, our results show that the optimal parameters are very difficult to determine without numerical modeling and optimization.

Optimization of the same parameters that were parameterized was carried out; however two non-equality constraints (one for volume of irreversible electroporation and one for total current) were added to the fitness function to guarantee that the final solution would not cause significant damage to the muscle tissue. Since the optimization algorithm reached the optimum without problems, notwithstanding the constraints, it seems that the addition of any such constraints does not significantly affect its performance.

4.6 Treatment planning for electrochemotherapy of a deep-seated tumor – ECT

(articles IV,V)

After the designed treatment procedure was tested, it was used to for treatment planning of the first clinical electrochemotherapy of a deep-seated tumor. The optimization algorithm was used to determine the best position of several electrodes and the voltages between them for two possible numbers of electrodes. Although the treatment was only partly successful, this clinical case demonstrates that treatment of deep-seated tumor nodules by electrochemotherapy is feasible and that optimization of the treatment approach by numerical modeling of the tumor is of significant help.

A reevaluation of the treatment plan has shown that errors in electrode positioning could have been responsible for the insufficient coverage of the tumor, however, other possibilities, such as inaccurate data on tissue properties (conductivity, electroporation thresholds), could not be ruled out. For example, several studies have shown that transport a heterogeneous multicellular environments, such as a large tumor, is impaired compared to simpler tissue [Canatella et al., 2004; Minchinton and Tannock, 2006; Wasungu et al., 2009], therefore it is possible that the tumor did not respond as expected to the treatment, because the used electrochemotherapeutic was not present in the whole tumor. If that is the case,

intratumoral injection of the chemotherapeutic drug or the use of irreversible electroporation could improve the treatment outcome [Mir, 2010]. However, if errors in electrode positioning were responsible for the treatment outcome, then similar errors should be avoided in the future by using a quality assurance system for electrode positioning, possibly one based on computer tomography or ultrasound imaging [Phee and Yang, 2010].

Robustness analysis of the treatment planning procedure has shown that the choice of electroporation thresholds and tissue conductivity as well as electrode positioning during the treatment setup have the greatest influence on the difference between predicted electric field distribution and the electric distribution achieved during treatment. Since both electroporation thresholds and conductivity values are not readily available, more research in the field of tissue electroporation is needed to improve the efficiency of electrochemotherapy treatment planning. On the other hand, robustness can be increased by using conservative estimates of electroporation thresholds and conductivity, as well as by using more electrodes for electric pulse delivery.

A certain number of errors are likely to be made during the treatment, due to reasons already mentioned. To ensure that the treatment outcome is not affected by these errors, a suitable safety margin should be employed during the treatment planning stage. The robustness analysis suggests that setting conservative values for conductive properties (higher $\sigma_{TUMOR}/\sigma_{FAT}$) and higher electroporation thresholds can increase the robustness of the treatment, but care must be taken to avoid excessive electric fields that would cause extensive tissue damage.

4.7 Electric field distribution in a subcutaneous tumor - ECT, IRE, EGT

In all the presented studies the same numerical models of electroporation (i.e. static or sequential) and the same optimization algorithm (genetic algorithm) were used for the optimization of electrode positions and voltages between the electrodes; the main difference between the optimization was the choice of fitness functions. We proposed that by changing the weights of the fitness function factors (e.g. volume of target tissue exposed to electric fields over the reversible or irreversible electroporation threshold) it is possible to obtain treatment plans that would suit individual electroporation-based treatment, similarly as is done in radiotherapy treatment planning [Bevilacqua et al., 2007]. In section 3.7 we showed that by choosing appropriate fitness functions, it is possible to obtain completely different

solutions for electrochemotherapy, tissue ablation with irreversible electroporation and gene electrotransfection. This suggests that the designed treatment planning procedure can be used for treatment planning of all three electroporation-based treatments.

5.   CONCLUSIONS

The main focus of the presented doctoral work was to design a treatment planning procedure for electrochemotherapy of deep-seated tumors and to test its various components on different models of electrochemotherapy, irreversible electroporation, and gene electrotransfer. The high number of numerical calculations performed, whether single calculations or as part of parameterization or optimization, not only tested the treatment planning algorithm but also enabled the creation of guidelines for the effective use of electroporation in all three electroporation-based treatments.

When using electroporation-based treatments to target a well-defined tissue, e.g. electrochemotherapy of cutaneous and subcutaneous tumors, clinical studies have shown that good results can be obtained even without numerical treatment planning. Nevertheless, numerical modeling and optimization carried out during the presented doctoral studies have shown that the homogeneity of the electric field in the target tissue and thereby the probability of covering the whole target tissue with the desired electric field could be increased by positioning the electrodes around the target tissue in such a way that the active parts of the electrodes (or their projections) cover a bigger volume than the tumor. The same guidelines are useful for electrochemotherapy and tissue ablation by irreversible electroporation.

The first component of the designed treatment planning procedure was building a 3D geometry from medical images. The planar contour method and voxel import were both successfully used to import geometry data from medical images into Comsol Multiphysics. It was determined that voxel import was unsuitable for sequential models of electroporation, where changes of tissue properties had to be defined in geometry objects; it was, however, appropriate for use in static models. If the geometry objects were imported by the planar contour method, the drawback was that electrodes could not be modeled in the immediate vicinity of the tumor, as this resulted in a meshing problem. Both drawbacks are directly related to Comsol Multiphysics; it might therefore be possible to avoid them by using different software.

Numerical modeling represents the second stage of the treatment planning procedure that evaluates the electroporation parameters with respect to the induced electric field distribution. It was determined that sequential electroporation models on average predict higher volumes of tissue to be electroporated than the static models (20 % higher) and higher total currents (145 % higher). This suggests that static models could be used to provide a conservative estimate of the volume of electroporated tissue, however, sequential models have

to be used for the prediction of the total electric current during electroporation. Furthermore, for electroporation currently used in tissue ablation, it was determined that modeling temperature distribution during optimization was unnecessary, as it takes too much computational time. Instead, a conservative estimate of the temperature increase was suggested.

The third stage of the treatment planning procedure – the genetic algorithm – was tested several times against different fitness functions, different numbers of parameters to optimize, and different constraints. When tested on the same problem several times, the algorithm always returned an adequate solution in a reasonable amount of time, regardless of the complexity and number of used geometries, constraints or parameters that were optimized. The complete treatment planning procedure was used for the world's first electrochemotherapy of a deep-seated tumor. It provided two treatment plans for two different numbers of electrodes used, whereupon one was chosen for the treatment. Although complete response of the tumor was not achieved, the tumor did decrease in volume considerably before regrowing. A reevaluation of the treatment plan has shown that inaccuracies in electrode positioning were most likely responsible for the treatment failure.

In all the presented studies the same numerical models of electroporation (i.e. static or sequential) and the same optimization algorithm (genetic algorithm) were used for the optimization of electrode positions and voltages between the electrodes; the main difference between the optimization was the choice of fitness functions. We showed that by choosing appropriate fitness functions, it is possible to obtain completely different solutions for electrochemotherapy, tissue ablation with irreversible electroporation and gene electrotransfection.

By designing a complete treatment planning procedure (importing anatomical data from medical images into numerical analysis software, accurate modeling of electroporation and optimization of electroporation parameters) the ground has been set for future use of electrochemotherapy in treatment of deep-seated tumor nodules. Testing the treatment planning procedure on various models enabled identification of current limitations and pointed towards two areas that need to be addressed in future work. The first is to improve the flow of the treatment planning process, which can be done by designing a graphical user interface that will enable segmentation of the medical images as well as definition of feasible options for insertions of needle electrodes. This will enable faster and more accurate generation of 3D anatomical geometries. The second is to improve the accuracy of the electroporation models by improving the accuracy of input data. The treatment planning

robustness analysis showed that the accuracy of the used tissue properties (i.e. electrical conductivity and electroporation thresholds) contribute significantly to the accuracy of the treatment plan. A lack of tissue specific experimental data on tissue properties remains one of the last hurdles towards reliable numerical treatment planning in electroporation-based treatments.

ORIGINAL CONTRIBUTIONS TO THE SCIENTIFIC FIELD

Electrochemotherapy treatment planning

We designed a treatment planning procedure that uses realistic geometries obtained from medical images of the tumor and surrounding tissue, finite element modeling and optimization to determine the optimal electrode positions and voltages between the electrodes for electrochemotherapy. We established two different ways of translating data from medical images into a commercial finite element package. We also determined that sequential electroporation models have to be used for the evaluation of total current during electric pulses, but not necessarily for the evaluation of electric field distribution, and designed a genetic algorithm that takes input from numerical models and optimizes the treatment parameters that enable successful electrochemotherapy with minimum side effects. The treatment planning procedure was used for the planning of the first electrochemotherapy treatment of a deep-seated tumor; our work has thus already been used to promote a novel cancer treatment.

In cases where treatment planning is necessary, we proposed simple guidelines for electrode positioning during electrochemotherapy that the attending physicians should follow to achieve adequate electric field coverage of the tumor and surrounding tissue. The electrodes should be positioned around the tumor on all sides, so that the volume between the active parts of the electrodes is greater than the tumor volume.

Ablation by irreversible electroporation treatment planning

Tissue ablation with irreversible electroporation has lately been shown to be an effective method of ablation of tumors and other tissues. We demonstrated that the treatment planning procedure designed for electrochemotherapy can also be used in the treatment planning of tissue ablation with irreversible electroporation, as can be the guidelines for electrode positioning when treatment planning cannot be carried out. We also determined that temperature distribution modeling during the treatment planning of tissue ablation with irreversible electroporation is unfeasible, as it takes almost 20 times longer than evaluation of the electric field distribution alone. Instead we proposed a simpler conservative estimation of temperature that is always evaluated, while the differential equations are only evaluated if the

estimate exceeds a predefined value. Furthermore, we established that current parameters used in clinical trials of tissue ablation with irreversible electroporation do not increase the temperature in the tissue by more than a few °C.

Optimization of gene electrotransfection of muscle tissue

Gene electrotransfer into skeletal muscle is showing great promise for gene therapy and gene vaccination, two upcoming medical treatments. We built a numerical model of muscle tissue and used it to analyze electrode positions and voltages between electrodes to achieve the optimal electric field distribution for gene electrotransfer. The model took into account anisotropy of muscle tissue and two different electroporation thresholds for two directions of electric field with respect to the orientation of muscle fibers (perpendicular and parallel). We determined that anisotropic tissue properties have to be taken into account when modeling electroporation in muscle tissue. We also determined that large volumes of reversible electroporation can be achieved without damaging too much muscle tissue by irreversible electroporation if: 1) rows of needle electrodes are used, with large distances between the rows and electrodes in a row, large needle insertion depths, and by inducing an electric field in the direction perpendicular to the direction of muscle fibers; or 2) one needle electrode pair is used, inducing electric field in the direction parallel to muscle fibers. We demonstrated that numerical modeling and optimization can be used to determine an optimal electric field distribution for the electroporation part of gene electrotransfection.

REFERENCES

Aihara H, Myazaki J. Gene electrotransfer into muscle by electroporation in vivo. *Nat Biotechnol* 16: 867-870, 1998.

Al-Sakere B, Bernat C, Connault E, Opolon P, Rubinsky B, Davalos R, Mir LM. Tumor ablation with irreversible electroporation. *PLoS ONE* 2: 135, 2007.

Andre F, Gehl J, Sersa G, Preat V, Hojman P, Eriksen J, Golzio M, Cemazar M, Pavselj N, Rols MP, Miklavcic D, Neumann E, Teissie J, Mir LM. Efficiency of high- and low-voltage pulse combinations for gene electrotransfer in muscle, liver, tumor, and skin. *Hum Gene Ther* 19: 1261-1271, 2008.

Astrom M, Zrinzo LU, Tisch S, Tripoliti E, Hariz MI, Wardell K. Method for patient-specific finite element modeling and simulation of deep brain stimulation. *Med Biol Eng Comp*, 47: 21-28, 2009.

Benedek GB, Villars FMH. Physics with illustrative examples from medicine and biology: electricity and magnetism (second edition), Springer, 2000.

Bettan M, Ivanov MA, Mir LM, Boissiere F, Delaere P, Scherman D. Efficient DNA electrotransfer into tumors. *Bioelectrochemistry* 52: 83-90, 2000.

Bevilacqua V, Mastronardi G, Piscopo G. Evolutionary approach to inverse planning in coplanar radiotherapy. *Image Vis Comp* 25: 196-203, 2007.

Brahme A. Biologically based treatment planning. *Acta Oncol Suppl* 13: 61-68, 1999.

Bureau MF, Gehl J, Deleuze V, Mir LM, Scherman D. Importance of association between permeabilization and electrophoretic forces for intramuscular DNA electrotransfer. *Biochim Biophys Acta* 1474: 353-359, 2000.

Campana LG, Mocellin S, Basso M, Puccetti O, De Salvo GL, Chiarion-Sileni V, Vecchiato A, Corti L, Rossi CR, Nitti D. Bleomycin-based electrochemotherapy: clinical outcome from a single institution's experience with 52 patients. *Ann Surg Oncol* 16: 191-199, 2009.

Canatella PJ, Karr JF, Petros JA, Prausnitz MR. Quantitative study of electroporation-mediated molecular uptake and cell viability. *Biophys J* 80: 755-764, 2001.

Canatella PJ, Black MM, Bonnichsen DM, McKenna C, Prausnitz MR. Tissue electroporation: quantification and analysis of heterogeneous transport in multicellular environments. *Biophys J* 86: 3260-3268, 2004.

Cemazar M, Jarm T, Miklavcic D, Macek-Lebar A, Ihan A, Kopitar NA, Sersa G. Effect of electric-field intensity on electropermeabilization and electrosensitivity of various tumor-cell lines in vitro. *Electro Magnetobiol* 17: 263-272, 1998.

Corovic S, Pavlin M, Miklavcic D. Analytical and numerical quantification and comparison of the local electric field in the tissue for different electrode configurations. *Biomed Eng Online* 6: 37, 2007.

Corovic S, Zupanic A, Kranjc S, Al-sakere B, Leroy-Willig A, Mir LM, Miklavcic D. In vivo electroporation detection based on magnetic resonance imaging, propidium iodide fluorescence and numerical modeling of anisotropic muscle tissue, 2010. Accepted for publication in *Med Biol Eng Comp*.

Curatolo P, Mancini M, Ruggiero A, Clerico R, Di Marco P, Calvieri S. Successful treatment of penile kaposi's sarcoma with electrochemotherapy. *Dermatol Surg* 34: 1–5, 2008.

Cukjati D, Batiuskaite D, André F, Miklavcic D, Mir LM. Real time electroporation control for accurate and safe in vivo non-viral gene therapy. *Bioelectrochemistry* 70: 501-507, 2007.

Daud AI, DeConti RC, Andrews S, Urbas P, Riker AI, Sondak VK, Munster PN, Sullivan DM, Ugen KE, Messina JL, Heller R. Phase I trial of interleukin-12 plasmid electro oration in patients with metastatic melanoma. *J Clin Oncol* 26: 896-903, 2008.

Davalos R, Rubinsky B, Otten DM. A feasibility study for electrical impedance tomography as a means to monitor tissue electroporation for molecular medicine. *IEEE Trans Biomed Eng* 49: 400–403, 2002.

Davalos RV, Otten DM, Mir LM, Rubinsky B. Electrical impedance tomography for imaging tissue electroporation. *IEEE Trans Biomed Eng* 51: 761–767, 2004.

Davalos R, Mir LM, Rubinsky B. Tissue ablation with irreversible electroporation. *Annals Biomed Eng* 33:223-231, 2005.

Davalos RV, Rubinsky B. Temperature considerations during irreversible electroporation. *Int J Heat Mass Transfer* 51: 5617-5622, 2008.

DeBruin KA, Krassowska W. Modeling electroporation in a single cell. I. Effects of field strength and rest potenatial. *Biophys J* 77: 1213-1224, 1999.

Denet AR, Vanbever R, Preat V. Skin electroporation for transdermal and topical delivery. *Adv Drug Deliv Rev* 56: 659–674, 2004.

Dev BS, Dhar D, Krassowska W. Electric field of a six-needle array electrode used in drug and DNA delivery in vivo: analytical versus numerical solutions. *IEEE T Biomed Eng* 50: 1296-1300, 2003.

Durieux AC, Bonnefoy R, Busso T, Freyssenet D. In vivo gene electrotransfection into skeletal muscle: effects of plasmid DNA on the occurence and extent of muscle damage. *J Gene Med* 6: 809-816, 2004.

Edd JF, Horowitz L, Davalos RV, Mir LM, Rubinsky B. In vivo results of a new focal tissue ablation technique: Irreversible electroporation. *IEEE Trans Biomed Eng* 53: 1409–1415, 2006.

Edd JF, Davalos RV. Mathematical modeling of irreversible electroporation for treatment planning. *Technol Cancer Res Treat* 6: 275–286, 2007.

Esser AT, Smith KC, Gowrishankar TR, Weaver JC. Towards solid tumor treatment by irreversible electroporation: intrinsic redistribution of fields and currents in tissue. *Technol Cancer Res Treat* 6: 261-273, 2007.

Ezzell GA. Genetic and geometric optimization of three-dimensional radiation therapy treatment planning. *Med Phys* 23**:** 293-305, 1996.

Fantini F, Gualdi G, Cimitan A, Giannetti A. Metastatic basal cell carcinoma with squamous differentiation. *Arch Dermatol* 144:1186-1188, 2008.

Gabriel B, Teissie J. Control by electrical parameters of short- and long-term cell death resulting from electropermeabilization of Chinese hamster ovary cells. *Biochim Biophys Acta* 1266: 171-178, 1995.

Gabriel B, Teissie J. Direct observation in the millisecond time range of fluorescent molecule asymmetrical interaction with the electropermeabilized cell membrane. *Biophys J* 73: 2630-2637, 1997.

Gabriel C, Peyman A, Grant EH. Electrical conductivity of tissue at frequencies below 1 MHz. *Phys Med Biol* 54: 4863-4878, 2009.

Gabriel S, Lau RW, Gabriel C. The dielectric properties of biological tissues .2. Measurements in the frequency range 10 Hz to 20 GHz. *Phys Med Biol* 41: 2251-2269, 1996.

Gehl J, Sorensen TH, Nielsen K, Raskmark P, Nielsen SL, Skovsgaard T, Mir LM. In vivo electroporation of skeletal muscle: Threshold, efficacy and relation to electric field distribution. *Biochim Biophys Acta* 1428: 233–240, 1999.

Gehl J. Electroporation: theory and methods, perspectives for drug delivery, gene therapy and research. *Acta Physiol Scand* 177:437-447, 2003.

Gilbert RA, Jaroszeski MJ, Heller R. Novel electrode designs for electrochemotherapy. *Biochim Biophys Acta*, 1334: 9-14, 1997.

Golberg A, Rubinsky B. A statistical model for multidimensional irreversible electroporation cell death in tissue. *Biomed Eng Online* 9:13, 2010.

Golzio M, Teissie J, Rols MP. Direct visualization at the single-cell level of electrically mediated gene delivery. *Proc Nat Acad Sci* 99: 1292-1297, 2002.

Gowrishankar TR, Weaver JC. Electrical behavior and pore accumulation in a multicellular model for conventional and supra-electroporation. *Biochem Biophys Res Comm* 349: 643-653, 2006.

Haemmerich D, Schutt DJ, AW Wright, Webster JG, Mahvi DM. Electrical conductivity measurement of excised human metastatic liver tumours before and after thermal ablation. *Physiol Meas* 30: 459-466, 2009.

Heinz V, Alvarez I, Angersbach A, Knorr D. Preservation of liquid foods by high intensity pulsed electric field - basic concepts for process design. *Trends Food Sci Technol* 12: 103-111, 2002.

Heller LC, Heller R. In vivo electroporation for gene therapy. *Hum Gene Ther* 17: 890-897, 2006.

Heller R, Jaroszeski M, Leo-Messina J, Perrot R, Van Voorhis N, Reintgen D, Gilbert R. Treatment of B16 mouse melanoma with the combination of electropermeabilization and chemotherapy. *Bioelectrochem Bioenerg* 36: 83-87, 1995.

Heller R, Jaroszeski MJ, Reintgen DS, Puleo CA, DeConti RC, Gilbert R, Glass LF. Treatment of cutaneous and subcutaneous tumors with electrochemotherapy using intralesional bleomycin. *Cancer* 83:148-157, 1998.

Heller R, Gilbert R, Jaroszeski MJ. Clinical application of electrochemotherapy. *Adv Drug Deliv Rev* 35: 119-129, 1999.

Hibino M, Shigemori M, Itoh H, Nagayama K, Kinosita K Jr. Membrane conductance of an electroporated cell analyzed by submicrosecond imaging of transmembrane potential. *Biophys J* 59: 209-220, 1991.

Holland JH. Adaptation in natural and artificial systems: an introductory analysis with applications to biology, control, and artificial intelligence. Cambridge: MIT Press, Cambridge, 1992.

Ivorra A, Al-Sakere B, Rubinsky B, Mir LM. In vivo electrical conductivity measurements during and after tumor electroporatio: conductivity changes reflect the treatment outcome. *Phys Med Biol*, 54: 5949-5963, 2009.

Ivorra A, Mir LM. Electric field redistribution due to conductivity changes during tissue electroporation: experiments with a simple vegetal model, Proceedings of the 11th World Congress on Medical Physics and Biomedical Engineering, Springer, Heidelberg, pp 59-62, 2009.

Jaroszeski M, Gilbert RA, Heller R. In vivo antitumor effects of electrochemotherapy in a hepatoma model. *Biochim Byophys Acta* 1334: 15-18, 1997.

Jaroszeski M, Illingworth P, Pottinger C, Hyacinthe M, Heller R. Electrically mediated drug delivery for treating subcutaneous and orthotopic pancreatic adenocarcinoma in a hamster model. *Anticancer Res* 19: 989-994, 1999a.

Jaroszeski M, Gilbert R, Nicolau C, Heller R. In vivo gene delivery by electroporation. *Adv Drug Deliv Rev* 35: 131-137, 1999b.

Kanduser M, Miklavcic D. Electroporation in biological cell and tissue: an overview. In Vorobiev E, Lebovka N (eds.), Electrotechnologies for extraction from food plants and biomaterials, Springer Science, New York, 1-37, 2008.

Kanthou C, Kranjc S, Sersa G, Tozer G, Zupanic A, Cemazar M. The endothelial cytoskeleton as a target of electroproation-based therapies. *Mol Cancer Ther* 5: 3145-3152, 2006.

Kennedy SM, Ji Z, Rockweiler NB, Hahn AR, Booske JH, Hagness SC. The role of plasmalemmal-cortical anchoring on the stability of transmembrane electropores. *IEEE Trans Diel Elec Insul* 16: 1251-1258, 2009.

Kinosita K, Tsong 1979. Voltage induced conductance in human erythrocyte. *Biochim Biophys Acta* 554: 479-497, 1979.

Kotnik T, Bobanovic F, Miklavcic D. Sensitivity of transmembrane voltage induced by applied electric fields – a theoretical analysis. *Bioelectrochem Bioenerg* 43: 285-291, 1997.

Kotnik T, Miklavcic D. Analytical description of transmembrane voltage induced by electric fields on spheroidal cells. *Biophys J* 79: 670-679, 2000.

Krassowska W, Gurvinder SN, Austin MB, Dev SB, Rabussay DP. Viability of cancer cells exposed to pulsed electric fields: the role of pulse charge. *Ann Biomed Eng* 31: 80-90, 2003.

Krassowska W, Filev PD. Modeling electroporation in a single cell. *Biophys J* 92: 404-417, 2007.

Lackovic I, Magjarevic R, Miklavcic D. Three-dimensional Finite-element Analysis of Joule Heating in Electrochemotherapy and in vivo Gene Electrotransfer. *IEEE T Diel Elec Insul* 16: 1338-1347, 2009.

Lavee J, Onik G, Mikus P, Rubinsky B. A novel nonthermal energy source for surgical epicardial atrial ablation: Irreversible electroporation. *Heart Surg Forum* 10: E162–E167, 2007.

Lee EW, Loh CT, Kee ST. Imaging guided percutaneous irreversible electroporation: Ultrasound and immunohistological correlation. *Technol Cancer Res Treat* 6: 287–293, 2007.

Leveillee R, Salas N, Moore C, Jorda M, Sierra M, Shields J. Preliminary investigations with irreversible electroporation in in-vivo porcine kidneys *J Endourology* 23: A3-A3, Supplement, 2009.

Liang XH, Wu XX, Liang AM, Wang CP. Constructing 3D surface from planar contours with grid adjustment analysis. In: Zha H, Pan ZG, Thwaites H, Addison AC, Forte M (eds.) Interactive technologies and sociotechnical systems, Spinger, Berlin, 2006.

Loganathan AG, Ellis TL, Rossmeisl JH, Garcia PA, Robertson J, Davalos RV. Irreversible electroporation for intracranial surgery: a pilot study in a canine model. *Neuro-Oncol* 11: 588-588, 2009.

Macek-Lebar A, Miklavcic D. Cell electropermeabilization to small molecules in vitro: control by pulse parameters. *Radiol Oncol* 35: 193-202, 2001.

Macek-Lebar A, Sersa G, Kranjc S, Groselj A, Miklavcic D. Optimisation of pulse parameters in vitro for in vivo electrochemotherapy. *Anticancer Res* 22: 1731-1736, 2002.

Maor E, Ivorra A, Leor J, Rubinsky B. The effect of irreversible electroporation on blood vessels. *Technol Cancer Res Treat* 6: 307–312, 2007.

Maor E, Ivorra A, Leor J, Rubinsky B. Irreversible electroporation attenuates neointimal formation after angioplasty. *IEEE Trans Biomed Eng* 55: 2268–2274, 2008.

Maor E, Rubinsky B. Endovascular non-thermal irreversible electroporation: a finite element analysis. *J Biomech Eng* 132: 031008, 2010.

Marty M, Sersa G, Garbay JR, Gehl J, Collins CG, Snoj M, Billard V, Geertsen PF, Larkin JO, Miklavcic D, Pavlovic I, Paulin-Kosir SM, Cemazar M, Morsli N, Soden DM, Rudolf Z, Robert C, O'Sullivan GC, Mir LM. Electrochemotherapy – an easy, highly effective and safe treatment of cutaneous and subcutaneous metastases: results of ESOPE (European Standard Operating Procedures of Electrochemotherapy) study. *Eur J Cancer Suppl* 4: 3-13, 2006.

Miklavcic D, Beravs K, Semrov D, Cemazar M, Demsar F, Sersa G. The importance of electric field distribution for effective in vivo electroporation of tissues. *Biophys J* 74: 2152-2158, 1998.

Miklavcic D, Semrov D, Mekid H, Mir LM. A validated model of in vivo electric field distribution in tissues for electrochemotherapy and for DNA electrotransfer for gene therapy. *Biochim Biophys Acta* 1523: 73-83, 2000.

Miklavcic D, Pucihar G, Pavlovec M, Ribaric S, Mali M, Macek-Lebar A, Petkovsek M, Nastran J, Kranjc S, Cemazar M, Sersa G. The effect of high frequency electric pulses on muscle contractions and antitumor efficiency in vivo for a potential use in clinical electrochemotherapy. *Bioelectrochemistry* 65: 121-128, 2005.

Miklavcic D, Corovic S, Pucihar G, Pavselj N. Importance of tumour coverage by sufficiently high local electric field for effective electrochemotherapy. *Eur J Cancer Suppl* 4: 45-51, 2006a.

Miklavcic D, Pavselj N, Hart FX. Electric Properties of Tissues. Wiley Encyclopedia of Biomedical Engineering, John Wiley & Sons, New York, 2006b.

Miklavcic D, Puc M. Electroporation. Wiley Encyclopedia of Biomedical Engineering, John Wiley & Sons, New York, 2006c.

Miller CE, Henriquez CS. Finite element analysis of bioelectric phenomena. *Crit Rev Biomed Eng* 18: 207-233, 1990.

Miller L, Leor J, Rubinsky B. Cancer cells ablation with irreversible electroporation. *Technol Cancer ResTreat* 4: 699–705, 2005.

Minchinton AI, Tannock IF. Drug penetration in solid tumours. *Nature Rev Cancer* 6: 583-592, 2006.

Mir LM, Orlowski S, Belehradek J, Paoletti C. Electrochemotherapy potentiation of antitumor effect of bleomycin by local electric pulses. *Eur J Cancer* 27: 68-72, 1991.

Mir LM, Bureau MF, Rangara R, Schwartz B, Scherman D. Long - term, high level in vivo gene expression after electric pulse - mediated gene transfer into skeletal muscle. *Medical sciences* 321: 893-899, 1998.

Mir LM, Bureau MF, Gehl, Rangara R, Rouy D, Caillaud JM, Delaere P, Branellec D, Schwartz B, Scherman D. High-efficiency gene transfer into skeletal muscle mediated by electric pulses. *Proc Natl Acad Sci USA*, 74: 4262-4267, 1999a.

Mir LM, Orlowski S. Mechanisms of electrochemotherapy. *Adv Drug Deliv Rev* 35: 107-118, 1999b.

Mir LM, Moller PH, Andre F, Gehl J. Electric-pulse mediated gene delivery to various animal tissues. *Adv Genet* 54: 83-114, 2005.

Mir LM, Gehl J, Sersa G, Collins CG, Garbay JR, Billard V, Geertsen PF, Rudolf Z, O'Sullivan GC, Marty M. Standard operating procedures of the electrochemotherapy: Instructions for the use of bleomycin or cisplatin administered either systemically or locally and electric pulses delivered by the Cliniporator by means of invasive or non-invasive electrodes. *Eur J Cancer* Suppl. 4: 14-25, 2006.

Mir LM. The Place of the Electroporation-Based Antitumor Therapies in the Electrical Armamentarium against Cancer. In Rubinsky B (ed.), Irreversible Electroporation, Springer Verlag, Berlin, 223-234, 2010.

Neumann E, Schaefer-Ridder M, Wang Y, Hofschneider PH. Gene transfer into mouse lyoma cells by electroporation in high electric fields. *EMBO J* 1: 841-845, 1982.

Neumann E, Kakorin S, Toensing K. Fundamentals of electroporative delivery of drugs and genes. *Bioelectrochem Bioenerg* 48: 3-16, 1999.

Okino M, Mohri H. Effects of a high-voltage electrical impulse and an anticancer drug on in vivo growing tumors. *Jpn J Cancer Res* 78: 1319-21, 1987.

Onik G, Mikus P, Rubinsky B. Irreversible electroporation: implications for prostate ablation. *Technol Cancer Res Treat* 6: 295-300, 2007.

Orlowski S, Belehradek J, Paoletti C, Mir LM. Transient electropermeabilization of cells in culture - increase of the cyto-toxicity of anticancer drugs. *Biochem Pharm* 37: 4727-4733, 1988.

Otten G, Schaefer M, Doe B, Liu H, Srivastava I, zur Megede J, O'Hagan D, Donnelly J, Widera G, Rabussay D, Lewis MG, Barnett S, Ulmer JB. Enhancement of DNA vaccine potency in rhesus macaques by electroporation. *Vaccine* 22: 2489-2493, 2004.

Pavselj N, Bregar Z, Cukjati D, Batiuskaite D, Mir LM, Miklavcic D. The course of tissue permeabilization studied on a mathematical model of a subcutaneous tumor in small animals. *IEEE Trans Biomed Eng* 52: 1373-1381, 2005.

Pavselj N, Miklavcic D. Numerical modeling in electroporation-based biomedical applications. *Radiol Oncol* 42: 159-168, 2008.

Pavlin M, Pavselj N, Miklavcic D. Dependence of induced transmembrane potential on cell density, arrangement, and cell position inside a cell system. *IEEE Trans Biomed Eng* 49: 605-612, 2002.

Pavlin M, Miklavcic D. Effective conductivity of a suspension of permeabilized cells: a theoretical analysis. *Biophys J* 85:719–729, 2003.

Payen E, Bettan M, Rouyer-Fessard P, Beuzard Y, Scherman D. Improvement of mouse beta-thalassemia by electrotransfer of erythropoietin cDNA. *Exp Hematol* 29: 295-300, 2001.

Pearce JA. Relationship between Arrhenius models of thermal damage and the CEM 43 thermal dose. In Ryan TP (ed.) Energy-based Treatment of Tissue and Assessment. Proceedings of the SPIE, 7181: 718104-718115, 2009.

Pennes HH. Analysis of tissue and arterial blood temperature in the resting human forearm. *J Appl Physiol* 85: 5-34, 1948.

Perez N, Bigey P, Scherman D, Danos O, Piechaczyk M, Pelegrin M. Regulatable systemic production of monoclonal antibodies by in vivo muscle electroporation. *Genet Vaccines Ther* 2: 2, 2004.

Phee SY, Yang K. Interventional navigation systems for treatment of unresectable liver tumor. *Med Biol Eng Comp* 48: 103-111, 2010.

Prud'homme GJ, Glinka Y, Khan AS, Draghia-Akli R. Electroporation enhanced nonviral gene transfer for the prevention or treatment of immunological, endocrine and neoplastic diseases. *Curr Gene Ther* 6: 243-273, 2006.

Poddevin B, Orlowski S, Belehradek J, Mir LM. Very high cytotoxicity of bleomycin introduced into the cytosol of cells in culture. *Biochem Pharmacol* 42: 67-75, 1991.

Puc M, Corovic S, Flisar K, Petkovsek M, Nastran J, Miklavcic D. Techniques of signal generation required for electropermeabilization. Survey of electropermeabilization devices. *Bioelectrochemistry* 64: 113-124, 2004.

Pucihar G, Mir LM, Miklavcic D. The effect of pulse repetition frequency on the uptake into electropermeabilized cells in vitro with possible applications in electrochemotherapy. *Bioelectrochemistry* 57: 167-172, 2002.

Pucihar G, Kotnik T, Valic B, Miklavcic D. Numerical determination of transmembrane voltage induced on irregularly shaped cells. *Annals Biomed Eng* 34: 642-652, 2006.

Pucihar G, Kotnik T, Teissie J, Miklavcic D. Electroporation of dense cell suspensions. *Eur Biophys J* 36: 173-185, 2007.

Pucihar G, Kotnik T, Miklavcic D. Measuring the induced membrane voltage with di-8-ANEPPS (Video Article). *J Visual Exp* 33: 1659, 2009.

Quaglino P, Mortera C, Osella-Abate S, Barberis M, Illengo M, Rissone M, Savoia P, Bernengo MG. Electrochemotherapy with intravenous bleomycin in the local treatment of skin melanoma metastases. *Ann Surg Oncol* 15: 2215-2222, 2008.

Rebersek M, Cufer T, Cemazar M, Kranjc S, Sersa G. Electrochemotherapy with cisplatin of cutaneous tumors lesions in breast cancer. *Anticancer drugs*, 15:593-597, 2004.

Rols MP, Teissie J. Electropermeabilization of mammalian cells: quantitative analysis of the phenomenon. *Biophys J* 58: 1089–1098, 1990.

Rols MP, Teissie J. Experimental evidence for the involvement of the cytoskeleton in mammalian cell electropermeabilization. *Biochim Biophys Acta* 1111: 45-50, 1992.

Rols MP, Bachaud JM, Giraud P, Chevreau C, Roche H, Teissie J. Electrochemotherapy of cutaneous metastases in malignant melanoma. *Melanoma Res* 10: 468-474, 2000.

Rowbottom M, Susskind C. Electricity and medicine: history of their interaction. San Francisco Press, San Francisco, 1984.

Rubinsky B. Technology in cancer research and treatment. *Technol Cancer Res Treat* 6: 255-259.

Rubinsky B, Onik G, Mikus P. Irreversible electroporation: A new ablation modality - Clinical implications. *Technol Cancer Res Treat* 6: 37–48, 2007.

Rubinsky J, Onik G, Mikus P, Rubinsky B. Optimal Parameters for the Destruction of Prostate Cancer Using Irreversible Electroporation. *J Urology* 180: 2668-2674, 2008.

Rudolf Z, Stabuc B, Cemazar M, Miklavcic D, Vodovnik L, Sersa G. Electrochemotherapy with bleomycin: the first clinical experience in malignant melanoma patients. *Radiol Oncol* 29: 229-235, 1995.

Sale AJH, Hamilton WA. Effects of electric fields on microorganizms I killing of bacteria and yeasts. *Biochim Biophys Acta* 148: 781-788, 1967.

Salford LG, Persson RBR, Brun A, Ceberg CP, Kongstad PC, Mir LM. A new brain tumor therapy combining bleomycin with in vivo electropermeabilisation. *Biochem Biophys Res Commun* 194: 938-943, 1993.

Satkauskas S, Bureau MF, Puc M, Mahfoudi A, Scherman D, Miklavcic D, Mir LM. Mechanisms of in vivo DNA electrotransfer: Respective contributions of cell electropermeabilization and DNA electrophoresis. *Mol Ther* 5: 133-140, 2002.

Satkauskas S, Andre F, Bureau MF, Scherman D, Miklavcic D, Mir LM. Electrophoretic component of electric pulses determines the efficacy of In Vivo DNA electrotransfer. *Hum Gene Ther* 16: 1194-1201, 2005.

Saulis G. Pore dissapearance in a cell after electroporation: theroretical simulation and comparison with experiments. *Biophys J* 73: 1299-1309, 1997.

Schwan HP, Kay CF. The conductivity of living tissues. *Ann NY Acad Sci*, 65: 1007, 1957.

Shafiee H, Garcia PA, Davalos RV. A preliminary study to delineate irreversible electroporation from thermal damage using the Arrhenius equation. *J Biomech Eng* 131: 074509, 2009.

Sel D, Cukjati D, Batiuskaite D, Slivnik T, Mir LM, Miklavcic D. Sequential finite element model of tissue electropermeabilization. *IEEE Trans Biomed Eng* 52: 816-827, 2005.

Sel D, Macek-Lebar A, Miklavcic D. Feasibility of employing model-based optimization of pulse amplitude and electrode distance for effective tumor electropermeabilization. *IEEE T Biomed Eng* 54: 773-781, 2007.

Semrov D, Miklavcic D. Calculation of the electrical parameters in electrochemotherapy of solid tumours in mice. *Comput Biol Med* 28: 439-448, 1998.

Sersa G, Cemazar M, Miklavcic D. Antitumor effectivness of electrochemotherapy with cis-diamminedichloroplatinium (II) in mice. *Cancer Res* 55:3450-3455, 1995.

Sersa G, Cemazar M, Semrov D, Miklavcic D. Changing electrode orientation improves the efficacy of electrochemotherapy of solid tumors in mice. *Bioelectrochem Bioenerg* 39: 61-66, 1996.

Sersa G, Cemazar M, Rudolf Z. Electrochemotherapy: advantages and drawbacks in treatment of cancer patients. *Cancer Ther* 1:133-142, 2003.

Sersa G, Miklavcic D. Electrochemotherapy of tumours (Video article). *J Visual Exp* 22: 1038, 2008a.

Sersa G, Jarm T, Kotnik T, Coer A, Podkrajsek M, Sentjurc M, Miklavcic D, Kadivec M, Kranjc S, Secerov A, Cemazar M. Vascular disrupting action of electroporation and electroche-motherapy with bleomycin in murine sarcoma. *Br J Cancer* 98: 388-398, 2008b.

Silverster PP, Ferrari LM. Finite elements for electrical engineers, Cambridge University Press, Cambridge, 1992.

Smith SR, Foster KR, Wolf GL. Dielectric properties of VX-2 carcinoma versus normal liver tissue. *IEEE Trans Biomed Eng* 33: 522–524, 1986.

Snoj M, Rudolf Z, Cemazar M, Jancar B, Sersa G. Succsessful sphincter-saving treatment of anorectal malignant melanoma with electrochemotherapy, local excision and adjuvant brachytherapy. *Anti-Cancer Drugs* 16: 345-348, 2005.

Snoj M, Cemazar M, Srnovrsnik T, Kosir SP, Sersa G. Limb sparing treatment of bleeding melanoma recurrence by electrochemotherapy. *Tumori* 95: 398-402, 2009.

Soden DM, Larkin JO, Collins CG, Tangney M, Aarons S, Piggott J, Morrissey A, Dunne C, O'Sullivan GC. Successful application of targeted electrochemotherapy using novel flexible electrodes and low dose bleomycin to solid tumors. *Cancer Lett* 232: 300-310, 2006.

Strang WG, Fix GJ. Analysis of the finite elements method. Prentice Hall, 1973.

Sugar IP, Neumann E. Stochastic model for electric field-induced membrane pores electroporation. *Biophys Chem* 19: 211-225, 1984.

Sukhorukov VL, Reuss R, Zimmermann D, Held C, Muller KJ, Kiesel M, Gessner P, Steinbach A, Schenk WA, Bamberg E, Zimmermann U. Surviving high-intensity field pulses: startegies for improving robustness and performance of electrotransfection and electrofusion. *J Memb Biol* 206: 187-201, 2005.

Sung W, Park PJ. Dynamics of pore growth in membranes and membrane stability. *Biophys J* 73: 1797-1804, 1997.

Susil R, Semrov D, Miklavcic D. Electric field-induced transmembrane potential depends on cell density and organization. *Electro Magnetobiol* 17: 391-399, 1998.

Suzuki T, Shin B, Fujikura K, Matsuaki T, Takata K. Direct gene transfer into rat liver cells by in vivo electro oration. *FEBS Lett* 425: 436-440, 1998.

Teissie J, Eynard N, Vernhes MC, Benichou A, Ganeva V, Galutzov B, Cabanes PA. Recent biotechnological developments of electropulsation: A prospective review. *Bioelectrochemistry* 55: 107–112, 2002.

Teissie J, Golzio M, Rols MP. Mechanisms of cell membrane electropermeabilization: A minireview of our present (lack of ?) knowledge. *Biochim Biophys Acta* 1724: 270-280, 2005.

Tevz G, Pavlin D, Kamensek U, Kranjc S, Mesojednik S, Coer A, Sersa G, Cemazar M. Gene electrotransfer into murine skeletal muscle: a systematic analysis of parameters for long-term gene expression. *Technol Cancer Res Treat* 7: 91-101, 2008.

Toepfl S, Mathys A, Heinz V, Knorr D. Review: potential of high hydrostatic pressure and pulsed electric fields for energy efficient and environmentally frinedly food processing. *Food Rev Int* 22: 405-423, 2006.

Tsong TY. Electroporation of cell membranes. *Biophys J* 60: 297–306, 1991.

Usaj M, Trontelj K, Hudej R, Kanduser M, Miklavcic D. Cell size dynamics and viability of cells exposed to hypotonic treatment and electroporation for electrofusion optimization. *Radiol Oncol* 43: 108-119, 2009.

Valic B, Golzio M, Pavlin M, Schatz A, Faurie C, Gabriel B, Teissie J, Rols MP, Miklavcic D. Effect of electric field induced transmembrane potential on spheroidal cells: theory and experiments. *Eur Biophys J* 32: 519–528, 2003.

Valic B. Vpliv implantov na porazdelitev elektromagnetnega polja v človeku, Doctoral dissertation, University of Ljubljana, Faculty of Electrical Engineering, 2006.

Viovy JL. Electrophoresis of DNA and other polyelectrolytes: Physical mechanisms. *Rev Mod Phys* 72: 813-872, 2000.

Wasungu L, Escoffre JM, VAlette A, Teissie J, Rols MP. A 3D in vitro spheroid model as a way to study mechanisms of electroporation. *Int J Pharm* 379: 278-284, 2009.

Weaver JC, Chizmadzhev YA. Theory of electroporation: A review. *Bioelectrochem Bioenerg* 41: 135-60, 1996

Wolf H, Rols MP, Boldt E, Neumann E, Teissie J. Control by pulse parameters of electric field-mediated gene-transfer in mammalian-cells. *Biophys J* 66: 524-531, 1994.

Wu X, Zhu Y. An optimization method for importance factors and beam weights based on genetic algorithms for radiotherapy treatment planning. *Phys Med Biol* 46: 1085-1099.

Zaharoff DA, Barr RC, Li CY, Yuan F. Electromobility of plasmid DNA in tumor tissues during electric field-mediated gene delivery. *Gene Ther* 9: 1286-1290, 2002.

Zampaglione I, Arcuri M, Cappelletti M, Ciliberto G, Perretta G, Nicosia A, La Monica N, Fattori E. In vivo DNA gene electro-transfer: a systematic analysis of different electrical parameters. *J Gene Med* 7: 1475-1481, 2005.

Zhang Y, Zhu CN, Pardridge WM. Antisense gene therapy of brain cancer with an artificial virus gene delivery system. *Mol Ther* 6: 67-72, 2002.

Zimmerman U, Pilwat G, Reimann F. Dielectric breakdown of cell membranes. *Biophys J* 14: 881-899, 1974.

Zimmermann U. Electric field-mediated fusion and related electrical phenomena. *Biochim Biophys Acta* 694: 227-277, 1982.

APPENDIX A

```matlab
%% track index changes

% INPUTS:
% INDEX - the original indexes of the model (before the geometry is
    % changed due to moving the electrodes)

% OUTPUTS:
% bi_old, di_old, bi_old2, di_old2 - current indexes of the model
% zz_boundary, zz_domain, zz_boundary2, zz_domain2 - indexes transformed into
    % comsol syntax - these indexes are later used in calculations

function
[bi_old, di_old, bi_old2, di_old2, zz_domain, zz_boundary, zz_domain2, zz_boundary2]=trackIndex(I
NDEX)

% read the original indexes for each application mode
    % for application mode 1
di_old=1:length(INDEX.domain);
bi_old=1:length(INDEX.boundary);
    % for application mode 2
di_old2=1:length(INDEX.domain2);
bi_old2=1:length(INDEX.boundary2);

% LOOP for all the different solutions in the generation:
i=1;
while i<=Nturnover+1-lessSolutionToSolve

    %%%%%%%%%%%%%%%%%%%%%%%%%%%%%%%%%%%%%%%%%%%%%%%%%%%%%%%%%%%%%%%%%%%%%

    % code that moves the electrodes

    %%%%%%%%%%%%%%%%%%%%%%%%%%%%%%%%%%%%%%%%%%%%%%%%%%%%%%%%%%%%%%%%%%%%%

    % read the changes in indexes (geomanalyze is a COMSOL native function)
    [fem, assocmap]=geomanalyze(fem);
    di_now=assocmap{4};
    bi_now=assocmap{3};

    % change index numbers
    di=di_old(di_now);
    bi=bi_old(bi_now);
    di2=di_old2(di_now);
    bi2=bi_old2(bi_now);

    % for application mode 1
    % for domains
    for ii=1:max(INDEX.domain)
```

```matlab
        di_temp=[];
        for kk=1:iod(ii).size
            ddi_temp=find(di==iod(ii).ind(kk));
            di_temp=[di_temp,ddi_temp];
        end
            din(ii).i=di_temp;
end
% for boundaries
for ii=1:max(INDEX.boundary)
    bi_temp=[];
    for kk=1:iob(ii).size
        bbi_temp=find(bi==iob(ii).ind(kk));
        bi_temp=[bi_temp,bbi_temp];
    end %for kk
    bin(ii).i=bi_temp;
end


% these are the true new indexes for domains
clear zz_domain
for ii=1:max(INDEX.domain)
    zz_domain(din(ii).i)=ii;
end
% for boundaries
clear zz_boundary
for ii=1:max(INDEX.boundary)
    zz_boundary(bin(ii).i)=ii;
end
clear din bin

% for application mode 2
% for domains
for ii=1:max(INDEX.domain2)
    di_temp2=[];
    for kk=1:iod2(ii).size
        ddi_temp2=find(di2==iod2(ii).ind(kk));
        di_temp2=[di_temp2,ddi_temp2];
    end
        din2(ii).i=di_temp2;
end
% for boundaries
for ii=1:max(INDEX.boundary2)
    bi_temp2=[];
    for kk=1:iob2(ii).size
        bbi_temp2=find(bi2==iob2(ii).ind(kk));
        bi_temp2=[bi_temp2,bbi_temp2];
    end %for kk
    bin2(ii).i=bi_temp2;
end


% these are the true new indexes for domains
clear zz_domain2
for ii=1:max(INDEX.domain2)
    zz_domain2(din2(ii).i)=ii;
```

```matlab
    end
    % for boundaries
    clear zz_boundary2
    for ii=1:max(INDEX.boundary2)
        zz_boundary2(bin2(ii).i)=ii;
    end     %for ii
    clear din2 bin2

    % current indexes will be used in the next iteration
    di_old=di;
    bi_old=bi;
    di_old2=di2;
    bi_old2=bi2;

    i=i+1;
end
```

APPENDIX B

I: Corovic S, **Zupanic A,** Miklavcic D. Numerical modeling and optimization of electric field distribution in subcutaneous tumor treated with electrochemotherapy using needle electrodes. *IEEE Trans Plasma Sci* 36: 1665-1672, 2008.

II: Zupanic A, Corovic S, Miklavcic D. Optimization of electrode position and electric pulse amplitude in electrochemotherapy. *Radiol Oncol* 42: 93-101, 2008.

III: Zupanic A, Miklavcic D. Optimization and numerical modeling in irreversible electroporation treatment planning. In Rubinsky B (ed.), Irreversible electroporation, Springer Verlag, Berlin, 203-222, 2010.

IV: Miklavcic D, Snoj M, **Zupanic A,** Kos B, Cemazar M, Kropivnik M, Bracko M, Pecnik T, Gadzijev E, Sersa G. Towards treatment planning and treatment of deep-seated solid tumors by electrochemotherapy. *Biomed Eng Online* 9:10, 2010.

V: Kos B, **Zupanic A,** Kotnik T, Snoj M, Sersa G, Miklavcic D. Robustness of treatment planning for electrochemotherapy of deep-seated tumors. Submitted to *J Memb Biol.*

VI: Pavselj N, **Zupanic A,** Miklavcic D. Modeling electric field distribution in vivo. In Pakhomov AG, Miklavcic D, Markov MS (eds.) Advanced electroporation techniques in biology and medicine, CRC Press, New York, 2010. (In press)

I

Corovic S, **Zupanic A,** Miklavcic D. Numerical modeling and optimization of electric field distribution in subcutaneous tumor treated with electrochemotherapy using needle electrodes. *IEEE Trans Plasma Sci* 36: 1665-1672, 2008.

Numerical Modeling and Optimization of Electric Field Distribution in Subcutaneous Tumor Treated With Electrochemotherapy Using Needle Electrodes

Selma Corovic, Anze Zupanic, and Damijan Miklavcic

Abstract—Electrochemotherapy (ECT) is an effective antitumor treatment employing locally applied high-voltage electric pulses in combination with chemotherapeutic drugs. For successful ECT, the entire tumor volume needs to be subjected to a sufficiently high local electric field, whereas, in order to prevent damage, the electric field within the healthy tissue has to be as low as possible. To determine the optimum electrical parameters and electrode configuration for the ECT of a subcutaneous tumor, we combined a 3-D finite element numerical tumor model with a genetic optimization algorithm. We calculated and compared the local electric field distributions obtained with different geometrical and electrical parameters and different needle electrode geometries that have been used in research and clinics in past years. Based on this, we established which model parameters had to be taken into account for the optimization of the local electric field distribution and included them in the optimization algorithm. Our results showed that parallel array electrodes are the most suitable for the spherical tumor geometry, because the whole tumor volume is subjected to sufficiently high electric field while requiring the least electric current and causing the least tissue damage. Our algorithm could be a useful tool in the treatment planning of clinical ECT as well as in other electric field mediated therapies, such as gene electrotransfer, transdermal drug delivery, and irreversible tissues ablation.

Index Terms—Electrochemotherapy (ECT), electropermeabilization, finite element method, genetic algorithm, optimization, subcutaneous tumor.

I. INTRODUCTION

ELECTROCHEMOTHERAPY (ECT) is a nonthermal and local tumor treatment, clinically proven to be effective, safe, and well tolerated by patients [1], [2]. ECT standard operating procedures have been defined for the treatment of cutaneous and subcutaneous tumor nodules of different histologies. Numerous published research and clinical reports have shown that it can be used as an efficient local tumor treatment for various tumor types [3]–[8].

ECT is performed using either intravenous or intratumoral chemotherapeutic injection, followed by the application of high-voltage electric pulses locally delivered to the target tissue via appropriate sets of electrodes. Electric pulses induce a local electric field (E) within the treated tissue, which depends on the tissue's electrical and geometrical properties. Namely, for efficient ECT, it is necessary that the entire tumor tissue is subjected to a local electric field in the range between reversible and irreversible electropermeabilization threshold values $(E_{rev} < E < E_{irrev})$, which causes transient structural changes in cell membranes (termed reversible electropermeabilization) and allows for increased entrance of chemotherapeutics into target tissues. This increased membrane permeabilization potentiates the effect of chemotherapeutic drugs, thus significantly lowering the required dose and improving the effectiveness of the treatment [9]. Other requirements for efficient ECT are that the healthy tissue volume subjected to $E > E_{rev}$ has to be kept minimal so as not to expose the healthy tissue to an E higher than necessary and to prevent the excessive irreversible tissue damage $(E > E_{irrev})$. At the same time, the electric current through the tissue has to be as low as possible due to the technical limitations of the high voltage pulse generator.

The magnitude and distribution of local electric field and thus the degree of tissue electropermeabilization can be controlled by electrode configuration and polarity and the amplitude of electric pulses [10], [11]. Local electric field, however also depends on the geometrical and electrical properties of treated tissues; therefore, both have to be taken into account when planning the treatment. Electrode types currently most often used for therapeutic and research purposes are external parallel plate electrodes and different geometries of needle electrode arrays [6], [12]–[14]. External plate electrodes are suitable for the treatment of protruding cutaneous tumors as the local electric field can be easily controlled by the contact surface between electrodes and the treated tissue, the interelectrode distance, and the amplitude of the applied electric pulses. If the target tissue cannot be fixed between the electrodes or is seated in deeper tissue, an array of needle electrodes is more effective as it can penetrate into the tissue to assure the necessary magnitude of electric field within the deeper parts of the tumor. The choice of the suitable electrode type and geometry can be determined by means of a numerical model [13], [15]. Numerical modeling can therefore serve as a vital component in ECT treatment planning; moreover, it can predict the treatment outcome for each tumor type with its specific electrical and geometrical properties, as has already been demonstrated [16].

The authors are with the Faculty of Electrical Engineering, University of Ljubljana, 1000 Ljubljana, Slovenia (e-mail: selma.corovic@fe.uni-lj.si; anze.zupanic@fe.uni-lj.si; damijan.miklavcic@fe.uni-lj.si).

Color versions of one or more of the figures in this paper are available online at http://ieeexplore.ieee.org.
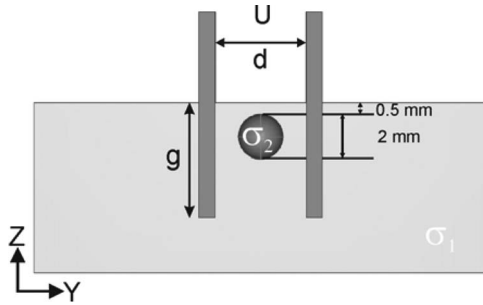
Fig. 1. Central YZ view across the subcutaneous tumor model, where U is the applied voltage between the electrode rows, g is the depth of needle insertion, d is the distance between the electrodes as shown in Fig. 3, and σ_1 and σ_2 are the healthy and tumor tissue conductivities, respectively. The tumor is positioned 0.5 mm below the surface of the model.

In this paper, we used finite element method and genetic algorithm to investigate and optimize the local electric field distribution within a given 3-D model of a subcutaneous tumor. The electric properties of the modeled tissues are based on the fact that the tumor tissue is more conductive than its surrounding healthy tissue [16], [17]. We investigated the influence of the number of needle electrodes, depth of electrode insertion, configuration of electrodes with respect to the treated tissue, and amplitude of electric pulses. We quantified local electric field distribution inside the tumor and its surrounding healthy tissue obtained with four needle electrode geometries that have been used in clinics and research in past years [1], [14], [18]. Based on the calculated distributions of electric field, we established which model parameters had to be taken into account for the optimization of the local electric field distribution and included them in the genetic optimization algorithm that we developed in order to determine the optimum electrode configuration in the target tissue. As the output of the algorithm, we obtained the optimum solution of the analyzed treatment parameters. Our algorithm can be used in local electric field optimization and thus in ECT treatment planning for arbitrary tumor geometries and electrical properties. Our optimization approach can be beneficial also in the treatment planning of other electric field mediated treatments, such as gene electrotransfer [19], transdermal drug delivery [20], and tissue ablation treatments [21].

II. METHODS

A. Tissue Properties and Model Geometry

Our model of a subcutaneous tumor consisted of two tissues, the target tumor tissue (a sphere with a diameter of 2 mm), and its surrounding healthy tissue (Figs. 1–3). Both tissues were considered isotropic and homogeneous, the assigned conductivity values being 0.4 S/m for the tumor and 0.2 S/m for the healthy tissue. These values describe the conductivity at the end of the electropermeabilization process. The values were chosen in accordance with previous measurements of tumor and tissue conductivity and models of subcutaneous tumor and skin electropermeabilization [16], [17], [19].

The electric field distribution was calculated for four different electrode geometries: three different parallel needle electrode arrays [Fig. 2(a)–(c)] and a hexagonal electrode array
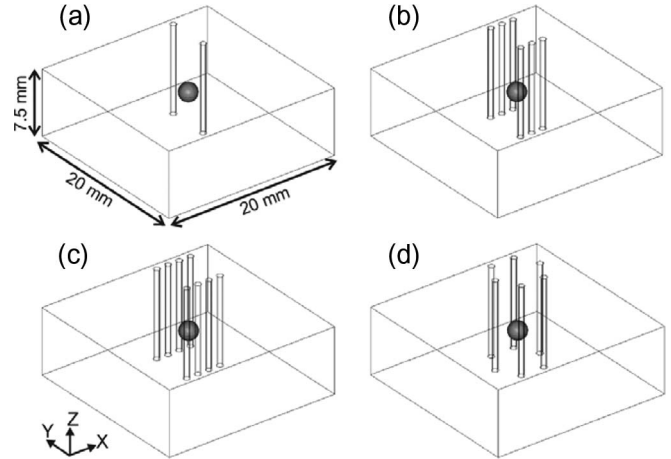
Fig. 2. Three-dimensional geometry of subcutaneous tumor with four needle electrode geometries analyzed: (a) One needle electrode pair, (b) three needle electrode pairs, (c) four needle electrode pairs, and (d) hexagonal needle electrode array.
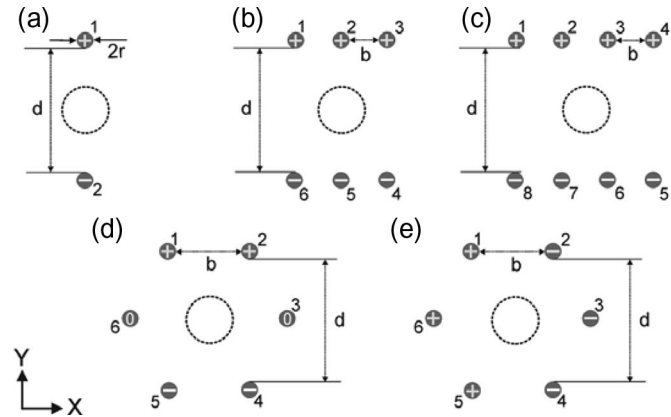
Fig. 3. XY view of the model with electrode geometries, polarities, and arrangement with respect to (the circled region) the target/tumor tissue: (a) One needle electrode pair, (b) three needle electrode pairs, (c) four needle electrode pairs, (d) 2 × 2 hexagonal needle electrode array (two electrodes on positive potential, two on negative potential, and two grounded), and (e) 3 × 3 hexagonal needle electrode array (three electrodes on positive potential and three on negative potential). d and b stand for the distance between opposite sets of electrodes and distance between electrodes of the same row (parallel needle electrode arrays) or distance between neighboring electrodes (hexagonal needle electrode array), respectively.

[Fig. 2(d)], and five electrode polarities: three for the parallel needle electrode arrays [Fig. 3(a)–(c)] and two for the hexagonal electrode array [Fig. 3(d) and (e)]. These geometries and polarities were chosen as they are the most often used in ECT research and therapy.

B. Numerical Modeling

All numerical calculations were performed with a commercial finite element software package COMSOL Multiphysics 3.3a (COMSOL AB, Sweden) and run on a desktop PC (Windows XP, 3.0-GHz Pentium 4, 1-GB RAM). Electric field distribution in the tissue, caused by an electric pulse, was determined by solving the Laplace equation for static electric currents

$$-\nabla \cdot (\sigma \cdot \nabla \varphi) = 0 \qquad (1)$$

where σ and φ stand for the electric conductivity of the tissue and electric potential, respectively. The boundary conditions used in our calculations were a constant potential on the surface of the electrodes (Fig. 3) and electric insulation on all outer boundaries of the model. Results were controlled for numerical errors by increasing the size of our model and increasing the mesh density, until the electric insulation condition and error due to meshing irregularities were insignificant—a further increase in domain size or mesh density only increased the computation time; however, the results changed less than 0.5%.

The electric field distributions obtained in our models were displayed in the range from the reversible $E_{\mathrm{rev}} = 400$ V/cm to the irreversible electropermeabilization threshold value $E_{\mathrm{irrev}} = 900$ V/cm. These values were taken from a previously published study, in which we estimated them by comparing *in vivo* measurements and the numerical modeling of the electropermeabilization of a subcutaneous tumor [16], [22]. Namely, E_{rev} was estimated to be the same for the tumor and skin tissue (400 V/cm), whereas the E_{irrev} values were estimated to be 800 and 1000 V/cm for the tumor and skin, respectively. The E_{irrev} in our model was set as the average of these two values (900 V/cm) in the tumor and healthy tissue.

C. Optimization

The genetic algorithm [23] was written with MATLAB 2007a (Mathworks, USA) and run together with the numerical calculation using the link between MATLAB and COMSOL. The initial population of chromosomes (vectors of real numbers: $X = (x_1, x_2, \ldots, x_n)$) was generated randomly, taking into account the following model constraints: range of distances between electrodes, range of depth of electrode insertion into tissue, and range of voltages between the electrodes. These constraints were chosen so that the calculation domain size, COMSOL meshing capabilities, and oncology experts' demands for a safety margin [24], when treating solid tumors, were all respected. Chromosomes for reproduction were selected proportionally to their fitness, according to the fitness function

$$F = 12 + 100 \cdot V_{\mathrm{Trev}} - 10 \cdot V_{\mathrm{Hirrev}} - V_{\mathrm{Hrev}} - V_{\mathrm{Tirrev}} \quad (2)$$

where F stands for fitness, V_{Trev} and V_{Tirrev} stand for tumor volume subjected to the local electric field above E_{rev} and E_{irrev}, respectively, and V_{Hrev} and V_{Hirrev} stand for the volume of healthy tissue subjected to local electric field above E_{rev} and E_{irrev}, respectively. The weights in the fitness function were set accordingly to the importance of the individual parameters for efficient ECT. Namely, V_{Trev} is crucial for efficient ECT; therefore, its weight is largest (100) in comparison to the weight of V_{Hirrev} (10), which was in turn larger than the weights of V_{Hrev} and V_{Tirrev}, as their significance for successful ECT is still debated. Other weight values that kept a similar ratio gave similar results. The integer 12 is present only to assure that the fitness function is always positive.

The selected chromosomes reproduced by crossover or mutation. When crossover takes place, each new chromosome

TABLE I
GENETIC ALGORITHM PARAMETERS

Size of initial population	Number of generations	Fraction of elite chromosomes [%]	Probability of cross-over	Probability of mutation
20 - 30	100	10	0.95	0.05

$Z = (z_1, z_2, \ldots, z_n)$ is a random linear combination of parent chromosomes X and Y

$$z_i = a_i \cdot x_i + (1 - a_i) \cdot y_i, \qquad a_i \in [0, 1]. \quad (3)$$

When mutation takes place, each new chromosome $M = (m_1, m_2, \ldots, m_n)$ is a random variation of one parent chromosome X

$$m_i = x_i + b_i \cdot x_i, \qquad b_i \in [-0.3, 0.3]. \quad (4)$$

Crossover and mutation were chosen according to the probabilities in Table I, with the exception that the top ranking solutions (elite) could not be subjected to mutation. The genetic algorithm was terminated after 100 generations, when the fitness of the highest ranking solution usually reached a plateau. The algorithm always converged to a possible optimum solution. The average computation time of the algorithm was two hours. Other genetic algorithm parameters can be found in Table I.

D. Protocol

To select the optimum electrode configuration for ECT of the subcutaneous tumor model, we first analyzed the local electric field distribution inside the tissue model for several discrete values of applied voltage between electrodes for all electrode geometries and polarities (Fig. 3). Distance between opposite sets of electrodes d and distance between electrodes of the same row b (parallel needle electrode arrays) or distance between neighboring electrodes b (hexagonal needle electrode array) were kept constant, at $b = 0.65$ mm (parallel arrays), $b = 4/\sqrt{3}$ mm (hexagonal array), and $d = 4$ mm, in all simulations. For each electrode geometry and two electrode depths ($g = 3$ mm—as deep as the bottom of the tumor; $g = 5$ mm—double the depth of the tumor), we calculated the minimum voltage U_c (critical voltage) that had to be applied between the electrodes so that the minimum electric field over the entire tumor volume exceeded E_{rev}. This was done by a sequence of calculations, in which we decreased the voltage by increments of 10 V, until the lowest needed amplitude was reached. We then selected the calculated critical voltage U_c that resulted in the lowest calculated values of reversibly electropermeabilized volume of healthy tissue V_{Hrev} and total electric current I and applied it to each electrode configuration. We examined the influence of the depth of insertion on the local electric field distribution within the target tumor tissue and its surrounding healthy tissue by visualization of the electric field and by quantification of electric distribution by calculating V_{Trev}, V_{Hrev}, V_{Hirrev}, and I.

TABLE II
CALCULATED VALUES OF CRITICAL VOLTAGE U_C, TOTAL ELECTRIC CURRENT I, REVERSIBLY ELECTROPERMEABILIZED TUMOR VOLUME V_{Trev}, AND REVERSIBLY AND IRREVERSIBLY ELECTROPERMEABILIZED HEALTHY TISSUE V_{Hrev} AND V_{Hirrev}, RESPECTIVELY, ARE GIVEN FOR ALL ANALYZED ELECTRODE GEOMETRIES AND POLARITIES AND FOR DEPTHS OF ELECTRODE INSERTIONS $g = 3$ mm AND $g = 5$ mm. ALL VOLUME VALUES ARE NORMALIZED BY THE TUMOR VOLUME V_T. DISTANCE BETWEEN OPPOSITE SETS OF ELECTRODES d AND DISTANCE BETWEEN ELECTRODES OF THE SAME ROW b (NEEDLE ELECTRODE ARRAYS) OR DISTANCE BETWEEN NEIGHBORING ELECTRODES b (HEXAGONAL NEEDLE ELECTRODE ARRAY) WERE KEPT CONSTANT AT $b = 0.65$ mm (PARALLEL NEEDLE ELECTRODE ARRAYS), $b = 4/\sqrt{3}$ mm (HEXAGONAL NEEDLE ELECTRODE ARRAY), AND $d = 4$ mm, IN ALL SIMULATIONS

Electrode configuration and polaririty	g [mm]	U_C [V]	I [A]	$\dfrac{V_{Trev}}{V_T}$	$\dfrac{V_{Hrev}}{V_T}$	$\dfrac{V_{Hirrev}}{V_T}$
one-needle pair	5	400	0.248	1	29.96	6.14
	3	440	0.175	1	21.00	5.14
three-needle pairs	5	260	0.270	1	31.86	1.71
	3	290	0.198	1	24.86	2.35
four-needle pairs	5	240	0.294	1	43.78	2.43
	3	280	0.234	1	29.21	2.14
2x2 hexagonal array	5	290	0.301	1	38.36	3.64
	3	350	0.234	1	30.64	4.92
3x3 hexagonal array	5	280	0.463	1	42.43	9.71
	3	310	0.330	1	31.4	8.07

TABLE III
CALCULATED VALUES OF TOTAL ELECTRIC CURRENT I, REVERSIBLY ELECTROPERMEABILIZED TUMOR VOLUME V_{Trev}, AND REVERSIBLY AND IRREVERSIBLY ELECTROPERMEABILIZED HEALTHY TISSUE V_{Hrev} AND V_{Hirrev}, RESPECTIVELY, ARE GIVEN FOR ALL ANALYZED ELECTRODE GEOMETRIES AND POLARITIES AND FOR DEPTHS OF ELECTRODE INSERTIONS $g = 3$ mm AND $g = 5$ mm. ALL VOLUME VALUES ARE NORMALIZED BY THE TUMOR VOLUME V_T. DISTANCE BETWEEN OPPOSITE SETS OF ELECTRODES d AND DISTANCE BETWEEN ELECTRODES OF THE SAME ROW b (NEEDLE ELECTRODE ARRAYS) OR DISTANCE BETWEEN NEIGHBORING ELECTRODES b (HEXAGONAL NEEDLE ELECTRODE ARRAY) WERE KEPT CONSTANT AT $b = 0.65$ mm (PARALLEL NEEDLE ELECTRODE ARRAYS), $b = 4/\sqrt{3}$ mm (HEXAGONAL NEEDLE ELECTRODE ARRAY), AND $d = 4$ mm, IN ALL SIMULATIONS. VOLTAGE WAS SET TO $U = 290$ V IN ALL SIMULATIONS

Electrode configuration and polaririty	g [mm]	U [V]	I [A]	$\dfrac{V_{Trev}}{V_T}$	$\dfrac{V_{Hrev}}{V_T}$	$\dfrac{V_{Hirrev}}{V_T}$
one-needle pair	5	290	0.180	0.08	17.21	2.71
	3	290	0.115	0.03	10.42	2.00
three-needle pairs	5	290	0.301	1.00	37.21	2.79
	3	290	0.198	1.00	24.86	2.36
four-needle pairs	5	290	0.354	1.00	45.86	2.86
	3	290	0.236	1.00	30.64	2.42
2x2 hexagonal array	5	290	0.291	1.00	36.86	3.29
	3	290	0.190	0.41	22.93	2.71
3x3 hexagonal array	5	290	0.471	1.00	44.07	10.57
	3	290	0.308	0.99	29.07	7.00

Because the first part of our study showed that voltage (U), distances between electrodes (b and d), and depth of electrode insertion (g) are all relevant for the distribution of electric field in the model, all four parameters were chosen for the optimization procedure. We ran the genetic algorithm for all electrode geometries and polarities in two distinct stages. In the first stage, ten runs of the algorithm were performed using a random initial population. To calculate solutions closer to the true optimum, the ten best solutions acquired from the first stage were "seeded" into the initial population of the second stage and five more solutions were calculated, all being of better fitness than the first-stage solutions. However, the difference between the best first- and second-stage solutions was less than 1% (if compared by V_{Hirrev}); therefore, no third stage was required, and the best second stage solution was considered to be the optimum.

III. RESULTS

The calculated critical voltage U_c needed to cover the entire tumor tissue with electric field above reversible electropermeabilization threshold E_{rev} for each electrode geometry and polarity is given in Table II. The shallower insertion of the electrodes generally increased the necessary U_C; however, the total current I through the model decreased. Increasing the number of the electrodes had the opposite effect: Lower U_C and higher I were calculated. Both observations can be explained

Erev<E   Erev<E<Eirrev   E>Eirrev
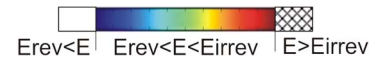
Fig. 4. False color legend used in Figs. 5–7, indicating the local electric field E distribution within the tissue models (i.e., the degree of tissue electropermeabilization). The white region represents insufficiently electropermeabilized regions of tissue ($E < E_{\mathrm{rev}}$), and the patterned region represents irreversibly electropermeabilized regions of tissue ($E > E_{\mathrm{irrev}}$).

by the size of contact surface between electrodes and treated tissue—larger contact surface increases I and decreases the necessary U_C.

When we applied the same voltage (290 V) to all electrode configurations, complete electropermeabilization of the tumor was not obtained in all cases. Namely, one needle electrode pair was completely unsuccessful, whereas both hexagonal geometries did not provide adequate coverage at $g = 3$ mm [Table III, Figs. 4, 5(a) and (b), and 6(b) and (d)]. Figs. 5 and 6 show a definite influence of electrode configuration on electric field distribution in the tumor and healthy tissue. This influence is most clearly seen by comparing electric field distributions of both hexagonal needle electrode arrays—electric field penetrates deeper for 3×3 geometry and V_{Hirrev} is considerably larger than in 2×2 geometry (Fig. 6). It can also be observed that deeper insertion of electrodes $(g = 5$ mm) and insufficient voltage applied on the electrodes cause the electric field to be higher within the healthy tissue below the tumor compared to

Fig. 5.   Local electric field distribution for the models of (a) and (b) one needle electrode pair, (c) and (d) three needle electrode pairs, and (e) and (f) four needle electrode pairs is shown for two depths of electrodes' insertion $g = 5$ mm [(a), (c), (e)] and $g = 3$ mm [(b), (d), (f)]. Electric field distribution is shown in three central perpendicular planes: XY, YZ, and XZ all passing through the center of the tumor. Distance between opposite sets of electrodes d, distance between electrodes of the same row b (needle electrode arrays) or distance between neighboring electrodes b (hexagonal needle electrode array) and voltage U are given in the caption of Table III.
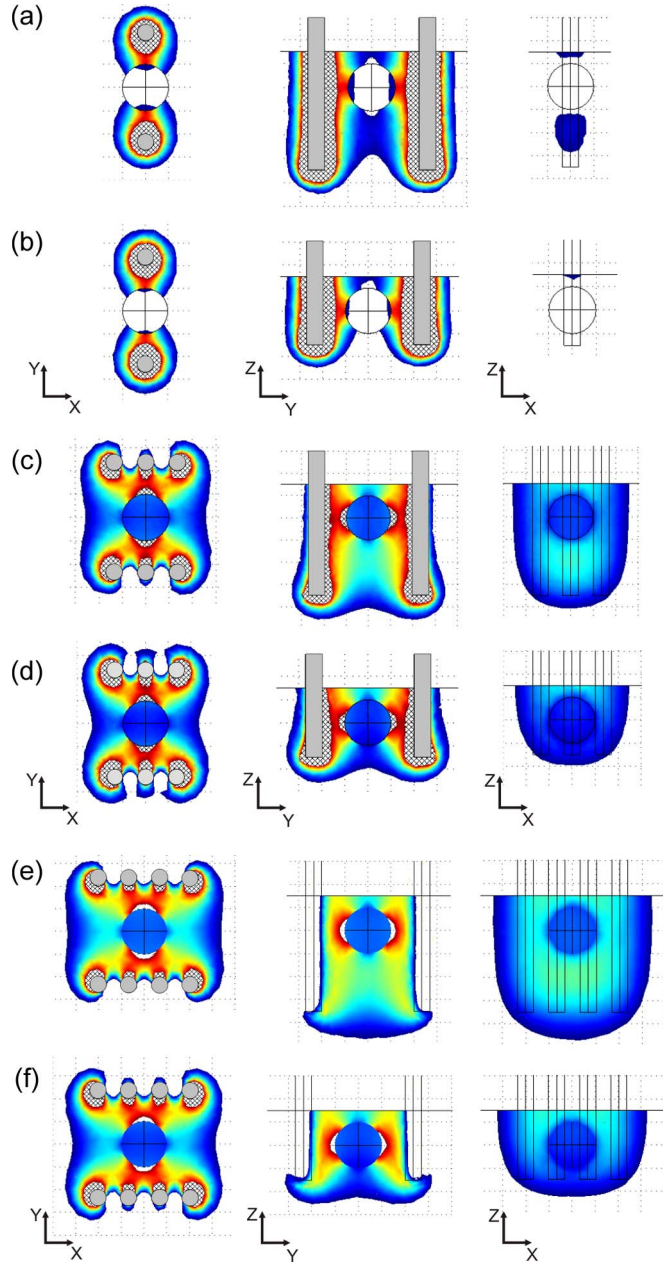

Fig. 6.   Local electric field distribution for the models of (a) and (b) 2 × 2 hexagonal needle electrode array and (c) and (d) 3 × 3 hexagonal needle electrode array is shown for two depths of electrodes' insertion $g = 5$ mm [(a), (c)] and $g = 3$ mm [(b), (d)]. Electric field distribution is shown in three central perpendicular planes: XY, YZ, and XZ all passing through the center of the tumor. Distance between opposite sets of electrodes d, distance between electrodes of the same row b (needle electrode arrays) or distance between neighboring electrodes b (hexagonal needle electrode array) and voltage U are given in the caption of Table III.

the electric field inside the tumor (Fig. 5(a), (c), and (e) in ZX orientation).

To assure complete electropermeabilization of the tumor and with the least healthy tissue damage in our model, all geometrical and electrical parameters have to be accounted for. When all parameters were optimized simultaneously, the required U_C was significantly lower (Table IV) than when determining the U_C for only two depths of needle insertion (Table II). At the same time, I, V_{Hrev}, and V_{Hirrev} were also

decreased, thus minimizing healthy tissue damage and required electric energy. Interestingly, the optimum depth of insertion depended very much on the electrode geometry, i.e., at similar applied voltages, the 2 × 2 hexagonal needle electrode array has to be inserted deeper than the 3 × 3 needle electrode array to achieve similar coverage of the target tumor tissue. The results of optimization using our algorithm are shown in Table IV and Fig. 7.

IV. DISCUSSION AND CONCLUSION

The aim of our study was to investigate and optimize the local electric field within a simple 3-D model of a subcutaneous tumor. We report the results of optimization of the geometrical and electrical parameters (voltage, distances between electrodes, depth of electrode insertion: U, b, d, and g; Figs. 1 and 3) of various needle electrode geometries used in research and clinical ECT for a 3-D numerical model of a subcutaneous tumor (Fig. 2). We show by using our optimization algorithm, how the local electric field distribution depends on the number, arrangement, depth of electrodes' insertion, and the amplitude

TABLE IV

OPTIMIZED VALUES OF DISTANCE BETWEEN ELECTRODES OF THE SAME ROW b (NEEDLE ELECTRODE ARRAYS), DISTANCE BETWEEN NEIGHBORING ELECTRODES b (HEXAGONAL NEEDLE ELECTRODE ARRAY), DISTANCE BETWEEN OPPOSITE SETS OF ELECTRODES d, DEPTH OF ELECTRODES' INSERTION g, AND CRITICAL VOLTAGE U_C FOR ALL ANALYZED ELECTRODE GEOMETRIES AND POLARITIES ARE GIVEN. CALCULATED VALUES OF TOTAL ELECTRIC CURRENT I, REVERSIBLY ELECTROPERMEABILIZED TUMOR VOLUME V_{Trev}, REVERSIBLY AND IRREVERSIBLY ELECTROPERMEABILIZED HEALTHY TISSUE V_{Hrev} AND V_{Hirrev}, RESPECTIVELY, ARE GIVEN FOR ALL OPTIMUM SOLUTIONS. ALL VOLUME VALUES ARE NORMALIZED BY THE TUMOR VOLUME V_T

Electrode configuration and polarity	b [mm]	d [mm]	g [mm]	U_C [V]	I [A]	$\dfrac{V_{Trev}}{V_T}$	$\dfrac{V_{Hrev}}{V_T}$	$\dfrac{V_{Hirrev}}{V_T}$
three-needle pairs	0.70	4.04	3.15	272	0.20	1	23.64	1.86
four-needle pairs	0.67	4.10	3.20	265	0.25	1	28.29	1.65
2x2 hexagonal array	1.71	3.47	3.57	256	0.24	1	21.86	2.34
3x3 hexagonal array	1.71	3.47	2.90	246	0.32	1	21.64	5.14

of electric pulses (Figs. 5–7, Tables II–IV). The complete coverage of the target tumor tissue with the local electric field magnitude required for successful ECT ($E_{\text{rev}} < E < E_{\text{irrev}}$) was achieved, whereas the volumes of healthy tissue exposed to the magnitude of the local electric field above reversible and irreversible thresholds were minimized (thus minimizing healthy tissue damage) for all analyzed electrode geometries.

Our study was built on previous research works done by our group and others, in which the usefulness of numerical modeling in predicting electropermeabilization outcomes was demonstrated. Already, the early numerical plate and needle electrode models in combination with *in vivo* experiments showed great promise in analysis of tissue electropermeabilization *in vivo* [18], [25]. However, only after the experimental validation of a numerical model was performed by comparing the numerical calculations to histological examinations of electropermeabilized tissue did numerical modeling gain ground in ECT research [11]. Different geometries of needle electrodes have been since then compared by [14], [26], and [27]; however, none of these included optimization and only Sel *et al.* [28] used a 3-D model. In our study, three needle electrode pairs, four needle electrode pairs, and 2×2 hexagonal needle electrode array all gave similar results, whereas the 3×3 hexagonal needle electrode array was significantly worse than the others. We examined the adequacy of needle electrode geometries by calculating values of total electric current through the model and volumes of reversibly and irreversibly electropermeabilized (damaged) healthy tissue. By analyzing all three measures, we can conclude that three needle electrode pairs gave the best results—they required the lowest total electric current, which caused a small volume of healthy tissue to be reversibly and even less to be irreversibly electropermeabilized (Fig. 7(a), Table IV). Four needle electrode pairs caused the
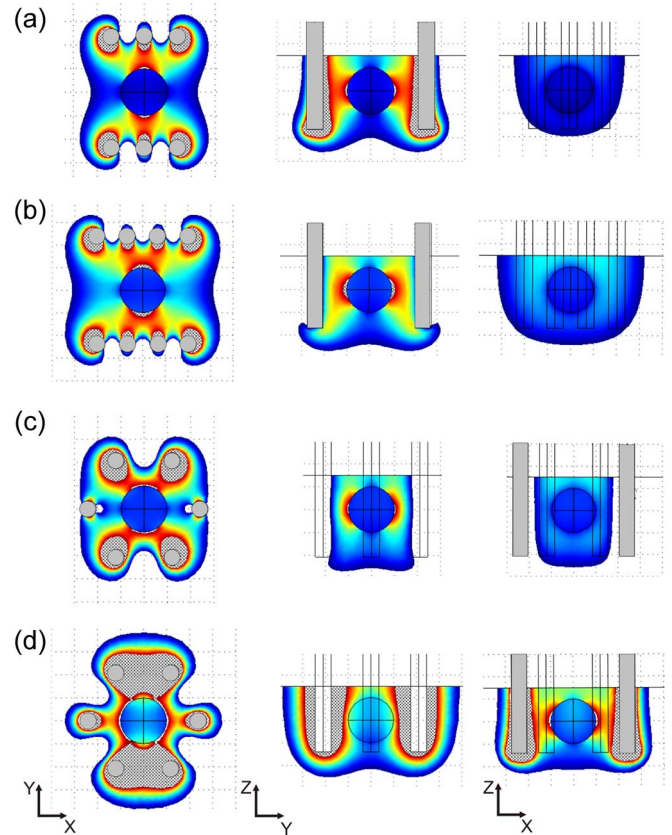

Fig. 7. Local electric field distribution for the optimized models of (a) three needle electrode pairs, (b) four needle electrode pairs, (c) 2×2 hexagonal needle electrode array, and (d) 3×3 hexagonal needle electrode array is shown. The electric field distribution is shown in three central perpendicular planes: XY, YZ, and XZ all passing through the center of the tumor. Corresponding optimized parameters which are distance between electrodes of the same row b (needle electrode arrays), distance between neighboring electrodes b (hexagonal needle electrode array), distance between opposite sets of electrodes d, depth of electrodes' insertion g, and critical voltage U_C are given in Table IV.

least healthy tissue damage; however, they required more current and more healthy tissue to be reversibly electropermeabilized (Fig. 7(b), Table IV), confirming previous results of our group—more electrodes mean a more invasive procedure, higher needed current, and lower needed voltage to obtain the same target tissue coverage [11], [26]. The 2×2 hexagonal needle electrode array caused the least volume of healthy tissue to be reversibly electropermeabilized and more to be irreversibly electropermeabilized (Fig. 7(c), Table IV). The 3×3 hexagonal needle electrode array optimization lead to the highest values of total electric current and the largest area of irreversibly permeabilized healthy tissue (Fig. 7(d), Table IV). The preference for three needle electrode pairs is also in agreement with our previous 2-D study [27].

The only other ECT optimization study was performed by Sel *et al.* who optimized the distance and voltage between electrodes for a realistic brain tumor using four pairs of needle electrodes as a proof of principle [28]. In our study, we used a simpler tumor model; however, we took the optimization one step further by optimizing for four different electrode geometries and polarities and for four different parameters, one of them being the depth of needle insertion, which turned

out to be significant. We demonstrated that inserting needle electrodes deeper than necessary, using inadequate electrode geometries, polarities, and arrangement with respect to the target tumor tissue, and applying insufficient voltage can result in unsuccessful electropermeabilization ($E < E_{\text{rev}}$) of the tumor. Moreover, the electric field within the healthy tissue below the tumor can be higher compared to the electric field inside the tumor [Figs. 5(a) and 6(d)]. This effect can be even more pronounced if the tumor is much more conductive than the surrounding tissue, because the electric field is then lower in the tumor and higher in the surrounding tissue [27]. The importance of insertion depth can also be seen if we compare the optimum depth for hexagonal needle electrode arrays—deeper insertion is required for the 2×2 needle electrode array, although all other geometrical parameters are the same for both configurations.

Even though our algorithm gives good results, significant challenges remain before it can be used for the optimization of *in vivo* ECT of large tumors. Our study does not analyze the possibility of changing electric field orientation in consecutive pulses, which can lead to less tissue damage, because such protocols can require lower voltage and total current [14]. Unfortunately, increasing the number of pulses can increase the unpleasantness of the treatment [29]. We also did not take into account the dynamic changes in tissue conductivities due to the tissue electropermeabilization [19], [28], [30] because this would significantly increase the computation time and would not considerably contribute to the results. Instead, we incorporated the change in conductivity into our model by choosing conductivity values at the end of the electropermeabilization process. Stratum corneum was not added to the model, as needle electrodes penetrate the skin and thus bypass its high resistivity [13]; however, if plate electrodes were to be used, we would most probably have to take into account also the stratum corneum and the skin conductivity changes due to electropermeabilization.

We chose the genetic algorithm as our optimization method, as it is relatively easy to develop and, unlike classical optimization methods, it does not require the fitness function to be differentiable. Linear and nonlinear constraints, such as the realistic technical limitations of high-voltage electric pulse generator (maximum output voltage and current), can be easily implemented into the algorithm, and it also allows optimization of a large number of continuous, discrete, and categorical parameters, e.g., type of electrodes. The drawbacks of the method are that it gives only an approximate solution to the optimization problem and requires a relatively long computation time. However, because the solutions of the algorithm are very close to the true optimum and computation times can be shortened by using a more powerful computer, we do not consider these to be significant drawbacks and believe that the suggested approach is well suited to the problem being addressed.

Numerical modeling and optimization can be efficiently combined to control the extent of tissue electropermeabilization in ECT and to produce the optimum electrode configuration for different types of tumors taking into account their electric properties. Our algorithm is a step forward to an effective treatment planning, not only in clinical ECT, but also in other electroporation-based treatments, such as gene electrotransfer [19], transdermal drug delivery [20], and irreversible tumor ablation [21].

REFERENCES

[1] M. Marty, G. Sersa, J. R. Garbay, J. Gehl, C. G. Collins, M. Snoj, V. Billard, P. F. Geertsen, J. O. Larkin, D. Miklavcic, I. Pavlovic, S. M. Paulin-Kosir, M. Cemazar, N. Morsli, Z. Rudolf, C. Robert, G. C. O'Sullivan, and L. M. Mir, "Electrochemotherapy—An easy, highly effective and safe treatment of cutaneous and subcutaneous metastases: Results of ESOPE (European Standard Operating Procedures of Electrochemotherapy) study," *Eur. J. Cancer, Suppl.*, vol. 4, no. 11, pp. 3–13, Nov. 2006.

[2] G. Sersa, "The state-of-the-art of electrochemotherapy before the ESOPE study; advantages and clinical uses," *Eur. J. Cancer, Suppl.*, vol. 4, no. 11, pp. 52–59, Nov. 2006.

[3] R. Heller, R. Gilbert, and M. J. Jaroszeski, "Clinical applications of electrochemotherapy," *Adv. Drug Deliv. Rev.*, vol. 35, no. 1, pp. 119–129, Jan. 1999.

[4] A. Gothelf, L. M. Mir, and J. Gehl, "Electrochemotherapy: Results of cancer treatment using enhanced delivery of bleomycin by electroporation," *Cancer Treat. Rev.*, vol. 29, no. 5, pp. 371–387, Oct. 2003.

[5] B. M. Tijink, R. De Bree, G. Van Dongen, and C. R. Leemans, "How we do it: Chemo-electroporation in the head and neck for otherwise untreatable patients," *Clin. Otolaryngol.*, vol. 31, no. 5, pp. 447–451, Oct. 2006.

[6] L. M. Mir, J. Gehl, G. Sersa, C. G. Collins, J. R. Garbay, V. Billard, P. F. Geertsen, Z. Rudolf, G. C. O'Sullivan, and M. Marty, "Standard operating procedures of the electrochemotherapy: Instructions for the use of bleomycin or cisplatin administered either systemically or locally and electric pulses delivered by the Cliniporator by means of invasive or non-invasive electrodes," *Eur. J. Cancer, Suppl.*, vol. 4, no. 11, pp. 14–25, Nov. 2006.

[7] M. Snoj, Z. Rudolf, M. Cemazar, B. Jancar, and G. Sersa, "Successful sphincter-saving treatment of anorectal malignant melanoma with electrochemotherapy, local excision and adjuvant brachytherapy," *Anti-Cancer Drugs*, vol. 16, no. 3, pp. 345–348, Mar. 2005.

[8] G. Sersa, M. Cemazar, D. Miklavcic, and Z. Rudolf, "Electrochemotherapy of tumours," *Radiol. Oncol.*, vol. 40, no. 3, pp. 163–174, 2006.

[9] C. Domenge, S. Orlowski, B. Luboinski, T. De Baere, G. Schwaab, J. Belehradek, and L. M. Mir, "Antitumor electrochemotherapy: New advances in the clinical protocol," *Cancer*, vol. 77, no. 5, pp. 956–963, Mar. 1996.

[10] D. Miklavcic, K. Beravs, D. Semrov, M. Cemazar, F. Demsar, and G. Sersa, "The importance of electric field distribution for effective in vivo electroporation of tissues," *Biophys. J.*, vol. 74, no. 5, pp. 2152–2158, May 1998.

[11] D. Miklavcic, D. Semrov, H. Mekid, and L. M. Mir, "A validated model of in vivo electric field distribution in tissues for electrochemotherapy and for DNA electrotransfer for gene therapy," *Biochim. Biophys. Acta*, vol. 1523, no. 1, pp. 73–83, Sep. 2000.

[12] M. Puc, S. Corovic, K. Flisar, M. Petkovsek, J. Nastran, and D. Miklavcic, "Techniques of signal generation required for electropermeabilization. Survey of electropermeabilization devices," *Bioelectrochemistry*, vol. 64, no. 2, pp. 113–124, Sep. 2004.

[13] D. Miklavcic, S. Corovic, G. Pucihar, and N. Pavselj, "Importance of tumour coverage by sufficiently high local electric field for effective electrochemotherapy," *Eur. J. Cancer, Suppl.*, vol. 4, no. 11, pp. 45–51, Nov. 2006.

[14] R. A. Gilbert, M. J. Jaroszeski, and R. Heller, "Novel electrode designs for electrochemotherapy," *Biochim. Biophys. Acta*, vol. 1334, no. 1, pp. 9–14, Feb. 1997.

[15] J. F. Edd, L. Horowitz, R. V. Davalos, L. M. Mir, and B. Rubinsky, "In vivo results of a new focal tissue ablation technique: Irreversible electroporation," *IEEE Trans. Biomed. Eng.*, vol. 53, no. 7, pp. 1409–1415, Jul. 2006.

[16] N. Pavselj, Z. Bregar, D. Cukjati, D. Batiuskaite, L. Mir, and D. Miklavcic, "The course of tissue permeabilization studied on a mathematical model of a subcutaneous tumor in small animals," *IEEE Trans. Biomed. Eng.*, vol. 52, no. 8, pp. 1373–1381, Aug. 2005.

[17] D. Miklavcic, N. Pavselj, and F. X. Hart, "Electric properties of tissues," in *Wiley Encyclopedia of Biomedical Engineering*. New York: Wiley, 2006.

[18] J. Gehl, T. H. Sorensen, K. Nielsen, P. Raskmark, S. L. Nielsen, T. Skovsgaard, and L. M. Mir, "In vivo electroporation of skeletal muscle:

Threshold, efficacy and relation to electric field distribution," *Biochim. Biophys. Acta*, vol. 1428, no. 2, pp. 233–240, Aug. 1999.

[19] D. Cukjati, D. Batiuskaite, F. Andre, D. Miklavcic, and L. M. Mir, "Real time electroporation control for accurate and safe in vivo non-viral gene therapy," *Bioelectrochemistry*, vol. 70, no. 2, pp. 501–507, May 2007.

[20] U. F. Pliquett, R. Vanbever, V. Preat, and J. C. Weaver, "Local transport regions (LTRs) in human stratum corneum due to long and short "high voltage" pulses," *Bioelectrochem. Bioenerg.*, vol. 47, no. 1, pp. 151–161, Nov. 1998.

[21] B. Al-Sakere, C. Bernat, E. Connault, P. Opolon, B. Rubinsky, R. Davalos, and L. M. Mir, "Tumor ablation with irreversible electroporation," *PLoS ONE*, vol. 2, no. 11, p. e1 135, 2007.

[22] D. Semrov and D. Miklavcic, "Calculation of the electrical parameters in electrochemotherapy of solid tumours in mice," *Comput. Biol. Med.*, vol. 28, no. 4, pp. 439–448, Jul. 1998.

[23] J. H. Holland, *Adaptation in Natural and Artificial Systems: An Introductory Analysis With Applications to Biology, Control, and Artificial Intelligence*. Cambridge, MA: MIT Press, 1992.

[24] J. Gehl and P. F. Geertsen, "Palliation of haemorrhaging and ulcerated cutaneous tumours using electrochemotherapy," *Eur. J. Cancer, Suppl.*, vol. 4, no. 11, pp. 35–37, Nov. 2006.

[25] G. Sersa, M. Cemazar, D. Semrov, and D. Miklavcic, "Changing electrode orientation improves the efficacy of electrochemotherapy of solid tumors in mice," *Bioelectrochem. Bioenerg.*, vol. 39, no. 1, pp. 61–66, Feb. 1996.

[26] D. Sel, S. Mazeres, J. Teissie, and D. Miklavcic, "Finite-element modeling of needle electrodes in tissue from the perspective of frequent model computation," *IEEE Trans. Biomed. Eng.*, vol. 50, no. 11, pp. 1221–1232, Nov. 2003.

[27] S. Corovic, M. Pavlin, and D. Miklavcic, "Analytical and numerical quantification and comparison of the local electric field in the tissue for different electrode configurations," *Biomed. Eng. Online*, vol. 6, no. 1, p. 37, 2007.

[28] D. Sel, A. M. Lebar, and D. Miklavcic, "Feasibility of employing model-based optimization of pulse amplitude and electrode distance for effective tumor electropermeabilization," *IEEE Trans. Biomed. Eng.*, vol. 54, no. 5, pp. 773–781, May 2007.

[29] A. Zupanic, S. Ribaric, and D. Miklavcic, "Increasing the repetition frequency of electric pulse delivery reduces unpleasant sensations that occur in electrochemotherapy," *Neoplasma*, vol. 54, no. 3, pp. 246–250, 2007.

[30] R. V. Davalos, B. Rubinsky, and D. M. Otten, "A feasibility study for electrical impedance tomography as a means to monitor tissue electroporation for molecular medicine," *IEEE Trans. Biomed. Eng.*, vol. 49, no. 4, pp. 400–403, Apr. 2002.

Anze Zupanic was born in 1981. He received the B.Sc. degree in electrical engineering from the University of Ljubljana, Ljubljana, Slovenia, where he is currently working toward the Ph.D. degree in electrical engineering in the Faculty of Electrical Engineering.

He is a Young Researcher with the Faculty of Electrical Engineering, University of Ljubljana. His main research interests are multiphysics numerical modeling and optimization of electroporation-based treatments.

Damijan Miklavcic was born in Ljubljana, Slovenia, in 1963. He received the Ph.D. degree in electrical engineering from the University of Ljubljana, Ljubljana.

He is a Professor with the Faculty of Electrical Engineering, University of Ljubljana, and the Head of the Laboratory of Biocybernetics. He is active in the field of biomedical engineering. His interest in the last years focuses on electroporation-assisted drug and gene delivery, including cancer treatment by means of electrochemotherapy, tissue oxygenation, modeling of biological processes, and hardware development.

Selma Corovic was born in 1976. She received the B.Sc. and M.Sc. degrees in electrical engineering from the University of Ljubljana, Ljubljana, Slovenia. She is currently working toward the Ph.D. degree at the Faculty of Electrical Engineering, University of Ljubljana and at the Paris University-Sud XI, Châtenay-Malabry 92 296, France.

She is an Assistant Researcher with the Faculty of Electrical Engineering, University of Ljubljana. Her main research interests are multiphysics numerical modeling and *in vivo* studies of electroporation process in biological tissues and web-based e-learning application development for electroporation-based treatments.

II

Zupanic A, Corovic S, Miklavcic D. Optimization of electrode position and electric pulse amplitude in electrochemotherapy. *Radiol Oncol* 42: 93-101, 2008.

Optimization of electrode position and electric pulse amplitude in electrochemotherapy

Anže Županič, Selma Čorović and Damijan Miklavčič

University of Ljubljana, Faculty of Electrical Engineering, Ljubljana, Slovenia

Background. *In addition to the chemotherapeutic drug being present within the tumor during electric pulse delivery, successful electrochemotherapy requires the entire tumor volume to be subjected to a sufficiently high electric field, while the electric field in the surrounding healthy tissue is as low as possible to prevent damage. Both can be achieved with appropriate positioning of the electrodes and appropriate amplitude of electric pulses.*

Methods. *We used 3D finite element numerical models and a genetic optimization algorithm to determine the optimum electrode configuration and optimum amplitude of electric pulses for treatment of three subcutaneous tumor models of different shapes and sizes and a realistic brain tumor model acquired from medical images.*

Results. *In all four tumor cases, parallel needle electrode arrays were a better choice than hexagonal needle electrode arrays, since their utilization required less electric current and caused less healthy tissue damage. In addition, regardless of tumor geometry or needle electrode configuration, the optimum depth of electrode insertion was in all cases deeper than the deepest part of the tumor.*

Conclusions. *Our optimization algorithm was able to determine the best electrode configuration in all four presented models and with further improvement it could be a useful tool in clinical electrochemotherapy treatment planning.*

Key words: electrochemotherapy; electroporation; subcutaneous tumor; finite element method; numerical modeling; optimization

Introduction

Electrochemotherapy (ECT) is an effective local tumor therapy performed by the administration of chemotherapeutic drugs followed by the application of local high-voltage electric pulses.[1, 2] The electric

pulses cause transient structural changes (electroporation) of tumor cell membranes and thus increase the entrance of the chemotherapeutic drugs. This potentiates the chemotherapeutic effect and lowers the required drug dose.[3] Numerous studies have demonstrated ECT to be a very efficient treatment in various tumor types; in recent years, it has become a treatment of choice for cutaneous and subcutaneous tumor nodules of different histologies.[4-9]

Two conditions have to be met for ECT to be efficient: 1) a sufficient amount of chemotherapeutic drug has to be present in the
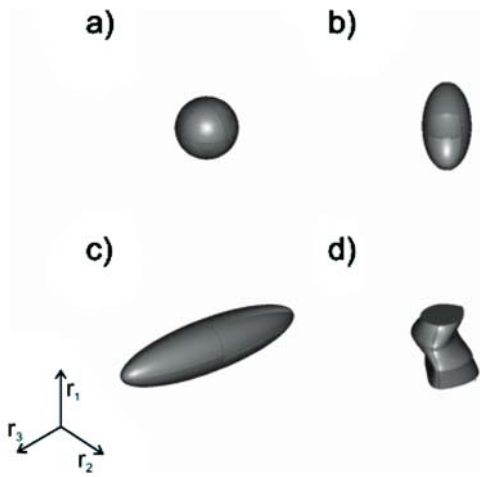
Figure 1. 3D subcutaneous tumor geometries. a) sphere (r_{1-3} = 2 mm); b) ellipsoid positioned deeper in tissue (r_1 = 4 mm, $r_{2,3}$ = 2 mm); c) ellipsoid ($r_{1,2}$ = 2 mm, r_3 = 8 mm); d) realistic tumor geometry from medical images (r_1 = 3.8 mm, r_2 = 2.4 mm, r_3 = 2.6 mm).

Figure 2. Electrode geometries and polarities: a) three needle electrode pairs (3 pairs); b) four needle electrode pairs (4 pairs); c) hexagonal needle electrode array with two electrodes on positive potential, two on negative and two neutral (2x2); d) hexagonal needle electrode array with three electrodes on positive potential and three on negative potential (3x3). Distances between electrodes d_{1-3} were among the optimized parameters in our optimization process. Diameter of all electrodes was 0.7 mm.

target tissue, when the electric pulses are applied; 2) the electric pulses have to reversibly electroporate the entire tumor volume, which means that the electric field established by the pulses should be of a magnitude between the reversible and irreversible electroporation threshold ($E_{rev} < E < E_{irrev}$). The optimal ECT protocol should thus destroy all tumor cells, while minimising electrically induced damage to healthy tissue due to irreversible electroporation. This can be achieved by choosing the most suitable electrode configuration and the lowest amplitude of electric pulses that guarantees whole tumor electroporation.[10,11] Finding the optimum treatment parameters is often difficult, since it requires a complete understanding of the treatment mechanisms. Since the electric field is one of the most important factors in ECT efficiency, modeling the electric field distribution is not only necessary for understanding the treatment, but is also a crucial step towards treatment planning.[12-14] This study presents the first use of an ECT optimization algorithm on several different tumor geometries.

The goal of our study was to optimize the electric field distribution in four different 3D subcutaneous tumor models (Figure 1) by optimizing the electrode configuration around the tumor tissue and the amplitude of the electric pulses for each of the four different electrode geometries that have been used in clinics in recent years (Figure 2).[1,15] Optimization was performed using a combination of finite element numerical modeling and a genetic algorithm. All tumor/electrode cases were optimized for the following parameters: distances between electrodes (Figure 2), depth of electrode insertion and amplitude of electric pulses. Our optimization algorithm successfully found the best parameters in all cases and with some further improvement it could be a useful tool in clinical ECT treatment planning as well as in treatment planning of other electroporation based treatments.[16-18]

Materials and methods

Tissue properties and model geometry

Each model of a subcutaneous tumor consisted of two tissues: the target/tumor tissue and the surrounding healthy tissue. Four different tumor geometries were chosen, a small sphere, an ellipsoid positioned deeper in the tissue, an elongated ellipsoid and a realistic tumor geometry taken from a previous study and scaled for better comparison with the other tumor geometries (Figure 1).[14] All tissues were considered isotropic and homogeneous, the assigned conductivity values being 0.4 S/m for the tumors and 0.2 S/m for the healthy tissue. These values describe the conductivity at the end of the electroporation process.[19] The values were chosen in accordance with previous measurements of tumor and tissue conductivity and models of subcutaneous tumor and skin electroporation.[13,16,20] The electric field distribution was calculated for three different electrode geometries: two different parallel needle electrode arrays (Figure 2a,b) and a hexagonal electrode array with two different electrode polarities (Figure 2c,d). These geometries and polarities were chosen because they are frequently used in ECT research and therapy.

Numerical modeling

Numerical calculations were performed with the commercial finite element software package COMSOL Multiphysics 3.4 (COMSOL AB, Sweden). The electric field distribution in the tissue, caused by the electroporative pulse, was determined by solving the Laplace equation for static electric currents:

$$-\nabla \cdot (\sigma \cdot \nabla \varphi) = 0 \ ,$$

where σ and ϕ are the conductivity of the tissue and electric potential, respectively. The boundary conditions used in our cal-
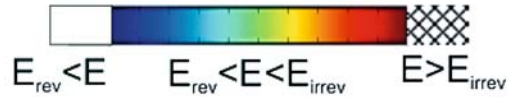
Figure 3. False color legend of Figs. 4, 5 indicating the degree of tissue permeabilization. The white region represents insufficiently permeabilized regions of tissue ($E < E_{rev}$) and the patterned region represents irreversibly permabilized regions of tissue ($E \geq E_{irrev}$).

culations were a constant potential on the surface of the electrodes and electric insulation on all outer boundaries of the model.

The electric field distributions obtained in our models were displayed in the range from the reversible $E_{rev} = 400$ V/cm to the irreversible electroporation threshold value $E_{irrev} = 900$ V/cm (Figure 3). These values were taken from a previously published study, in which we estimated them by comparing *in vivo* measurements and numerical modeling of electroporation of a subcutaneous tumor.[13,21]

Optimization

The genetic algorithm[22] was written in MATLAB 2007a (Mathworks, USA) and was run together with the finite element model using a link between MATLAB and COMSOL. The initial population of possible solutions was generated randomly, taking into account the following model constraints: range of distances between electrodes (d_1: 0.7-4.0 mm; d_2: 3.4-5.0 mm; d_3: 1.3-5.0 mm), range of depths of electrode insertion into tissue (-1.0-5.0 mm below the tumor) and range of amplitudes of electric pulses (1-1200 V). These constraints were chosen so that the calculation domain size, COMSOL meshing capabilities and oncology experts' demands for a safety margin[23] when treating solid tumors, were all respected. Solutions for reproduction were selected proportionally to their fitness, according to the fitness function:

Table 1. Optimized distances between electrodes (d_{1-3}), depth of electrode insertion below the tumor and amplitude of electric pulse (U) are given for all analyzed tumor models and electrode geometries. Qualities of individual optimized solutions are described by the calculated values of total electric current through tissue (I), fraction of reversibly permeabilised target tissue (V_{Trev}/V_T) and normalized volume of damaged healthy tissue (V_{Hirrev}/V_{sph}).

Tumor	Electrode geometry	d_1 [mm]	d_2 [mm]	d_3 [mm]	Insertion depth [mm]	U [V]	I [A]	V_{Trev}/V_T	$V_{Hirrevv}/V_{sph}$
	3 pairs	0.70	3.4		1.1	210	0.45	1	1.00
	4 pairs	0.70	3.4		0.9	210	0.52	1	1.03
	3x3			1.3	0.3	200	0.55	1	3.58
	2x2x2			1.3	0.3	220	0.32	1	1.77
	3 pairs	0.70	3.4		0.9	220	0.65	1	1.59
	4 pairs	0.70	3.6		0.9	220	0.75	1	1.39
	3x3			1.3	0.3	210	0.89	1	6.31
	2x2x2			1.3	0.7	220	0.47	1	2.51
	3 pairs	2.60	3.4		0.9	320	0.88	1	7.40
	4 pairs	1.60	3.4		0.7	320	0.96	1	7.08
	3x3			4.3	0.5	550	1.19	1	15.84
	2x2x2			4.6	0.1	1160	1.25	1	31.22
	3 pairs	0.75	3.4		0.9	270	0.65	1	3.17
	4 pairs	0.70	3.4		0.7	270	0.70	1	3.39
	3x3			1.8	1.1	320	1.07	1	11.44
	2x2x2			1.6	0.9	320	0.55	1	5.45

$$F = 12 + 100 \cdot V_{Trev} - 10 \cdot V_{Hirrev} - V_{Hrev} - V_{Tirrev} \, ,$$

where F stands for fitness, V_{Trev} and V_{Tirrev} stand for the tumor volume subjected to the local electric field above E_{rev} and above E_{irrev}, and V_{Hrev} and V_{Hirrev} stand for the volume of healthy tissue subjected to the local electric field above E_{rev} and above E_{irrev}, respectively. The weights in the fitness function were set according to the importance of the individual parameters for efficient ECT. Namely, V_{Trev} is crucial for efficient ECT, so its weight is largest (100) in comparison to the weight of V_{Hirrev} (10), which was in turn larger than the weights of V_{Hrev} and V_{Tirrev}, since their significance for successful electrochemotherapy is still debated. Other weight values that kept a similar ratio gave similar results. The integer 12 is present only to ensure that the fitness function is always positive.

The selected solutions reproduced by cross-over or by mutation. The genetic algorithm was terminated after 100 generations, when the fitness of the highest ranking solution usually reached a plateau. The average computation time of the algorithm was two hours on a standard desktop PC (Windows XP, 3.0 GHz, 1 GB RAM).

Results

The optimized parameters of electrochemotherapy (ECT) for all tumor/electrode cases are given in Table 1. The optimum distance
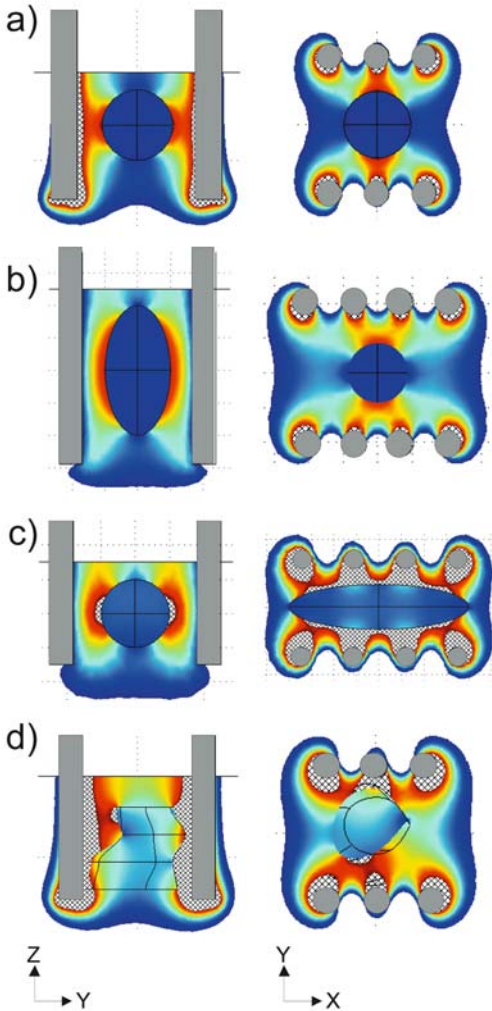
Figure 4. Electric field distribution for the optimized models of subcutaneous tumors is shown. In each case, only the best electrode configuration is given: a) three needle pairs for the spherical tumor; b) four needle pairs for the ellipsoid; c) four needle pairs for the ellipsoid deeper in tissue; d) three needle pairs for the realistic tumor. The electric distribution is shown in two central perpendicular planes: YZ and XY both passing through the center of the tumor. Corresponding values of parameters are given in Table 1.

between electrodes in a parallel row (d_1) was similar for all tumor models, except, due to its size, for the elongated ellipsoid tumor geometry, for which successful electroporation required the electrodes to be

further apart. The electrodes were as close to each other as possible considering the parameter constraints, which guaranteed that the electric field distribution in the target tissue was homogeneous as possible (comparison of Figure 4b and Figure 4c). The optimum distance between electrode rows (d_2) was also similar for all tumor geometries and as small as possible, the reason being that small inter-electrode distances required a lower voltage to ensure electroporation, thus also requiring less electric energy and causing less damage to tissue. The same is true for the distance between electrodes in a hexagonal array (d_3), the reason this time being a combination of both homogeneity of the local electric field and lower required voltage. In contrast, the optimum depth of electrode insertion varied with the tumor and electrode geometry. Nevertheless, the optimum position for the electrodes was in all cases below the tumor. The optimum electric pulse amplitude did not differ much in cases of a spherical tumor and ellipsoid tumor deep in tissue but in other tumor geometries, parallel electrode arrays required considerably lower amplitudes than their hexagonal counterparts.

We compared the quality of the optimized solution in terms of total electric current through the tissue and extent of healthy tissue damage (Table 1 – V_{Hirrev}/V_{sph}). We normalized the volumes of irreversibly electroporated tumor with the volume of a spherical tumor better to compare the amount of tissue damage between individual treatment cases. Parallel electrode arrays gave better results for all four tumor geometries. Three needle pairs always resulted in less total electric current. However, four needle pairs produced a more homogeneous field, which, in combination, caused three needle pairs to be a slightly better choice (less healthy tissue damage) for the spherical and the realistic
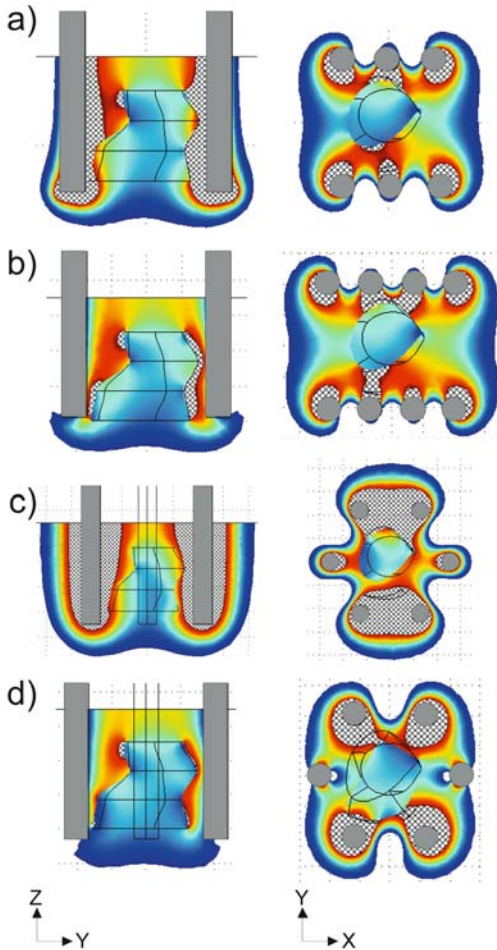
Figure 5. Electric field distribution for the optimized model of the realistic tumor with a) three needle pairs; b) four needle pairs; c) 3x3 hexagonal needle electrode array; d) 2x2x2 hexagonal needle electrode array is shown. The electric distribution is shown in two central perpendicular planes: YZ and XY both passing through the center of the tumor. Corresponding values of parameters are given in Table 1.

in Figure 5 for the realistic tumor geometry. The 3x3 hexagonal electrode array caused more healthy tissue damage than the other three geometries and also required the highest total electric current, mostly because the electric current ran between the closest positive and negative electrodes, instead of through the target tissue (Figure 5).

Discussion

The aim of our study was to optimize the electrode configuration around the target tissue and electric pulse amplitude for ECT of four 3D models of subcutaneous tumors treated with four different needle electrode array geometries. In all 16 cases, the optimization resulted in reversible electroporation of the entire tumor (Table 1: $V_{Trev}/V_T = 1$), which was the parameter with the highest weight in our fitness function. At the same time, the damage to healthy tissue was minimal. When treating a spherical tumor, only a volume of healthy tissue equal to the tumor volume was irreversibly electroporated (Table 1: V_{Hirrev}/V_{sph}). Treatment of larger tumors caused more healthy tissue damage.

The usefulness of numerical modeling in predicting electroporation outcomes has already been demonstrated.[14,15,19,24-26] We examined the adequacy for ECT of needle electrode array geometries by calculating the values of total electric current through the model (must be as low as possible to avoid nerve stimulation[27] and not exceed the capacities of the electric pulse generator[28]) and volumes of reversibly and irreversibly electroporated tumor tissue and healthy tissue. Three-needle electrode pairs were best for the spherical and the realistic tumor geometry; they required the lowest total electric current and caused only a small volume of healthy tissue to be irreversibly electroporated (healthy tissue damage) (Figure 4).

tumor geometry and four needle pairs to be slightly better for the other two geometries. The best electrode configurations for all tumor geometries and the corresponding electric field distributions are shown in Figure 4. Hexagonal electrodes caused considerably more healthy tissue damage ($E > E_{irrev}$) than parallel electrodes, which can be seen

Four-needle electrode pairs caused the least healthy tissue damage in the other tumor geometries, but they required more electric current (Figure 4), confirming previous results of our group - more electrodes mean a more invasive procedure, higher required current and lower required voltage to obtain the same target tissue coverage. Parallel electrode arrays gave much better results than the 2x2 and 3x3 hexagonal needle electrode arrays, mostly because they induced a much more homogeneous field and, consequently, a lower electric current density.

Our work built on a previous study by our group that optimized the distance and voltage between electrodes for a realistic brain tumor (the same tumor geometry that we used in a scaled form in this study).[14] Our present study took optimization one step further by optimizing for four different electrode geometries and for two additional parameters, *i.e.* distance between electrodes in a row and depth of electrode insertion, which lead to perhaps the most important practical result. It is very difficult to guess the best possible insertion depth, since it depends in complex ways on tumor geometry, electrode geometry, electroporation thresholds and the conductivities of tumor and healthy tissue. However, based on our results, electrodes should always be inserted deeper than the deepest part of the tumor (Table 1).

We chose a genetic algorithm as the optimization method, since different linear and non-linear constraints, such as the technical limitations of the high-voltage electric pulse generator (maximum output voltage and current) can be easily taken into account. A genetic algorithm also allows optimization of a large number of continuous, discrete and categorical parameters, *e.g.* type of electrodes and can give as a result many solutions of similar quality, which can nevertheless be topologically very different. This gives the treating physician more alternatives for the positioning of electrodes, which can be very valuable if some of them are not easy to access. The major drawback of a genetic algorithm is the relatively long computation time. However, since it can be considerably shortened by using a more powerful computer or by making the optimization parameters discrete instead of continuous, we do not consider this to be a significant issue and believe that this approach is well suited to the problem being addressed.

Even though our algorithm gives good results, several challenges remain to be addressed before it can be used for treatment planning of ECT. We must determine the most appropriate level of complexity of our numerical models. In this study, we did not take into account changes to tissue conductivity due to electroporation, the possibility of several consecutive pulses being used, of changing the electric field orientation or of moving the electrodes during treatment of a larger tumor; all of which options must be considered in the future.[13,15,25] Another crucial development would be an algorithm that would convert medical images of the treatment area into 3D structures ready to import into numerical modeling software.

In conclusion, we demonstrated that numerical modeling and optimization can be efficiently combined to control the extent of tissue electroporation in ECT and to produce the optimum electrode configuration and amplitude of electric pulses. Our algorithm is a step towards effective treatment planning, not only in clinical ECT, but also in other electroporation based treatments, such as gene electrotransfer, transdermal drug delivery and irreversible tumor ablation.16-18

References

1. Marty M, Sersa G, Garbay JR, et al. Electrochemotherapy - An easy, highly effective and safe treatment of cutaneous and subcutaneous metastases: Results of ESOPE (European Standard Operating Procedures of Electrochemotherapy) study. *Eur J Cancer Suppl* Nov 2006; **4:** 3-13.

2. Sersa G. The state-of-the-art of electrochemotherapy before the ESOPE study; advantages and clinical uses. *Eur J Cancer Suppl* 2006; **4:** 52-9.

3. Domenge C, Orlowski S, Luboinski B, DeBaere T, Schwaab G, Belehradek J, et al. Antitumor electrochemotherapy - New advances in the clinical protocol. *Cancer* 1996; **77:** 956-63.

4. Heller R, Gilbert R, Jaroszeski MJ. Clinical applications of electrochemotherapy. *Adv Drug Deliv Rev* 1999; **35:** 119-29.

5. Gothelf A, Mir LM, Gehl J. Electrochemotherapy: results of cancer treatment using enhanced delivery of bleomycin by electroporation. *Cancer Treat Rev* 2003; **29:** 371-87.

6. Tijink BM, De Bree R, Van D, Leemans CR. How we do it: Chemo-electroporation in the head and neck for otherwise untreatable patients. *Clin Otolaryngol* 2006; **31:** 447-51.

7. Mir LM, Gehl J, Sersa G, et al. Standard operating procedures of the electrochemotherapy: Instructions for the use of bleomycin or cisplatin administered either systemically or locally and electric pulses delivered by the Cliniporator (TM) by means of invasive or non-invasive electrodes. *Eur J Cancer Suppl* 2006; **4:** 14-25.

8. Snoj M, Rudolf Z, Cemazar M, Jancar B, Sersa G. Successful sphincter-saving treatment of anorectal malignant melanoma with electrochemotherapy, local excision and adjuvant brachytherapy. *AntiCancer Drugs* 2005; **16:** 345-8.

9. Sersa G, Cemazar M, Miklavcic D, Rudolf Z. Electrochemotherapy of tumours. *Radiol Oncol* 2006; **40:** 163-74.

10. Miklavcic D, Beravs K, Semrov D, Cemazar M, Demsar F, Sersa G. The importance of electric field distribution for effective in vivo electroporation of tissues. *Biophys J* 1998; **74:** 2152-8.

11. Miklavcic D, Semrov D, Mekid H, Mir LM. A validated model of in vivo electric field distribution in tissues for electrochemotherapy and for DNA electrotransfer for gene therapy. *Biochim Biophys Acta* 2000; **1523:** 73-83.

12. Miklavcic D, Corovic S, Pucihar G, Pavselj N. Importance of tumour coverage by sufficiently high local electric field for effective electrochemotherapy. *Eur J Cancer Suppl* 2006; **4:** 45-51.

13. Pavselj N, Bregar Z, Cukjati D, Batiuskaite D, Mir LM, Miklavcic D. The course of tissue permeabilization studied on a mathematical model of a subcutaneous tumor in small animals. *IEEE Trans Biomed Eng* 2005; **52:** 1373-81.

14. Sel D, Lebar AM, Miklavcic D. Feasibility of employing model-based optimization of pulse amplitude and electrode distance for effective tumor electropermeabilization. *IEEE Trans Biomed Eng* 2007; **54:** 773-81.

15. Gilbert RA, Jaroszeski MJ, Heller R. Novel electrode designs for electrochemotherapy. *Biochim Biophys Acta* 1997; **1334:** 9-14.

16. Cukiati D, Batiuskaite D, Andre F, Miklavcic D, Mir LM. Real time electroporation control for accurate and safe in vivo non-viral gene therapy. *Bioelectrochemistry* 2007; **70:** 501-7.

17. Pliquett UF, Vanbever R, Preat V, Weaver JC. Local transport regions (LTRs) in human stratum corneum due to long and short 'high voltage' pulses. *Bioelectrochem Bioener* 1998; **47:** 151-61.

18. Al Sakere B, Bernat C, Connault E, Opolon O, Rubinsky B, Davalos R, et al. Tumour ablation with irreversible electroporation. *PLoS ONE* 2007:11.

19. Corovic S, Pavlin M, Miklavcic D. Analytical and numerical quantification and comparison of the local electric field in the tissue for different electrode configurations. *Biomed Eng Online* 2007; **6.**

20. Miklavcic D, Pavselj N, Hart FX. Electric properties of tissues. *Wiley Encyclopedia of Biomedical Engineering.* New York: John Wiley & Sons; 2006.

21. Semrov D, Miklavcic D. Calculation of the electrical parameters in electrochemotherapy of solid tumours in mice. *Comput Biol Med 1998*; **28:** 439-48.

22. Holland JH. *Adaptation in Natural and Artificial Systems: An Introductory Analysis with Applications to Biology, Control, and Artificial Intelligence.* Cambridge: MIT Press; 1992.

23. Gehl J, Geertsen PF. Palliation of haemorrhaging and ulcerated cutaneous tumours using electrochemotherapy. *Eur J Cancer Suppl* 2006; **4:** 35-7.

24. Gehl J, Sorensen TH, Nielsen K, Raskmark P, Nielsen SL, Skovsgaard T, et al. In vivo electroporation of skeletal muscle: threshold, efficacy and relation to electric field distribution. *Biochim Biophys Acta* 1999; **1428:** 233-40.

25. Sersa G, Cemazar M, Semrov D, Miklavcic D. Changing electrode orientation improves the efficacy of electrochemotherapy of solid tumors in mice. *Bioelectrochem Bioener* 1996; **39:** 61-6.

26. Sel D, Mazeres S, Teissie J, Miklavcic D. Finite-element modeling of needle electrodes in tissue from the perspective of frequent model computation. *IEEE Trans Biomed Eng* 2003; **50:** 1221-32.

27. Zupanic A, Ribaric S, Miklavcic D. Increasing the repetition frequency of electric pulse delivery reduces unpleasant sensations that occur in electrochemotherapy. *Neoplasma* 2007; **54:** 246-50.

28. Puc M, Corovic S, Flisar K, Petkovsek M, Nastran J, Miklavcic D. Techniques of signal generation required for electropermeabilization. Survey of electropermeabilization devices. *Bioelectrochemistry* 2004; **64:** 113-24.

III

Zupanic A, Miklavcic D. Optimization and numerical modeling in irreversible electroporation treatment planning. In Rubinsky B (ed.), irreversible electroporation, Springer Verlag, Berlin, 203-222, 2010.

Optimization and Numerical Modeling in Irreversible Electroporation Treatment Planning

Anže Županič and Damijan Miklavčič*

Faculty of Electrical Engineering, University of Ljubljana, Ljubljana, SI-1000, Slovenia
* Corresponding author E-mail: `damijan.miklavcic@fe.uni-lj.si`

Introduction

When you overhear someone mention treatment planning, you can bet the conversation is about one of the forms of radiation therapy (RT). In the 1960s, when high powered x-ray delivery systems were readily available to radiation oncologists, the biggest challenge remained to improve the accuracy in locating the tumor and in directing the beams of charged particles. This changed when the first computed tomography (CT) scanners were invented (Lampert et al, 1974). Availability of 3D anatomical data and ever increasing computer processing power gave rise to numerical treatment planning. Together with improved beam generation and delivery technology, treatment planning has enabled RT to better target the tumor and to reduce adverse effects on vital organs (Jaffray et al, 2007). This is exactly what researchers would also like to achieve with irreversible electroporation (IRE): ablate the target tissue and spare as much healthy tissue as possible. Just as treatment planning in RT provides radiation oncologist with the radiation beam intensities and directions that cover the tumor without causing extensive damage to healthy tissue, so can treatment planning in IRE provide physicians with electrode configurations and amplitudes of electric pulses that result in adequate electric field distribution in and around the target tissue.

It might seem a bit early to talk about treatment planning for IRE as it is still in the phase of clinical experimentation. However, RT has been around for more than fifty years and has only become one of the most successful cancer treatments after treatment planning procedures were implemented. And while in RT one had to wait for medical imaging and powerful computers to appear, everything is readily available for IRE. There is also no need to wait for IRE to become a recognized and widely implemented ablation technique, treatment planning is just as important in the experimental stage, as experiences from electrochemotherapy, an application of reversible electroporation that has already made it to the clinic, have shown (Miklavcic et al, 1998; Miklavcic et al, 2000; Semrov & Miklavcic, 1998). Careful experiment planning not only increases the reproducibility of experiments, it also lowers the number of needed experimental animals, and thus improves the overall quality of research.

    In this chapter we compare features of external beam radiation therapy (and brachytherapy, when probe/electrode insertion questions are analyzed) with IRE features, which are relevant for the treatment planning procedure. By careful analysis we try to determine which features of RT treatment planning can be applied directly to IRE, which could be applied after adjustments and which cannot be applied due to overly different natures of both therapies. At the end we present our recent work in electroporation numerical modeling and genetic algorithm optimization in two illustrative (but hypothetical) examples of treatment planning of tumor ablation by IRE.

A Brief Overview of Irreversible Electroporation Basics

Cell membranes can be permeabilized by exposing them to a high enough electric field, a phenomenon termed electroporation (Neumann et al, 1982). The nature of electrically-induced membrane permeabilization can be predominantly controlled by the amplitude of local electric field. Permeabilization can be either reversible – the membrane stays permeabilized for up to minutes, allowing entrance of molecules that do not normally cross the membrane, and later recovers (Orlowski et al, 1988); or, if electric field strength is increased, irreversible – membranes do not recover and the cells die (Rubinsky et al, 2007). In biomedical research reversible electroporation has become widely used in the last decade, e.g. for electrochemotherapy (Belehradek et al, 1991; Heller et al, 1999; Mir et al, 1998; Serša et al, 2006), gene electrotransfer (Golzio et al, 2004; Hojman et al, 2007; Mir et al, 1999), transdermal drug delivery (Denet et al, 2004; Prausnitz, 1999) and electrofusion of cells (Scott-Taylor et al, 2000; Trontelj et al, 2008), while IRE has gained momentum in the last few years, since Davalos et al showed it can be used to kill cells without considerable thermal effects (Davalos et al, 2005). Further studies on ablation capacity of IRE have confirmed the absence of significant resistive heating during IRE (Al-Sakere et al, 2007; Edd et al, 2006; Miller et al, 2005) and have also demonstrated some additional advantages IRE has over more conventional thermal and chemical ablation techniques. These advantages include: 1) IRE is a non-thermal physical ablation modality, therefore not affected by blood flow (Miller et al, 2005); 2) delineation between treated (ablated) and untreated tissue after IRE is very sharp – only a few cells thick (Lee et al, 2007); 3) IRE affects only cell membranes and leaves extracellular structures intact – preservation of microvasculature is possible (Lee et al, 2007; Maor et al, 2007; Onik et al, 2007); 4) IRE elicits no immune response and can thus be used for treatment of patients with immune system deficiency (Al-Sakere et al, 2007); 5) the procedure is relatively fast compared to other ablation techniques (Lee et al, 2007); 6) IRE allows rapid regeneration of ablated tissue with healthy tissue (Rubinsky et al, 2007); 7) IRE can be accurately numerically modeled – numerical models of reversible electroporation that have been around for quite some time can be easily modified and implemented for IRE modeling (Corovic et al, 2007; Edd & Davalos, 2007; Pavselj & Miklavcic, 2008a).

IRE was tested as an ablation modality in various medical applications, such as ablation of cancer (Onik et al, 2007; Rubinsky et al, 2008), epicardial ablation (Lavee et al, 2007) and prevention of restenosis after angioplasty (Maor et al, 2008). After encouraging primary results of these studies, researchers expressed the need for accurate experimental planning that would: 1) guarantee that thermal effects are indeed negligible; 2) take advantage of the sharp physical delineation between treated and untreated tissue to enable surgically precise ablation and 3) make experimental (and later medical) procedures more reproducible.

Before setting guidelines for proper treatment planning, it seems appropriate to check whether sophisticated and time consuming numerical treatment planning procedures are necessary in all biomedical applications of IRE. If, for example, IRE takes place in homogeneous and isotropic tissues with no vital organ in the vicinity of the treated area, then a simple look-up database of appropriate treatment parameters calculated by simple numerical models validated by experiments would suffice. The same can be said for more complex tissue geometries that do not change much from patient to patient, as is the case in restenosis prevention where electric pulses are applied to blood vessel walls. The look-up database should include electric field distributions generated by the use of different electrode geometries, different electrode configurations and a range of electrical input parameters. Such databases can be constructed using numerical modeling alone, without optimization, and have to provide enough information for the treating physician to choose the proper set of electrodes and electric parameters for each treatment. Optimization becomes important in more complex situations, when the target tissue is located near a vital organ whose function should not be compromised by the treatment. In such situations it is of vital importance to control the magnitude and distribution of the electric field so that as little as possible critical tissue (organ at risk) is compromised by the treatment. This can be effectively accomplished by numerical modeling of IRE and optimization based on anatomical medical imaging, as has been demonstrated recently for electrochemotherapy (Corovic et al, 2008; Zupanic et al, 2008). Numerical modeling may also be necessary for treatment planning in tissues with highly anisotropic properties and highly non-homogeneous tissues, where electric field distribution is otherwise difficult to predict (Pavselj & Miklavcic, 2008b). In all such cases the treatment planning procedure will have to be applied individually for each patient and the electric field distribution will have to be sculpted carefully to ablate all of the target tissue and preserve as much of the critical tissue as possible.

Radiation Therapy vs. Irreversible Electroporation Procedure

Over the past decades progress in imaging technology and computer processors have modernized RT through use of more accurate radiation dose calculation algorithms, more complex dose delivery techniques and modern imaging

modalities (Dawson & Sharpe, 2006; Jaffray et al, 2007). Modern radiation therapy techniques, such as 3D conformal RT (Purdy & Starkschall, 1999) and intensity-modulated RT (Boyer et al, 2001) are completely image-guided and computerized, which has enabled more accurate sculpting of radiation doses to clinical volumes (target volumes and critical volumes). RT treatment planning procedure has accordingly become extremely sophisticated, which makes it an ideal benchmark for treatment planning of other biomedical application based on physical agents. A typical RT treatment today generally consists of five major phases: simulation, treatment planning, set-up verification, dose delivery and response assessment (Lecchi et al, 2008). In the simulation phase, data on patients' anatomy are acquired via modern 3D imaging devices. In treatment planning, clinical volumes are first delineated, dose constraints are defined and the treatment plan is determined. Before treatment, imaging is again utilized for control of the clinical set-up. After the radiation dose is delivered the treatment success is periodically evaluated by following tumor response. In this chapter we analyze the first three phases with emphasis on the treatment planning phase.

Similar major phases as for RT can also be defined for IRE treatment: simulation, treatment planning, set-up verification, electric pulse delivery and response assessment. Simulation is probably not necessary in all biomedical applications of IRE; however, it is necessary in all situations that require numerical treatment planning. Treatment planning is currently limited to experienced researchers that are able to "predict" the appropriate electrode configuration and electric pulse amplitude, whether from experience alone or with help of modeling. The appropriate positioning of electrodes can be controlled by real time ultrasound measurements (Lee et al, 2007). Electric pulses are delivered by a clinical electroporator (Bertacchini et al, 2007) and evaluation of treatment success depends on individual IRE application, e.g. when using IRE for tumor ablation, tumor size is periodically measured.

Medical Imaging

The first phase in RT is medical imaging of the whole region surrounding the target tumor tissue. This is usually accomplished with computer tomography (CT), although, if necessary, other imaging modalities, such as magnetic resonance imaging (MRI) and positron emission tomography (PET) are also used as they can provide additional anatomical and physiological information (Lecchi et al, 2008; Newbold et al, 2006; Vanuytsel et al, 2000). If MRI or PET are used, their images are later aligned to the CT images using image-fusion algorithms (Skerl et al, 2007; Slomka, 2004). It is vital for the success of the therapy that the patient's position during imaging is as close as possible to the actual treatment position. In external beam RT this is usually achieved with laser positioning control and patient immobilization (Heinzerling et al, 2008). In brachytherapy, on the other hand, it is very important that imaging is done with probes already implanted inside the body, as their insertion can significantly change the internal organ

positions (Potter et al, 2008a; Potter et al, 2008b). During treatment, ultrasound can be used to control internal organ movement (Chandra et al, 2003).

The exact same imaging procedures as in RT can also be used in IRE; however, since IRE is a local treatment, less extensive imaging is necessary. Ultrasound imaging can be very useful in IRE, e.g. for real-time ultrasound guidance of electrode insertion and real-time ablation zone monitoring (Lee et al, 2007). Electrical impedance imaging has also been suggested as a real-time electroporation monitoring modality (Davalos et al, 2004; Davalos et al, 2002; Granot & Rubinsky, 2007; Ivorra & Rubinsky, 2007), as has been current and voltage measurement during pulse delivery (Cukjati et al, 2007). As precise positions of electrodes for IRE are only available after the treatment planning procedure, it would be no use to insert them prior to imaging. Instead, ultrasound imaging will probably have to be relied upon to assure adequate positioning of the electrodes with respect to the target volume and critical volumes.

Delineation of Clinical Volumes and Definition of Dose Constraints

Oncology experts examine the acquired medical images slice by slice and delineate the target volumes and critical volumes for the treatment as defined by the International commission on radiation units and measurements (ICRU) reports 50 and 62 (ICRU-50, 1993; ICRU-62, 1999). If the location of the target tissue is such that target and critical volumes coincide, the expert has to use his/her experience and adjust the volumes with respect to the patient's best interest. Dose constraints for each critical volume and target dose are also defined according to the same ICRU reports. In RT there is no threshold effect: lower doses already cause tissue damage and by increasing the dose the damage increases up to the point where the dose necessary to kill all cancer cells is achieved.

The ICRU reports define clinical volumes mainly according to the probability of error in accurate delineation, according to the probability of microscopic spread of tumor cells outside the main tumor mass and accordingly to the set-up and delivery errors, which were all evaluated by a vast collection of clinically acquired data. As only the set-up and delivery error are radiation specific and are analyzed separately, tumor volumes treated by IRE can also be defined using ICRU reports. In IRE electric field strength is believed to be the main factor controlling the treatment outcome. IRE is apparently, contrary to RT, a threshold phenomenon. Electric fields below the irreversible threshold permeabilize cells reversibly, but do not kill them, while electric fields over the threshold irreversibly permeabilize cells and thus destroy them. This effectively means that tissue damage can theoretically be sculpted to the target tissue and around all critical tissues with great accuracy. IRE thresholds have, however, been found to be tissue specific. Furthermore, several electric pulse parameters affect the threshold values: pulse duration, number of pulses and to some extent also pulse repetition frequency (Edd & Davalos, 2007; Miklavcic & Kotnik, 2004). Prior to any treatment planning, data on thresholds for all target tissues and all critical tissues should be available for a range of electroporation parameters.

Tissue Properties

For radiation therapy data on tissue properties is readily available directly through CT imaging. Namely, CT values correlate well with electron density, the main tissue property used in computation of Compton scattering, which is the most probable interaction of high energy X rays with atomic nuclei in living beings. It is also considered that electron density remains the same during the entire treatment (Ruchala et al, 2000).

Data on human tissue electrical properties (electrical conductivity and electrical permittivity) are harder to come by. Although several reports have been published (Gabriel et al, 1996a; Gabriel et al, 1996b; Miklavcic et al, 2006b; Polk & Postow, 1996), the data between individual studies differ by a factor of 2 or more. A database of electrical properties is desperately needed, preferably with additional data on electrical property variation with age, gender and pathological changes (e.g. different tumors or scarred tissues). Furthermore, because electric tissue properties change dramatically during electroporation (Pavlin & Miklavcic, 2008; Pliquett & Weaver, 1996), these data should be available not only for pre-electroporation, but also for permeabilized tissues. Models of electroporation that take this dynamic change in tissue properties into account, provide us with much more detailed description of electroporation and can describe in vivo phenomena that cannot be explained with models that use constant tissue properties. Data on electrical tissue properties after electroporation are, however, very scarce, although they may prove crucial for accurate treatment planning.

Dose Calculation Algorithms

In modern radiation therapy two main calculation methods are used: convolution-superposition, where the patients dose is computed and lateral transport of radiation, beam energy, beam modifiers and electron density distribution are accounted for (Mackie et al, 1985; Sharpe & Battista, 1993); and Monte-Carlo where the dose is computed directly from first principles (Reynaert et al, 2007). While convolution-superposition is faster, Monte-Carlo is more accurate. Medical physicists in oncology usually choose the method according to necessity (and availability); when time is very important and many calculations are needed, convolution-superposition is used, and when high accuracy is needed, Monte-Carlo based methods are used.

In tissue electroporation modeling several algorithms are used, mostly utilizing the finite element method (for details on finite element modeling in electroporation based applications consult *Finite element modeling of in vivo electroporation* by Pavselj and Miklavcic). The difference between individual models is mostly whether they take into account the changes in tissue electrical properties during electroporation or not. Steady-state models calculate the electric field distribution without incorporating changes in tissue properties. These models give reasonably good results, if the tissues modeled are homogeneous and isotropic. (Edd & Davalos, 2007; Miklavcic et al, 2006a; Miklavcic et al, 2000). When this is not the case, sequential models can be used. These models approximate changes in electrical properties as a function of the magnitude of

electric field and thus approximately describe the time course of conductivity increase during electroporation (Sel et al, 2005). Further improvements in accuracy can be achieved by taking into account a certain time-dependency of changes in electrical properties (Pucihar et al, 2008), or even by multiscale modeling that combines single cell electroporation into the bulk tissue models (Esser et al, 2007; Smith & Weaver, 2008; Weaver, 2003). Each of these improvements is computationally more intensive than the previous one, thus taking more time. For treatment planning purposes it is necessary to choose the model that takes the least time to compute, while at the same time maintains an adequate level of accuracy. Since steady-state models cannot accurately simulate IRE in complex anatomies, and multiscale models are so computer intensive that so far they have only been used in 2D, currently the only achievable options are sequential models.

Multiphysics (Applicable to Irreversible Electroporation Only)

One of the main advantages of irreversible electroporation is its non-thermal ablation capacity. When electric pulses are applied to biological tissue, heat is generated in the form of resistive heating and the temperature increases. In order to guarantee non-thermal ablation IRE treatment planning must involve a control for the heat generated by electric pulses. Coupling of electrical and thermal phenomena can provide an estimate of temperature rise and distribution due to IRE (Davalos & Rubinsky, 2008; Edd & Davalos, 2007; Pliquett, 2003); thus it can be used to calculate temperature increases for each individual application of IRE or to generate a conservative range of electric pulse parameters (pulse duration, number of pulses, pulse repetition frequency) that do not elevate tissue temperatures excessively. When the electric field distribution is highly non-homogeneous, with high local peaks, calculation of resistive heating should be included in the treatment planning process.

Forward and Inverse Treatment Planning Procedure

Forward planning is a technique used in RT to produce a treatment plan that consists of a set of physically deliverable modulated beam fluence profiles, which in practice means that, for each beam, a direction, duration and modulated intensity have to be chosen. In forward planning, an initial plan is made by a treatment planner (usually a medical physicist) who uses his/her experience to produce a set of treatment parameters that can deliver sufficient radiation to a tumor while sparing vital organs and also minimizing the dose to other healthy tissues. The treatment dose is then calculated and evaluated by an oncology expert. If necessary, improvements to the plan are made and radiation doses are recalculated. This cycle is repeated until a satisfactory plan is produced. Forward planning is used for the majority of RT treatments.

In more complex cases, when vital organs are near the target volume or the target volume is of complex shape, inverse planning produces better results (Ezzell et al, 2003; Galvin et al, 2004; Lindegaard et al, 2008; Webb, 2003). In inverse planning, which is used in intensity-modulated radiation therapy, a desired dose

distribution (dose constraints) in and around the target volume is defined. Then a computer optimization technique is used together with the dose calculation algorithm to determine the optimal set of treatment parameters resulting in a dose distribution that most closely matches the desired one. The optimization algorithm compares the quality of different treatment plans according to an objective function that incorporates dose constraints defined earlier. The constraints are usually implemented using dose-volume criteria: how much target volume and critical volume is covered by the appropriate dose; how much is overdosed and how much underdosed. Biological effects models, such as tumor control probability and normal tissue complication probability are also used: what are the biological consequences of covering a certain volume of the tumor and of critical tissues with a certain dose (Bortfeld, 1999; Lyman & Wolbarst, 1987). Currently, gradient based optimization algorithms and stochastic optimization algorithms are used in radiation therapy (Bortfeld, 2006; Ezzell, 1996). Gradient algorithms are faster, but require a good initial guess to reach a satisfactory solution, while stochastic algorithms, such as simulated annealing and genetic algorithms are slower, but do not require an initial guess.

In IRE, a treatment plan should consist of appropriate electric pulse parameters, i.e. pulse duration, number of pulses, pulse repetition frequency and pulse amplitude, and of appropriate electrode parameters, i.e. electrode geometry, configuration of electrode arrays and sequence of electrode activation in cases when multiple pulses (that would induce different electric field distributions) would have to be delivered. The effect of number of pulses, their duration and repetition frequency to treatment success can be substantial; increasing the number of pulses or pulse duration increases electroporation efficiency, increasing repetition frequency decreases efficiency. Increasing any of the three increases tissue temperature (Macek-Lebar et al, 2002; Pucihar et al, 2002). Since the sequential models cannot currently evaluate the effect of these parameters on electroporation efficiency, all three parameters have to be chosen according to the experimental results and the non-thermal criteria. Numerical treatment planning procedure should therefore only deal with pulse amplitude and electrode related parameters, unless appropriate biological effects models are included.

Forward planning in IRE is possible, but probably not sensible, since inverse planning is not much more time consuming and produces better results. The choice between gradient and stochastic methods is less straight-forward. Gradient methods are faster and more accurate, if a good initial guess is available and if the number of parameters optimized for is not too large. Increasing the number of parameters can result in gradient optimization methods becoming stuck in one of the local optimums a long way away from the global optimum. In such a case, stochastic methods, such as genetic algorithm and simulated annealing, are much more likely to come close to the global optimum (since the methods are stochastic, the probability of reaching the global optimum in a reasonable amount of time are slim, however, they do find an acceptably good solution in a fixed amount of time). An additional advantage of genetic algorithm optimization is its ability to return more than one high-quality suggestion for the optimal parameters, thus giving the treatment planner more than one option of similar quality into consideration. No matter which methods (gradient

or stochastic) are used, the IRE treatment planning procedure should follow the RT procedure closely. Target volumes, critical volumes and the appropriate electric field distributions should be defined. Optimization algorithm should then compare the quality of different treatment plans according to an objective function that takes into account that the electric field must be over the IRE threshold in all the target tissue and under the IRE threshold in vital organs and as low as possible elsewhere. If biological effect models ever become available for IRE, they should also be included in the objective function.

Tumor Ablation with Irreversible Electroporation Treatment Planning Examples

We present two examples of treatment planning of ablation by IRE using numerical modeling and a genetic optimization algorithm. In both examples we try to determine the best possible configuration and electric potentials of six electrodes surrounding a subcutaneous tumor - the target tissue. Our goal is to irreversibly electroporate ($E > E_{irr}$) the entire tumor volume, while sparing as much as possible of the hypothetical spherical organ at risk, situated next to the tumor (Figure 1).

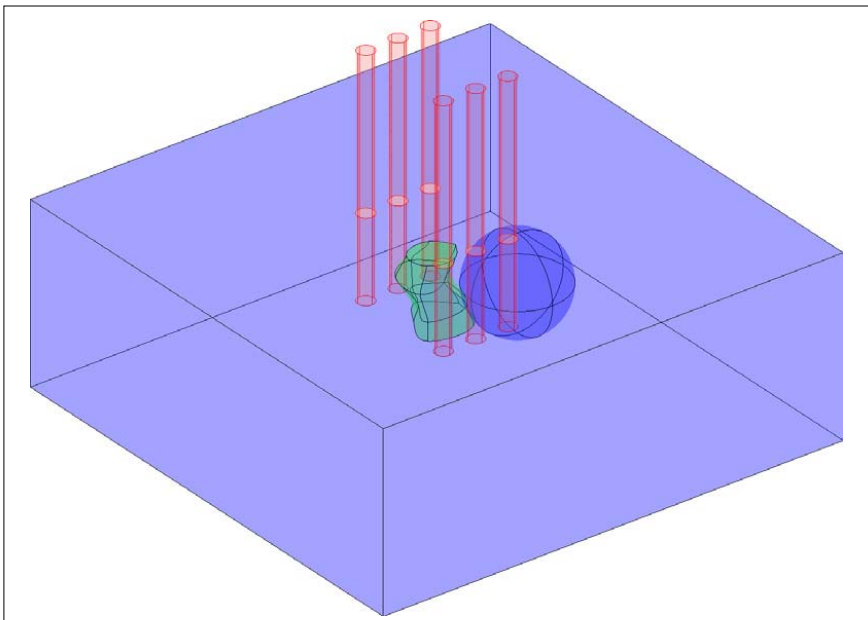**Fig. 1.** Model geometry: biological tissue (light blue); tumor (green) – geometry taken from (Sel et al, 2007); organ at risk (dark blue). Needle electrodes (pink – two rows of needle electrodes as in example 1) are inserted into the tissue and appropriate electric potentials are assigned to each electrode so that the entire tumor volume and the least possible volume of the organ at risk is irreversibly electroporated.

In both examples we use the same steady-state numerical model of electroporation; i.e. electric field distribution in the tissue caused by an electric pulse is determined by solving the Laplace equation for static electric currents. All tissues are considered isotropic and homogeneous, the assigned conductivity values being 0.4 S/m for the tumor and 0.2 S/m for healthy tissue and for organ at risk (Cukjati et al, 2007; Pavselj et al, 2005). The IRE threshold is taken to be 800 V/cm, which is the average threshold reported in literature (Davalos et al, 2005). However, this value is only used for demonstration purposes, as the exact threshold is tissue dependent and also depends on electric pulse duration and number.

The genetic algorithm (Holland, 1992) was written in Matlab and was run together with the numerical calculation using the link between Matlab and COMSOL Multiphysics, a finite element software. In both examples the initial population of chromosomes is generated randomly, taking into account the following model constraints: range of distances between electrodes, range of depth of electrode insertion into the tissue and range of electric potential values on individual electrodes. Chromosomes for reproduction are selected proportionally to their fitness, according to the fitness function:

$$F = 10000 \cdot V_{Tir} - 200 \cdot V_{OARir} - 2 \cdot V_{HTir},$$

where F stands for fitness, V_{Tir} stands for fraction of tumor volume subjected to local electric field above irreversible threshold ($E > E_{irrev}$), V_{OARir} stands for fraction of volume of organ at risk subjected to $E > E_{irrev}$ and V_{HTir} stands for volume of healthy tissue subjected to $E > E_{irrev}$. The weights in the fitness function are set arbitrarily, but with respect to the importance of the individual parameters for efficient IRE. Namely, V_{Tir} is crucial for efficient IRE of the target tissue, therefore its weight is largest (10000) than the weight of V_{OARir} (-200), which is in turn larger than the weight of V_{HTir}, because the organ at risk needs to be preserved, if possible.

Example 1. – two rows of three needle electrodes.

In our first example we optimize the positions of two rows of three needle electrodes, which is a needle electrode array often used in electrochemotherapy (Gilbert et al, 1997; Puc et al, 2004). The optimized parameters are: distance between rows of electrodes, distance between electrodes in a row, depth of electrode insertion, x and y coordinates of the electrode array central point and the voltage between rows of electrodes; altogether six parameters.

The final treatment plan is presented in Figures 2 and 3. We can see that the electric field distribution is rather homogeneous; the field is very high only very close to the electrodes and just above the E_{irr} inside the tumor. Electric field is quite high in the organ at risk closest to the tumor as well – all in all E_{irr} is exceeded in 2.43 % of the organ at risk (Table 1).
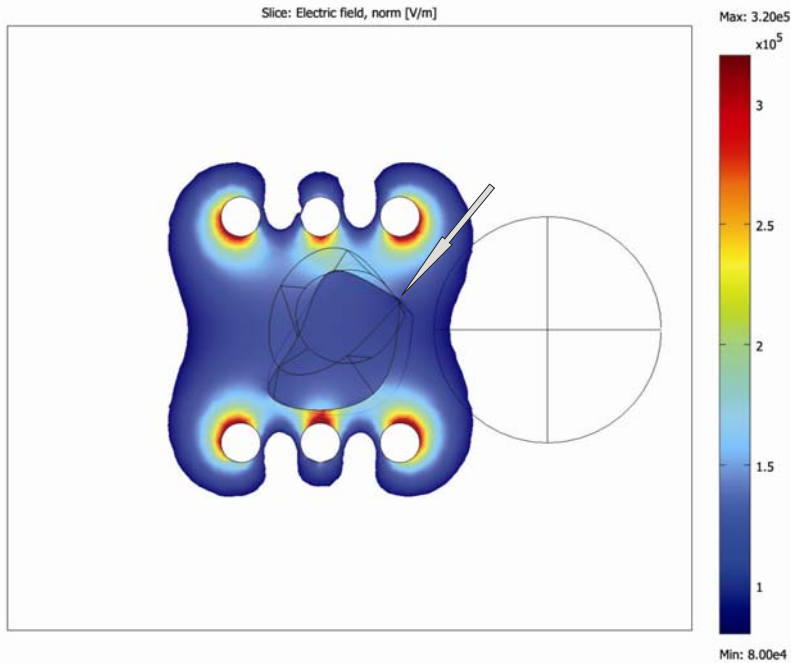
Fig. 2. Local electric field distribution for treatment plan 1 is shown in the XY plane through the center of the tumor. White arrow marks part of the tumor, where electric field is barely over IRE threshold (800 V/cm).

At a first glance it seems that the electric field exceeds E_{irr} in a large volume outside the target tissue and that the treatment planning algorithm should give better results. The obvious change to improve the result would be to put the electrodes more to the left, so that less of the organ at risk gets affected, or perhaps to use only four electrodes instead of six. Actually, none of these two obvious improvements work (data not shown). Moving the electrodes further left causes the electric field on the edge of the tumor (Figure 2) to fall below E_{irr} – as a result the potential on the electrodes has to increase so that the whole tumor volume is covered and this in turn increases the affected volume of organ at risk. Using only four electrodes leads to a similar result.

Example 2. – six needle electrodes.

In our second example we optimize the positions of six individual needle electrodes. Optimized parameters are: x and y coordinates of each of the electrodes separately, electric potential of each electrode and depth of electrode insertion (the same for all electrodes); altogether 19 parameters.

Fig. 3. Target tissue, organ at risk and IRE are presented as contours in the XY plane (left) at three different depths (top: 8 mm; middle: 23 mm; bottom: 38 mm) and in the XZ plane (right) at three different cross-sections (middle: tumor center; top and bottom: 1.2 mm from tumor center).

Table 1. Quality of treatment planning parameters V_{Tir}, V_{OARir}, V_{HT} and treatment planning (computational) time. V_{Tir} and V_{OARir} are normalized by their tissues' respective volumes, V_T and V_{OAR}. All values were calculated using the optimal parameters acquired by the optimization procedure.

	F	V_{Tir}/V_T [%]	V_{OARir}/V_{OAR} [%]	V_{HTir} [mm^3]	No. of parameters	Calculation time [h]
Example 1	9995.0	100	2.4	89	6	1.5
Example 2	9998.1	100	0.8	149	19	4.2
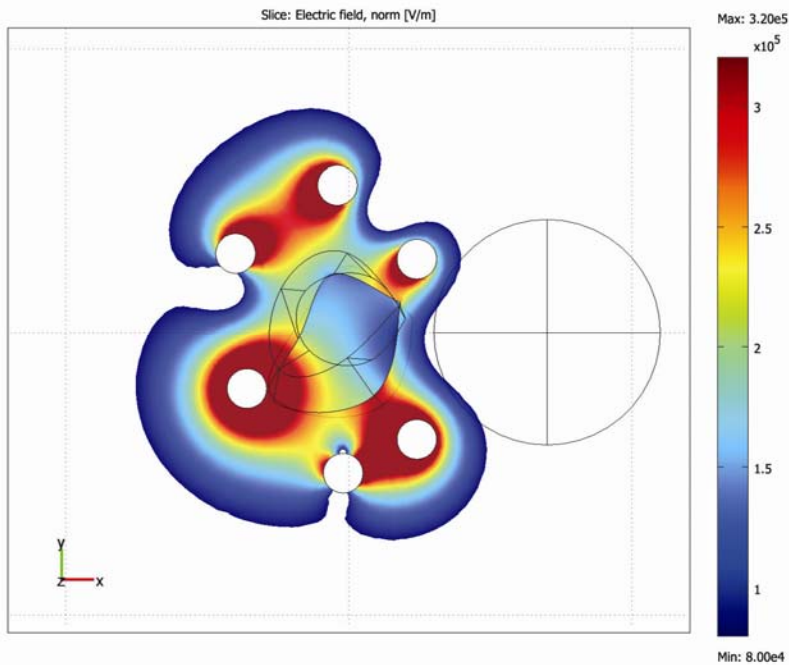
Fig. 4. Electric field distribution for the treatment plan 2 is shown in the XY plane through the center of the tumor. For better comparison, the same color legend (800 V/cm – 3200 V/cm) as in Figure 2 is used. Values over 3200 V/cm are shown in dark red.

The final treatment plan is presented in figures 4 and 5. We can see that the electric field distribution in this case is not at all homogeneous; the field around the electrodes and also in the tumor is much higher than in example 1. Nevertheless, only 0.8 % of the organ at risk is affected (Table 1). We can clearly see that the irregular positioning of the electrodes and different potentials on each electrode result in an electric field distribution "avoiding" high electric fields in the organ at risk on the expense of higher electric field elsewhere.

Both treatment plans provide the treating physician with a set of treatment parameters that successfully ablate the entire target tissue. The treatment plan 2 causes less damage to the organ at risk, however, it takes longer to calculate and causes more damage to the non-critical healthy tissue (Table 1). According to our fitness function F, treatment plan 2 is in fact better than treatment plan 1. However, in the clinical environment, the treating physician has control over the fitness function weights, which can be chosen according to expert knowledge and the choice may well be significantly different from ours, which may result in treatment plan 1 winning out over treatment plan 2.
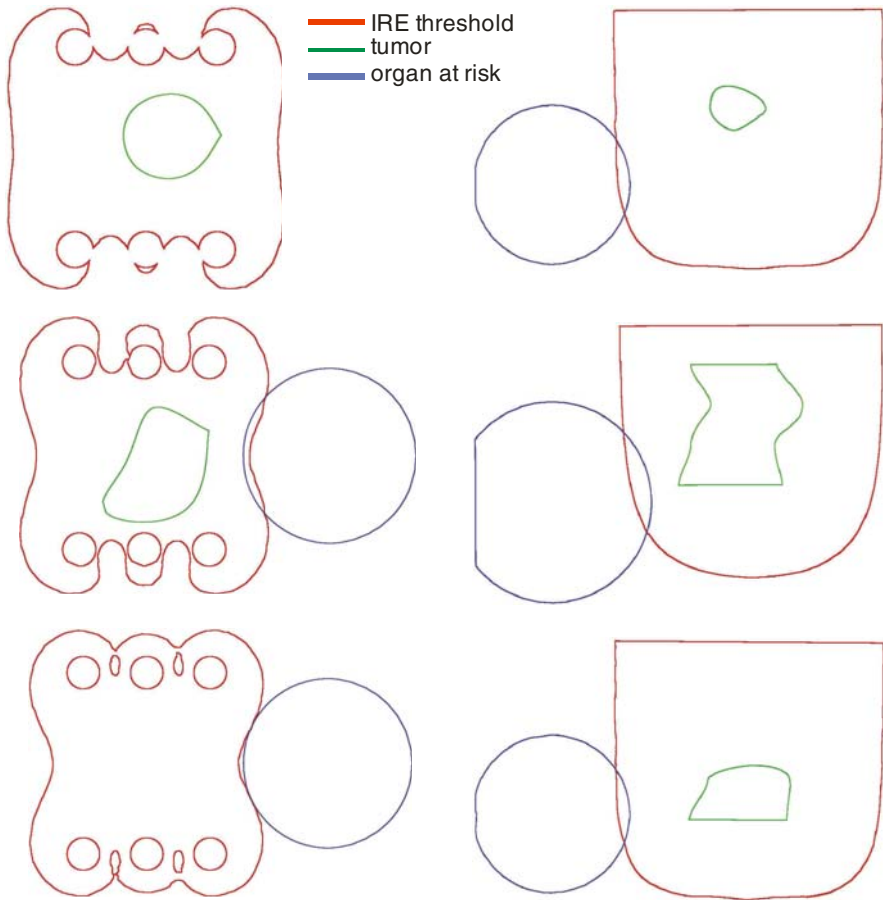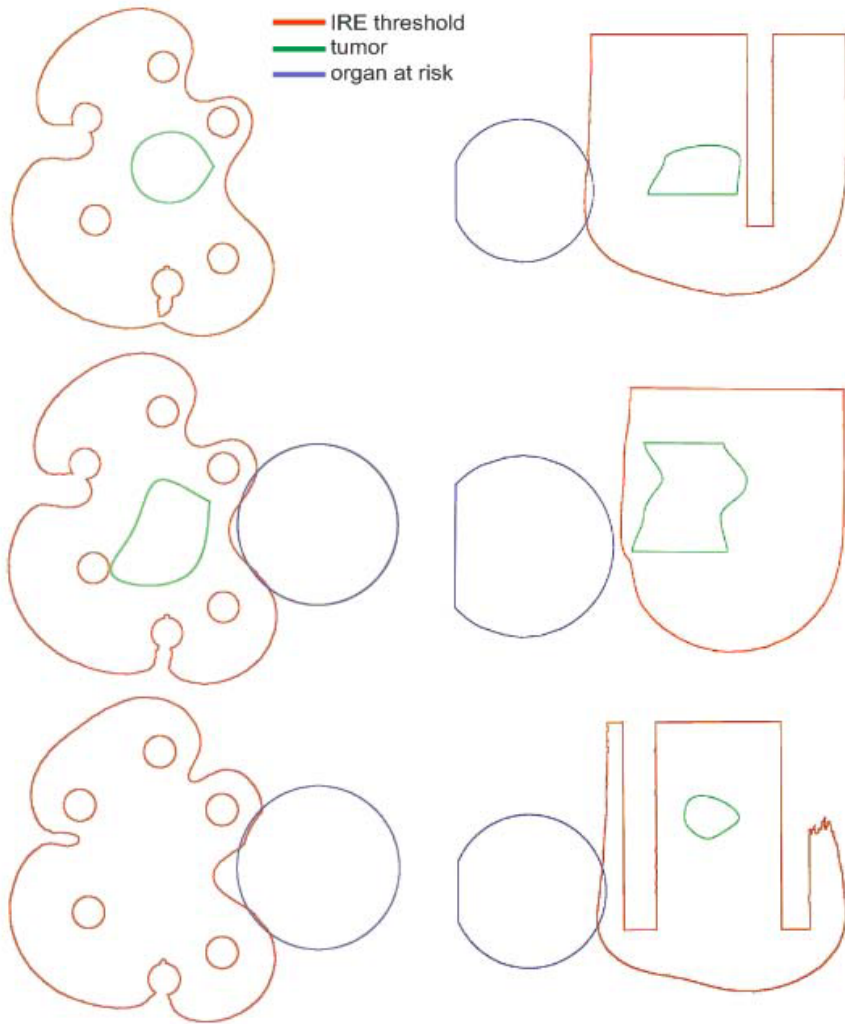
Fig. 5. Target tissue, organ at risk and IRE are presented as contours in the XY plane (left) at three different depths (top: 8 mm; middle: 23 mm; bottom: 38 mm) and in the XZ plane (right) at three different cross-sections (middle: tumor center; top and bottom: 1.2 mm from tumor center)

Conclusions

There are many similarities between radiation therapy and irreversible electroporation. Both treatments depend on the knowledge of the treated anatomy and on medical imaging. Both treatments are based on harmful effects of a

physical agent, which can be efficiently and accurately numerically modeled. Both treatments are local – they target a certain volume of tissue and try not to affect the rest. That is why the RT treatment planning methodology can at least partially be translated to IRE treatment planning, while keeping in mind the relevant differences between the two treatments.

RT and IRE treatment planning both rely on medical imaging to provide patient anatomical data. RT also relies on imaging to provide patient tissue properties, while IRE relies on average electrical properties of excised human tissue measured by different researchers. While tissue properties do not change significantly during RT, they do during IRE. Tissue properties and tissue specific IRE thresholds seems to be the biggest challenge that IRE planning has still to address. Before IRE treatment planning takes off, additional research will have to be performed on human tissue electrical properties, before, during and after electroporation. More data on tissue specific IRE thresholds are also needed, at the very least for all target tissues and critical tissues. At the moment IRE thresholds are only available for few tissue types and limited pulse parameters (Miklavcic et al, 2000; Pavselj et al, 2005). Only after these crucial parameters are available will it become possible to accurately model IRE and provide high accuracy treatment plans.

Choosing the appropriate mathematical model and the appropriate optimization algorithm are also very important steps in treatment planning, as is the decisions, which parameters should the algorithm optimize. Currently, the most viable option seems to be the sequential model of electroporation in combination with one of the stochastic optimization algorithms, which generally provide the best results for higher numbers of optimized parameters (Corovic et al, 2008; Sel et al, 2007; Zupanic et al, 2008). When non-homogeneous electric field distributions are expected, electroporation models should also include modeling of the thermal effects to guarantee non-thermal ablation of target tissue (Davalos & Rubinsky, 2008; Edd & Davalos, 2007).

The presented (hypothetical) IRE treatment planning procedure used the steady-state electroporation model, i.e. no changes in tissue conductivity due to electroporation is taken into consideration, and the genetic optimization algorithm to plan IRE treatment of a subcutaneous tumor. Two different numbers of optimized parameters were chosen and two completely different treatment plans resulted in completely covering the tumor with sufficiently high electric field and only minimally affecting the organ at risk. The presented approach represents the basis for developing future IRE treatment planning algorithms.

Acknowledgements

References

Al-Sakere, B., Bernat, C., Andr, F., Connault, E., Opolon, P., Davalos, R.V., Mir, L.M.: A study of the immunological response to tumor ablation with irreversible Electroporation. Technology in Cancer Research & Treatment 6(4), 301–305 (2007)

Belehradek, J., Orlowski, S., Poddevin, B., Paoletti, C., Mir, L.M.: Electrochemotherapy of spontaneous mammary-tumors in mice. European Journal of Cancer 27(1), 73–76 (1991)

Bertacchini, C., Margotti, P.M., Bergamini, E., Lodi, A., Ronchetti, M., Cadossi, R.: Design of an irreversible Electroporation system for clinical use. Technology in Cancer Research & Treatment 6(4), 313–320 (2007)

Bortfeld, T.: Optimized planning using physical objectives and constraints. Seminars in Radiation Oncology 9(1), 20–34 (1999)

Bortfeld, T.: IMRT: a review and preview. Physics in Medicine and Biology 51(13), R363–R379 (2006)

Boyer, A.L., Butler, E.B., DiPetrillo, T.A., Engler, M.J., Fraass, B., Grant, W., Ling, C.C., Low, D.A., Mackie, T.R., Mohan, R., Purdy, J.A., Roach, M., Rosenman, J.G., Verhey, L.J., Wong, J.W., Cumberlin, R.L., Stone, H., Palta, J.R.: Intensity Modulated Radiation T Intensity modulated radiotherapy: Current status and issues of interest. International Journal of Radiation Oncology Biology Physics 51(4), 880–914 (2001)

Chandra, A., Dong, L., Huang, E., Kuban, D.A., O'Neill, L., Rosen, I, Pollack, A.: Experience of ultrasound-based daily prostate localization. International Journal of Radiation Oncology Biology Physics 56(2), 436–447 (2003)

Corovic, S., Pavlin, M., Miklavcic, D.: Analytical and numerical quantification and comparison of the local electric field in the tissue for different electrode configurations. Biomedical Engineering Online 6 (2007)

Corovic, S., Zupanic, A., Miklavcic, D.: Numerical modeling and optimization of electric field distribution in subcutaneous tumor treated with electrochemotherapy using needle electrodes. IEEE Transactions on Plasma Science 36(4), 1665–1672 (2008)

Cukjati, D., Batiuskaite, D., Andre, F., Miklavcic, D., Mir, L.M.: Real time electroporation control for accurate and safe in vivo non-viral gene therapy. Bioelectrochemistry 70(2), 501–507 (2007)

Davalos, R.V., Mir, L.M., Rubinsky, B.: Tissue ablation with irreversible electroporation. Annals of Biomedical Engineering 33(2), 223–231 (2005)

Davalos, R.V., Otten, D.M., Mir, L.M., Rubinsky, B.: Electrical impedance tomography for imaging tissue electroporation. IEEE Transactions on Biomedical Engineering 51(5), 761–767 (2004)

Davalos, R.V., Rubinsky, B.: Temperature considerations during irreversible electroporation. International Journal of Heat and Mass Transfer 51(23-24), 5617–5622 (2008)

Davalos, R.V., Rubinsky, B., Otten, D.M.: A feasibility study for electrical impedance tomography as a means to monitor tissue electroporation for molecular medicine. IEEE Transactions on Biomedical Engineering 49(4), 400–403 (2002)

Dawson, L.A., Sharpe, M.B.: Image-guided radiotherapy: rationale, benefits, and limitations. Lancet Oncology 7(10), 848–858 (2006)

Denet, A.R., Vanbever, R., Preat, V.: Skin electroporation for transdermal and topical delivery. Advanced Drug Delivery Reviews 56(5), 659–674 (2004)

Edd, J.F., Davalos, R.V.: Mathematical Modeling of irreversible Electroporation for treatment planning. Technology in Cancer Research & Treatment 6(4), 275–286 (2007)

Edd, J.F., Horowitz, L., Davalos, R.V., Mir, L.M., Rubinsky, B.: In vivo results of a new focal tissue ablation technique: Irreversible electroporation. IEEE Transactions on Biomedical Engineering 53(7), 1409–1415 (2006)

Esser, A.T., Smith, K.C., Gowrishankar, T.R., Weaver, J.C.: Towards solid tumor treatment by irreversible electroporation: Intrinsic redistribution of fields and currents in tissue. Technology in Cancer Research & Treatment 6(4), 261–273 (2007)

Ezzell, G.A.: Genetic and geometric optimization of three-dimensional radiation therapy treatment planning. Medical Physics 23(3), 293–305 (1996)

Ezzell, G.A., Galvin, J.M., Low, D., Palta, J.R., Rosen, I., Sharpe, M.B., Xia, P., Xiao, Y., Xing, L., Yu, C.X.: Guidance document on delivery, treatment planning, and clinical implementation of IMRT: Report of the IMRT subcommittee of the AAPM radiation therapy committee. Medical Physics 30(8), 2089–2115 (2003)

Gabriel, C., Gabriel, S., Corthout, E.: The dielectric properties of biological tissues.1. Literature survey. Physics in Medicine and Biology 41(11), 2231–2249 (1996a)

Gabriel, S., Lau, R.W., Gabriel, C.: The dielectric properties of biological tissues.2. Measurements in the frequency range 10 Hz to 20 GHz. Physics in Medicine and Biology 41(11), 2251–2269 (1996b)

Galvin, J.M., Ezzell, G., Eisbrauch, A., Yu, C., Butler, B., Xiao, Y., Rosen, I., Rosenman, J., Sharpe, M., Xing, L., Xia, P., Lomax, T., Low, D.A., Palta, J.: Implementing IMRT in clinical practice: A joint document of the American Society for Therapeutic Radiology and Oncology and the American Association of Physicists in Medicine. International Journal of Radiation Oncology Biology Physics 58(5), 1616–1634 (2004)

Gilbert, R.A., Jaroszeski, M.J., Heller, R.: Novel electrode designs for electrochemotherapy. Biochimica Et Biophysica Acta-General Subjects 1334(1), 9–14 (1997)

Golzio, M., Rols, M.P., Teissie, J.: In vitro and in vivo electric field-mediated permeabilization, gene transfer, and expression. Methods 33(2), 126–135 (2004)

Granot, Y., Rubinsky, B.: Methods of optimization of electrical impedance tomography for imaging tissue electroporation. Physiological Measurement 28(10), 1135–1147 (2007)

Heinzerling, J.H., Papiez, L., Chien, S., Anderson, J., Forster, K., Zhang, G., Timmerman, R.: Stereotactic body radiation therapy: Evaluation of setup accuracy and targeting methods for a new couch integrated immobilization system. Technology in Cancer Research & Treatment 7(3), 197–206 (2008)

Heller, R., Gilbert, R., Jaroszeski, M.J.: Clinical applications of electrochemotherapy. Advanced Drug Delivery Reviews 35(1), 119–129 (1999)

Hojman, P., Zibert, J.R., Gissel, H., Eriksen, J., Gehl, J.: Gene expression profiles in skeletal muscle after gene electrotransfer. Bmc. Molecular Biology 8 (2007)

Holland, J.H.: Adaptation in Natural and Artificial Systems: An Introductory Analysis with Applications to Biology, Control, and Artificial Intelligence. MIT Press, Cambridge (1992)

ICRU-50, Prescribing, recording, and reporting photon beam therapy. Bethesda (1993)

ICRU-62, Prescribing, recording, and reporting photon beam therapy (supplement to ICRU Report 50). Bethesda (1999)

Ivorra, A., Rubinsky, B.: In vivo electrical impedance measurements during and after electroporation of rat liver. Bioelectrochemistry 70(2), 287–295 (2007)

Jaffray, D., Kupelian, P., Djemil, T., Macklis, R.M.: Review of image-guided radiation therapy. Expert Review of Anticancer Therapy 7(1), 89–103 (2007)

Lampert, V.L., Zelch, J.V., Cohen, D.N.: Computed tomography of orbits. Radiology 113(2), 351–354 (1974)

Lavee, J., Onik, G., Mikus, P., Rubinsky, B.: A novel nonthermal energy source for surgical epicardial atrial ablation: Irreversible electroporation. Heart Surgery Forum 10(2), E162–E167 (2007)

Lecchi, M., Fossati, P., Elisei, F., Orecchia, R., Lucignani, G.: Current concepts on imaging in radiotherapy. European Journal of Nuclear Medicine and Molecular Imaging 35(4), 821–837 (2008)

Lee, E.W., Loh, C.T., Kee, S.T.: Imaging guided percutaneous irreversible electroporation: Ultrasound and immunohistological correlation. Technology in Cancer Research & Treatment 6(4), 287–293 (2007)

Lindegaard, J.C., Tanderup, K., Nielsen, S.K., Haack, S., Gelineck, J.: MRI-guided 3D optimization significantly improves DVH parameters of pulsed-dose-rate brachytherapy in locally advanced cervical cancer. International Journal of Radiation Oncology Biology Physics 71(3), 756–764 (2008)

Lyman, J.T., Wolbarst, A.B.: Optimization of radiation-therapy.3. A method of assessing complication probabilities from dose-volume histograms. International Journal of Radiation Oncology Biology Physics 13(1), 103–109 (1987)

Macek-Lebar, A., Sersa, G., Kranjc, S., Groselj, A., Miklavcic, D.: Optimisation of pulse parameters in vitro for in vivo electrochemotherapy. Anticancer Research 22(3), 1731–1736 (2002)

Mackie, T.R., Scrimger, J.W., Battista, J.J.: A convolution method of calculating dose for 15-MV X-rays. Medical Physics 12(2), 188–196 (1985)

Maor, E., Ivorra, A., Leor, J., Rubinsky, B.: The effect of irreversible electroporation on blood vessels. Technology in Cancer Research & Treatment 6(4), 307–312 (2007)

Maor, E., Ivorra, A., Leor, J., Rubinsky, B.: Irreversible electroporation attenuates neointimal formation after angioplasty. IEEE Transactions on Biomedical Engineering 55(9), 2268–2274 (2008)

Miklavcic, D., Beravs, K., Semrov, D., Cemazar, M., Demsar, F., Sersa, G.: The importance of electric field distribution for effective in vivo electroporation of tissues. Biophysical Journal 74(5), 2152–2158 (1998)

Miklavcic, D., Corovic, S., Pucihar, G., Pavselj, N.: Importance of tumour coverage by sufficiently high local electric field for effective electrochemotherapy. Ejc Supplements 4(11), 45–51 (2006a)

Miklavcic, D., Kotnik, T.: Electroporation for electrochemotherapy and gene therapy. In: Rosch, P., Markov, M. (eds.) Bioelectromagnetic medicine, pp. 637–656. Marcel Decker, New York (2004)

Miklavcic, D., Pavselj, N., Hart, F.X.: Electric properties of tissues. In: Wiley Encyclopedia of Biomedical Engineering. John Wiley & Sons, New York (2006b)

Miklavcic, D., Semrov, D., Mekid, H., Mir, L.M.: A validated model of in vivo electric field distribution in tissues for electrochemotherapy and for DNA electrotransfer for gene therapy. Biochimica Et Biophysica Acta-General Subjects 1523(1), 73–83 (2000)

Miller, L., Leor, J., Rubinsky, B.: Cancer cells ablation with irreversible electroporation. Technology in Cancer Research & Treatment 4(6), 699–705 (2005)

Mir, L.M., Bureau, M.F., Gehl, J., Rangara, R., Rouy, D., Caillaud, J.M., Delaere, P., Branellec, D., Schwartz, B., Scherman, D.: High-efficiency gene transfer into skeletal muscle mediated by electric pulses. Proceedings of the National Academy of Sciences of the United States of America 96(8), 4262–4267 (1999)

Mir, L.M., Glass, L.F., Sersa, G., Teissie, J., Domenge, C., Miklavcic, D., Jaroszeski, M.J., Orlowski, S., Reintgen, D.S., Rudolf, Z., Belehradek, M., Gilbert, R., Rols, M.P., Belehradek, J., Bachaud, J.M., DeConti, R., Stabuc, B., Cemazar, M., Coninx, P., Heller, R.: Effective treatment of cutaneous and subcutaneous malignant tumours by electrochemotherapy. British Journal of Cancer 77(12), 2336–2342 (1998)

Neumann, E., Schaeferridder, M., Wang, Y., Hofschneider, P.H.: Gene transfer into mouse lyoma cells by electroporation in high electric-fields. Embo Journal 1(7), 841–845 (1982)

Newbold, K., Partridge, M., Cook, G., Sohaib, A., Charles-Edwards, E., Rhys-Evans, P., Harrington, K., Nutting, C.: Advanced imaging applied to radiotherapy planning in head and neck cancer: a clinical review. British Journal of Radiology 79(943), 554–561 (2006)

Onik, G., Mikus, P., Rubinsky, B.: Irreversible electroporation: Implications for prostate ablation. Technology in Cancer Research & Treatment 6(4), 295–300 (2007)

Orlowski, S., Belehradek, J., Paoletti, C., Mir, L.M.: Transient electropermeabilization of cells in culture - increase of the cyto-toxicity of anticancer drugs. Biochemical Pharmacology 37(24), 4727–4733 (1988)

Pavlin, M., Miklavcic, D.: Theoretical and experimental analysis of conductivity, ion diffusion and molecular transport during cell electroporation — Relation between short-lived and long-lived pores. Bioelectrochemistry 74, 38–46 (2008)

Pavselj, N., Bregar, Z., Cukjati, D., Batiuskaite, D., Mir, L.M., Miklavcic, D.: The course of tissue permeabilization studied on a mathematical model of a subcutaneous tumor in small animals. IEEE Transactions on Biomedical Engineering 52(8), 1373–1381 (2005)

Pavselj, N., Miklavcic, D.: Numerical modeling in electroporation-based biomedical applications. Radiology and Oncology 42(3), 159–168 (2008a)

Pavselj, N., Miklavcic, D.: Numerical models of skin electropermeabilization taking into account conductivity changes and the presence of local transport regions. IEEE Transactions on plasma science, 1650–1658 (2008b)

Pliquett, U.: Joule heating during solid tissue electroporation. Medical & Biological Engineering & Computing 41(2), 215–219 (2003)

Pliquett, U., Weaver, J.C.: Electroporation of human skin: Simultaneous measurement of changes in the transport of two fluorescent molecules and in the passive electrical properties. Bioelectrochemistry and Bioenergetics 39(1), 1–12 (1996)

Polk, C., Postow, E.: Handbook of Biological Effects of Electromagnetic Fields. CRC Press, Boca Raton (1996)

Potter, R., Fidarova, E., Kirisits, C., Dirnopoulos, J.: Image-guided adaptive brachytherapy for cervix carcinoma. Clinical Oncology 20(6), 426–432 (2008a)

Potter, R., Kirisits, C., Fidarova, E.F., Dimopoulos, J.C.A., Berger, D., Tanderup, K., Lindegaard, J.C.: Present status and future of high-precision image guided adaptive brachytherapy for cervix carcinoma. Acta Oncologica 47(7), 1325–1336 (2008b)

Prausnitz, M.R.: A practical assessment of transdermal drug delivery by skin electroporation. Advanced Drug Delivery Reviews 35(1), 61–76 (1999)

Puc, M., Corovic, S., Flisar, K., Petkovsek, M., Nastran, J., Miklavcic, D.: Techniques of signal generation required for electropermeabilization. Survey of electropermeabilization devices. Bioelectrochemistry 64(2), 113–124 (2004)

Pucihar, G., Kotnik, T., Miklavcic, D., Teissie, J.: Kinetics of transmembrane transport of small molecules into electropermeabilized cells. Biophysical Journal 95(6), 2837–2848 (2008)

Pucihar, G., Mir, L.M., Miklavcic, D.: The effect of pulse repetition frequency on the uptake into electropermeabilized cells in vitro with possible applications in electrochemotherapy. Bioelectrochemistry 57(2), 167–172 (2002)

Purdy, J., Starkschall, G.: A practical guide to 3-D planning and conformal radiation therapy. Advanced Medical Publishing, Madison (1999)

Reynaert, N., van der Marck, S.C., Schaart, D.R., Van der Zee, W., Van Vliet-Vroegindeweij, C., Tomsej, M., Jansen, J., Heijmen, B., Coghe, M., De Wagter, C.: Monte Carlo treatment planning for photon and electron beams. Radiation Physics and Chemistry 76(4), 643–686 (2007)

Rubinsky, B., Onik, G., Mikus, P.: Irreversible electroporation: A new ablation modality - Clinical implications. Technology in Cancer Research & Treatment 6(1), 37–48 (2007)

Rubinsky, J., Onik, G., Mikus, P., Rubinsky, B.: Optimal Parameters for the Destruction of Prostate Cancer Using Irreversible Electroporation. Journal of Urology 180(6), 2668–2674 (2008)

Ruchala, K.J., Olivera, G.H., Schloesser, E.A., Hinderer, R., Mackie, T.R.: Calibration of a tomotherapeutic MVCT system. Physics in Medicine and Biology 45(4), N27–N36 (2000)

Scott-Taylor, T.H., Pettengell, R., Clarke, I., Stuhler, G., La Barthe, M.C., Walden, P., Dalgleish, A.G.: Human tumour and dendritic cell hybrids generated by electrofusion: potential for cancer vaccines. Biochimica Et Biophysica Acta-Molecular Basis of Disease 1500(3), 265–279 (2000)

Sel, D., Cukjati, D., Batiuskaite, D., Slivnik, T., Mir, L.M., Miklavcic, D.: Sequential finite element model of tissue electropermeabilization. IEEE Transactions on Biomedical Engineering 52(5), 816–827 (2005)

Sel, D., Lebar, A.M., Miklavcic, D.: Feasibility of employing model-based optimization of pulse amplitude and electrode distance for effective tumor electropermeabilization. IEEE Transactions on Biomedical Engineering 54(5), 773–781 (2007)

Semrov, D., Miklavcic, D.: Calculation of the electrical parameters in electrochemotherapy of solid tumours in mice. Computers in Biology and Medicine 28(4), 439–448 (1998)

Serša, G., Čemažar, M., Miklavčič, D., Rudolf, Z.: Electrochemotherapy of tumours. Radiology & Oncology 40, 163–174 (2006)

Sharpe, M.B., Battista, J.J.: Dose calculations using convolution and superposition principles - the orientation of dose spread kernels in divergent X-ray beams. Medical Physics 20(6), 1685–1694 (1993)

Skerl, D., Likar, B., Fitzpatrick, J.M., Pernus, F.: Comparative evaluation of similarity measures for the rigid registration of multi-modal head images. Physics in Medicine and Biology 52(18), 5587–5601 (2007)

Slomka, P.J.: Software approach to merging molecular with anatomic information. Journal of Nuclear Medicine 45, 36S–45S (2004)

Smith, K.C., Weaver, J.C.: Active mechanisms are needed to describe cell responses to submicrosecond, megavolt-per-meter pulses: Cell models for ultrashort pulses. Biophysical Journal 95(4), 1547–1563 (2008)

Trontelj, K., Rebersek, M., Kanduser, M., Curin-Serbec, V., Sprohar, M., Miklavcic, D.: Optimization of bulk cell electrofusion in vitro for production of human–mouse heterohybridoma cells. Bioelectrochemistry 74, 124–129 (2008)

Vanuytsel, L.J., Vansteenkiste, J.F., Stroobants, S.G., De Leyn, P.R., De Wever, W., Verbeken, E.K., Gatti, G.G., Huyskens, D.P., Kutcher, G.J.: The impact of F-18-fluoro-2-deoxy-D-glucose positron emission tomography (FDG-PET) lymph node staging on the radiation treatment volumes in patients with non-small cell lung cancer. Radiotherapy and Oncology 55(3), 317–324 (2000)

Weaver, J.C.: Electroporation of biological membranes from multicellular to nano scales. IEEE Transactions on Dielectrics and Electrical Insulation 10(5), 754–768 (2003)

Webb, S.: The physical basis of IMRT and inverse planning. British Journal of Radiology 76(910), 678–689 (2003)

Zupanic, A., Corovic, S., Miklavcic, D.: Optimization of electrode position and electric pulse amplitude in electrochemotherapy. Radiology and Oncology 42(2), 93–101 (2008)

IV

Miklavcic D, Snoj M, **Zupanic A,** Kos B, Cemazar M, Kropivnik M, Bracko M, Pecnik T, Gadzijev E, Sersa G. Towards treatment planning and treatment of deep-seated solid tumors by electrochemotherapy. *Biomed Eng Online* 9:10, 2010.

BioMedical Engineering OnLine

RESEARCH

Open Access

Towards treatment planning and treatment of deep-seated solid tumors by electrochemotherapy

Damijan Miklavcic[1], Marko Snoj[2], Anze Zupanic[1], Bor Kos[1], Maja Cemazar[2], Mateja Kropivnik[2], Matej Bracko[2], Tjasa Pecnik[2], Eldar Gadzijev[2], Gregor Sersa[2*]

Abstract

Background: Electrochemotherapy treats tumors by combining specific chemotherapeutic drugs with an intracellular target and electric pulses, which increases drug uptake into the tumor cells. Electrochemotherapy has been successfully used for treatment of easily accessible superficial tumor nodules. In this paper, we present the first case of deep-seated tumor electrochemotherapy based on numerical treatment planning.

Methods: The aim of our study was to treat a melanoma metastasis in the thigh of a patient. Treatment planning for electrode positioning and electrical pulse parameters was performed for two different electrode configurations: one with four and another with five long needle electrodes. During the procedure, the four electrode treatment plan was adopted and the patient was treated accordingly by electrochemotherapy with bleomycin. The response to treatment was clinically and radiographically evaluated. Due to a partial response of the treated tumor, the metastasis was surgically removed after 2 months and pathological analysis was performed.

Results: A partial response of the tumor to electrochemotherapy was obtained. Histologically, the metastasis showed partial necrosis due to electrochemotherapy, estimated to represent 40-50% of the tumor. Based on the data obtained, we re-evaluated the electrical treatment parameters in order to correlate the treatment plan with the clinical response. Electrode positions in the numerical model were updated according to the actual positions during treatment. We compared the maximum value of the measured electric current with the current predicted by the model and good agreement was obtained. Finally, tumor coverage with an electric field above the reversible threshold was recalculated and determined to be approximately 94%. Therefore, according to the calculations, a small volume of tumor cells remained viable after electrochemotherapy, and these were sufficient for tumor regrowth.

Conclusions: In this, the first reported clinical case, deep-seated melanoma metastasis in the thigh of the patient was treated by electrochemotherapy, according to a treatment plan obtained by numerical modeling and optimization. Although only a partial response was obtained, the presented work demonstrates that treatment of deep-seated tumor nodules by electrochemotherapy is feasible and sets the ground for numerical treatment planning-based electrochemotherapy.

Trial registration: EudraCT:2008-008290-54

* Correspondence: gsersa@onko-i.si
[2]Institute of Oncology Ljubljana, Zaloska 2, SI-1000 Ljubljana, Slovenia

Background

Electrochemotherapy is a type of tumor treatment that combines the use of specific chemotherapeutic drugs which have an intracellular target and low membrane permeability, with application of electric pulses to the tumors to increase drug uptake into cells. It provides good local tumor control when the two modalities combined are optimized; *i.e.* drug choice, distribution and concentration in the tumors, in addition to adequate electric pulse parameter selection and pulse delivery leading to cell membrane electroporation of the tumor tissue [1-4].

The drug used in electrochemotherapy needs to be adequately distributed in the tumor and present at a sufficient concentration. For treatment of small subcutaneous tumor nodules, such as melanoma metastases, intratumoral bleomycin or cisplatin administration is recommended, whereas for treatment of bigger tumor nodules, intravenous injection of bleomycin is used. Drug doses needed for treatment are provided in the published Standard Operating Procedures [5]. For optimal drug distribution within the tumor after intratumoral injection, only a few minutes are needed between the drug injection and electroporation of tumors. After intravenous bleomycin injection, at least 8 minutes are needed for the drug to be in a pharmacological peak in the tumor and the drug remains at a sufficient concentration for at least another 20 minutes [6].

The second prerequisite for successful electrochemotherapy is that the whole tumor mass is exposed to a sufficiently high electric field. This can be achieved by appropriate selection and placement of electrodes, and application of electric pulses of adequate amplitude. The distribution of the electric field after application of electric pulses by plate or needle electrodes has already been extensively elaborated for small tumor nodules [2]. These settings and electrodes provide efficient treatment of superficial tumor nodules up to 3 cm in diameter in a single electrochemotherapy session and have even been used to treat bone cancer [7-9]. However, to enable treatment of deep-seated tumors, a design of long needle electrodes and in particular their positioning with respect to the tumor is needed. If solid tumors of 3-4 cm diameter are located deep in the body, choosing electrical parameters that would result in a good clinical response and that would have no or minimal damage to normal tissue is of the outmost importance, especially in cases where tumors are located close to vital organs. Numerical modeling in treatment planning is the proposed approach that also allows verification of the electrical parameters based on the clinical response to electrochemotherapy [10].

In order to also develop electrochemotherapy for treatment of deep-seated tumors, the aim of our study was to treat a deep-seated melanoma metastasis in the thigh of a patient by custom-made long needle electrodes. Based on treatment planning, the electric pulse parameters and positioning of electrodes were determined. The patient was treated accordingly by electrochemotherapy with bleomycin. The response to treatment was clinically, radiographically and histologically evaluated. Due to a partial response of the treated tumor (reduction in size by more than 50%), the metastasis was surgically removed after 2 months and pathological analysis was performed. Based on the data obtained, we re-evaluated the electrical treatment parameters in order to correlate the treatment plan with the clinical response of the electrochemotherapy-treated metastasis.

Materials and methods

Clinical data of the patient

A 51-year-old male Caucasian patient with a diagnosis of melanoma had been previously treated by electrochemotherapy with bleomycin given intravenously. The treated small superficial metastases on the right leg regressed completely after the treatment. In October 2008, a PET-CT was performed, which revealed a deep-seated metastasis in the right thigh (Figure 1). In December 2008, electrochemotherapy with long needle electrodes was performed using bleomycin given intravenously (15,000 IU/m^2) and electric pulses were delivered 10-12 minutes after injection. The study was approved by the national Ethics committee and institutional board. The patient signed an informed consent to participate in the study. The positioning of the electrodes
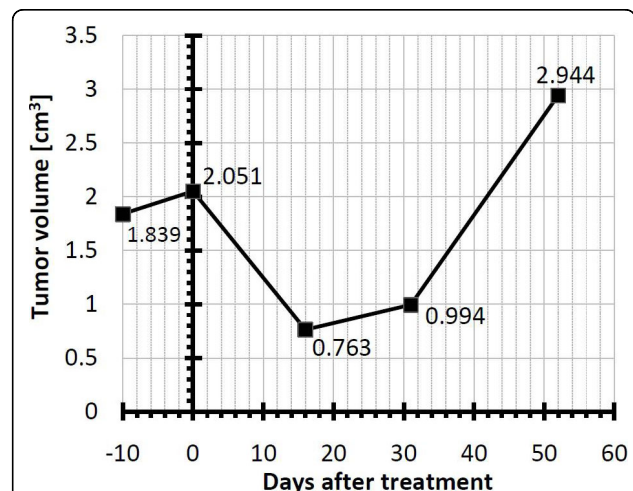

Figure 1 Size of the melanoma metastasis determined by ultrasound. The figure shows the tumor size shortly before the treatment, at the time of the treatment itself and during the follow-up. Regrowth of the tumor was observed at day 31 and the tumor was excised at day 52.

was ultrasonographically guided. The treatment was performed in general anesthesia; in order to avoid strong muscle contractions induced by electric pulses the myorelaxant vercuronium bromide (Norcuron, Organon) was used. In February 2009, regrowth of the metastasis was observed by ultrasound. The metastasis was surgically removed by the end of February and a pathological analysis of the excised tissue was performed.

Numerical treatment planning

Based on the PET-CT radiographs, the position of the melanoma metastasis was determined. Its size was 20 × 14 mm in diameter and it was located in the right thigh, 20 mm under the skin. The location was estimated to be on or minimally invasive into thigh muscle fascia.

During preparation for electrochemotherapy, a slight growth of the metastasis was observed ultrasonographically (Figure 1). The anatomical model geometry used in the treatment planning procedure was obtained from CT images. All clinically relevant tissue structures (tumor, muscle, adipose tissue) were delineated and used to construct 3D geometry objects in the numerical computing environment Matlab (Mathworks, USA) by the planar contour method as previously described by [11] (Figure 2). The geometry of objects was then imported into the finite element analysis software Comsol Multiphysics 3.5 (COMSOL AB, Sweden). In the model, all tissues were considered homogeneous, the assigned conductivity values being: 0.2 S/m for the tumor, 0.018 S/m for adipose tissue, 0.135 S/m and 0.75

S/m for muscle tissue perpendicular and parallel to the muscle direction, respectively. These conductivity values were considered as approximations for DC values, and are extrapolated from measurements performed at 10 Hz. During the delivery of electric pulses, the conductivity of tissues changes as a consequence of electroporation. Measurements of conductivity during pulse application have shown that conductivity changes by a factor of around 3.5; therefore conductivity of electroporated tissue was increased by this factor, which agrees well with measurements taken on rat muscle and liver tissue and with the post-electroporation conductivity estimation performed by mathematical modeling for rabbit liver [12,13]. All conductivity values were chosen according to previous measurements of tumor and tissue conductivity and models of subcutaneous tumor and skin electroporation [12-14].
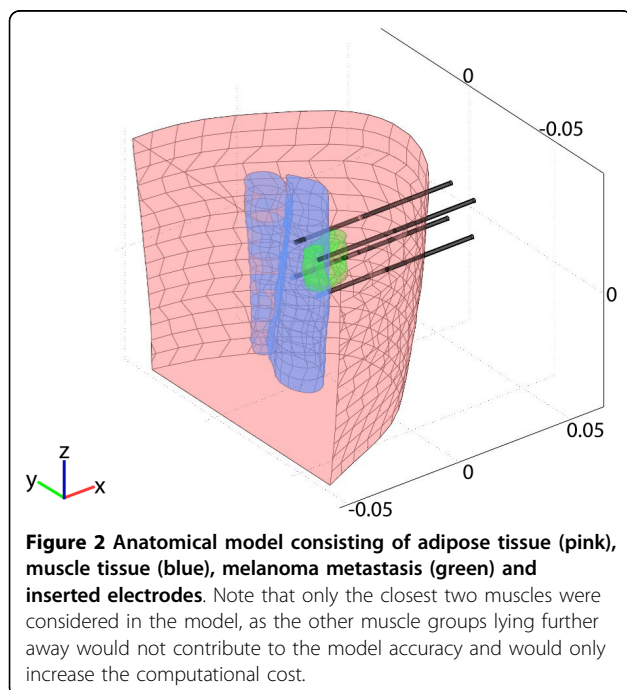
Numerical calculations were performed with Comsol. Electric field distribution in the tissue, caused by an electroporative pulse, was determined by solving the Laplace equation for static electric currents:

$$\nabla \cdot (\sigma \cdot \nabla \varphi) = 0$$

where σ and ϕ are tissue electric conductivity and electric potential, respectively. The boundary conditions used in our calculations were a constant potential on the surface of the electrodes and electrical insulation on all outer boundaries of the model. For tumors, the reversible electroporation threshold was considered to be 400 V/cm, for adipose tissue 100 V/cm, for muscle tissue 200 V/cm and 80 V/cm, in the perpendicular direction to muscle fibers and in the parallel direction, respectively. The irreversible threshold was set to 900 V/cm for all tissues.

In treatment planning, a numerical model of electroporation was used that did not take into account changes in tissue conductivity during electroporation. After the treatment, in order to compare the measured electric currents during electric pulse delivery and the currents predicted by the model, a model that took into account the changes in tissue conductivity was used. The conductivity dependencies on the electric field $\sigma(E)$ of all tissues were approximated by a step function [14].

Electrode positions and voltages to be applied between individual electrodes were optimized using a genetic algorithm, described in more detail in previous studies [15,16]. In short, the algorithm optimized the position of each electrode (x, y, z) - in discrete steps of 1 mm and the voltage between each pair of electrodes in discrete steps of 100 V. Feasible ranges of all these parameters were taken into account, as well as the specifications of the electric pulse generator (see below). First, a population of treatment plans (consisting of all electrode

Figure 2 Anatomical model consisting of adipose tissue (pink), muscle tissue (blue), melanoma metastasis (green) and inserted electrodes. Note that only the closest two muscles were considered in the model, as the other muscle groups lying further away would not contribute to the model accuracy and would only increase the computational cost.

positions and all used voltages) was randomly generated. The treatment plans then evolved over several hundred generations by mathematical operations cross-over and mutation according to the fitness function:

$$F = 100 \cdot V_{Trev} - 10 \cdot V_{Hirrev}$$

where F is fitness, V_{Trev} is the tumor volume subjected to the local electric field above the reversible threshold and V_{Hirrev} is the volume of healthy tissue subjected to a local electric field above the irreversible threshold. The weights in the fitness function were chosen to reflect the importance of the individual parameters for efficient ECT. Namely, V_{Trev} is crucial for efficient ECT; therefore its weight is larger (100) than the weight of V_{Hirrev}. The algorithm was stopped after 500 iterations - this number of iterations gave good solutions in previous studies [15,16] and the quality of the treatment plan was compared to previously set treatment plan requirements - when a sufficiently high quality treatment plan was achieved, *i.e.* the whole tumor was covered with a sufficiently high electric field and very little of the surrounding tissue was affected by the field. The optimization took 5 h on a Windows XP, 3.0 GHz, 2 GB RAM desktop computer.

Electrodes, pulse generator and pulse parameters

Four custom-made electrodes made of stainless steel, 1.8 mm in diameter with sharpened tips, insulated except for the upper 4 cm, were used. An additional 1.2 mm in diameter electrode was considered for direct insertion into the center of the tumor. The electrodes were connected to independently controlled generator outputs of the Cliniporator Vitae (IGEA, Carpi, Italy). The Cliniporator Vitae device is a pulse generator with 6 independently controlled and electrically insulated outputs each providing up to 3000 V, max current 50 A, delivering 8 rectangular electrical pulses (rise time 1 μs) of 100 μs duration at a pulse repetition frequency of 4 Hz [17]. The current and voltage are measured and logged with a precision better than 3%, which allows for pulse delivery control and post-treatment evaluation. Pulses were delivered 10-12 minutes after i.v. bolus injection of bleomycin.

Results
Optimized treatment plan
Treatment planning was performed for two different electrode configurations. The first configuration was with five electrodes with a central electrode inserted in the tumor and four electrodes distributed around the tumor, while the second configuration was with four electrodes outside the tumor (Figure 3). Although the five-electrode option was recognized as superior and was the primary choice for treatment, the central electrode could not be
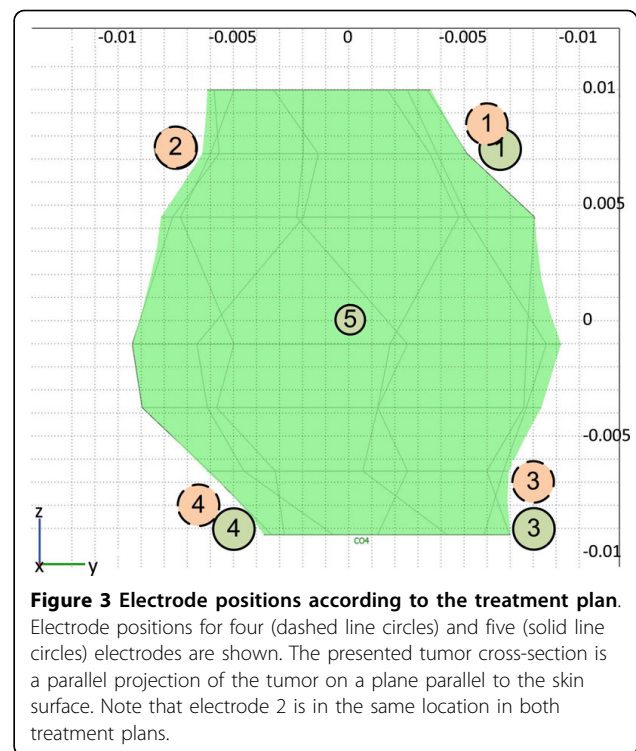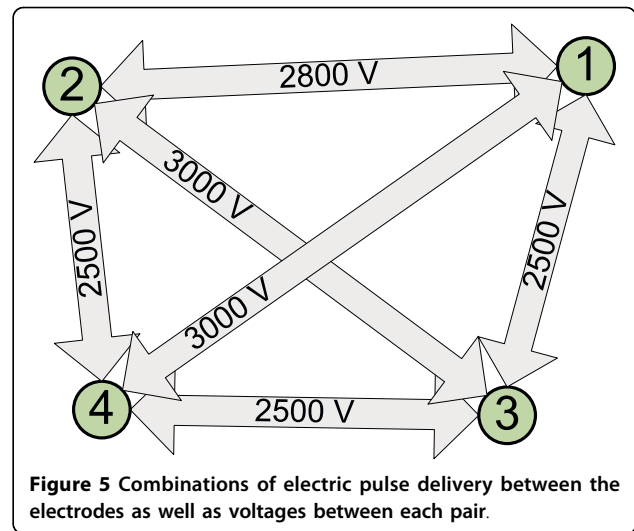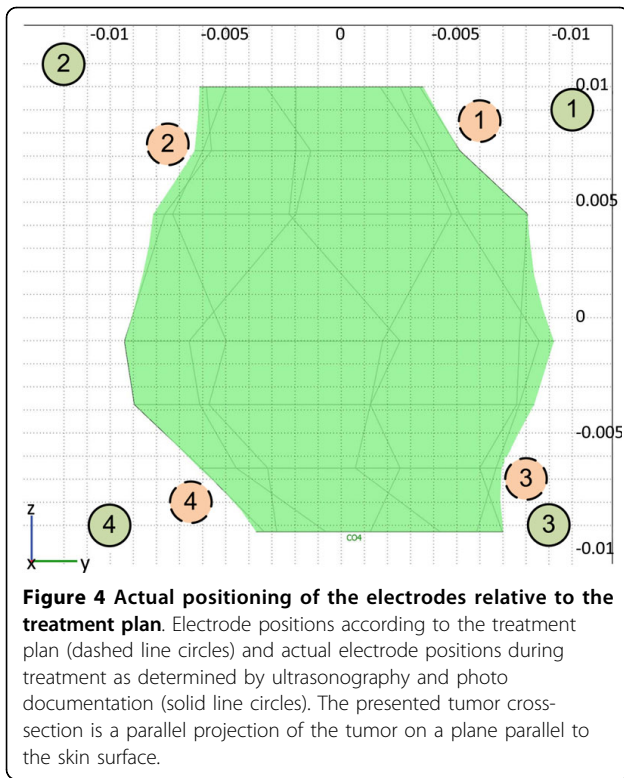

Figure 3 Electrode positions according to the treatment plan. Electrode positions for four (dashed line circles) and five (solid line circles) electrodes are shown. The presented tumor cross-section is a parallel projection of the tumor on a plane parallel to the skin surface. Note that electrode 2 is in the same location in both treatment plans.

inserted into the tumor as the tumor was very mobile, effectively "floating" in the surrounding adipose tissue. This mobility of the tumor also made it very difficult to rigorously follow the treatment plan for four electrodes, and as a result the electrodes were positioned farther away from the tumor than originally planned.

The results of optimization were electrode positions and minimum voltages for each electrode pair. Electrode positions outside the tumor were similar in both configurations, *i.e.* very close to the tumor surface; however the fifth electrode inside the tumor significantly reduced the required voltage to achieve efficient membrane electroporation of cells in the whole tumor, thereby also reducing damage to healthy tissue. The maximum voltages required were 3000 V and 2500 V in the four and five electrode configuration, respectively. The volume of irreversibly permeabilized healthy tissue according to the treatment plan was 13.8 cm^3 (of that 11.5 cm^3 adipose tissue and 2.33 cm^3 muscle tissue) in the four electrode configuration and 12.3 cm^3 (of that 10.4 cm^3 adipose tissue and 1.88 cm^3 muscle tissue) in the five electrode configuration. Depth of insertion was a few millimeters deeper than the tumor, slightly penetrating the muscle tissue.

Treatment and response to the treatment
During the procedure, the four-electrode treatment plan was adopted. The electrodes were placed according to the treatment plan as depicted in Figure 4. Electrodes

Figure 4 Actual positioning of the electrodes relative to the treatment plan. Electrode positions according to the treatment plan (dashed line circles) and actual electrode positions during treatment as determined by ultrasonography and photo documentation (solid line circles). The presented tumor cross-section is a parallel projection of the tumor on a plane parallel to the skin surface.

Figure 5 Combinations of electric pulse delivery between the electrodes as well as voltages between each pair.
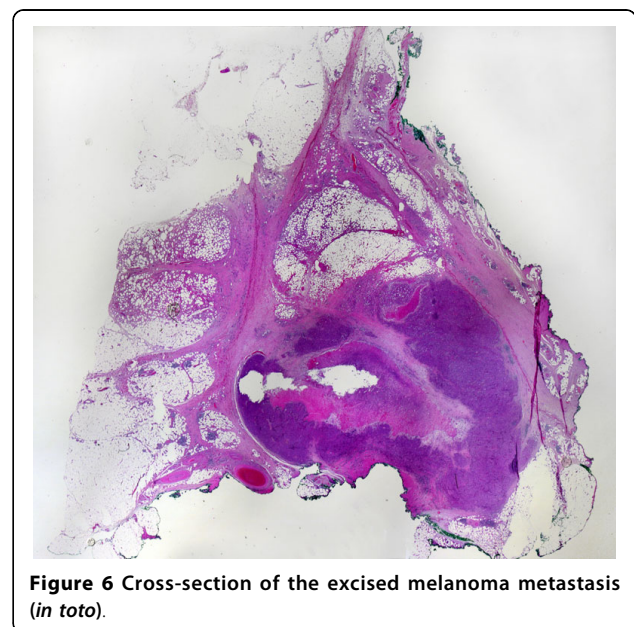
were positioned under ultrasonographic guidance in the four outer corners of the tumor in the fat tissue, the deepest location being minimally inserted into the muscle (Figure 4). Eight pulses of 100 μs each were delivered between each pair of electrodes. In total, 6 times 8 pulses were delivered to the tumor with amplitudes of 2800 V between electrodes (pair 1-2) 25 mm apart, 2500 V between electrodes (1-3, 2-4 and 3-4) 20 mm apart, and 3000 V between diagonal electrodes (1-4 and 2-3) (Figure 5). The currents recorded during electric pulse delivery were between 9 and 19 A.
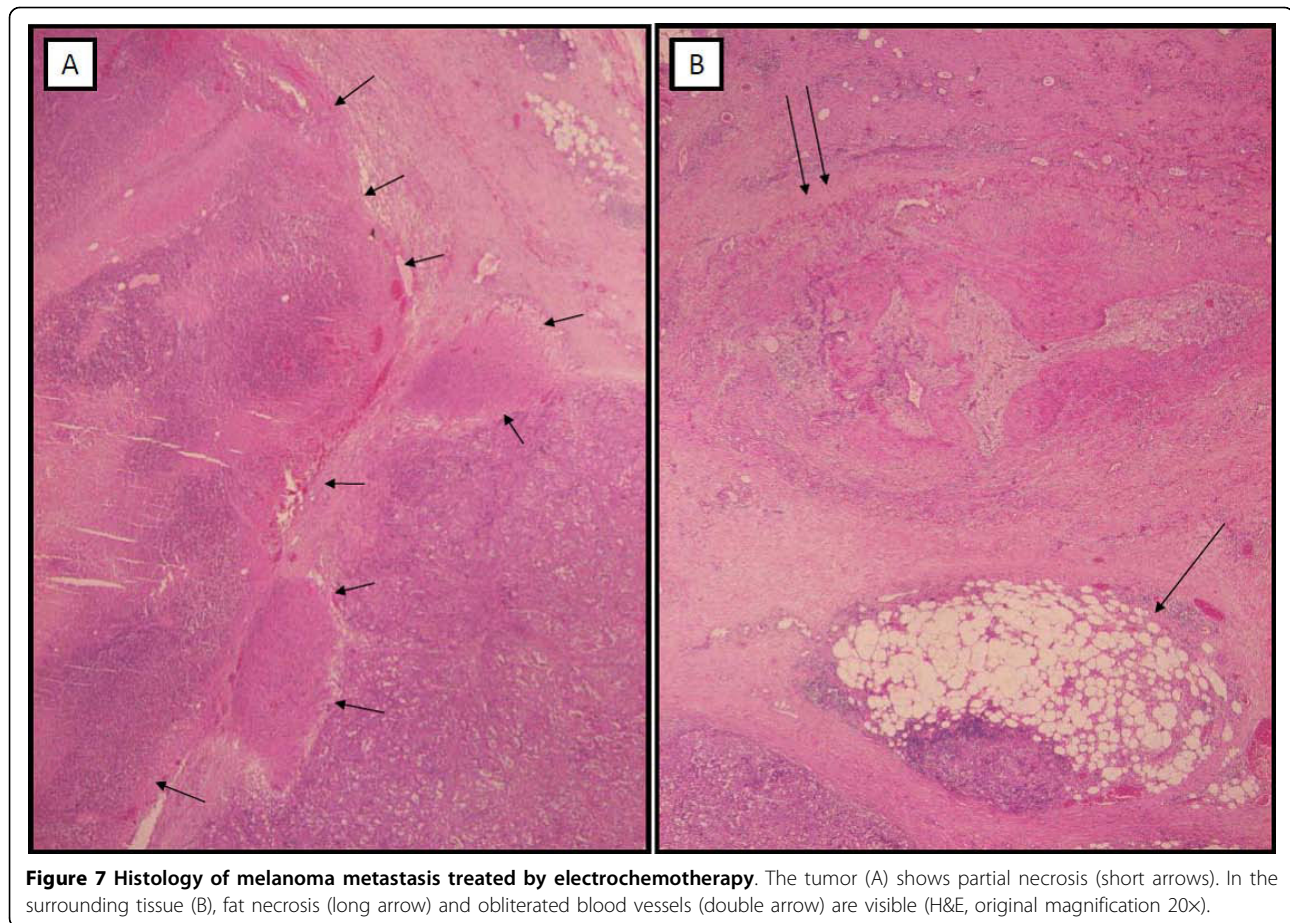
The treatment was performed in general anesthesia and due to the myorelaxant given to the patient, only minor muscle contractions were observed. No other side-effects were noticed. The patient reported no discomfort after the treatment, and left the hospital after 2 days. The response to treatment with electrochemotherapy was followed ultrasonographically at regular time intervals (Figure 1). The first post-operative ultrasound showed a substantial decrease in the tumor volume (more than 50%), while the second showed a regrowth of tumor tissue.

In February 2009, *i.e.* 52 days after electrochemotherapy was performed, the metastasis was excised. It was located 2 cm under the skin in the deep subcutaneous fat tissue, abutting on the muscle fascia. The size of the metastasis measured after excision (22 × 15 mm) was determined on the pathological cross-section (Figure 6).

Histologically, the metastasis showed partial necrosis, estimated to represent 40-50% of the tumor. It was not possible to discriminate between spontaneous and induced necrosis. However, there was indirect evidence of the effect of electrochemotherapy; *i.e.* the presence of fat necrosis and obliterated blood vessels in the tissue around the tumor (Figure 7). These observations would not be expected in a fast-growing, untreated metastasis.

Numerical model validation

After the treatment, the geometry of the numerical model was updated according to measurements taken during the operating procedure and photo documentation of the treatment. Specifically, the four electrode positions in the model were changed according to these

Figure 6 Cross-section of the excised melanoma metastasis (*in toto*).

Figure 7 Histology of melanoma metastasis treated by electrochemotherapy. The tumor (A) shows partial necrosis (short arrows). In the surrounding tissue (B), fat necrosis (long arrow) and obliterated blood vessels (double arrow) are visible (H&E, original magnification 20×).

measurements (Figure 4). We compared the maximum value of the electric current measured by the Cliniporator Vitae during electric pulse delivery with the current predicted by the numerical model. Good agreement was obtained between the measurements and calculations, as presented in Table 1. Finally, tumor coverage with an electric field above the reversible threshold was recalculated using the revised geometry and the volume of the reversibly permeabilized tumor was determined to be approximately 94% (Figure 8).

Table 1 Agreement between maximum measured electrical currents and currents calculated in the numerical model

Electrode pair	Measured current [A]	Calculated current [A]	Error [%]
1-2	16	16.2	1
1-3	18	17.3	-4
1-4	10	9.5	-5
2-3	19	17.2	-9
2-4	9	8.4	-7
3-4	9	8.0	-11

Discussion

We present here the first study of deep-seated tumor electrochemotherapy based on numerical treatment planning. Namely, electrochemotherapy was, until now only used for superficial and accessible tumor nodules, with an approximately 80% objective response rate [1,7,18-22]. In this, the first reported clinical case, a deep-seated melanoma metastasis in the thigh of the patient was treated by insertion of long needle electrodes around the tumor. A new electric pulse generator was used that provides higher voltages and currents and has six independently controlled insulated outputs, which thus allow for treatment of deeper-seated tumors by delivering electric pulses between different pairs of electrodes.

The electric conductivity values taken into account in the numerical model have been obtained from measurements done mostly on large animal tissues, which are not necessarily valid for human tissue as well [13]. Furthermore, these values are not valid for electroporated tissue, as electroporation increases tissue conductivity. In one of our previous studies, we measured the conductivity of rat muscle and liver tissue and the conductivity increased between 3.2-3.8 times for both tissue types [12]. Also,
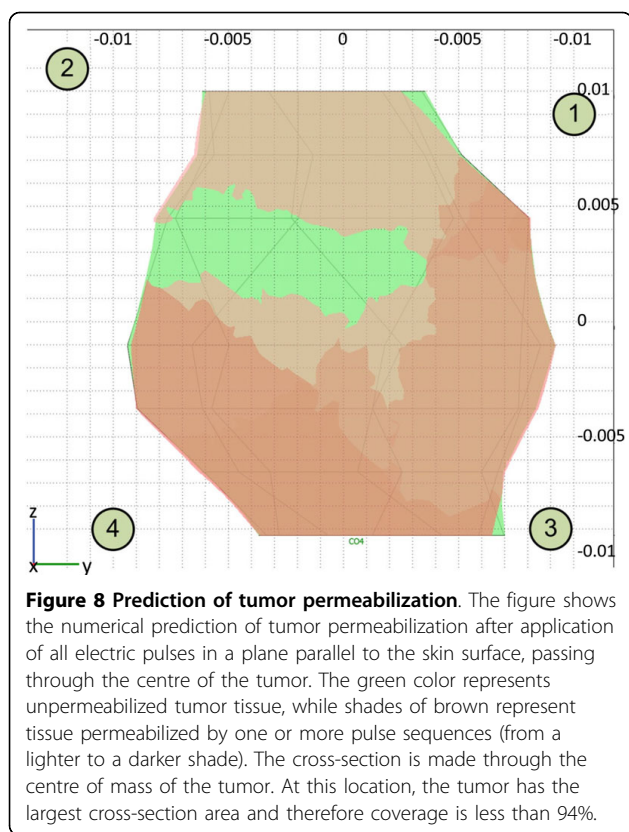
Figure 8 Prediction of tumor permeabilization. The figure shows the numerical prediction of tumor permeabilization after application of all electric pulses in a plane parallel to the skin surface, passing through the centre of the tumor. The green color represents unpermeabilized tumor tissue, while shades of brown represent tissue permeabilized by one or more pulse sequences (from a lighter to a darker shade). The cross-section is made through the centre of mass of the tumor. At this location, the tumor has the largest cross-section area and therefore coverage is less than 94%.

comparing the measured and calculated electric current for rabbit liver resulted in an estimated conductivity increase of 3.6 [11]. In this study, an increase in conductivity of 3.5 as a result of electroporation was used for all tissues, a choice which seems to be at least partly validated by the agreement between the measured and calculated electric current in our study (Table 1).

In our post-treatment model, tissue electroporation thresholds for muscle and tumor were taken from previous studies in which these thresholds were determined by comparing *in vivo* measurements and numerical modeling of electroporation of different tissues [14,23,24]. In all these studies, the assumption was made that the values of the electric field, at which a change in tissue properties occur, coincides with the electroporation thresholds. This assumption was already considered both theoretically and practically in previous studies and can be considered as justified [25-27].

Two different electroporation models were used in our present study; the first which took into account changes in tissue properties and the second which did not, a simplification that made the calculation much faster. Both models predicted similar electroporation volumes (results not shown), while only the first model could predict the electric current density. As such, the second model was used for optimization-based treatment

planning and the first one for validation by comparing the measured and calculated electric currents.

According to the model used after the treatment, inaccuracies in positioning of the electrodes are most likely responsible for the inadequate electroporation of the entire tumor volume, although possible deviation from the assigned electrical conductivities and/or deviations from the assigned electroporation threshold for the tissues cannot be disregarded. Nevertheless, good agreement between the predicted and the measured delivered currents implies that the conductivity values chosen were very close to the real values. Under the assumption that the positioning of the electrodes was responsible for the inadequate tumor electroporation, calculations show that only a small percent of the tumor was not successfully electroporated (app. 6%); however this was enough for the tumor to survive and start growing again. While normally these relatively small errors in electrode positioning (Figure 4) would not lead to an unsuccessful treatment, the proximity of three different tissues with very different conductivities made the treatment very sensitive to electrode positioning. Adipose tissue that surrounded the tumor had by far the lowest conductivity, which meant that according to the voltage divider principle the electric field was largest in the adipose tissue around the tumor and not in the tumor [28].

Conclusions

Electrochemotherapy of a deep-seated tumor was performed in a patient with the aim to verify the treatment approach, and the use of treatment planning in optimizing the positioning of the electrodes and electrical parameters. Although the configuration of five electrodes was recognized as the best in treatment planning, it was not possible to execute it due to "floating" of the tumor in the adipose tissue. The four-electrode position was thus used and at follow-up of the tumor growth, significant tumor reduction was observed (Figure 1). For effective treatment, however, all viable tumor cells have to be destroyed in order to prevent tumor regrowth. Therefore, as calculated in this tumor model, even a small percentage of remaining viable tumor tissue (6%) after electrochemotherapy was enough for tumor regrowth. Nevertheless, this clinical case demonstrates that treatment of deep-seated tumor nodules by electrochemotherapy is feasible and that optimization of the treatment approach by tumor numerical modeling is of significant help.

Author details

[1]University of Ljubljana, Faculty of Electrical Engineering, Trzaska cesta 25, SI-1000 Ljubljana, Slovenia. [2]Institute of Oncology Ljubljana, Zaloska 2, SI-1000 Ljubljana, Slovenia.

Authors' contributions

DM, MS, MC, MK, TP, EG and GS were involved in treatment of the patient. MB performed pathology of the metastasis. DM, AZ and BK carried out medical image segmentation and performed numerical calculations. DM, AZ, BK and GS prepared the manuscript. All authors read and approved the final manuscript.

Competing interests

The authors declare that they have no competing interests.

References

1. Sersa G, Miklavcic D, Cemazar M, Rudolf Z, Pucihar G, Snoj M: Electrochemotherapy in treatment of tumours. *EJSO* 2008, **34**:232-240.
2. Miklavcic D, Corovic S, Pucihar G, Pavselj N: Importance of tumour coverage by sufficiently high local electric field for effective electrochemotherapy. *EJC Suppl* 2006, **4**:45-51.
3. Gothelf A, Mir LM, Gehl J: Electrochemotherapy: results of cancer treatment using enhanced delivery of bleomycin by electroporation. *Cancer Treat Rev* 2003, **29**:371-387.
4. Larkin JO, Collins CG, Aarons S, Tangney M, Whelan M, O'Reily S, Breatnach O, Soden DM, O'Sullivan GC: Electrochemotherapy: aspects of preclinical development and early clinical experience. *Ann Surg* 2007, **245**:469-479.
5. Mir LM, Gehl J, Sersa G, Collins CG, Garbay JR, Billard V, Geertsen PF, Rudolf Z, O'Sullivan GC, Marty M: Standard operating procedures of the electrochemotherapy: Instructions for the use of bleomycin or cisplatin administered either systemically or locally and electric pulses delivered by Cliniporator™ by means of invasive or non-invasive electrodes. *EJC Suppl* 2006, **4**:14-25.
6. Domenge C, Orlowski S, Luboinski B, De Baere T, Belehradek J-Jr, Mir LM: Antitumor electrochemotherapy. New advances in the clinical protocol. *Cancer* 1996, **77**:956-963.
7. Marty M, Sersa G, Garbay JR, Gehl J, Collins CG, Snoj M, Billard V, Geertsen PF, Larkin JO, Miklavcic D, Pavlovic I, Paulin-Kosir SM, Cemazar M, Morsli N, Soden DM, Rudolf Z, Robert C, O'Sullivan GC, Mir LM: Electrochemotherapy - An easy, highly effective and safe treatment of cutaneous and subcutaneous metastases: Results of ESOPE (European Standard Operating Procedures of Electrochemotherapy) study. *EJC Suppl* 2006, **4**:3-13.
8. Snoj M, Rudolf Z, Cemazar M, Jancar B, Sersa G: Successful sphincter-saving treatment of anorectal malignant melanoma with electrochemotherapy, local excision and adjuvant brachytherapy. *Anti-Cancer Drugs* 2005, **16**:345-348.
9. Shimizu T, Nikaido T, Gomyo H, Yoshimura Y, Horiuchi A, Isobe K, Ebara S, Takaoka K: Electrochemotherapy for digital chondrosarcoma. *J Orthop Sci* 2003, **8**:248-51.
10. Sel D, Macek-Lebar A, Miklavcic D: Feasibility of employing model-based optimization of pulse amplitude and electrode distance for effective tumor electropermeabilization. *IEEE T Biomed Eng* 2007, **54**:773-781.
11. Sel D, Cukjati D, Batiuskaite D, Slivnik T, Mir LM, Miklavcic D: Sequential finite element model of tissue electropermeabilization. *IEEE T Biomed Eng* 2005, **52**:816-827.
12. Cukjati D, Batiuskaite D, Andre F, Miklavcic D, Mir LM: Real time electroporation control for accurate and safe in vivo non-viral gene therapy. *Bioelectrochemistry* 2007, **70**:501-507.
13. Gabriel C, Peymann A, Grant EH: Electrical conductivity of tissue at frequencies below 1 MHz. *Phys Med Biol* 2009, **54**:4863-4878.
14. Pavselj N, Bregar Z, Cukjati D, Batiuskaite D, Mir LM, Miklavcic D: The course of tissue permeabilization studied on a mathematical model of a subcutaneous tumor in small animals. *IEEE T Biomed Eng* 2005, **52**:1373-1381.
15. Corovic S, Zupanic A, Miklavcic D: Numerical modeling and optimization of electric field distribution in subcutanoues tumors treated with electrochemotherapy using needle electrodes. *IEEE T Plasm Sci* 2008, **36**:1665-1672.
16. Zupanic A, Corovic S, Miklavcic D: Optimization of electrode position and electric pulse amplitude in electrochemotherapy. *Radiol Oncol* 2008, **42**:93-101.
17. Campana LG, Mocellin S, Basso M, Puccetti O, De Salvo G, Chiarion-Sileni V, Vecchiato A, Corti L, Rossi CR, Nitti D: Bleomycin-based electrochemotherapy: clinical outcome from a single institution's experience with 52 patients. *Ann Surg Oncol* 2008, **16**:191-199.
18. Bertacchini C, Margotti PM, Bergamini E, Ronchetti M, Cadossi R: Irreversible electroporation systems for clinical use. *Irreversible electroporation* Berlin: Springer VerlagRubinsky B 2010, 255-272.
19. Quaglino P, Mortera C, Osella-Abate S, Barberis M, Illengo M, Rissone M, Savoia P, Bernengo MG: Electrochemotherapy with intravenous bleomycin in the local treatment of skin melanoma metastases. *Ann Surg Oncol* 2008, **15**:2215-2222.
20. Heller R, Jaroszeski MJ, Reintgen DS, Puleo CA, DeConti RC, Gilbert RA, Glass LF: Treatment of cutaneous and subcutaneous tumors with electrochemotherapy using intralesional bleomycin. *Cancer* 1998, **83**:148-157.
21. Sersa G, Cufer T, Cemazar M, Rebersek M, Zvonimir R: Electrochemotherapy with bleomycin in the treatment of hypernephroma metastasis: case report and literature review. *Tumori* 2000, **86**:163-165.
22. Sersa G: The state-of-the-art of electrochemotherapy before the ESOPE study: advantages and clinical uses. *EJC Suppl* 2006, **4**:52-59.
23. Semrov D, Miklavcic D: Calculation of the electrical parameters in electrochemotherapy of solid tumours in mice. *Comput Biol Med* 1998, **28**:439-448.
24. Miklavcic D, Semrov D, Mekid H, Mir LM: A validated model of in vivo electric field distribution in tissues for electrochemotherapy and for DNA electrotransfer for gene therapy. *Biochim Biophys Acta* 2000, **1523**:73-83.
25. Pavlin M, Miklavcic D: Effective conductivity of a suspension of permeabilized cells: a theoretical analysis. *Biophys J* 2003, **85**:719-729.
26. Pavlin M, Kanduser M, Rebersek M, Pucihar G, Hart FX, Magjarevic R, Miklavcic D: Effect of cell electroporation on the conductivity of a cell suspension. *Biophys J* 2005, **88**:4378-4390.
27. Ivorra A, Al-Sakere B, Rubinsky B, Mir LM: In vivo electrical conductivity measurements during and after tumor electroporation: conductivity changes reflect treatment outcome. *Phys Med Biol* 2009, **54**:5949-5963.
28. Pavselj N, Miklavcic D: Numerical modeling in electroporation-based biomedical applications. *Radiol Oncol* 2008, **42**:159-168.

V

Kos B, **Zupanic A,** Kotnik T, Snoj M, Sersa G, Miklavcic D. Robustness of treatment planning for electrochemotherapy of deep-seated tumors. Submitted to *J Memb Biol.*

Robustness of Treatment Planning for Electrochemotherapy of Deep-Seated Tumors

Bor Kos[1], Anže Zupanic[1], Tadej Kotnik[1], Marko Snoj[2], Gregor Sersa[2] and Damijan Miklavcic[1]

[1] *Faculty of Electrical Engineering, University of Ljubljana, Trzaska 25, SI-1000 Ljubljana, Slovenia*

[2] *Institute of Oncology, Zaloska 2, SI-1000 Ljubljana, Slovenia*

ABSTRACT

Treatment of cutaneous and subcutaneous tumors with electrochemotherapy has become a regular clinical method, while treatment of deep-seated tumors is still at an early stage of development. We present a method for preparing a dedicated-patient specific, computer optimized treatment plan for electrochemotherapy of deep-seated tumors based on medical images. The treatment plan takes into account the patient's anatomy, tissue conductivity changes during electroporation and the constraints of the pulse generator. An analysis of robustness of a treatment plan made with this method shows that the effectiveness of the treatment is not affected significantly by small single errors in positioning. When many errors occur simultaneously however, the resulting drop in effectiveness is larger, which means that it is necessary to be as accurate as possible in electrode positioning. The largest effect on treatment effectiveness stems from uncertainties in dielectric properties and electroporation thresholds of treated tumors and surrounding tissues, which emphasizes the need for more accurate measurements and more research. The presented methods for treatment planning and robustness analysis allow quantification of the treatment reproducibility and enable the setting of suitable safety margins to improve the likelihood of successful treatment of deep-seated tumors by electrochemotherapy.

INTRODUCTION

Electrochemotherapy (ECT) is a treatment in which a specific chemotherapeutic drug having an intra-cellular target is combined with a strong pulsed electric field that increases the cell membrane

permeability - electroporation (Orlowski et al., 1988; Sersa, Cemazar & Miklavcic, 1995). This increases the amount of molecules that enter cancer cells and have a cytotoxic effect. To achieve a complete response of the treated tumors, the electric field used for electroporation has to exceed a threshold value over the whole tumor volume (Miklavcic et al., 2006a; Sersa et al., 2008). In the last decade ECT has been successfully used for treatment of cutaneous and subcutaneous tumors, mainly melanoma (Campana et al., 2009; Marty et al., 2006). The success of ECT, its clinical applicability and recent development of more powerful electric pulse generators and new electrodes have resulted in the first clinical uses of ECT for treatment of deep-seated tumors (Miklavcic et al., – submitted for publication).

In the ESOPE study a standard operating protocol was developed for ECT of cutaneous and subcutaneous tumors that provides the physicians with a set of appropriate electrodes and electric pulse parameters depending on tumor size and location (Mir et al., 2006). This protocol, however, cannot be used for ECT of deep-seated tumors because of increased treatment complexity. The shape of the tumor can be irregular, tumors can be much bigger, can be surrounded by vital organs, damage to which has to be avoided, and the electric properties of the surrounding tissue as well as of the tumor can vary significantly. Since it is necessary to cover the whole tumor with electric field above the threshold to achieve a desirable effect, the choice of electrode position and voltages applied between the electrodes is different from case to case, which is why an individualized treatment plan, similar to radiotherapy treatment plans, is necessary (Bortfeld, 1999). As the electric field distribution inside the target tissues is one of the most important predictors of electroporation (Miklavcic et al., 1998), the use of numerical models of electroporation have been proposed, in combination with optimization algorithms, as means of ECT treatment planning (Corovic, Zupanic & Miklavcic, 2008; Sel, Lebar & Miklavcic, 2007).

The treatment plan should be robust enough to prevent uncertainties both in the treatment planning stage and in the treatment itself from influencing the treatment outcome. The uncertainties include: 1)

all the input parameters for the numerical model and 2) the difficulty in precisely positioning the electrodes. These uncertainties have to be carefully analyzed and their significance for the success of the treatment evaluated.

In this paper we present a method of creating a dedicated patient-specific treatment plan for deep-seated tumor ECT, its application on a case of melanoma metastasis in the thigh and a qualitative assessment of the treatment plan robustness.

METHODS

Assembling a patient-specific numerical model

The first step in ECT treatment planning is the construction of a sufficiently detailed patient-specific model of the anatomy. Medical images (MRI) of the region of interest were first segmented, and then used to build a 3D geometry by approximating the segmented tissue with a closed spline curve and connecting the curves in the third dimension using Matlab (Mathworks, USA) as described in previously published work (Sel et al., 2007). This geometry was then imported into COMSOL Multiphysics (COMSOL, Sweden), where finite-element analysis was performed.

In the presented case (Miklavcic et al., submitted for publication) the geometry consisted of a melanoma metastasis in the right thigh, two nearby muscles (Sartorius and Gracilis) and surrounding adipose tissue. After the tissue geometry was built, the geometry of the electrodes chosen for the treatment were added (in the presented case, four stainless steel needle electrodes with a 30 millimeter exposed tip and the rest of the length insulated were used) (Figure 1). As the skin is penetrated by the needle electrodes, its high impedance does not affect the calculations; therefore it was not considered in the model along with other tissues located away from the tumor (e.g. Femur and other thigh muscles). At the location of these tissues, the electric field strength is very low and is not significant for the treatment.

In the presented model, tumor, muscle and adipose tissue were modeled; their bulk conductivities were taken from the literature (0.135 S/m, 0.75 S/m, 0.2 S/m and 0.02 S/m, for muscle in the direction perpendicular to muscle fibers, muscle in the direction parallel to muscle fibers, tumor and adipose tissue, respectively) (Gabriel, Lau & Gabriel, 1996; Haemmerich et al., 2009). These values present conductivities at a frequency of 10 Hz or 50 Hz, and have been previously used to accurately predict tissue electroporation and the total current delivered during electric pulses (Pavselj et al., 2005).

The mathematical model of electroporation used in the study is described in more detail in (Sel et al., 2005). In short, the Laplace equation for static electric currents was used to calculate the electric field distribution in the model. A sequential model of electroporation was used that takes into account the conductivity changes during electric pulse delivery due to electroporation (Cukjati et al., 2007; Ivorra et al., 2009). In the model, electroporation-increased tissue conductivities were increased by a factor of 3.5 (Cukjati et al., 2007) and the reversible thresholds for electroporation were considered to be 400 V/cm for tumor tissue, 100 V/cm for adipose tissue, and 200 V/cm and 80 V/cm for muscle tissue in perpendicular direction to muscle fibers and in parallel direction, respectively (Miklavcic et al., 2000) (Corovic et al., submitted for publication).

Treatment planning

The assembled numerical model was used together with a genetic algorithm, as previously described, to provide an optimal treatment plan (Corovic et al., 2008; Zupanic, Corovic & Miklavcic, 2008). When setting up the optimization, constraints had to be taken into account, e.g. feasible positions of the electrodes and specifications of the pulse generator (Cliniporator Vitae[TM]; IGEA, Carpi, Italy). The position constraints were that the electrodes are not to be put inside the tumor and not farther than 1 cm outside the tumor, while the pulse generator constraints were the maximum available voltage (3000 V), and current (50 A). In addition, only two electrodes at a time can have a set potential during electric pulse delivery. In the presented case the algorithm searched for the optimal

positions of each of the four electrodes and the optimal voltage between each pair of electrodes. Optimization algorithm was set to maximize the volume of the tumor covered with electric fields over the reversible electroporation threshold and reduce the volume of nearby healthy tissue covered with fields over the irreversible electroporation threshold (Davalos, Mir & Rubinsky, 2005; Rubinsky, Onik & Mikus, 2007). Since the tumor coverage is essential for successful treatment, tumor coverage was given 10 times more weight than damage to healthy tissue. The final number of parameters optimized for the treatment was fifteen: depth of insertion of all electrodes, y and z position of each electrode and voltage between each pair of electrodes.

Robustness analysis

To verify the robustness of the presented treatment plan, we used the same numerical model as in the treatment planning and calculated the volume of tumor covered with an electric field over the reversible electroporation threshold, while varying a single model parameter at a time. In this parameterization study the parameters analyzed were the model inputs that were taken from the literature, such as electrical conductivity values and reversible electroporation thresholds for each tissue as well as the treatment planning parameters acquired from the optimization (electrode positions and voltages).

Every parameter was varied in five steps from the optimal position, and percentage of tumor volume coverage was determined each time. Electrode positions perpendicular to the axis of insertion were varied in 0.5 mm steps away from the tumor in two perpendicular directions (y,z); depth of electrode insertion was varied in 1 mm steps in both directions (deeper and shallower penetration than optimal); voltages were varied in steps of 100 V below the optimal values; electrical conductivities were varied in steps of 10 % of the values used in the model in both directions (higher and lower values than those used in the model); and electroporation thresholds were varied in steps of 50 V/cm above the values used in the model. This approach highlights the most critical parameters for the

success of ECT treatment and can also serve in determining the safety factors needed for treatment and predicting the treatment outcome.

RESULTS AND DISCUSSION

We applied the described methods to build a three-dimensional patient-specific model, optimize the positioning of four electrodes outside the tumor and necessary minimum voltage to apply between each electrode pair. Current drawn from all electrode pairs was calculated and we established that it was below the maximum 50 A current limit of the Cliniporator Vitae™ electroporation pulse generator. The optimized treatment plan was successful in covering the whole tumor volume with an electric field of no less than 400 V/cm, the tumor electroporation threshold value; the details of the treatment plan are presented in Figures 1 and 2 and Table 1. Figure 2 shows tumor coverage after each pulse application; it can be seen that the whole tumor is covered after the application of pulses to all six electrode pairs. It would be possible to cover the whole tumor with just two electrodes, however the required voltage would be much higher, and the amount of healthy tissue damage would increase significantly as well. An additional benefit of using multiple electrodes is that many parts of the tumor are covered more than once, and with different directions of the electric field, which has been shown to increase electroporation efficiency and molecular uptake (Rebersek et al., 2007). All this should increase the robustness of the treatment.
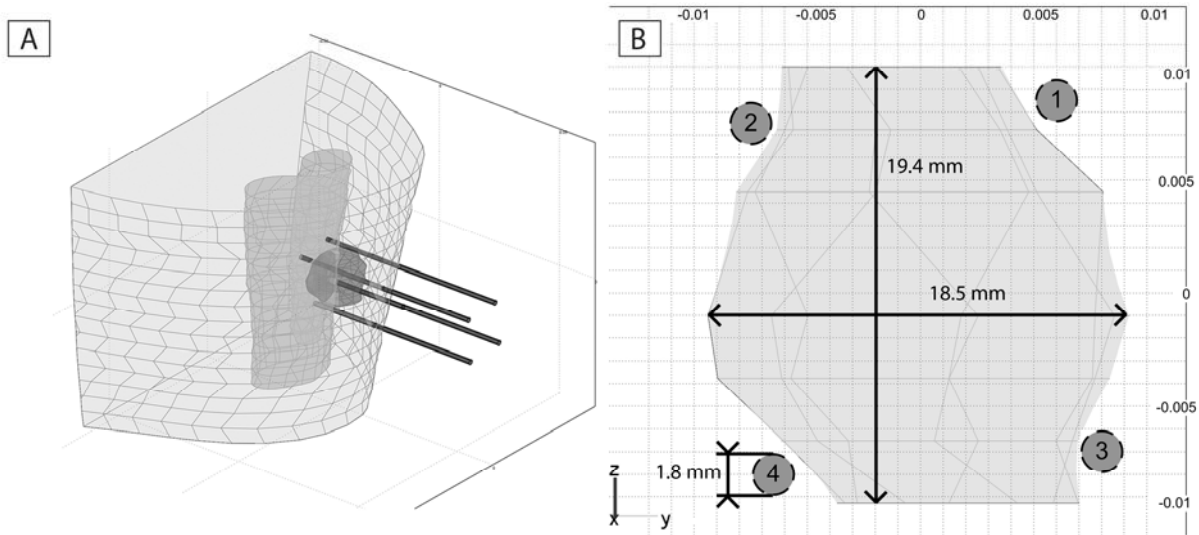
Figure 1: A: Model geometry. Four electrodes are inserted into the thigh (light grey) around the tumor (dark grey) according to the treatment plan. Also shown are two adjoining muscles that the electrodes penetrate by a few millimeters. B: Electrode positions in the cross-section perpendicular to the electrodes' axis, through the centre of mass of the tumor.
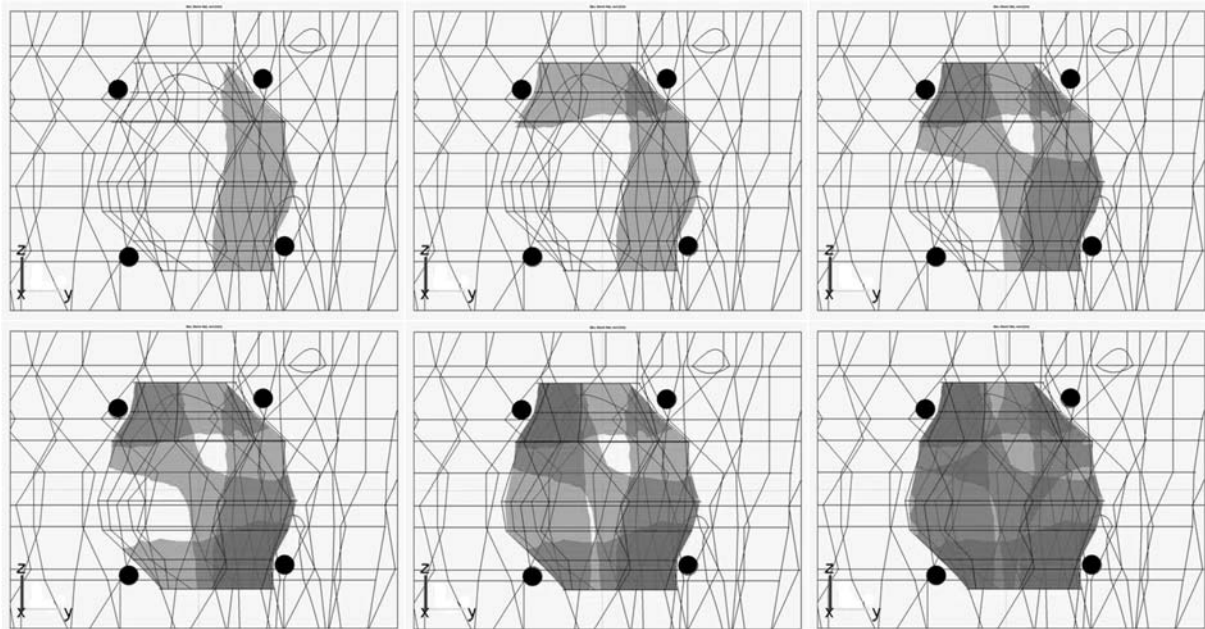
Figure 2: Tumor electroporation after application of each pulse in the sequence. Grey areas show where the electric field exceeded the threshold value

Electrode pair	Voltage
1-2	1100 V
1-3	1600 V
2-4	1600 V
3-4	1100 V
1-4	1800 V
2-3	1900 V

Table 1: Optimized electrode voltages for all electrode pairs. Electrode numbering is the same as in Figure 1B.

Figure 3: Robustness analysis - dependence of tumor coverage with an electric field over the electroporation threshold on different parameters. Effect of reducing voltage on a single electrode pair in steps of 100 V.
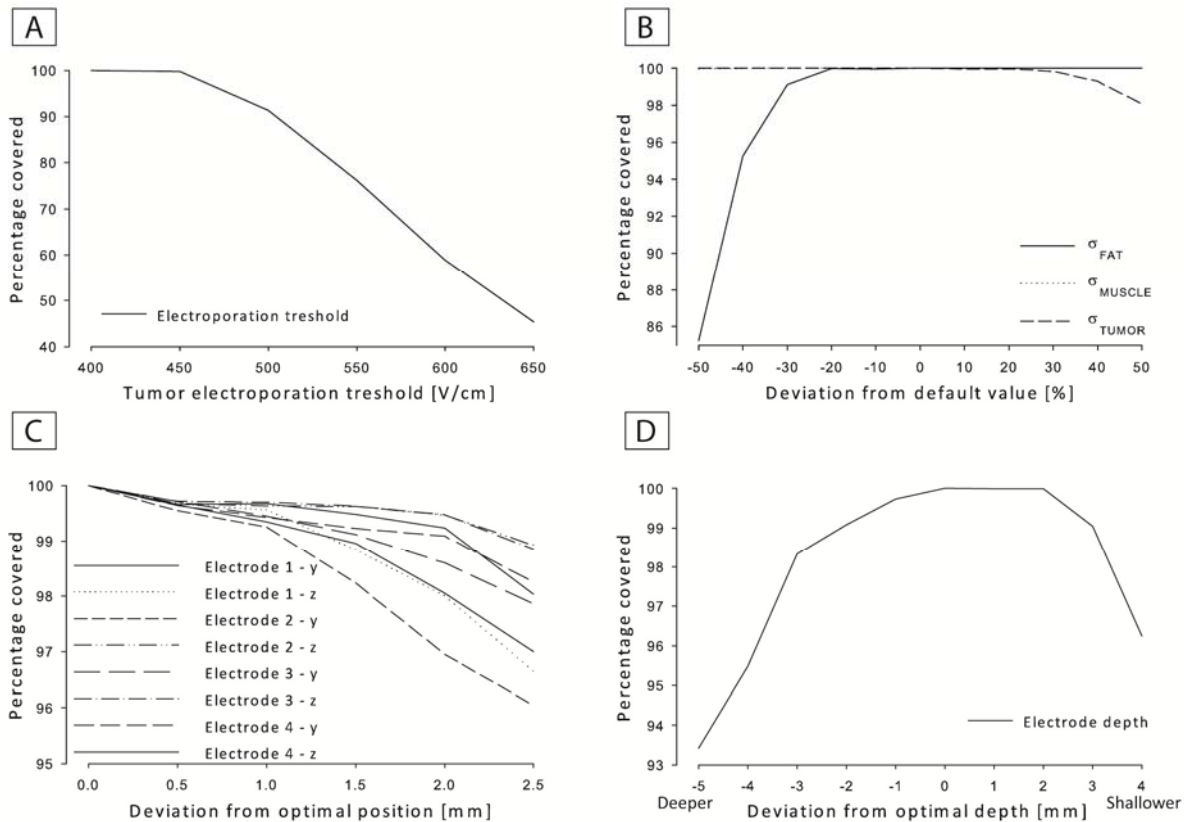
Figure 4: Robustness analysis - dependence of tumor coverage with an electric field over the electroporation threshold on different parameters. A: effect of deviations of tumor electroporation threshold in steps of 50 V/cm. 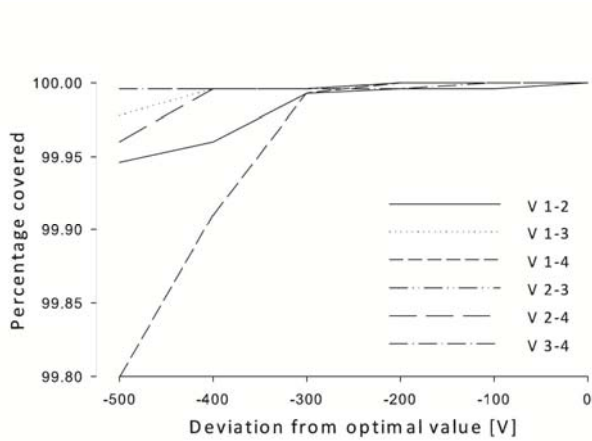B: effect of deviations of tissue conductivities from values used in treatment planning in steps of 10 % of the values used. C: effect of errors in electrode positions along a single axis in steps of 0.5 mm away from tumor surface, D: dependence on depth of insertion of all electrodes. Note that all plots do not share the same vertical scale.

In Figures 3 and 4 we show the results of the robustness analysis. Lowering the voltage on one electrode pair by 300 V does not affect the tumor coverage at all (Figure 3), while decreasing the voltage by 500 V causes a small volume (ranging from 0.05 to 0.2%) to be below the threshold. This can be explained by the fact that most of the tumor volume is covered by more than a single a pair of electrodes (Figure 2). Therefore, a drop in effectiveness of one electrode pair does not affect the end

result as dramatically as might be expected. The results also suggest that 100 V is an appropriate step in voltage optimization of ECT.

The highest drop in tumor coverage was observed when increasing the tumor electroporation threshold (Figure 4 A) - increasing the threshold to 650 V/cm reduces tumor coverage to just above 45 %. The electroporation threhsold is a critical parameter in many aspects. First, the thresholds are different for different tissues and this fact is mostly attributed to differences in cell shapes and sizes between the tissues (Cemazar et al., 1998). Threshold measurements have so far been scarce (Miklavcic et al., 2000)and are further complicated by the fact that many tissues, among them larger tumors, are inherently heterogeneous and therefore probably exhibit a range of thresholds instead of just one. Furthermore, it is hard to cover a large volume of tissue with very high electric fields as the voltages and currents required would be higher than available from commercial pulse generators. All this calls for more research into the tissue electroporation thresholds to improve the efficiency of ECT.

Deviations in tissue conductivity also affected the tumor coverage (Figure 4B). More precisely, it is the ratio of conductivities between the tumor and surrounding (in this case adipose) tissue, which is the (most) critical factor. When the conductivity of adipose tissue is lowered, or alternatively, the conductivity of the tumor is increased, the ratio of $\sigma_{TUMOR}/ \sigma_{FAT}$ is increased and the treatment effectiveness is reduced significantly. If this ratio is changed from 10 as in the original treatment plan to 20, tumor coverage is reduced to 85%. While this is not a parameter that can be controlled by the optimization or performing physician, it is necessary to note that data regarding low frequency conductivities of human healthy and cancerous tissues are scarce, difficult to measure, and the values published by different authors/studies vary significantly (Gabriel, Peyman & Grant, 2009; Miklavcic, Pavselj & Hart, 2006b).

Electrode positions are also a critical parameter (Figure 4C, D), since electrode insertion is the part of the procedure that is most prone to errors. Mispositioning a single electrode by 2 mm can already reduce tumor coverage from 100 % to less than 97 %. However, if all electrodes miss their target, the results are much more severely affected. When all electrodes are moved away from the tumor in a diagonal direction by 0.7 or 1.4 mm (effectively increasing the distance between the electrodes and the distance between the electrodes and the tumor), the tumor coverage decreases to 87 or 66 %, respectively. The depth of insertion is also important, although we assumed at this point that all electrodes were placed at the same depth. Since the needle electrodes used in this case have a 3 cm non-insulated tip (comparable in size to the tumor) that delivers the pulses, and the rest of the electrode length is insulated, inserting them either too deep or too shallow can cause significant reduction in tumor coverage, e.g. 6 % when electrodes are inserted 5 mm too deep (Figure 4D). These results seem to be in contradiction with previous research (Corovic et al., 2008) that suggested that deeper insertion can be considered as being on the safe side. The difference is due to a small size of tumors (compared to non-insulated electrode length) that were used in the calculations of Corovic et al. Current results suggest it is necessary to be as accurate as reasonably possible in the operative theatre, including use of medical imaging for positioning electrodes.

A certain number of errors is likely to be made during the treatment, due to reasons already mentioned previously. To ensure that the treatment outcome is not affected by these errors, a suitable safety margin should be employed during the treatment planning stage. The robustness analysis suggests that setting conservative values for dielectric properties (higher $\sigma_{TUMOR}/ \sigma_{FAT}$) and higher electroporation thresholds can increase the robustness of the treatment, but care must be taken to avoid excessive electric fields that would cause extensive tissue damage.

Our results show that the presented method for treatment planning is capable of producing efficient and robust treatment plans in the clinical setting. The robustness analysis indicates that further work is

necessary in determining tissue electroporation thresholds and conductivity values, as well as in enabling accurate electrode positioning during ECT, since these two parameters affect the treatment outcome to the highest degree. The presented work sets the ground for numerical treatment planning-based electrochemotherapy of deep-seated solid tumors, quantifying its reproducibility and enabling the setting of suitable safety margins to improve the likelihood of successful treatment.

References

Bortfeld, T. 1999. Optimized planning using physical objectives and constraints. *Seminars in Radiation Oncology* 9:20-+

Campana, L.G., Mocellin, S., Basso, M., Puccetti, O., De Salvo, G.L., Chiarion-Sileni, V., Vecchiato, A., Corti, L., Rossi, C.R., Nitti, D. 2009. Bleomycin-Based Electrochemotherapy: Clinical Outcome from a Single Institution's Experience with 52 Patients. *Annals of Surgical Oncology* 16:191-199

Cemazar, M., Jarm, T., Miklavcic, D., Lebar, A.M., Ihan, A., Kopitar, N.A., Sersa, G. 1998. Effect of electric-field intensity on electropermeabilization and electrosensitivity of various tumor-cell lines in vitro. *Electro- and Magnetobiology* 17:263-272

Corovic, S., Zupanic, A., Miklavcic, D. 2008. Numerical modeling and optimization of electric field distribution in subcutaneous tumor treated with electrochemotherapy using needle electrodes. *Ieee Transactions on Plasma Science* 36:1665-1672

Cukjati, D., Batiuskaite, D., Andre, F., Miklavcic, D., Mir, L.M. 2007. Real time electroporation control for accurate and safe in vivo non-viral gene therapy. *Bioelectrochemistry* 70:501-507

Davalos, R.V., Mir, L.M., Rubinsky, B. 2005. Tissue ablation with irreversible electroporation. *Annals of Biomedical Engineering* 33:223-231

Gabriel, C., Peyman, A., Grant, E.H. 2009. Electrical conductivity of tissue at frequencies below 1 MHz. *Physics in Medicine and Biology* 54:4863-4878

Gabriel, S., Lau, R.W., Gabriel, C. 1996. The dielectric properties of biological tissues .2. Measurements in the frequency range 10 Hz to 20 GHz. *Physics in Medicine and Biology* 41:2251-2269

Haemmerich, D., Schutt, D.J., Wright, A.W., Webster, J.G., Mahvi, D.M. 2009. Electrical conductivity measurement of excised human metastatic liver tumours before and after thermal ablation. *Physiological Measurement* 30:459-466

Ivorra, A., Al-Sakere, B., Rubinsky, B., Mir, L.M. 2009. In vivo electrical conductivity measurements during and after tumor electroporation: conductivity changes reflect the treatment outcome. *Physics in Medicine and Biology* 54:5949-5963

Marty, M., Sersa, G., Garbay, J.R., Gehl, J., Collins, C.G., Snoj, M., Billard, V., Geertsen, P.F., Larkin, J.O., Miklavcic, D., Pavlovic, I., Paulin-Kosir, S.M., Cemazar, M., Morsli, N., Rudolf, Z., Robert, C., O'Sullivan, G.C., Mir, L.M. 2006. Electrochemotherapy - An easy, highly effective and safe treatment of cutaneous and subcutaneous metastases: Results of ESOPE (European Standard Operating Procedures of Electrochemotherapy) study. *Ejc Supplements* 4:3-13

Miklavcic, D., Beravs, K., Semrov, D., Cemazar, M., Demsar, F., Sersa, G. 1998. The importance of electric field distribution for effective in vivo electroporation of tissues. *Biophysical Journal* 74:2152-2158

Miklavcic, D., Corovic, S., Pucihar, G., Pavselj, N. 2006a. Importance of tumour coverage by sufficiently high local electric field for effective electrochemotherapy. *Ejc Supplements* 4:45-51

Miklavcic, D., Pavselj, N., Hart, F.X. 2006b. Electric properties of tissues. *In:* Wiley Encyclopedia of Biomedical Engineering. John Wiley & Sons, New York

Miklavcic, D., Semrov, D., Mekid, H., Mir, L.M. 2000. A validated model of in vivo electric field distribution in tissues for electrochemotherapy and for DNA electrotransfer for gene therapy. *Biochimica Et Biophysica Acta-General Subjects* 1523:73-83

Mir, L.M., Gehl, J., Sersa, G., Collins, C.G., Garbay, J.R., Billard, V., Geertsen, P.F., Rudolf, Z., O'Sullivan, G.C., Marty, M. 2006. Standard operating procedures of the electrochemotherapy: Instructions for the use of bleomycin or cisplatin administered either systemically or locally and electric pulses delivered by the Cliniporator (TM) by means of invasive or non-invasive electrodes. *Ejc Supplements* 4:14-25

Orlowski, S., Belehradek, J., Paoletti, C., Mir, L.M. 1988. Transient electropermeabilization of cells in culture - increase of the cyto-toxicity of anticancer drugs. *Biochemical Pharmacology* 37:4727-4733

Pavselj, N., Bregar, Z., Cukjati, D., Batiuskaite, D., Mir, L.M., Miklavcic, D. 2005. The course of tissue permeabilization studied on a mathematical model of a subcutaneous tumor in small animals. *Ieee Transactions on Biomedical Engineering* 52:1373-1381

Rebersek, M., Faurie, C., Kanduser, M., Xorovic, S., Teissie, J., Rols, M.P., Miklavcic, D. 2007. Electroporator with automatic change of electric field direction improves gene electrotransfer in-vitro. *Biomedical Engineering Online* 6

Rubinsky, B., Onik, G., Mikus, P. 2007. Irreversible electroporation: A new ablation modality - Clinical implications. *Technology in Cancer Research & Treatment* 6:37-48

Sel, D., Cukjati, D., Batiuskaite, D., Slivnik, T., Mir, L.M., Miklavcic, D. 2005. Sequential finite element model of tissue electropermeabilization. *Ieee Transactions on Biomedical Engineering* **52:816-827**

Sel, D., Lebar, A.M., Miklavcic, D. 2007. Feasibility of employing model-based optimization of pulse amplitude and electrode distance for effective tumor electropermeabilization. *Ieee Transactions on Biomedical Engineering* **54:773-781**

Sersa, G., Cemazar, M., Miklavcic, D. 1995. Antitumor effectiveness of electrochemotehrapy with cis-diamminedichloroplatinum(II) in mice. *Cancer Research* **55:3450-3455**

Sersa, G., Miklavcic, D., Cemazar, M., Rudolf, Z., Pucihar, G., Snoj, M. 2008. Electrochemotherapy in treatment of tumours. *Ejso* **34:232-240**

Zupanic, A., Corovic, S., Miklavcic, D. 2008. Optimization of electrode position and electric pulse amplitude in electrochemotherapy. *Radiology and Oncology* **42:93-101**

VI

Pavselj N, **Zupanic A,** Miklavcic D. Modeling electric field distribution in vivo. In Pakhomov AG, Miklavcic D, Markov MS (eds.) Advanced electroporation techniques in biology and medicine, CRC Press, New York, 2010. In press.

15

Modeling Electric Field Distribution In Vivo

Nataša Pavšelj
University of Ljubljana

Anže Županič
University of Ljubljana

Damijan Miklavčič
University of Ljubljana

15.1 Introduction

The application of electric pulses to cells, either in suspension or tissue, causes the electroporation of the cell membrane, increasing its permeability and making it possible for larger molecules that otherwise cannot cross the membrane, such as drug molecules or DNA, to enter the cell. If the pulse is of adequate amplitude, the electric field and consequently the induced transmembrane voltage are high enough to cause cell membrane permeabilization. For any given cell, the induced transmembrane voltage is proportional to the electric field; more precisely, it is proportional to the local electric field in which the cell is placed. More details on induced transmembrane voltage and electroporation on the cell level are given in Chapter 3, titled "Induced transmembrane voltage—Theory, modeling, and experiments" by Kotnik and Pucihar. In this chapter, the focus is on the electroporation on a tissue level, more specifically on how the electric field is distributed in different electrode-tissue setups in the applied use of electroporation.

Numerous experiments, both in vitro and in vivo, have to be performed before a biomedical application is put to practical use in the clinical environment. As a complementary work to in vivo experimenting, analytical and numerical models can be used to represent, as realistically as possible, real biological phenomena. In this way, we can better understand some of the processes involved and analyze and explain the experimental results. Different electrical parameters can be evaluated in advance, such as pulse amplitude, duration, and number of pulses. All of that can help us plan new protocols, design electroporation devices, facilitate the design of electrodes and their placement with respect to target tissue, and plan new experiments and treatments (Šemrov and Miklavčič 1998, Brandisky and Daskalov 1999,

Miklavčič et al. 2000, Dev et al. 2003, Miklavčič et al. 2006a, Šel et al. 2007, Čorović et al. 2008b, Županič et al. 2008). Of course, models have to be validated by experiments and, if necessary, improved. Experimenting with such models is easier and sometimes the only possible or ethically acceptable alternative to experimenting on real biological systems. Both experimental work and numerical modeling combined give us valuable information and help us to understand the underlying mechanisms of the process(es) we are aiming to describe.

As a simple definition, a mathematical model is a representation of the chosen essential aspects of a real system (may it be a living, engineering, or social system), described by a set of variables and a set of equations that establish relationships between the variables. Mathematical models represent an important tool in the study of the effects of the electromagnetic fields and accompanying coupled phenomena on cells, tissues, and organs (Fear and Stuchly 1998, Debruin and Krassowska 1999a,b, Miklavčič et al. 2000, Šel et al. 2005, Pavšelj and Miklavčič 2008a). These biological systems are often geometrically highly intricate, so analytical methods are, in most cases, entirely replaced by numerical methods. In continuation, we provide the basics of electromagnetic field theory, describe the characteristics of biological tissues, explain the basic steps in constructing numerical models of tissue electroporation, and give some reference to numerical modeling–based treatment planning.

15.2 Electromagnetic Field Theory

15.2.1 Maxwell's Equations

In 1865, Maxwell had put forward a set of equations that describe the properties of the macroscopic electric and magnetic fields and relate them to their sources: Ampere's law (Equation 15.1), Faraday's law of induction (Equation 15.2), Gauss's laws (Equation 15.3), Gauss's law for magnetism (Equation 15.4), and the continuity equation (Equation 15.5)

$$\nabla \times \vec{B} = \mu_0 \vec{J} + \mu_0 \varepsilon_0 \frac{\partial \vec{E}}{\partial t} \tag{15.1}$$

$$\nabla \times \vec{E} = -\frac{\partial \vec{B}}{\partial t} \tag{15.2}$$

$$\nabla \cdot \vec{E} = \frac{\rho}{\varepsilon_0} \tag{15.3}$$

$$\nabla \cdot \vec{B} = 0 \tag{15.4}$$

$$\nabla \cdot \vec{J} = -\frac{\partial \rho}{\partial t} \tag{15.5}$$

where
  B is the magnetic flux density
  J is the total current density
  E is the electric field
  ρ is the electric charge
  μ_0 is the permeability of free space
  ε_0 is the permittivity of free space

When complemented by the constitutive relations pertaining to the media under consideration and by their relevant boundary conditions, these equations are suitable for initiating the numerical or analytical

solution of a given problem. Today, numerical calculations of the distribution of macroscopic electric and magnetic fields are usually performed using different sets of equations (Equations 15.6 and 15.7), usually derived from Maxwell's equations and the definitions of the electric potential *V* (Equation 15.8) and the magnetic vector potential *A* (Equation 15.9):

$$\nabla^2 V + \frac{\partial}{\partial t}\left(\nabla \cdot \vec{A}\right) = -\frac{\rho}{\varepsilon_0} \tag{15.6}$$

$$\left(\nabla^2 \vec{A} - \frac{1}{c^2}\frac{\partial^2 \vec{A}}{\partial t^2}\right) - \nabla\left(\nabla \cdot \vec{A} + \frac{1}{c^2}\frac{\partial V}{\partial t}\right) = -\mu_0 \vec{J} \tag{15.7}$$

$$\vec{E} = -\nabla V - \frac{\partial \vec{A}}{\partial t} \tag{15.8}$$

$$\vec{B} = \nabla \times \vec{A} \tag{15.9}$$

By working with potentials instead of fields, the number of degrees of freedom of the calculations is reduced, as *V* and *A* only have four components to be solved for instead of six for *E* and *B*.

15.2.2 Constitutive Relations

When electromagnetic fields are applied to matter, the polarization and magnetization of bound charges and currents take place. By considering the constitutive relations for dielectric and magnetic materials (Equations 15.10 and 15.11)

$$\vec{D} = \varepsilon \vec{E} \tag{15.10}$$

$$\vec{B} = \propto \vec{H} \tag{15.11}$$

where
  D is the electric flux density
  H is the magnetic field intensity
  ε is the permittivity
  μ is the permeability,

A new set of Maxwell's equation is derived (Equations 15.12 through 15.15)

$$\nabla \times \left(\frac{\vec{B}}{\mu}\right) = \vec{J}_f + \varepsilon \frac{\partial \vec{E}}{\partial t} \tag{15.12}$$

$$\nabla \times \vec{E} = -\frac{\partial \vec{B}}{\partial t} \tag{15.13}$$

$$\nabla \cdot \left(\varepsilon \vec{E}\right) = \rho_f \tag{15.14}$$

$$\nabla \cdot \vec{B} = 0 \tag{15.15}$$

where
  J_f is the free current
  ρ_f is the free charge

It is worth noting that neither ε nor μ are necessarily constants, rather they are functions that can depend on position, field strength, field direction, or frequency. The same is true for the electrical conductivity that describes the relation between electric fields and electric currents in matter—Ohm's law (Equation 15.16). We focus on the physical properties of biological materials relevant to electroporation in Section 15.3 of this chapter.

$$\vec{J} = \sigma \vec{E} \tag{15.16}$$

15.2.3 Boundary Conditions

Since calculation of electromagnetic fields is usually limited to a finite region of space and time, it is necessary to use boundary and initial conditions. In modeling electric fields in biological tissues, the fields are introduced into the region of interest via Dirichlet (Equation 15.17) and Neumann (Equation 15.18) boundary conditions:

$$V = V_0 \tag{15.17}$$

$$\frac{\partial V}{\partial n} = q_0 \tag{15.18}$$

While the Dirichlet boundary condition specifies the value that the solution (in our case electric potential) takes on the boundary, the Neumann boundary condition specifies the value of the derivative of the solution on the boundary.

15.2.4 Electric Field Calculations for Electroporation

According to the theory of electroporation (see Chapter 3 by Kotnik and Pucihar in this book), when a cell is exposed to an external electric field, a transmembrane potential proportional to the field is induced on the cell plasma membrane. Since the magnitude of the induced transmembrane potential is related to the level of membrane permeabilization, bulk electroporation can be related to the local electric field distribution.

Most often, the electric fields used for electroporation are delivered in the form of unipolar rectangular electric pulses. These pulses are much longer than the membrane charging time; therefore, the induced transmembrane voltage reaches its final value long before the end of the pulse. This means that the electric field distribution can be modeled in its steady-state, disregarding the transients that occur during the pulse rise time. In practice, this means that equations used to calculate the local electric field distribution in electroporation modeling become much simpler. Note that the equations are still nonlinear, the nonlinearity being hidden in the material properties. The equations are reduced to the Laplace steady-state equation (Equation 15.19), which can be derived from Equations 15.5, 15.8, and 15.16 by taking into account that all time derivatives are equal to zero.

$$\nabla \cdot (\sigma \nabla V) = 0 \tag{15.19}$$

15.3 Biological Tissues

Biological tissues perform different physiological functions, which are reflected in a number of specific characteristics that have to be considered when representing them in a model at both the cellular and higher organizational level. These differences are also clearly reflected in highly different bulk properties of biological materials (Gabriel et al. 1996a,b, Miklavčič et al. 2006b). They define the current densities

and pathways that result from an applied electric stimulus and are thus very important in the analysis of a wide range of biomedical applications used for diagnosis and treatment. Biological tissues are, in general, inhomogeneous and nonlinear.

15.3.1 Biological Tissues in Electric Field

The electrical properties of any material, including biological tissue, can be broadly separated into two categories: conducting and insulating. In a conductor, the electric charges move freely in response to the applied electric field whereas in an insulator (dielectric) the charges are fixed and are not free to move. A more detailed discussion of the fundamental processes underlying the electrical properties of tissue can be found in Foster and Schwan (1989).

If a conductor is placed in an electric field, charges will move within the conductor until the interior field is zero. In the case of an insulator, there are no free charges; therefore, the net migration of charge does not occur. In polar materials, however, the positive and negative charge centers in the molecules do not coincide, which causes an electric dipole moment, p. An applied field, E_0, tends to orient the dipoles and produces a field inside the dielectric, E_p, which opposes the applied field. This process is called polarization. Most materials contain a combination of orientable dipoles and relatively free charges so that the electric field is reduced in any material. The net field inside the material, E, is then

$$\vec{E} = \vec{E}_0 - \vec{E}_p \tag{15.20}$$

The net field is lowered by a significant amount relative to the applied field if the material is an insulator and is essentially zero for a good conductor. This reduction is characterized by a factor ε_r, which is called the relative permittivity or dielectric constant, according to

$$\vec{E} = \frac{\vec{E}_0}{\varepsilon_r} \tag{15.21}$$

In practice, most materials, including biological tissue, actually display some characteristics of both insulators and conductors because they contain dipoles as well as free charges that can move, but in a restricted manner. For materials that are heterogeneous in structure, charges may become trapped at interfaces. Because positive and negative ions move in opposite directions in the applied field, internal charge separations can then result within the material, producing an effective internal polarization that acts like a very large dipole.

On the macroscopic level, we describe the material as having a permittivity, ε, and a conductivity, σ. The permittivity characterizes the material's ability to trap or store charge or to rotate molecular dipoles whereas the conductivity describes its ability to transport charge (Grimnes and Martinsen 2000):

$$\varepsilon = \varepsilon_r \varepsilon_0 \tag{15.22}$$

Consider a sample of material that has a thickness, d, and cross-sectional area, A. If the material is an insulator, then we treat the sample as a capacitor with a capacitance of

$$C = \varepsilon \cdot \frac{A}{d} \tag{15.23}$$

If it is a conductor, then we treat it as a conductor with a conductance of

$$G = \sigma \cdot \frac{A}{d} \tag{15.24}$$

If a constant (direct current, DC) voltage V is applied across this parallel combination, then a conduction current $I_C = GV$ will flow and an amount of charge $Q = CV$ will be stored.

Suppose, instead, we apply an alternating (alternating current, AC) voltage:

$$V(t) = V_0 \cos(\omega t) \tag{15.25}$$

where

    V_0 is the amplitude of the voltage

    $\omega = 2\pi f$, where f is the frequency of the applied signal

The charge on the capacitor plates is now changing with frequency f. This change is associated with a flow of charge or current in the circuit. We characterize this flow as a displacement current:

$$I_d = \frac{dQ}{dt} = -\omega C V_0 \sin(\omega t) \tag{15.26}$$

The total current flowing through the material is the sum of the conduction and displacement currents that are separated in phase by 90°. This phase difference can be expressed as

$$V(t) = V_0 e^{i\omega t} \quad \text{where } i = \sqrt{(-1)} \tag{15.27}$$

taking its real part for physical significance. The total current is $I = I_c + I_d$ (I_c being the conductive and I_d being the displacement current), hence

$$I = GV + C \cdot \frac{dV}{dt} = (\sigma + i\omega\varepsilon)A \cdot \frac{V}{d} \tag{15.28}$$

The actual material, then, can be characterized as having an admittance, $Y^\star$, given by

$$Y^\star = G + i\omega C = \left(\frac{A}{d}\right)(\sigma + i\omega\varepsilon) \tag{15.29}$$

where * indicates a complex-valued quantity. In terms of material properties, we define a corresponding, complex-valued conductivity or admittivity as

$$\sigma^\star = (\sigma + i\omega\varepsilon) \tag{15.30}$$

Describing a material in terms of its admittance emphasizes its ability to transport current. Alternatively, we could emphasize its ability to restrict the flow of current by considering its impedance $Z^\star = 1/Y^\star$, or for a pure conductance, its resistance, $R = 1/G$.

    Factoring $i\omega\varepsilon_0$ in Equation 15.28 yields

$$I = \left(\varepsilon_r - \frac{i\sigma}{\omega\varepsilon_0}\right)i\omega\varepsilon_0 A \cdot \frac{V}{d} = C\frac{dV}{dt} \tag{15.31}$$

We can define a complex-valued relative permittivity as

$$\varepsilon^\star = \varepsilon_r - \frac{i\sigma}{\omega\varepsilon_0} = \varepsilon_r' - i\varepsilon_r'' \tag{15.32}$$

with

    $\varepsilon_r' = \varepsilon_r$

    $\varepsilon'' = \sigma/(\omega\varepsilon_0)$

The complex conductivity and complex permittivity are related by

$$\sigma^* = i\omega\varepsilon^* = i\omega\varepsilon_0\varepsilon_r^* \tag{15.33}$$

In physical terms, we can consider the conductivity of a material as a measure of the ability of its charge to be transported throughout its volume due to the applied electric field. Similarly, its permittivity is a measure of the ability of its dipoles to rotate or its charge to be stored by an applied external field. Note that if the permittivity and conductivity of the material are constant, the displacement current will increase with frequency whereas the conduction current does not change. At low frequencies, the material will behave like a conductor, but capacitive effects will become more important at higher frequencies. For most materials, however, these material properties are not constant, but vary with the frequency of the applied signal. σ^* and ε^* are frequency-dependent.

15.3.2 Biological Tissue in DC Electric Field

The electrical response of biological tissues when stimulated with DC electroporative pulses can be seen as quasi-stationary. Namely, for any material whose electric properties are in the range of those of biological tissues or organs and whose dimensions do not exceed 1 m and the frequency of the electric field is low, the electrical behavior in any given moment as a response to electric current can be numerically described with a set of equations describing stationary fields. Although the impedance of biological tissue has a capacitive component, the electric field can be considered as time independent, thus, the capacitive effects and the finite propagation of the electric current in the biological tissue are disregarded.

The electric field in a tissue and electric current passing through the tissue are coexisting and are related by Ohm's law (Equation 15.16). The corresponding integral values are electric current I, conductance G (which is the reverse of resistance R), and voltage U. Ohm's law then takes the form of

$$U = R \cdot I \tag{15.34}$$

or

$$I = G \cdot U \tag{15.35}$$

Current passes through the tissue if a potential difference exists between two points in the tissue, and the current loop is closed. In practice, we generate the potential difference (voltage) on the electrodes with an electric pulse generator. When both electrodes (one needs at least two electrodes to close the loop) are placed on/in the tissue (which is a conductive material where charge carriers are ions as in electrolyte solutions), the current loop is closed and the current passes through the tissue.

As the electric current passes through a biological tissue, it is distributed through different parts of the tissue, depending on their electrical conductivity. In general, highly perfused tissues have higher conductivity; blood is highly conductive, as well as muscles, whereas bone and fatty tissue have low conductivity. The current will flow easier and for the same voltage in higher proportion through more conductive tissues (e.g., muscles). On the contrary, the electric field in these tissues will be lower than in tissues with low conductivity for the same current.

Nevertheless, as the electric current takes the shortest and easiest path through the tissue, the current will be contained predominantly between the electrodes if they are close enough to each other. This property allows for relatively good control and containment of electric field distribution predominantly between the electrodes (Miklavčič et al. 1998).

Even though the pulses usually used in electroporation are DC, the capacitive properties of the biological material cannot always be disregarded. This holds true for the cases where the transient of cell membrane charging may also be interesting to study. Namely, cell membrane charging time is on the order of microseconds, and typical pulses used for electropermeabilization of the cell membrane are 100 μs long, with the amplitude of around 500 V/cm (Kotnik et al. 1997, 1998). It has been found that if pulses of much higher

amplitude (e.g., 50 kV/cm) and much shorter duration are used—in the order of tens of ns—the charging effect also becomes pronounced on the membranes of intracellular organelles (Schoenbach et al. 2001, Tekle et al. 2005, Kotnik and Miklavčič 2006). For a qualitative analysis of these processes, the time courses of organelle and cell plasma membrane charging become important. Thus, the capacitive component describing the electrical properties of the cell, its organelle(s), and their membranes can no longer be neglected.

15.3.3 Some Biological Tissue Properties Important in the Applied Use of Electroporation

15.3.3.1 Tissue Anisotropy

When the properties of a material are the same in all directions, the material is said to be isotropic. However, some biological materials are distinctly anisotropic. Typical anisotropic tissues are, for example, skeletal muscle and tendon. Therefore, when referring to published electrical property data, the information about the orientation of the electrodes relative to the major axis of the tissue during impedance measurements is important (longitudinal, transversal, or a combination of both).

The conductivity of the material (in units: S/m) can, in the case of an anisotropic conductor, be represented by a tensor:

$$\sigma = \begin{bmatrix} \sigma_{xx} & \sigma_{xy} & \sigma_{xz} \\ \sigma_{yx} & \sigma_{yy} & \sigma_{yz} \\ \sigma_{zx} & \sigma_{zy} & \sigma_{zz} \end{bmatrix}$$

Whenever the material's conductivity can be described in the orthogonal Cartesian system and its spatial dependence can be aligned with the axes, the electric field and the current density can be described in the same way; the nondiagonal elements of the matrix equal zero, hence the matrix becomes diagonal:

$$\sigma = \begin{bmatrix} \sigma_{xx} & 0 & 0 \\ 0 & \sigma_{yy} & 0 \\ 0 & 0 & \sigma_{zz} \end{bmatrix}$$

If we take skeletal muscle for example, two different conductivity values can be measured in two different directions: one for the direction along the length of the muscle fibers and one that is perpendicular to it. If the muscle tissue is aligned with one of the axes of the coordinate system, two diagonal elements in the above matrix have the same value.

Tissue anisotropy is often related to the structure and physiological properties of the tissue. Skeletal muscles are composed of fibers that are very large, highly elongated individual cells and are aligned in the direction of muscle contraction. Electrical conduction along the length of the fiber is thus significantly easier than conduction between the fibers (the difference is about sevenfold) (Reilly 1998). The longitudinal conductivity is significantly higher than the transverse conductivity, especially in the low frequency range. Tissue anisotropy is also frequency-dependent (Hart et al. 1999). If the frequency of the current is high enough, the anisotropic properties disappear (specifically for skeletal muscle that happens in the MHz frequency range). At higher frequencies, charge movement takes place over shorter distances so large-scale structures become less important and capacitive coupling across membranes becomes more important.

15.3.3.2 Nonlinear Behavior

With respect to the intrinsic characteristics of a system or equations describing it, an important consideration is whether the system is linear. Mathematically speaking, a nonlinear system does not satisfy the superposition principle stating that the response of a system caused by two or more input stimuli is the sum of the responses, which would have been caused by each stimulus individually. In terms of

equations, a nonlinear system is any system where the variable(s) to be solved for cannot be written as a linear sum of independent components. Unfortunately, most physical systems are inherently nonlinear in their nature and, unfortunately, biological tissues are not an exception. Often, the physical property of a material is changed during a process (material's temperature coefficients, conductivity changes during tissue electroporation). For some applications, a linear approximation of a nonlinear function can be found at (or around) a given point, for specific input values. However, if the model has to cover the whole (or larger) range of input values, the nonlinearities have to be considered in the model.

If we speak strictly about tissue properties exposed to electric current, at least two important nonlinearities need to be considered.

One is the increase in tissue conductivity (σ) due to an increased electric field (E) causing cell membrane electroporation (Pliquett and Weaver 1996, Pavšelj et al. 2005, Šel et al. 2005). This change of material properties has two more nonlinear characteristics. First, it is considered to be a threshold phenomenon, meaning that the electric field has to reach a certain value, termed reversible electropermeabilization threshold E_{rev}, in order to cause conductivity changes. Second, for the duration of the pulse, this conductivity change is an irreversible phase transition process. More specifically, once the conductivity is increased in a given tissue volume, it cannot be changed back to its lower value during pulse delivery, even if the electric field strength drops below the threshold due to changed conductivities. Here, we would like to point out that one has to be careful to distinguish between the reversibility of cell electroporation (provided the electric field was below the irreversible threshold) after the cessation of electric pulses; and the irreversible nature of the conductivity changes during pulse delivery—the change is only possible in one direction, tissue conductivity can only increase (Pavlin et al. 2005).

The second nonlinearity comes from the electrical–thermal coupling (Pliquett 2003). Once a part of a tissue is permeabilized, it becomes more conductive and the current density increases several times, causing resistive heating. In turn, tissue conductivity increases even more, as the temperature coefficient of electrical conductivity of most biological materials is positive—in the range of 1%–3% °C^{-1} (Duck 1990).

15.3.3.3 Electric Field Threshold of Biological Tissues

The cell membrane is permeabilized when the threshold transmembrane potential is reached, thus, when the external electric field is above the threshold value. This increased cell membrane permeability is reversible, provided the electric field is not too high. However, if cells are exposed to an electric field above the irreversible threshold, they suffer permanent damage. For electroporation-based applications such as gene delivery (Golzio et al. 2004, André et al. 2008) or transdermal drug delivery (Prausnitz 1999, Denet and Préat 2003, Denet et al. 2004), this is not a desirable effect as the cells have to be viable after the treatment. On the other hand, for applications based on irreversible electroporation, the target cells can be irreversibly destroyed within a narrow range while leaving neighboring cells unaffected. This technique represents a promising new treatment for cancer, heart disease, and other conditions that require tissue ablation (Davalos et al. 2005, Lavee et al. 2007, Onik et al. 2007, Rubinsky et al. 2007).

In any case, it is important to determine the needed amplitude of electric pulses at a given electrode-tissue setup to achieve an electric field distribution in the tissue that is adequate for a given application. Electric field reversible and irreversible thresholds are both inherent characteristics of the tissue (also different for different tissues), no matter what kind of electrodes we use or if inhomogeneous or composed tissues are involved. Of course, the electropermeabilization process as well as cell viability depend on electrical parameters, i.e., pulse amplitude, pulse duration, and the number of pulses (see Figure 15.1) (Maček-Lebar et al. 2002, Puc et al. 2003).

However, accomplishing an adequate electric field distribution in the tissue is much more complex than merely calculating the voltage we need at a given electrode separation (U/d). Mathematically, this ratio gives an electric field only when delivering pulses to a homogeneous tissue through parallel plate electrodes whose surface is large (infinite) compared with the electrode separation (see Figure 15.2a). It can still be used as an approximation of the electric field in the area between the parallel plate electrodes
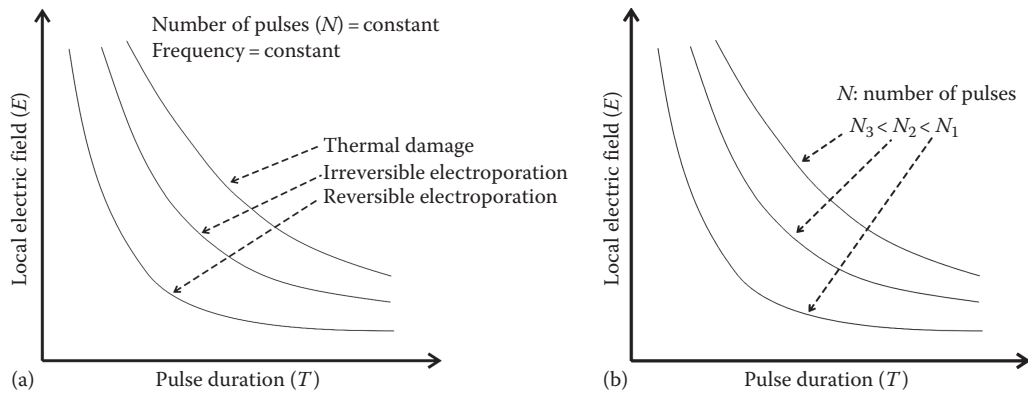
FIGURE 15.1 Electroporation process is (for a given tissue-electrode geometry) controlled by pulse parameters. (a) At constant number of pulses (N) and their frequency, lengthening pulse duration requires lower local electric field (pulse amplitude) for the same effect. If both are increased, the effects on the tissue become irreversible, or, at even higher values, tissue thermal damage can be observed, due to excessive resistive heating. (b) Similarly, for any of the curves, if number of applied pulses is larger, the same effect can be achieved with a lower pulse amplitude and/or duration.
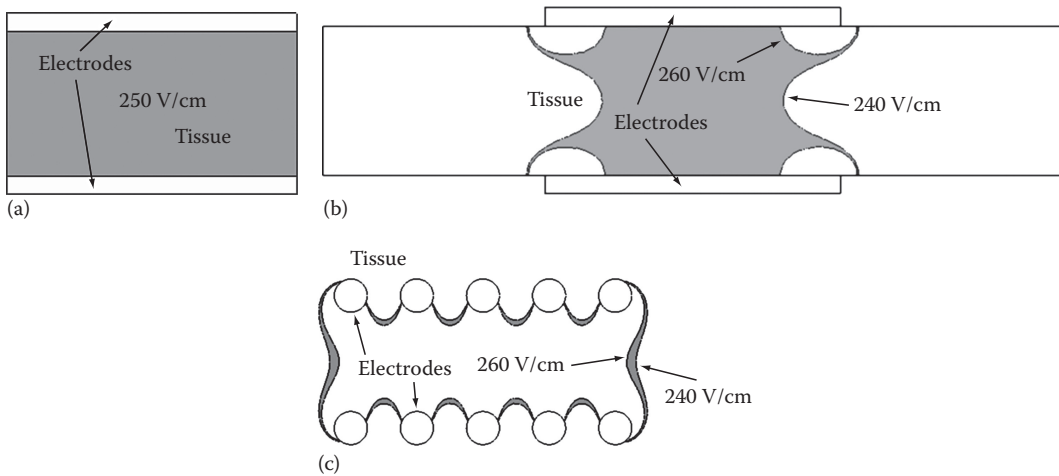

FIGURE 15.2 Curves of the same electric field in a homogeneous tissue in a section plane perpendicular to electrodes. (a) The electric field equals the ratio U/d (voltage/distance between electrodes) only in the theoretical case where electric pulses are delivered through plate electrodes of infinite surface. Here, only a portion of this infinite structure is modeled with boundary conditions set to represent an infinite volume. The distance between the electrodes (d) is 4 mm, the applied voltage (U) is 100 V, and thus the electric field equals U/d = 250 V/cm throughout the tissue between the electrodes. (b) A real situation where electrodes are of finite dimension. The electric field in the gray area between the two black isocontours is between 240 and 260 V/cm, so the voltage to distance ratio in this area is a good approximation, except near the edges of the electrodes. The U/d approximation is valid in a greater portion of the tissue between the electrodes if the electrode surface is increased or the distance between them is smaller. (c) Two rows of needle electrodes are used instead of plate electrodes. The length of the electrode array and the distance between the rows is the same as in (b). The gray area between the two black isocontours denoting electric field between 240 and 260 V/cm is very small and limited to a few narrow stripes. Throughout most of the area inside the electrode array the electric field is higher (around 300 V/cm or higher) and thus cannot be satisfactorily approximated by voltage to distance ratio.

of finite dimensions, away from their edges (Figure 15.2b). The *U*/*d* ratio is also often used to estimate the electric field between two parallel rows of needle electrodes. Some are referring to the *U*/*d* ratio as a "nominal" field; however, the approximation is extremely rough (Figure 15.2c). In the case of any other electrode geometry using plate, needle, microneedle, or surface electrodes or if more than one tissue is involved, a numerical analysis has to be performed beforehand, as a part of treatment planning, in order to choose the right electrode configuration and the pulse amplitude.

15.4 Modeling

Having acquired some basic knowledge about the electromagnetic field theory and specificities of biological tissues, we can set about constructing mathematical models representing different aspects of electroporation.

The starting point of the modeling process is deciding on the mathematical approach to adequately describe the modeled system by first acquiring enough observable and measurable information about it. Typically, more than one modeling approach is possible and choosing the most suitable one depends on the modeler's or end user's objective needs and personal preferences, as well as the physical and geometrical characteristics of the modeled system. In some cases, using more than one modeling approach can be beneficial in terms of model verification and validation. More than one phenomenon can determine a system, which is especially the case with biological systems. Generalizations and simplifications are possible and, in most cases, cannot be avoided. The model can refer only to some aspects of the real system, while disregarding the ones that either have a very limited influence on its accuracy or are out of the scope of this particular model. Prior to building a model, we need to define its scope, apply necessary simplifications while being aware of the circumstances or the range of input variables for which the model is valid.

Deciding on the right level of complexity for our model is not always an easy task as it involves a trade-off between simplicity and accuracy. As a general guideline, if we are choosing from different models giving comparable results, the simplest one is the most desirable. Namely, we need to be aware that adding complexity can make the model difficult to understand and experiment with and can pose computational problems.

Analytical methods are rather complicated and are only feasible for use on problems where the geometry, material properties, and boundary conditions can easily be described in a defined coordinate system (Cartesian, cylindrical, or spherical). Simple analytical models can have certain advantages over numerical models. First, the input data needed is typically less extensive than that of numerical models. Also, analytical solutions have no numerical and discretization errors. The obvious limitation of analytical models is that only the simple and uniform geometries, boundaries, and initial conditions can easily be modeled. In the last decades, analytical models have mostly been replaced by numerical models based on boundary element, finite difference, finite volume, or finite element methods, due to the miniaturization and accessibility of both computer hardware and software. Of these methods, the latter is preferred in the modeling of electroporation, due to its relatively easy implementation and its ability to handle more intricate geometries. The principle behind this method is the discretization of the geometry into smaller elements where the quantity to be determined is approximated with a function or is assumed to be constant throughout the element. Discrete elements can be of different shapes and sizes, which allows for the modeling of intricate geometries. In such models, the excitations can be changed easily, being that it only involves changing the boundary conditions on the same model. The model geometry, however, takes time and precision to be built and generalizations and simplifications need to be used when possible.

15.4.1 Building a Geometry

When designing a numerical model, we must decide for the appropriate details to be included. Geometrically more detailed models will inevitably consume more of both the modeler's and the

computer's time, but do not necessarily produce better quality results, as the inclusion of geometrical details depends on the purpose of the model.

15.4.1.1 Geometrical Symmetries

Taking advantage of the geometrical symmetries of the system we are modeling allows us to analyze a structure or a system by modeling only a portion of it by applying appropriate boundary conditions. This approach can be used when the same symmetry can be observed in both the geometry as well as the sources (in our case of electric current). It reduces the size of the model and consequently the analysis run time as well as the demands on computer resources. Alternatively, modeling only a portion of the whole geometry allows us to include more details in the model, when needed, thereby obtaining better results that would not have been possible with the full geometry (Pavšelj et al. 2007). For example, when representing a tumor with a simplified elliptical shape, supposing also the symmetry of the electric stimulation), only a quarter of the tumor can be modeled (see Figure 15.3a). A similar approach can be used when modeling a geometrical structure with a repetitive infinite or quasi-infinite pattern (Figure 15.3b). In this case, only a small portion of the whole array, a unit cell, needs to be modeled by applying the appropriate periodic boundary conditions (Susil et al. 1998, Pavlin et al. 2002).

Similarly, sometimes we are able to represent a 3D structure by a single 2D plane. For example, in Cartesian coordinates, a structure stretched along a straight line (Z-direction) can be represented with a structure in the X–Y plane, while the model is assumed to be uniform in the perpendicular Z-direction (see Figure 15.4a). Similarly, if the structure is axisymmetrical, the plane of symmetry is the cross section anywhere around the axis of symmetry. In this case, we are using a single 2D slice (r–z cylindrical coordinates) to represent the whole 360° of the structure (see Figure 15.4b).
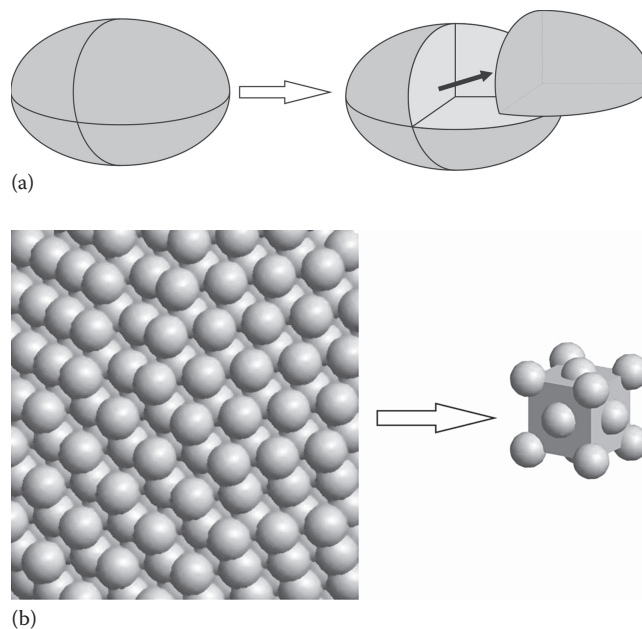

(a)

(b)

FIGURE 15.3 Representation of a large structure with only a portion of its geometry. (a) When modeling an elliptically shaped tumor during electrochemotherapy, supposing the electric stimulation exerts the same symmetry, only a quarter of the tumor need be modeled. (b) A finite representation of an infinite 3D lattice, such as cells in a cluster.
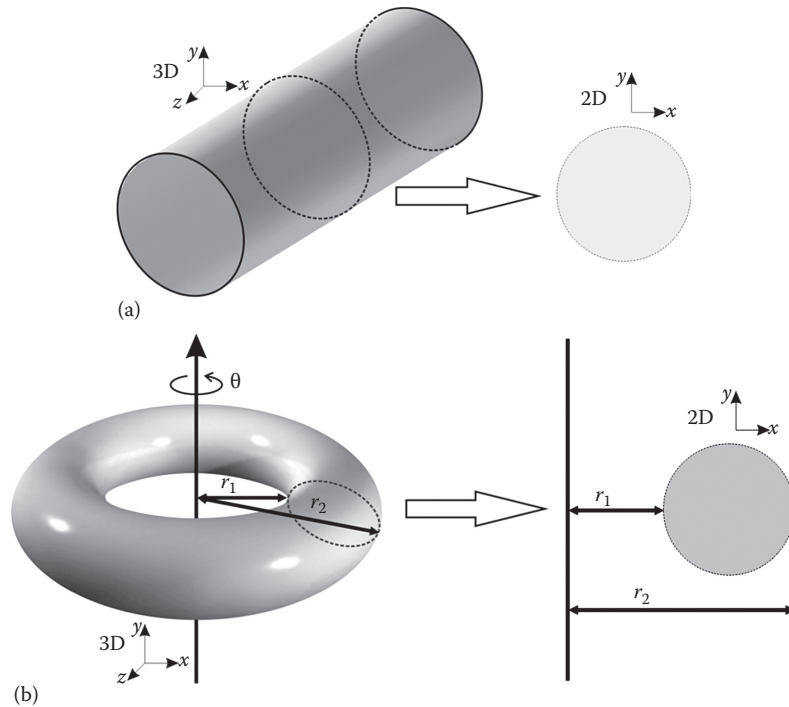
FIGURE 15.4 Representation of a 3D structure by a single 2D plane. (a) 2D representation of a 3D geometry. In this case, the cylinder was represented by its cross section. (b) 2D representation of a 3D axisymmetrical structure.

15.4.1.2 The Size of the Modeled Volume/Area

In some cases, the modeled system has no borders electrically insulating it from its surroundings; the electrical quantities are simply diminishing with increasing distance from the source. One such example is needle electrodes inserted in a tissue (Figure 15.5). In such cases, the outer boundaries of the model need to be far enough from the source(s), in order not to restrain the natural flow of the electric current (see Figure 15.5a). Namely, when modeling such a system, the borders of the model are artificially electrically insulated from the surroundings. This effectively means that the boundary condition is set in such a way that no electric current flows in or out of the enclosing box—only tangential components of the electric current exist on the outer tissue borders while the normal component equals zero. If these borders are too close to the source(s) of the electric current, such as in Figure 15.5b, the electric field and current distribution is deformed and does not reflect the true situation. The safest way to choose the right distance of the model borders from the source(s) is by changing the dimensions of the enclosing box and observing its effect on the results. The enclosing box is large enough when, if further increased, the effect on the calculated scalar and vector fields is negligible.

15.4.1.3 Modeling of Biological Entities

Numerous examples could be given to illustrate either the importance or futility of including physiological details in the geometry of the model. Already at the cell level, in vitro observations on cell suspensions can be represented numerically on different levels. For example, when studying the magnitude and the distribution of the electric field in a cell suspension, a material with homogeneous properties is an adequate model (Pavlin and Miklavčič 2003). However, if the aim of our research is to study the phenomena on the cell level or if we are looking into interactions between cells, the influence of their size, shape, density, and orientation, individual cells rather than bulk material have to be modeled (Susil et al. 1998, Pavlin et al. 2002, Valič et al. 2003, Pucihar et al. 2006, Pavlin and Miklavčič 2008, Towhidi et al.
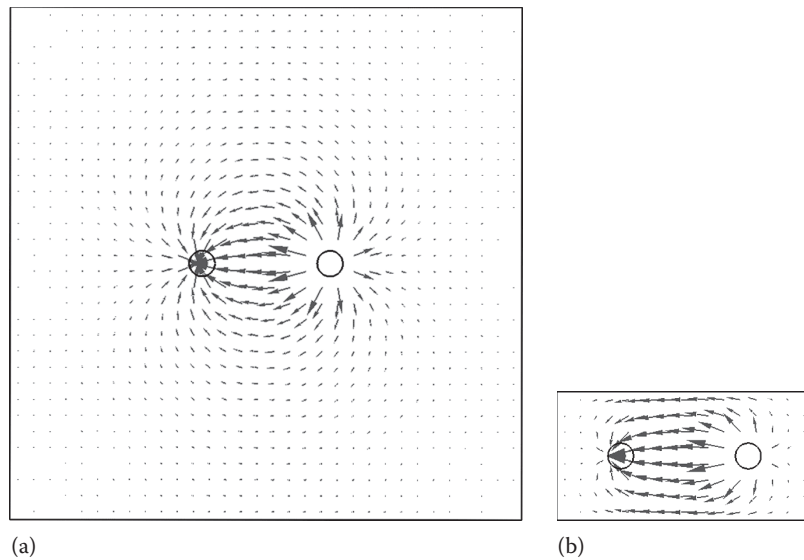
(a)   (b)

FIGURE 15.5 The electric current density—*J* (gray arrows) in a homogeneous material, electric pulse is delivered through needle electrodes (the two black circles). The electric current density is shown in a section plane cut through the material, perpendicular to electrodes. (a) The insulated borders of the model are far enough from the electrodes, which allows for the natural flow of the electric current, the electric field and the electric current near model borders are very close to zero. (b) The borders of the model are too close to the electrodes, the electric field close to the border is not zero, electric current is artificially constrained.

2008). Even further, if we are using nanopulses, cell organelles must be added to the geometry (Kotnik and Miklavčič 2006). Still, by using smart approaches, such as replacing a thin, non-zero conductivity cell membrane by a boundary condition between the cytoplasm and the exterior, getting rid of complexities while maintaining accuracy of the model is possible (Pucihar et al. 2006).

Similar observations hold true on the tissue level. Different levels of complexity and inhomogeneity can be observed in different tissues; however, including their particularities depends strongly on the purpose of the model. Skin, for example, is a very intricate tissue due to its highly inhomogeneous structure, leading to inhomogeneous electric properties. It consists of different layers in terms of dimensions (thickness) and electrical properties: the outer thin layer of dead flat skin cells, the stratum corneum, the viable epidermis, dermis, and the subcutaneous tissue (Yamamoto and Yamamoto 1976a,b, Chizmadzhev et al. 1998). If the aim of the model is to study the electroporation of skin as a target tissue, this layered structure needs to be included in the geometrical representation (Pavšelj et al. 2007). Moreover, even this bulk layered structure might sometimes prove inadequate. Smaller structures, such as hair follicles, sweat glands, and blood vessels, or local transport regions as a result of skin electroporation (Pavšelj et al. 2008a) may have to be added in order to study the processes on the microscale, where they occur, and only then compare them to bulk observations. On the one hand, such details, unavoidably adding to the overall complexity of the model, can be omitted in cases where skin electroporation is not studied directly, such as any application where electric pulses are delivered with external electrodes to tissues beneath the skin (Pavšelj et al. 2005). On the other hand, other structures, such as major blood vessels may be important and need to be included in the model when studying the mechanisms of the electrochemotherapy of tumors (Serša et al. 2008).

15.4.2 Setting the Physics of the Model

After the geometry of the model has been constructed, the next step in the modeling process is setting the physics of the model, such as underlying equations, material properties, boundary, and initial conditions.

15.4.2.1 Frequency-Dependent Component

First, the material's response will be different when exposed to either direct (DC) or alternating current (AC). If our material is purely resistive, the system exerts no frequency dependency; the current is proportional to the voltage irrespective of the frequency. However, in general, materials have their capacitive or inductive component so the voltage to current ratio does depend on frequency and is termed impedance (Z). Impedance is a complex quantity consisting of a resistance R (the real part) and a reactance X (the imaginary, frequency-dependent part):

$$\vec{Z} = R + jX \tag{15.36}$$

The resistance can only be positive, while the reactance can be either positive (inductive character, current lagging behind voltage—X_L) or negative (capacitive character, voltage lagging behind current—X_C).

$$X_L = j\omega L \tag{15.37}$$

$$X_C = -j\frac{1}{\omega C} \tag{15.38}$$

Voltage and current can be considered as vectors in the complex plane (phasors) that are out of phase, so the voltage to current ratio—the impedance—can also be given by its magnitude and phase angle:

$$\vec{Z} = |Z| \cdot e^{j\Theta} \tag{15.39}$$

$$|Z| = \sqrt{R^2 + X^2} \tag{15.40}$$

$$\Theta = arctg\frac{X}{R} \tag{15.41}$$

Resistance is only a special case of impedance, when the material we are considering exerts no or negligible capacitive or inductive character ($jX = 0$). Further, if a system is exposed to DC, the frequency-dependent part—the reactance X—plays no role when the system is in steady-state, after all the transients have faded out. It does, however, dictate the course of the transient of the system, which poses the next question in the modeling process: Are we interested only in the steady-state of our system or are we studying transient phenomena—changes over time from $t = 0$ until the system has reached its steady-state?

15.4.2.2 Transient vs. Steady-State

Transient behavior occurs when the magnitude and direction of electrical quantities change with time. On the contrary, if they are constant with time throughout the entire volume, the system is already in its steady-state. To avoid any ambiguity, the steady-state does not mean the absence of movement or flow in the system! If we take electric currents in a material as an example, it simply means that the "amount" of electric current in the system does not change within an observed time; the magnitude of the current exiting the system equals the current magnitude flowing into the system at any time when in steady-state. In other words, time becomes an irrelevant variable for the analysis, since the recently observed behavior of the system will continue into the future.

In many systems, steady-state is not achieved until sufficient time has elapsed after the system is started or stimulated (externally or internally). The situation after the occurrence of the described changes of the system and before all internal quantities (states) of the system reach the steady-state is defined as the transient state. As an example, in an electrical system of purely resistive character, no transients occur at $t = 0$, when the electrical stimulation is turned on. However, if the imaginary part (the reactance) is present in the impedance of the electrical system, its behavior exerts inertia, meaning that the change of electrical quantities in the system is not instantaneous. The capacitive or the inductive

component opposes the sudden change at $t = 0$ (applied voltage or current) and enforces the transient state onto the system that will, however, eventually fade out.

15.4.2.3 Multiphysics

The effects of various physical phenomena can be investigated by separately analyzing each individual phenomenon without any consideration of the interaction between them. However, often we are dealing with two or more interacting, simultaneous phenomena, such as the coupling between the electric and the magnetic fields. An important coupling of physical phenomena in applications using electric pulses on biological tissues is heat transfer in tissue due to resistive heating (Tungjitkusolmun et al. 2000). This coupling may give rise to tissue conductivity changes (due to temperature increase), which in turn changes the magnitude of the electric current. When constructing a model, the influence of such interactions have to be estimated and, if needed to obtain accurate results, mutual dependencies have to be included. To do so, we need data on how the material properties significant for one field (such as the electric field) vary with the magnitude of another field (such as temperature) and vice versa.

15.4.3 Interpretation of Results

When modeling the electroporation of biological tissues, much consideration has to be given to the interpretation of the results in relation to possible simplifications in the model or inherent characteristics of different biological tissues. Namely, some simplifications might not have much effect in isotropic, homogeneous tissues, such as the liver, but may yield useless results in inhomogeneous, composed biological structures, such as layered skin or subcutaneous tumors, where electric field distribution is much more complex (Pavšelj et al. 2005, Ivorra et al. 2008, Pavšelj and Miklavčič 2008b). To illustrate, when modeling electroporation in a homogeneous tissue, such as the liver, the results are still useful and comparable to experimental data even if the conductivity increase due to tissue electropermeabilization is neglected. In fact, early models did not take this nonlinear tissue behavior into account (Miklavčič et al. 2000). However, when more complicated electrode-tissue setups were being studied with numerical models, experimentally observed phenomena could not be satisfactorily modeled in this way. Namely, upon applying electric pulses on a composed or layered tissue with an inhomogeneous distribution of electrical conductivities, the voltage is divided among them proportionally to their electrical resistances (Pavšelj and Miklavčič 2008b). This leads to a more complex electric field distribution, meaning that some parts of the tissue, due to their low electrical conductivity (disproportionally lower than the rest of the tissue), are exposed to a much stronger electric field. The electric field is the highest in the layer with the highest resistivity (lowest conductivity). In the case of the subcutaneous tumor, this is the skin, which has the lowest electrical conductivity, and in the case of the skin fold, the highest electric field is in the nonconductive outermost skin layer, the stratum corneum. But more importantly, the electric field in the target tissues (tumor and viable skin layers) stays too low for successful electroporation. This fact raised the question of how the experimentally confirmed successful permeabilization of the target tissues theoretically is possible when external plate electrodes are used, which led to the inclusion of tissue conductivity changes due to electroporation in the numerical models.

15.4.4 Model Verification and Validation

The last, but nevertheless very important part of the modeling process is the verification and the validation of the constructed model, involving different aspects of evaluation. Mostly, these aspects should be taken into consideration from the very beginning of the process and can roughly be divided into three categories:

1. *Verification*: The main question here is whether we reached the aim of the model. Already in the planning phase of the modeling process, we have to set the scope of our model, the range of input data it should be valid for, as well as geometrical details to be included. However, as we build the model, some simplifications and trade-offs may have to be made. Comparing the actual result

with the requirements set during the planning phase will demonstrate whether our resulting model is still within the planned scope of the model or not.

2. *Descriptive realism*: Have we identified and explained the underlying physics? In cases where almost nothing is known about the phenomena describing the modeled system, we are dealing with the so-called black box problem that can only be treated in terms of its input and output characteristics. Our only option may be finding a curve that has the best fit to a series of data points, while respecting possible constraints without actual physical reference to the described process(es). However, different techniques of system identification (Ljung 1999) can be applied in order to identify the physics defining our "black box," which can then be modeled. Namely, the purpose of modeling is to gain insight and explain underlying phenomena, as well as using them for predicting the output at certain input data sets. We should therefore direct our efforts to turn the black box into a set of equations, if possible. Once again, as some trade-offs will most likely be necessary, we should assess if the modeled physical phenomena successfully explain the most important experimental observations.

3. *Validation*: Does our model agree with the empirical data? One way to justify the physics used in the model (sometimes the only way) is by comparing the output data obtained from the model to experimental data. Usually, or ideally, the experimental data can be divided into two groups: the training data and the validation data. The former is used to identify the process and to construct a model with its relevant parameters and constraints, while the latter is used to assess if the model is valid for any range of input parameters within the defined constraints.

15.5 Treatment Planning

When electroporation is used in biomedical experiments and medical treatments, the (steady-state) electric field distribution inside the target tissues is one of the most important predictors of success (Miklavčič et al. 1998). Models have helped us to understand that the electric field in tissue changes its magnitude during pulses, as the conductivity increases due to electroporation (Pavšelj et al. 2005, Šel et al. 2005). Also, modeling has shown the importance of ensuring good surface contact between the electrodes and tissue, when plate electrodes are used to deliver electric pulses (Čorović et al. 2008a), and the importance of the depth of insertion, when needle electrodes are used (Čorović et al. 2008b). It has also been shown that for a known number and duration of applied electric pulses, the electric field has to be higher than a threshold value ($E > E_{\mathrm{th}}$) for electroporation to occur (Šemrov and Miklavčič 1998). As such, the electric field distribution can serve as a predictor of treatment outcome. As has been mentioned in the previous sections, the local electric field distribution inside biological tissue is very hard to predict without numerical models. If a specific distribution is needed, as is the case in electroporation-based medical treatments, several attempts are needed before the right electrode positions relative to the target tissue and voltages between the electrodes are found. The more complex the case, the more time is needed to determine the treatment parameters by trial and error (forward planning), therefore, numerical optimization techniques (inverse planning) have to be used: a desired electric field distribution can be set and appropriate treatment parameters (electrode positions, voltages) can be determined by numerical optimization (Župan et al. 2008).

In practice, these more complex cases include target tissues that are located deep in the body or close to the vital organs. In such cases, it is important to control the magnitude and distribution of the electric field so that a minimum volume of vital tissue is compromised by the treatment. Numerical modeling may also be necessary for treatment planning in tissues with highly anisotropic properties and highly nonhomogeneous tissues (Pavšelj and Miklavčič 2008b). In such cases, the treatment planning procedure has to be applied individually for each patient and the electric field distribution has to be sculpted carefully to guarantee that the entire target tissue is exposed to a high enough electric field, while vital tissues are as unaffected as possible.

Treatment planning does not consist solely of optimization and modeling, but is instead an integral part of the whole treatment process. Normally, medical imaging (CT, MRI) is first used to obtain

information about the anatomical details of the treated volumes. The images are converted into mathematical representations and used in the numerical model to calculate the electric field distribution. The numerical model is used in the optimization algorithm to calculate the best treatment parameters (electrode positions and voltages). Additional measures can be taken to ensure that the treatment plan is successfully executed, e.g., the insertion of electrodes can be controlled by ultrasound imaging and the extent of electroporation can be monitored by current and voltage measurements (Cukjati et al. 2007) or electrical impedance imaging (Davalos and Rubinsky 2004, Ivorra and Rubinsky 2007). Therefore, it can be argued that the quality of numerical treatment planning for electroporation-based treatment depends on the quality of medical imaging, target and normal tissue identification, detailed knowledge of the biological effects of the electric field (changes in tissue properties, threshold values), and the quality of the underlying model. At present, not all of the requisites are met. For one, electroporation thresholds are tissue specific and are not yet readily available. Furthermore, several electric pulse parameters that affect the threshold values: pulse duration, number of pulses, and to some extent also pulse repetition frequency (Pucihar et al. 2002, Edd and Davalos 2007) have not yet been included in numerical models. Therefore, prior to any treatment planning, data on thresholds for all relevant tissues should be available for a range of electroporation parameters.

We present an example of treatment planning of the electrochemotherapy of a tumor nodule located near a vital organ using numerical modeling and a genetic optimization algorithm. The goal is to determine the best possible configuration and electric potentials of six electrodes surrounding a subcutaneous tumor—the target tissue. The treatment parameters must irreversibly electroporate ($E > E_{\text{rev}}$) the entire tumor volume while sparing the hypothetical spherical vital organ ($E < E_{\text{irr}}$) situated next to the tumor (Figure 15.6).

The steady-state numerical model of electroporation is used, taking into account the changes in tissue conductivities because of electroporation; i.e., electric field distribution in the tissue caused by an electric pulse is determined by solving the Laplace equation for static electric currents (2.19) with $\sigma(E)$. All tissues are considered isotropic and homogeneous. The assigned conductivity values and electroporation thresholds are given in Table 15.1. These values are mostly taken from existing literature (Gabriel et al. 1996a,b, Davalos et al. 2005, Pavšelj et al., 2005, Cukjati et al. 2007) or, in cases where data cannot be found in existing literature, are educated guesses, meant only for demonstration purposes.

A genetic algorithm is used for the optimization procedure. A population of possible solutions (treatment plans consisting of the positions and direction of each electrode [x, y, z, φ, θ] and all used voltages) is first randomly chosen. The solutions then evolve in iterations by mathematical operation cross-over and mutation according to their fitness function
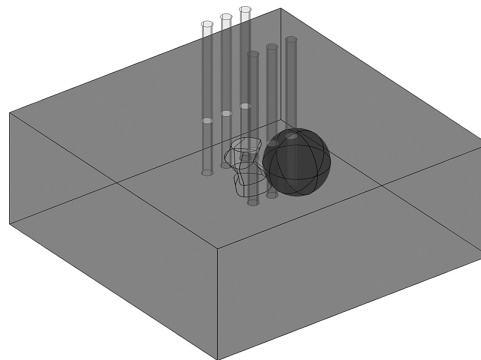

FIGURE 15.6 Model geometry: healthy tissue, tumor (between the electrodes)—geometry taken from Šel et al. (2007), vital organ (sphere). Needle electrodes are inserted into the tissue and appropriate electric potentials are assigned to each electrode so that the entire tumor volume is reversibly electroporated and the least possible volume of the vital organ is irreversibly electroporated.

TABLE 15.1   Tissue Properties Used in the Numerical Model

Tissue	σ_1 (S/m)	σ_2 (S/m)	E_{rev} (V/m)	E_{irr} (V/m)
Tumor	0.2	0.7	400	900
Vital organ	0.15	0.5	250	600
Healthy tissue	0.15	0.5	250	600

$$F = 10 \cdot V_{Trev} - 2 \cdot V_{VOir}, \tag{15.42}$$

where

    F is the fitness
    V_{Trev} is the fraction of tumor volume subjected to local electric fields above reversible thresholds
        ($E > E_{rev}$)
    V_{VOir} is the fraction of volume of the organ at risk subjected to $E > E_{irrev}$

The weights in the fitness function (importance factors) are set arbitrarily, but with respect to the importance of the individual parameters for efficient electroporation. Namely, the most important endpoint of the treatment is the reversible electroporation of the entire tumor (weight 10 in Equation 15.42), while sparing the vital organ is not as important (weight 2). In the clinical environment, these importance factors would have to be set by an experienced physician. In our case, the algorithm optimizes 36 different parameters (positions [x, y, z, φ, θ] and electric potentials of all six electrodes). It is presumed that it is possible to achieve a good enough electric field distribution using these parameters.

The final treatment plan is presented in Figure 15.7. The resulting electric field distribution is not at all homogeneous; the field around the electrodes and in some parts of the tumor is much higher than in other parts of the tissue. Nevertheless, the tumor is completely reversibly electroporated, while 0.3% of the vital organ is irreversibly electroporated. From that we can conclude that the treatment planning goals have been met.
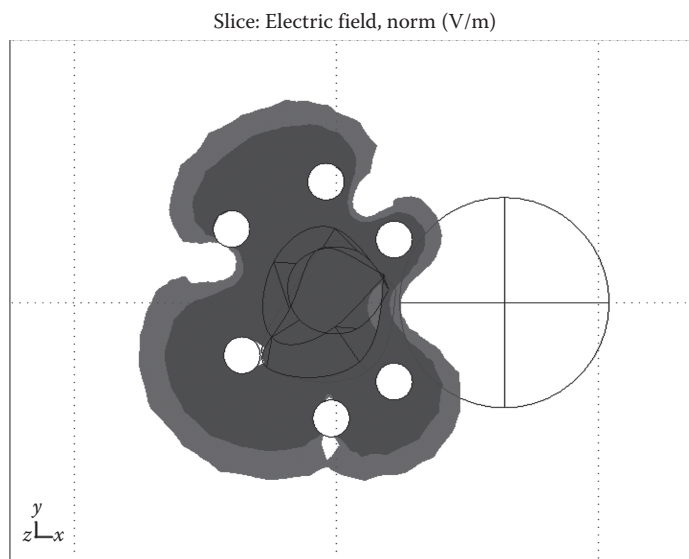
Slice: Electric field, norm (V/m)

FIGURE 15.7   Electric field distribution for the treatment plan 2 is shown in the *XY* plane through the center of the tumor. Light gray areas are reversible electroporated ($E > E_{rev}$), while dark gray areas are irreversibly electroporated ($E > E_{irr}$).

15.6 Summary

This chapter explains in detail the process of electric field distribution modeling in biological tissues. The equations used in modeling are derived from Maxwell's equation of the electromagnetic field, while taking into account the dynamics of the induced transmembrane potential compared with the duration of electric pulses and the behavior of biological tissue in the presence of external electric fields. Biological tissues, which can be heterogeneous, anisotropic, and nonlinear, are included in the equations in the form of electric fields and direction-dependent tissue properties. The model geometry has to be chosen carefully, according to the modeling aims—the simplest possible geometry and form of equations that give good results should be used to make the calculation as fast as possible and also easier to interpret. Finally, the numerical modeling of electric field distribution is not only useful for explaining the experimental results and hypothesis testing, but also in the clinical setting, where it can be used together with optimization techniques in the inverse treatment planning of electroporation-based treatments.

Acknowledgments

References

André F, Gehl J, Serša G, Préat V, Hojman P, Eriksen J, Golzio M et al. 2008. Efficiency of high- and low-voltage pulse combinations for gene electrotransfer in muscle, liver, tumor, and skin. *Human Gene Ther* 19:1261–1271.

Brandisky K, Daskalov I. 1999. Electrical field and current distributions in electrochemotherapy. *Bioelectrochem Bioenerg* 48:201–208.

Chizmadzhev YA, Indenbom AV, Kuzmin PI, Galichenko SV, Weaver JC, Potts RO. 1998. Electrical properties of skin at moderate voltages: Contribution of appendageal macropores. *Biophys J* 74:843–856.

Čorović S, Al Sakere B, Haddad V, Miklavčič D, Mir LM. 2008a. Importance of contact surface between electrodes and treated tissue in electrochemotherapy. *Technol Cancer Res Treat* 7:393–399.

Čorović S, Županič A, Miklavčič D. 2008b. Numerical modeling and optimization of electric field distribution in subcutaneous tumor treated with electrochemotherapy using needle electrodes. *IEEE Trans Plasma Sci* 36:1665–1672.

Cukjati D, Batiuskaite D, André F, Miklavčič D, Mir LM. 2007. Real time electroporation control for accurate and safe in vivo non-viral gene therapy. *Bioelectrochemistry* 70:501–507.

Davalos RV, Rubinsky B. 2004. Electrical impedance tomography of cell viability in tissue with application to cryosurgery. *J Biomech Eng* 126(2):305–309.

Davalos RV, Mir LM, Rubinsky B. 2005. Tissue ablation with irreversible electroporation. *Ann Biomed Eng* 33(2):223–231.

Debruin KA, Krassowska W. 1999a. Modeling electroporation in a single cell. I. Effects of field strength and rest potential. *Biophys J* 77:1213–1224.

Debruin KA, Krassowska W. 1999b. Modeling electroporation in a single cell. II. Effects of ionic concentrations. *Biophys. J.* 77:1225–1233.

Denet A-R, Préat V. 2003. Transdermal delivery of timolol by electroporation through human skin. *J Control Release* 88:253–262.

Denet A-R, Vanbever R, Préat V. 2004. Skin electroporation for transdermal and topical delivery. *Adv Drug Deliv Rev* 56(5):659–674.

Dev SB, Dhar D, Krassowska W. 2003. Electric field of a six-needle array electrode used in drug and DNA delivery in vivo: Analytical versus numerical solution. *IEEE Trans Biomed Eng* 50(11):1296–1300.

Duck FA. 1990. *Physical Properties of Tissue: A Comprehensive Reference Book*. Academic Press, London, U.K.

Edd JF, Davalos RF. 2007. Mathematical modeling of irreversible electroporation for treatment planning. *Technol Cancer Res Treat* 6(4):275–286.

Fear EC, Stuchly MA. 1998. Modeling assemblies of biological cells exposed to electric fields. *IEEE Trans Biomed Eng* 45(10):1259–1271.

Foster KR, Schwan HP. 1989. Dielectric properties of tissues and biological materials: A critical review. *Crit Rev Biomed Eng* 17:25–104.

Gabriel C, Gabriel S, Corthout E. 1996a. The dielectric properties of biological tissues: I. Literature survey. *Phys Med Biol* 41:2231–2249.

Gabriel S, Lau RW, Gabriel C. 1996b. The dielectric properties of biological tissues: II. Measurements in the frequency range 10 Hz to 20 GHz. *Phys Med Biol* 41:2251–2269.

Golzio M, Rols MP, Teissié J. 2004. In vitro and in vivo electric field-mediated permeabilization, gene transfer, and expression. *Methods* 33(2):126–135.

Grimnes S, Martinsen OG. 2000. *Bioimpedance & Bioelectricity Basics*. Academic Press, London, U.K.

Hart FX, Berner NJ, McMillen RL. 1999. Modelling the anisotropic electrical properties of skeletal muscle. *Phys Med Biol* 44:413–421.

Ivorra A, Rubinsky B. 2007. In vivo electrical impedance measurements during and after electroporation of rat liver. *Bioelectrochemistry* 70(2):287–295.

Ivorra A, Al-Sakere B, Rubinsky B, Mir LM. 2008. Use of conductive gels for electric field homogenization increases the antitumor efficacy of electroporation therapies. *Phys Med Biol* 53:6605–6618.

Kotnik T, Miklavčič D. 2006. Theoretical evaluation of voltage inducement on internal membranes of biological cells exposed to electric fields. *Biophys J* 90:480–491.

Kotnik T, Bobanović F, Miklavčič D. 1997. Sensitivity of transmembrane voltage induced by applied electric fields—A theoretical analysis. *Bioelectrochem Bioenerg* 43:285–291.

Kotnik T, Miklavčič D, Slivnik T. 1998. Time course of transmembrane voltage induced by time-varying electric fields—A method for theoretical analysis and its application. *Bioelectrochem Bioenerg* 45:3–16.

Lavee J, Onik G, Mikus P, Rubinsky B. 2007. A novel nonthermal energy source for surgical epicardial atrial ablation: Irreversible electroporation. *Heart Surg Forum* 10(2):96–101.

Ljung L. 1999. *System Identification—Theory for the User*, 2nd edn., PTR Prentice Hall, Upper Saddle River, NJ.

Maček-Lebar A, Serša G, Kranjc S, Grošelj A, Miklavčič D. 2002. Optimisation of pulse parameters in vitro for in vivo electrochemotherapy. *Anticancer Res* 22:1731–1736.

Miklavčič D, Beravs K, Šemrov D, Čemažar M, Demšar F, Serša G. 1998. The importance of electric field distribution for effective in vivo electroporation of tissues. *Biophys J* 74:2152–2158.

Miklavčič D, Šemrov D, Mekid H, Mir LM. 2000. A validated model of in vivo electric field distribution in tissues for electrochemotherapy and for DNA electrotransfer for gene therapy. *Biochim Biophys Acta* 1523:73–83.

Miklavčič D, Čorović S, Pucihar G, Pavšelj N. 2006a. Importance of tumour coverage by sufficiently high local electric field for effective electrochemotherapy. *Eur J Cancer Suppl* 4:45–51.

Miklavčič D, Pavšelj N, Hart FX. 2006b. *Electric Properties of Tissues. Wiley Encyclopedia of Biomedical Engineering*, John Wiley & Sons, New York.

Onik G, Mikus P, Rubinsky B. 2007. Irreversible electroporation: Implications for prostate ablation. *Technol Cancer Res Treat* 6(4):295–300.

Pavlin M, Miklavčič D. 2003. Effective conductivity of a suspension of permeabilized cells: A theoretical analysis. *Biophys J* 85:719–729.

Pavlin M, Miklavčič D. 2008. Theoretical and experimental analysis of conductivity, ion diffusion and molecular transport during cell electroporation—Relation between short-lived and long-lived pores. *Bioelectrochemistry* 74:38–46.

Pavlin M, Pavšelj N, Miklavčič D. 2002. Dependence of induced transmembrane potential on cell density, arrangement, and cell position inside a cell system. *IEEE Trans Biomed Eng* 49:605–612.

Pavlin M, Kandušer M, Reberšek M, Pucihar G, Hart FX, Magjarević R, Miklavčič D. 2005. Effect of cell electroporation on the conductivity of a cell suspension. *Biophys J* 88:4378–4390.

Pavšelj N, Miklavčič D. 2008a. Numerical models of skin electropermeabilization taking into account conductivity changes and the presence of local transport regions. *IEEE Trans Plasma Sci* 36:1650–1658.

Pavšelj N, Miklavčič D. 2008b. Numerical modeling in electroporation-based biomedical applications. *Radiol Oncol* 42:159–168.

Pavšelj N, Bregar Z, Cukjati D, Batiuskaite D, Mir LM, Miklavčič D. 2005. The course of tissue permeabilization studied on a mathematical model of a subcutaneous tumor in small animals. *IEEE Trans Biomed Eng* 52:1373–1381.

Pavšelj N, Préat V, Miklavčič D. 2007. A numerical model of skin electropermeabilization based on in vivo experiments. *Ann Biomed Eng* 35:2138–2144.

Pliquett U. 2003. Joule heating during solid tissue electroporation. *Med Biol Eng Comput* 41(2):215–219.

Pliquett U, Weaver JC. 1996. Electroporation of human skin: Simultaneous measurement of changes in the transport of two fluorescent molecules and in the passive electrical properties. *Bioelectrochem Bioenerg* 39(1):1–12.

Prausnitz MR. 1999. A practical assessment of transdermal drug delivery by skin electroporation. *Adv Drug Deliv Rev* 35:61–76.

Puc M, Kotnik T, Mir LM, Miklavčič D. 2003. Quantitative model of small molecules uptake after in vitro cell electropermeabilization. *Bioelectrochemistry* 60:1–10.

Pucihar G, Mir LM, Miklavčič D. 2002. The effect of pulse repetition frequency on the uptake into electropermeabilized cells in vitro with possible applications in electrochemotherapy. *Bioelectrochemistry* 57:167–172.

Pucihar G, Kotnik T, Valič B, Miklavčič D. 2006. Numerical determination of transmembrane voltage induced on irregularly shaped cells. *Ann Biomed Eng* 34:642–652.

Reilly JP. 1998. *Applied Bioelectricity, from Electrical Stimulation to Electropathology*, Springer-Verlag, New York.

Rubinsky B, Onik G, Mikus P. 2007. Irreversible electroporation: A new ablation modality—Clinical implications. *Technol Cancer Res Treat* 6(1):37–48.

Schoenbach KH, Beebe SJ, Buescher ES. 2001. Intracellular effect of ultrashort electrical pulses. *Bioelectromagnetics* 22:440–448.

Šel D, Cukjati D, Batiuskaite D, Slivnik T, Mir LM, Miklavčič D. 2005. Sequential finite element model of tissue electropermeabilization. *IEEE Trans Biomed Eng* 52:816–827.

Šel D, Maček-Lebar A, Miklavčič D. 2007. Feasibility of employing model-based optimization of pulse amplitude and electrode distance for effective tumor electropermeabilization. *IEEE Trans Biomed Eng* 54:773–781.

Šemrov D, Miklavčič D. 1998. Calculation of the electrical parameters in electrochemotherapy of solid tumors in mice. *Comput Biol Med* 28:439–448.

Serša G, Jarm T, Kotnik T, Coer A, Podkrajšek M, Šentjurc M, Miklavčič D et al. 2008. Vascular disrupting action of electroporation and electrochemotherapy with bleomycin in murine sarcoma. *Br J Cancer* 98:388–398.

Susil R, Šemrov D, Miklavčič D. 1998. Electric field induced transmembrane potential depends on cell density and organization. *Electro Magnetobiol* 17:391–399.

Tekle E, Oubrahim H, Dzekunov SM, Kolb JF, Schoenbach KH, Chock PB. 2005. Selective field effects on intracellular vacuoles and vesicle membranes with nanosecond electric pulses. *Biophys J* 89:274–284.

Towhidi L, Kotnik T, Pucihar G, Firoozabadi SMP, Mozdarani H, Miklavčič D. 2008. Variability of the minimal transmembrane voltage resulting in detectable membrane electroporation. *Electromagn Biol Med* 27:372–385.

Tungjitkusolmun S, Woo EJ, Cao H, Tsai J-Z, Vorperian VR, Webster JG. 2000. Thermal-electrical finite element modelling for radio frequency cardiac ablation: Effects of changes in myocardial properties. *Med Biol Eng Comput* 38:562–568.

Valič B, Golzio M, Pavlin M, Schatz A, Faurie C, Gabriel B, Teissié J, Rols MP, Miklavčič D. 2003. Effect of electric field induced transmembrane potential on spheroidal cells: Theory and experiment. *Eur Biophys J* 32:519–528.

Yamamoto T, Yamamoto Y. 1976a. Electrical properties of the epidermal stratum corneum. *Med Biol Eng* 14(2):151–158.

Yamamoto T, Yamamoto Y. 1976b. Dielectric constant and resistivity of epidermal stratum corneum. *Med Biol Eng* 14(5):494–500.

Županič A, Čorović S, Miklavčič D. 2008. Optimization of electrode position and electric pulse amplitude in electrochemotherapy. *Radiol Oncol* 42:93–101.